

**Complementary Approaches to Target Human Respiratory
Syncytial Virus Using Small Molecule Ligands**

Charles-Hugues Claude Jean Lardeau

Submitted in accordance with the requirements for the degree of
Doctor of Philosophy

The University of Leeds

Astbury Centre for Structural Molecular Biology

November 2012

The candidate confirms that the work submitted is his own and that appropriate credit has been given where reference has been made to the work of others.

This copy has been supplied on the understanding that it is copyright material and that no quotation from the thesis may be published without proper acknowledgement.

The right of Charles-Hugues Claude Jean Lardeau to be identified as Author of this work has been asserted by him in accordance with the Copyright, Designs and Patents Act 1988.

© 2012 The University of Leeds and Charles-Hugues Claude Jean Lardeau.

ACKNOWLEDGEMENTS

I would like to start by thanking my supervisors Adam Nelson, John Barr, and Julian Hiscox for their support and help over the last few years and for agreeing on this collaborative project between Chemistry and Virology; Olivier Ménard, my Maths teacher in Poitiers in 2002, whose strict methods during my first year of “Classes Préparatoires” are a consequence of my path to date. Finally, I would like to thank the Wellcome Trust, for funding the project.

I have been in England since mid-September 2006 and I have to thank my family for their continuous support, despite the distance and the fact that they barely saw me. Their support has been critical in the final year (I have been unable to travel home since mid-February). I have missed my little sister “Lili” the most, she is 16 and I feel like I have not seen her grow up. I also want to thank Bernard, a good friend from Toulouse for his continuous help and support but also for listening to my complaints. Thank you all!

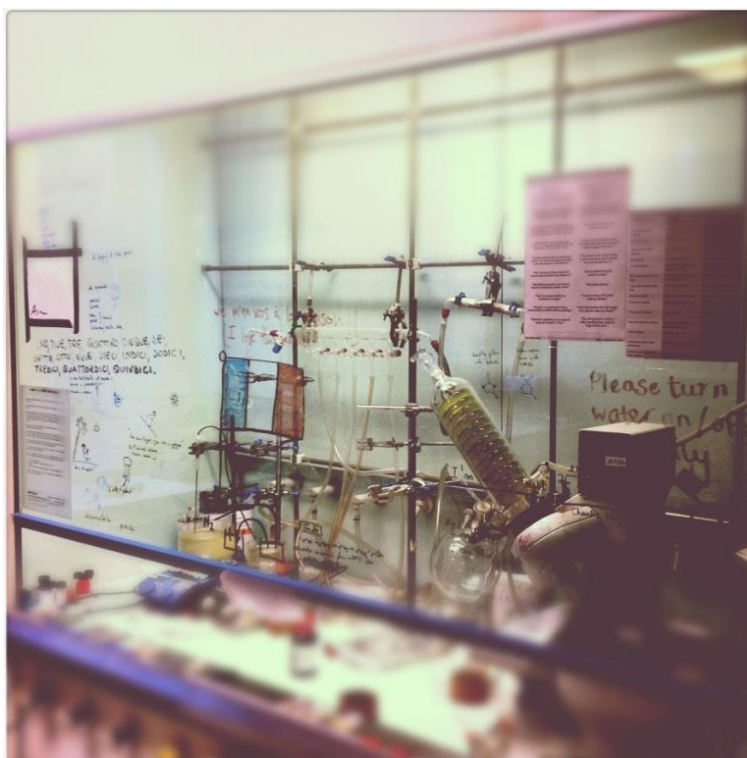
I would like to thank the following: Becky, Diane, Petra, and Weining for their help with virology techniques, Dr Jamel “buddy” Mankouri for his help with confocal imaging. I would also like to thank the following for making my time in Virology so enjoyable: Becky, Cheryl, Siân, Tosh, Zsofia, Barney, Björn, Carsten, Doug, Jamel, Mark V, Raj. Thank you (Siân and Carsten) for making me a better person by pointing out that white socks were a no-no.

I would like to thank everyone in Chemistry for help, friendship, and support. In particular: Francesco, Mark, Martin, Paul, and Tom J for helping me with Chemistry. I also want to thank Giorgia, Carlos, George B, Martin, and Dr Jeff “Kaboom” Plante for being awesome members of “team middle-bay”. I must thank George K and Mark for progresses made towards building blocks or final compound preparation. I also would like to thank Giorgia, “sneeze-tastic” Jenny, Alun, George B, George K, Mark, Richard, Steven for making it an enjoyable working environment. One person on this list meant that I got to visit the inside of a British hospital after 6 years.

I would also to thank Dr Chris Empson, Jim Titchmarsh, and Dr Stuart Warriner for their help with using the liquid-handling robot in the School of Chemistry; and Dr Katie Simmons, Dr Ian Yule, Dr Jayakanth Kankanala and Prof Peter Johnson for their help with the virtual screening software. Also, I would like to thank the technical staff in the School of Chemistry: Tanya Marinko-Covell, Simon Barrett, Francis “Matey” Billingham and his colleagues from Stores, and Martin Huscroft.

Adam, John, Giorgia, George B, George K, Paul, Richard have read part (or more) of the thesis and provided helpful feedback. Thank you!

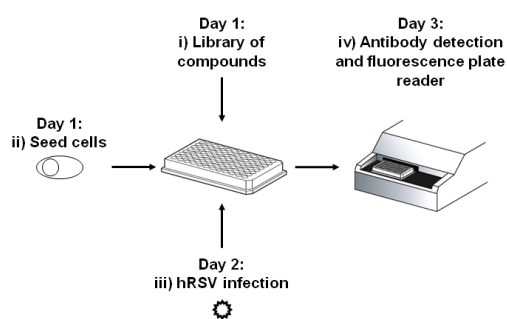
I must conclude by mention some names one more time: Adam for his continuous help, support, and patience since 2007, Giorgia, for being an amazing friend (*je ne suis pas facile, merci*), and the fantastic Italian community in Leeds, Björn and Carsten for the mutual amusement we provided each other, and Mark and Gemma for kindly providing me with shelter during the writing up period.



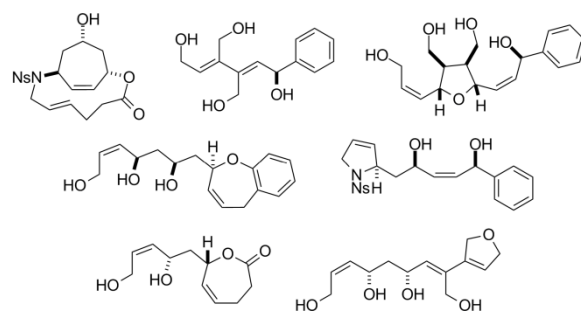
ABSTRACT

In the current project, situated at the interface of chemistry and virology, complementary drug discovery approaches (high-throughput screening and structure-based drug design) have been exploited in order to discover novel small molecule inhibitors of hRSV.

Thus, a novel fluorescence-based high-throughput screening assay was developed using known anti-virals for validation: EC₅₀ of Ribavirin *ca.* 30 μM, and EC₅₀ of JNJ-4749914 *ca.* 0.4 nM. This assay was then used to screen a natural product-like library.

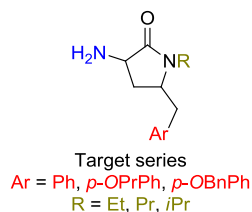


High-throughput screening assay setup



Library of natural product-like library

The crystal structure of a small molecule in complex with the fusion protein of hRSV was used in a virtual high-throughput screening campaign. A range of virtual libraries (libraries of likely synthetically accessible and commercially available molecule) were screened virtually using eHiTS against this binding cavity. This led to the identification of a potential novel series of hRSV fusion inhibitors, whose syntheses and biological evaluation have been described.



Novel confocal imaging experiments were also carried out on a known hRSV fusion inhibitor (JNJ-4749914) in order to gain more insight in the compound's mode of action by visualising virus entry inhibition in epithelial cells.

TABLE OF CONTENTS

ACKNOWLEDGEMENTS	i
ABSTRACT	iii
TABLE OF CONTENTS	iv
ABBREVIATIONS	ix
1 INTRODUCTION	1
1.1 Human respiratory syncytial virus	1
1.1.1 Historical background	1
1.1.2 Phylogenic relationships.....	1
1.1.3 The burden of hRSV.....	2
1.1.4 The hRSV genome and its expression.....	3
1.1.5 The role of hRSV proteins in the virus life cycle.....	5
1.1.6 Structural analysis of hRSV proteins	7
1.2 General introduction to drug discovery	14
1.2.1 Physico-chemical properties of compound collections	14
1.2.2 HTS and vHTS as techniques towards the discovery of new biologically active small molecules	16
1.3 hRSV therapies: from proof-of-concept to clinical trials	19
1.3.1 Overview of the therapies available to tackle hRSV.....	19
1.3.2 FDA-approved therapies	22
1.3.3 High-throughput screening to discover new small molecules anti-virals 22	
1.3.4 The use of biologics to tackle hRSV	26
1.3.5 Conclusions and future perspectives	26
1.4 Project outline	28

2	DEVELOPMENT OF A HIGH-THROUGHPUT SCREENING ASSAY	29
2.1	Introduction.....	29
2.1.1	Virus-induced cytopathic effects.....	29
2.1.2	Determination of the mode of action.....	31
2.1.3	Towards a robust HTS assay	31
2.2	Selectivity and range of antibody	34
2.2.1	Western blot analysis.....	34
2.2.2	Enzyme-linked immunosorbent assay.....	37
2.2.3	Fluorescence-based assay	38
2.3	Optimisation of a fluorescence-based assay for hRSV growth	41
2.3.1	The different steps composing the assay.....	41
2.3.2	Signal variation across the plate.....	42
2.3.3	Effect of the multiplicity of infection on the fluorescence signal	43
2.3.4	Study of the negative control (DMSO) effects.....	44
2.3.5	Study of the positive control (Ribavirin) effects	47
2.3.6	Robustness of the assay upon using a liquid-handling robot	52
2.3.7	Further assay validation with a known specific sub-nanomolar inhibitor 55	
2.4	Summary.....	62
3	DESIGN OF POTENTIAL LIGANDS USING VIRTUAL HIGH- THROUGHPUT SCREENING	63
3.1	vHTS approach to target hRSV	63
3.1.1	Selection of a target.....	64
3.1.2	Requirements for a virtual library	65
3.1.3	Virtual screening package	65
3.1.4	Selection criteria.....	66
3.1.5	Free energy minimisation.....	66

3.2	vHTS campaign	67
3.2.1	Enumeration of a virtual library	68
3.2.2	Identification of promising scaffolds for further development	69
3.2.3	Identification of potential hRSV fusion inhibitors to be prepared	72
3.2.4	Free energy minimisation	76
3.3	<i>In silico</i> evaluation of a virtual library with lead-like properties	80
3.3.1	Identification of an additional series of potential hRSV fusion inhibitors 80	
3.3.2	Predicted structure-activity relationships using eHiTS	84
3.4	vHTS on a virtual library of commercially available compounds.....	88
3.5	Summary.....	90
4	STUDIES TOWARDS THE SYNTHESIS OF POTENTIAL HRSV FUSION INHIBITORS	91
4.1	Retrosynthetic analyses.....	91
4.2	Synthesis of building blocks required for route development	94
4.2.1	Synthesis of building blocks required for the synthetic studies towards series 1	94
4.2.2	Synthesis of building blocks required for the studies towards series 2.	96
4.2.3	Synthesis of building blocks required for the synthetic studies towards series 3	97
4.3	Synthetic studies towards potential hRSV fusion inhibitors	98
4.3.1	Synthetic studies towards series 2	98
4.3.2	Synthetic studies towards series 3	101
4.4	Synthesis of building blocks required for a focused library of proposed inhibitors	102
4.4.1	Preparation of DL-O-benzyltyrosinol and DL-O-n-propyltyrosinol...	102
4.4.2	Preparation of the cyclic sulfamidates derived from DL-O- benzyltyrosinol and DL-O-n-propyltyrosinol	103
4.5	Synthesis of a focused library of proposed inhibitors.....	104

4.6	Summary	105
5	EVALUATION OF SELECTED COMPOUNDS AS INHIBITORS OF HRSV	106
5.1	Biological evaluation at a single concentration	106
5.1.1	Choice of a compound collection for HTS	106
5.1.2	High-throughput screening results	108
5.1.3	Evaluation of compounds identified through vHTS.....	111
5.1.4	Therapeutic index	114
5.1.5	Dose-response analyses on screening hits	115
5.1.6	Discussion	119
5.2	Biological testing of the intermediates in the synthesis of JNJ-4749914...	120
5.2.1	Dose-response curves	120
5.2.2	Confocal imaging of the mode of action of JNJ-4749914	122
5.2.3	Discussion	123
5.3	Summary	124
6	SUMMARY AND FUTURE WORK.....	125
7	MATERIALS AND METHODS	129
7.1	Buffers and solutions	129
7.2	Tissue culture techniques	130
7.2.1	Tissue culture plasticware	130
7.2.2	Maintaining cells	130
7.2.3	Freezing cells down.....	130
7.2.4	Using cells from a frozen stock	131
7.2.5	Counting cells	131
7.2.6	Virus propagation	131
7.3	Confocal imaging	132
7.4	Plaque assay	133
7.5	Preparation of cell lysates and western blot analyses	134

7.6	Spinoculation	135
7.7	Antiviral assay	136
7.8	Plate reader parameters	137
7.9	Cytotoxicity assay.....	138
7.10	Data analysis	138
7.11	Ribavirin stock and preparation of dilution series	141
7.12	Ribavirin master plate to test the robustness of the assay upon using the robot	143
7.13	Mode of action of JNJ-4749914.....	145
7.14	High-throughput screening.....	146
7.15	Compounds characterisation	147
8	REFERENCES.....	197
9	APPENDIX.....	212

ABBREVIATIONS

General abbreviations

°C	Celsius degrees
3D	Three dimensional
Å	Ångström
Ab	Antibody
Ac	Acetyl
App	Apparent
Aq	Aqueous
Ar	Aromatic
Bn	Benzyl
Boc	<i>tert</i> -Butyloxycarbonyl
br	Broad
Bu	Butyl
C	Concentration
<i>ca.</i>	Circa; about
CADp	Carbamoyl-phosphate synthetase 2, aspartate transcarbamylase, and dihydroorotase polypeptide
CC ₅₀	50% Cytotoxic concentration
CV	Coefficient of variation
δ	Chemical shift
Da	Dalton
dba	Dibenzylideneacetone
dppb	1,4-Bis(diphenylphosphino)butane
DCM	Dichloromethane
DEAD	Diethyl azodicarboxylate
DMAP	4-Dimethylaminopyridine

DHODH	Dihydroorotate dehydrogenase
Direct	Primary antibody conjugated to HRP or FITC
d	Doublet
dd	Double doublet
ddd	Double, double doublet
dddd	Double, double double doublet
dq	Double quadruplet
ddt	Double, double triplet
dt	Double triplet
DMAP	4-Dimethylaminopyridine
DMEM	Dulbecco's Modified Eagle's Media
DMF	<i>N,N</i> -Dimethylformamide
DMSO	Dimethyl sulfoxide
EC ₅₀	50% Effective concentration
<i>e.g.</i>	Exempli gratia; for example
Et	Ethyl
<i>et al.</i>	Et alii; and others
eHiTS	Electronic high-throughput screening
ELISA	Enzyme-linked immunosorbent assay
FBDD	Fragment-based drug design
FBS	Foetal bovine serum
FDA	Food and Drug Administration
FITC	Fluorescein isothiocyanate
GE / GS	Gene end / Gene start (sequences)
g	Gram
<i>g</i>	Acceleration
HCV	Hepatitis C virus
hept	Heptuplet
HIV	Human immunodeficiency virus
HR	Heptad repeat

HRP	Horseradish peroxidase
(v)HTS	(virtual) High-throughput screen
(h)RSV	(human) Respiratory syncytial virus
Hz	Hertz
IC ₅₀	50% Inhibitory concentration
IR	Infrared
iPr	<i>isopropyl</i>
<i>J</i>	Spin-spin coupling constant
(c)LE	(computational) Ligand efficiency
LiHMDS	Lithium bis(trimethylsilyl)amide
LIMS	Laboratory Information Management System
Lit	Literature
Log	Logarithm in base 10
LsA	Limits of Agreement
μ	Mean
m	Multiplet
M	Molar
MAD	Median absolute deviation
maj	Major
Me	Methyl
mg	Milligram
min	Minor
mL	Millilitre
mM	Millimolar
m.p.	Melting point
μL	Microlitre
μM	Micromolar
MOI	Multiplicity of infection
MR	Mean-ratio
Ms	Mesyl

MSR	Minimum significant ratio
MTT	3-(4,5-Dimethylthiazol-2-yl)-2,5-diphenyl tetrazolium bromide
MW	Molecular weight
N/A	Not available
NIH	National Institutes of Health
NIS	<i>N</i> -Iodosuccinimide
nM	Nanomolar
NMR	Nuclear magnetic resonance
Ns	2-Nitrobenzenesulfonyl
PBS	Phosphate-buffered saline
PDB	Protein databank
Petrol	Petroleum spirit (b.p. 40-60)
Pfu	Plaque forming units
pH	Potential hydrogen
Piv	<i>tert</i> -Butylcarbonyl
pM	Picomolar
Pr	Propyl
PSA	Polar surface area
q	Quadruplet
RCM	Ring-closing metathesis
RdRp	RNA-dependent RNA polymerase
R.F.U.	Relative fluorescence unit
(m / si)RNA	(messenger / small interfering) Ribonucleic acid
RNP	Ribonucleoprotein (complex)
rot	Rotamer
rpm	Rotation per minute
σ	Standard deviation
s	Singlet
S:B	Signal-to-background (ratio)
S:N	Signal-to-noise (ratio)

SAR(s)	Structure-activity relationship(s)
SBDD	Structure-based drug design
SDS	Sodium dodecyl sulphate
SW	Signal window
t	Triplet
tt	Triple triplet
TBAF	tetra- <i>n</i> -Butylammonium fluoride
TBS	<i>tert</i> -Butyldimethylsilyl
<i>t</i> Bu	<i>tert</i> -Butyl
<i>tert</i>	Tertiary
TFA	Trifluoroacetic acid
THF	Tetrahydrofuran
TI	Therapeutic index
XTT	2,3-bis[2-Methoxy-4-nitro-5-sulfohenyl]-2H-tetrazolium-5-carboxyanilide, inner salt

Amino acids

Alanine (Ala, A)

Arginine (Arg, R)

Asparagine (Asn, N)

Aspartic acid (Asp, D)

Cysteine (Cys, C)

Glutamic acid (Glu, E)

Glutamine (Gln, Q)

Glycine (Gly, G)

Histidine (His, H)

Isoleucine (Ile, I)

Leucine (Leu, L)

Lysine (Lys, K)

Methionine (Met, M)

Phenylalanine (Phe, F)

Proline (Pro, P)

Serine (Ser, S)

Threonine (Thr, T)

Tryptophan (Trp, W)

Tyrosine (Tyr, Y)

Valine (Val, V)

hRSV proteins

F = fusion protein

G = glycoprotein

L = large protein

M = matrix protein

N = nucleoprotein

NS = non-structural protein

P = phosphoprotein

SH = small hydrophobic protein

1 INTRODUCTION

1.1 Human respiratory syncytial virus

1.1.1 *Historical background*

Human respiratory syncytial virus (hRSV) was originally isolated in 1956 from chimpanzees presenting the symptoms of coryza¹ (respiratory infection with symptoms of a cold). As a result, it was known as the chimpanzee coryza agent. It was only designated hRSV when it was recovered from the lower respiratory tract of infants a year later and its cytopathic effects were characterised in human nasopharynx or liver cells². The observation of the formation of large cells with multiple nuclei led to the use of the term syncytium^{1,2} (from the Greek *syn-* together, and *kytos* cell).

1.1.2 *Phylogenic relationships*

hRSV is an enveloped virus from the *Paramyxoviridae* family (order *Mononegavirales*, genus *Pneumovirus*)³. hRSV is classified into two subgroups: hRSV-A and hRSV-B^{4,5} on the basis of membrane glycoprotein reactivity to a panel of monoclonal antibodies^{6,7}. Other members of this family include the human parainfluenza virus and measles virus⁸⁻¹⁰. Additional members of the *Mononegavirales* order include Ebola virus⁸ (family *Filoviridae*) or rabies virus⁸ (family *Rhabdoviridae*). RSV infections are not only limited to humans: several RSV species are also present across different hosts such as in bovine (*e.g.* cow) and ovine (*e.g.* sheep)⁹.

1.1.3 The burden of hRSV

hRSV is one of the major lower respiratory tract pathogens in infants with consistent annual outbreaks. 90% of infants are infected with hRSV at least once within the first two years of life¹¹. It is estimated that, each year, over 2 million children under five require hospitalisation as a consequence of hRSV infection in the United States of America alone¹². Elderly patients, patients with chronic heart and lung conditions and immunocompromised patients are also at risk^{4,13,14}. According to the World Health Organization, there are about 60 million people infected and 160,000 deaths every year¹⁵.

hRSV is spread by large respiratory droplets and can live for several hours on objects, requiring close proximity or contaminated objects for viral transmission^{16,17}. Replication occurs in the upper respiratory tract (nasopharynx) first with an incubation period of *ca.* four days prior to spreading to the lower respiratory tract (lung). The symptoms range from mild cough or fever to severe bronchiolitis or pneumonia^{18,19}. Early acute hRSV infection in infants has also been linked with the development of asthma^{20,21}.

hRSV targets superficial layers of ciliated polarised epithelial cells^{22,23} (bronchial, alveolar epithelial cells²⁴). Following infection, they do not display any signs of morphologic changes unlike in non-polarised cell lines (human cervix carcinoma epithelial cells also known as HEP-2 cells²⁵). However, syncytia are observed *in vivo* when there is a T cell* deficiency¹¹. hRSV has been shown to infect dendritic cells located in the respiratory tract^{26,27} that play a role in the immune response²⁸. Airway obstruction and breathing difficulties are a consequence of mucus discharge, debris and sloughing of infected epithelial cells^{11,14,24}.

* T cells lead the immune response to hRSV²⁴ Johnson, J. E., Gonzales, R. A., Olson, S. J., Wright, P. F. & Graham, B. S. The histopathology of fatal untreated human respiratory syncytial virus infection. *Mod. Pathol.* **20**, 108-119 (2006).

Over the course of ten years, during the epidemic season (November to March, with a peak in January or February in the Northern hemisphere^{4,5,11}), scientists in Belgium have studied the prevalence and circulation of hRSV-A and hRSV-B strains and observed that the two subgroups can co-exist but one subgroup can prevail from one year to the other⁵. The co-existence of the two subgroups is thought to be a factor that allows hRSV re-infection^{4,5}.

1.1.4 The hRSV genome and its expression

The hRSV genome is a single strand of negative-sense RNA, 15,222 nucleotides in length (Figure 1.1.A). The infecting hRSV genome is replicated by the virus-encoded RNA-dependent RNA polymerase (RdRp) to yield a positive sense anti-genome, which is used as a template for the subsequent synthesis of a progeny genome²⁹. The genome is transcribed sequentially by the RdRp into ten individual capped and polyadenylated mRNAs. During transcription, the RdRp can only enter the genome at the 3' leader region, and has a polarised movement (3' to 5')²⁹. Transcription is a start-and-stop process as a consequence of gene start (GS) and gene end (GE) sequences on either side of the viral genes. Initiation and capping of each mRNA is signalled by the GS sequence, and the synthesised mRNA is polyadenylated and released from the RdRp at the GE sequence. After reading the GE sequence, the RdRp scans the intergenic sequence until the next GS sequence is reached (Figure 1.1.B). Approximately 30% of RdRp molecules disengage from the template within the intergenic region, resulting in a polar abundance of transcription products; genes at the 3' end of the genome are transcribed with greater abundance than those at the 5' end^{11,29}. The replication of the hRSV genome and the synthesis of individual viral mRNAs occurs in the cytoplasm of infected cells^{9,11,30}.

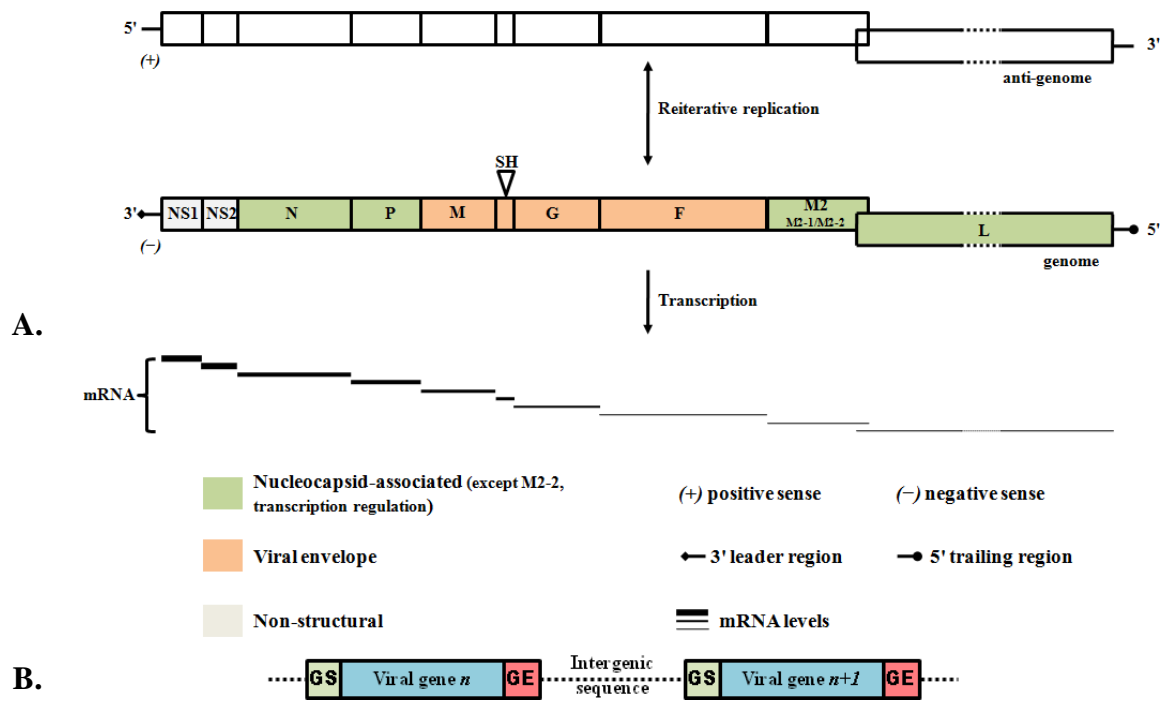


Figure 1.1. A schematic representation of the hRSV RNA genome and expression of the viral genes. **A.** The hRSV genome is replicated by the synthesis of a positive sense anti-genome (template for progeny genome). It is also expressed into individual mRNAs by start-and-stop synthesis with decreasing abundance (represented by the thickness of the line) from 3' to 5'. NS1, NS2: non-structural protein 1 and 2; N: nucleoprotein, P: phosphoprotein, M: matrix protein, SH: small hydrophobic, G: glycoprotein, F: fusion, L: large. Adapted from Collins *et al.*¹¹. **B.** Start-and-stop mRNA synthesis with the gene start (GS) and gene end (GE) sequences on either side of viral genes. The GE of a viral gene is separated from the GS of the next gene by an intergenic sequence (dotted line). Adapted from Fearn's *et al.*²⁹.

1.1.5 The role of hRSV proteins in the virus life cycle

There are ten viral genes in the hRSV genome that encode for eleven viral proteins: M2-1 and M2-2 are expressed from overlapping reading frames in the M2 gene¹¹. The genome and the viral proteins (except NS1, NS2 and M2-2 which are non structural) are components of the viral particle, also known as the virion^{11,31} (Figure 1.2). Collins *et al.*³² have demonstrated, using a minigenome system, that RNA replication was controlled by the N (role in RNA-binding¹¹), P (cofactor for elongation³³) and L (polymerase³⁴) proteins. However, it was observed that M2-1 was required for transcription of full length mRNAs, and proposed its role as a processivity factor of the polymerase^{19,34,35}. N, P, L and M2-1 proteins form the ribonucleoprotein complex (RNP) with RNA³. M2-2 regulates the relative levels of the synthesis of genomic RNA and viral mRNAs but its presence is not critical for replication³⁶. NS1 and NS2 inhibit the synthesis of interferons and have been linked with the inhibition of apoptosis^{11,19}. The matrix protein is important for viral assembly⁹ and it inhibits host cell transcription capabilities^{37,38}.

The remaining three proteins F, G and SH are membrane glycoproteins. The F proteins are conserved across hRSV strains (91% sequence conservation³⁹) while the G gene diverges between hRSV strains (53% sequence conservation⁴⁰). As a consequence, G is at the centre of hRSV antigenic variability and the classification of hRSV into two subgroups (hRSV-A and hRSV-B^{4,5}). hRSV infection and budding in epithelial cells is reported to be polarised and occurs preferentially through the apical face of the cell^{22,23}. hRSV virion entry and syncytia formation occur by cell membrane fusion with the F protein. The G protein plays a role in virus attachment⁴¹ (although is not critical for infection^{42,43} or replication⁴⁴ *in vitro*). The current model for hRSV binding is that hRSV binds to glycosaminoglycans⁴⁵ (e.g. heparin) on the cell surface *via* interactions with the G protein⁴⁶, which is followed by the binding of the F protein to nucleolin⁴⁷. Proteins involved in virus entry or replication could be attractive targets for therapeutic intervention^{37,48}. Recently, the SH protein has been classified as a viroporin^{49,50}, a group of pore-forming, oligomeric transmembrane proteins, which also include the hepatitis C virus p7 protein or the influenza A M2 protein⁵¹.

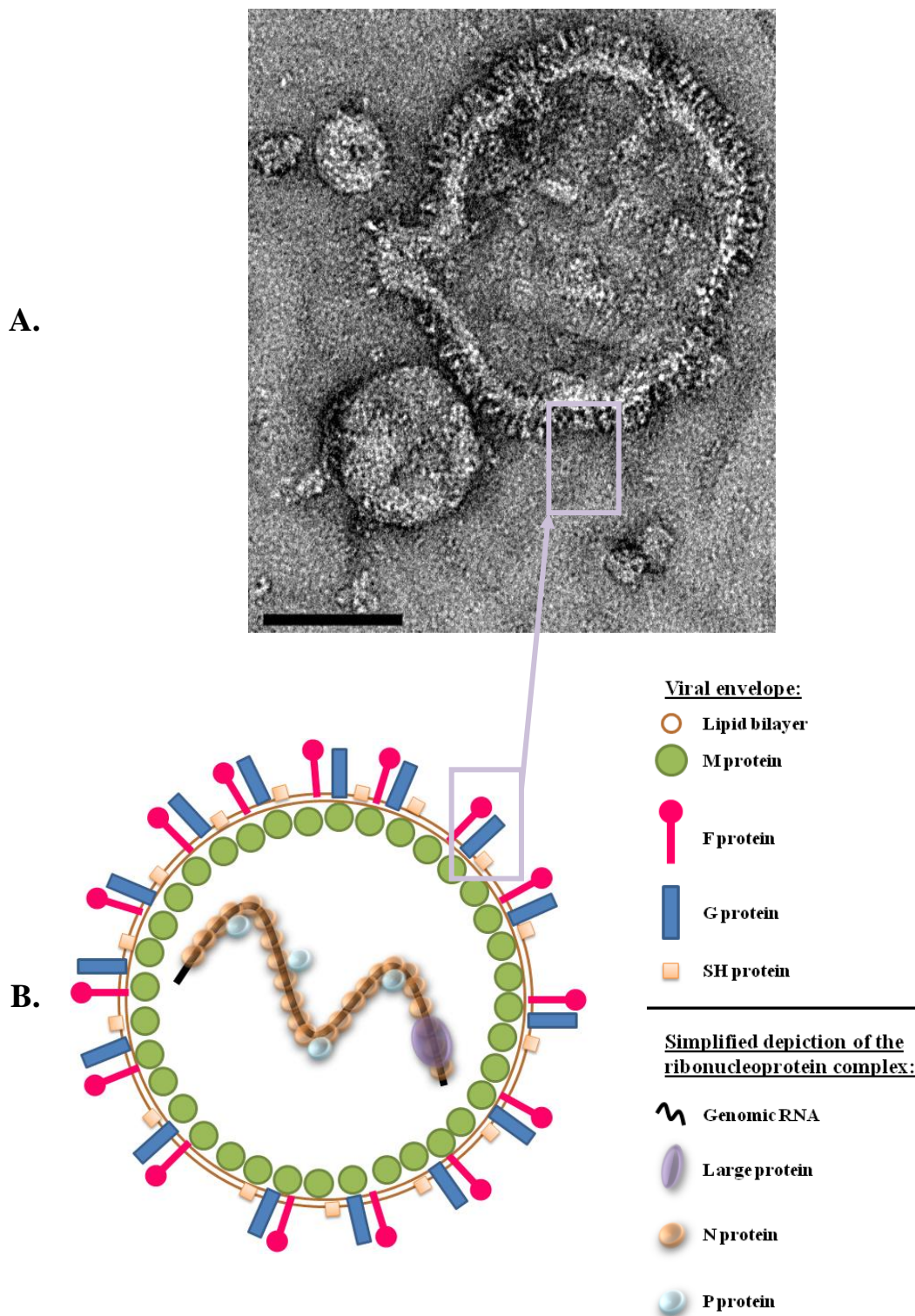


Figure 1.2. Organisation of the hRSV virion. **A.** Electron-microgram showing the membrane features of a hRSV virion (courtesy of Kyle Dent). Diameter: *ca.* 210 nm. Scale bar: 2 μm = 85 nm. **B.** Simplified diagram of the hRSV virion. On the outer and inner membranes, the proteins for the viral envelope (F, G, SH and M) are depicted individually. The ribonucleoprotein complex is located inside the virion: N is encapsidating the RNA genome, P has been found with a binding site on N⁵². Because its interaction partners are not defined, M2-1 is not depicted. NS1, NS2, and M2-2 are non-structural proteins and are not part of the virion. For ease of illustration, the viral proteins are not drawn to scale. Adapted from Ghildyal *et al.*⁹.

1.1.6 Structural analysis of hRSV proteins

Structure-based drug design requires high resolution structural data obtained by either X-ray crystallography or NMR spectroscopy ($< 2.5 \text{ \AA}$ in order to be confident about the positions of residues and side chains within the electron density map⁵³). Structural data is available for four hRSV proteins: N, M, SH and F.

1.1.6.1 Crystal structure of the N–RNA complex

A major component of the RNP is the nucleoprotein N, which is responsible for the encapsidation of the anti-genome and the progeny genome, as they are synthesised, with helical symmetry¹⁵. One turn of the helical N-RNA complex has been solved by X-ray crystallography (3.3 \AA) as a decameric ring⁵⁴ (Figure 1.3.A). The authors suggested that the polymerase might be able to access the genome without dissociating the N–RNA complex (Figure 1.3.B). The structure also revealed a cavity in which RNA bases 2 to 4 dock (Figure 1.3.C): the cavity–RNA bases interaction seems to be conserved across the *Mononegavirales* order⁵⁴. Finally, resistance that arose from the exposure of a specific inhibitor to the N protein has been mapped at the proposed N–polymerase binding site⁵⁴ (see Section 1.3.3.3).

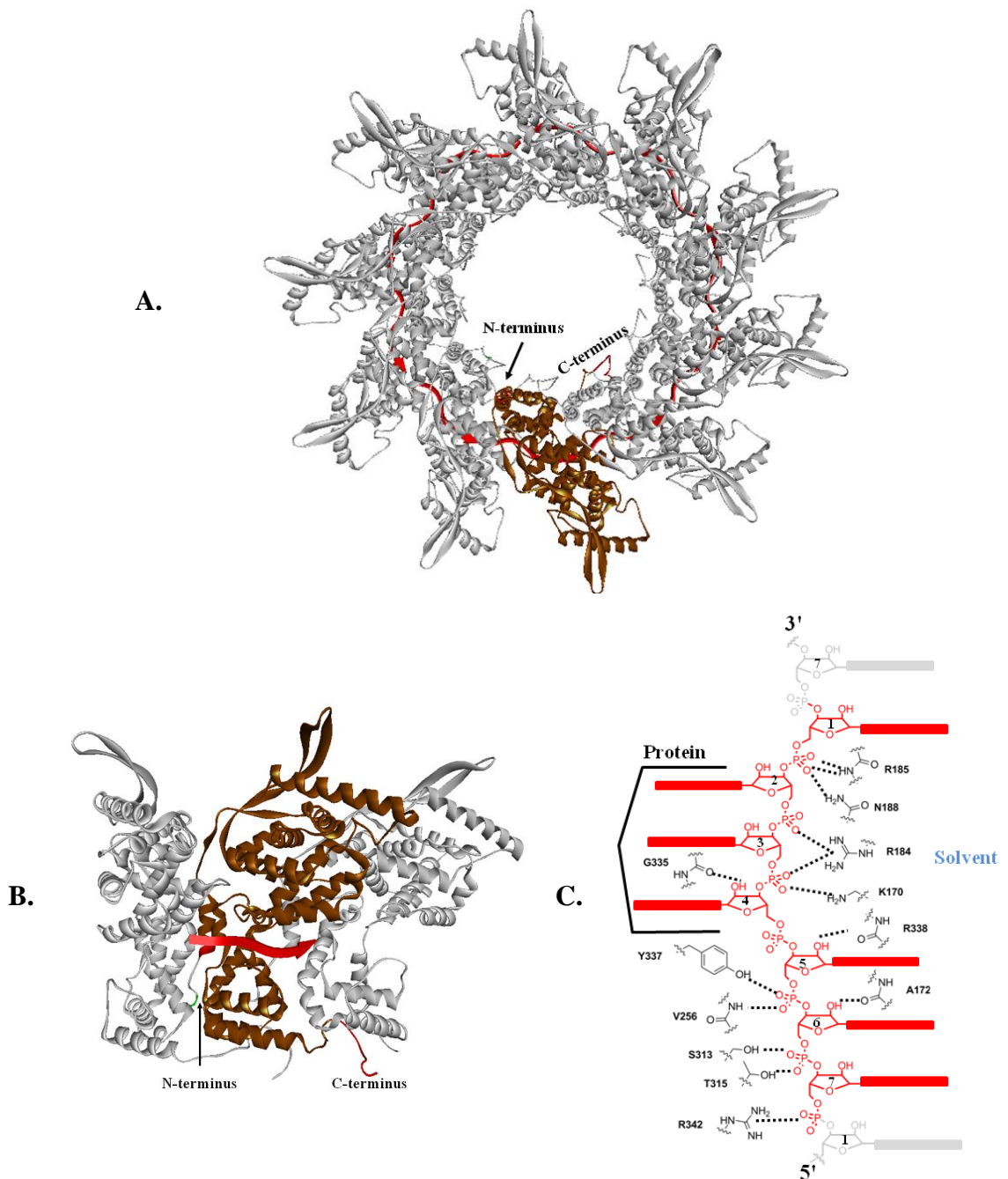


Figure 1.3. Crystal structure of the N-RNA complex⁵⁴. **A.** Top view of the crystal structure of a decameric N-RNA ring complex (PDB accession number 2WJ8, 3.3 Å), shown in solid ribbon. One turn of the helical symmetry of the N-encapsulation process is represented. A single N subunit is shown in brown and the RNA is shown in red arrows. The N- and C-terminus are buried on the inside of the decameric ring. **B.** Side view of three adjacent N subunits (RNA, shown in red, has been hidden from the subunits flanking the N-RNA complex in the middle). **C.** N-RNA interactions (dotted lines). Seven nucleotides are interacting with the N subunit. RNA from adjacent subunits is shown in grey. RNA from the main subunit is shown in red. RNA bases are shown as thick coloured lines. Adapted from Tawar *et al.*⁵⁴. Pictures generated with Discovery Studio (Accelrys).

1.1.6.2 Crystal structure of the M protein

The crystal structure of the M protein has been solved³¹ using X-ray crystallography (1.6 Å) (Figure 1.4.A) and consists of two β -sheet domains joined by a flexible linker, a feature that is found in other members of the *Mononegavirales* order⁵⁵. Additionally, calculation of the electrostatic potential⁵⁶ revealed an area of positively charged residues (Figure 1.4.B), ideally positioned to form complementary interactions with a membrane or alternatively with the RNP, both negatively charged³¹. Both of these potential interactions would be consistent with the matrix protein being important for viral entry⁵⁵ and assembly⁹.

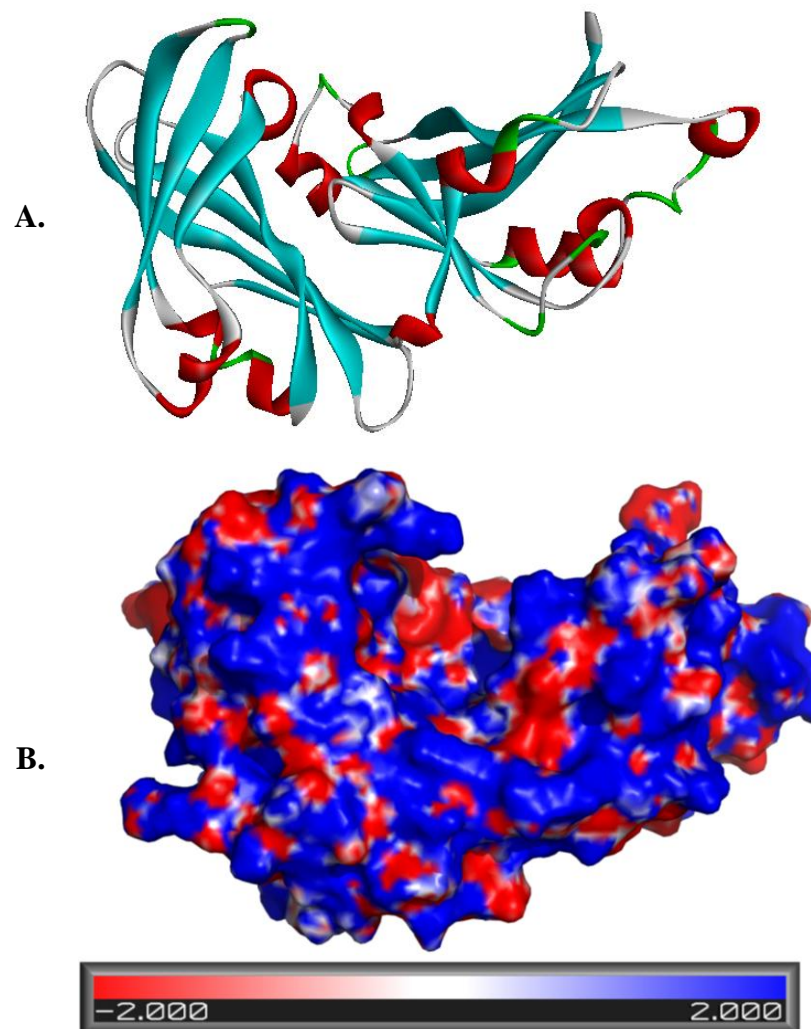


Figure 1.4. Crystal structure of the M protein³¹. **A.** Crystal structure of the M protein (PDB accession number 2VQP, 1.6 Å), shown in solid ribbon, reveals two β -sheet domains. Picture generated with Discovery Studio (Accelrys). **B.** Electrostatic potential solved with the Poisson-Boltzmann equations solver⁵⁶ using the CHARMM program⁵⁷ between -2 (red) and 2 (blue) kcal/mol/ e , e is the unit charge. Picture generated with PyMOL (Schrödinger).

1.1.6.3 NMR structure of the SH protein

Electron microscopy observation of the SH protein by Carter *et al.*⁴⁹ revealed pentameric and hexameric ring-like objects in liposomes or micelles with a central pore of 19 nm (pentamer) or 26 nm (hexamer) (Figure 1.5.A). After solution NMR studies in micelles and lipid bilayers, Gan *et al.*⁵⁰ observed that the SH protein adopted an α -helical conformation and concluded that the SH protein formed a pentamer (Figure 1.5.B, Figure 1.5.C).

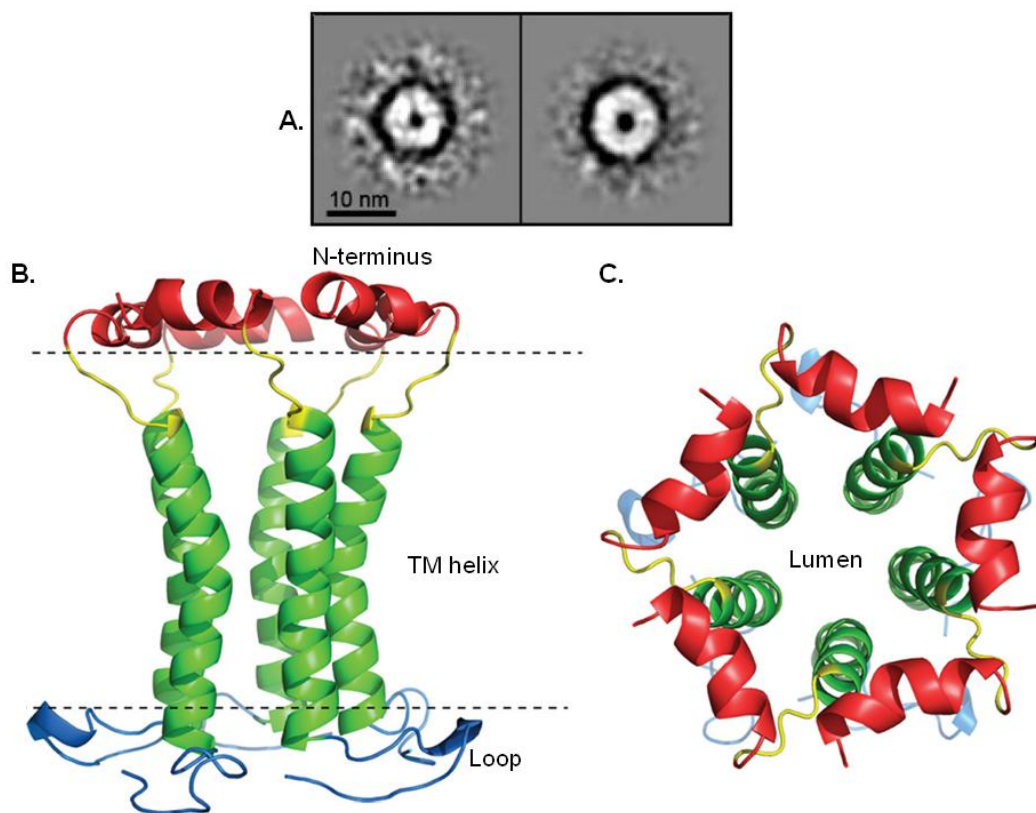


Figure 1.5. Structural studies on the SH protein. A. Putative five- and six-fold symmetries observed by electron microscopy. Image taken from Carter *et al.*⁴⁹. B. Side-view of the SH pentamer. The pentamer model was constructed from 2D NMR and structure refinement data. Within a membrane, the SH protein adopts an α -helical conformation. The length of the channel is *ca.* 45 Å. Image taken from Gan *et al.*⁵⁰, as PDB coordinates were not released. C. Top-view of the SH pentamer. The pentamer model was constructed from 2D NMR and structure refinement data. Image taken from Gan *et al.*⁵⁰, as PDB coordinates were not released.

1.1.6.4 F protein and its function

hRSV F protein is a class I fusion protein⁵⁸. Class I proteins are synthesised as an inactive precursor that is cleaved into the active fusion sequence. The well-studied human immunodeficiency virus type 1 (HIV-1) gp41⁵⁹ is also a class I fusion protein and its mechanism of action has been extended by analogy to hRSV⁶⁰. The F protein is synthesised as an inactive precursor (F₀) that is cleaved into two subunits (F₁ and F₂) (Figure 1.6.A), one of which (F₁) undergoes a series of conformational rearrangements involving the heptad repeats (HR) of the N- and C-terminus (Figure 1.6.B). Based on the structural data available for the parainfluenza virus 5 F protein^{61,62} (another class I fusion protein), HR-N is proposed to be buried in the globular domain in the pre-fusion state. Upon fusion, an initial conformational rearrangement results in the fusion peptide being directed towards the target cell membrane and the HR-C to be extracted from the globular domain. A key intermediate in the fusion mechanism is thought to be a 6-helix bundle⁶⁰, a homotrimer of antiparallel heterodimers (solved at 2.3 Å, Figure 1.6.C). The final intermediate is the more stable post-fusion conformation⁶³ (solved at 2.8 Å, Figure 1.6.D). Upon discovering resistant strains to a known small molecule inhibitor, mutations were observed in the globular domain, which has to undergo conformational rearrangement in order for the two heptad repeats to interact (Figure 1.6.B). It was proposed that mutation in the globular domain could affect the kinetics of the rearrangement⁶⁴.

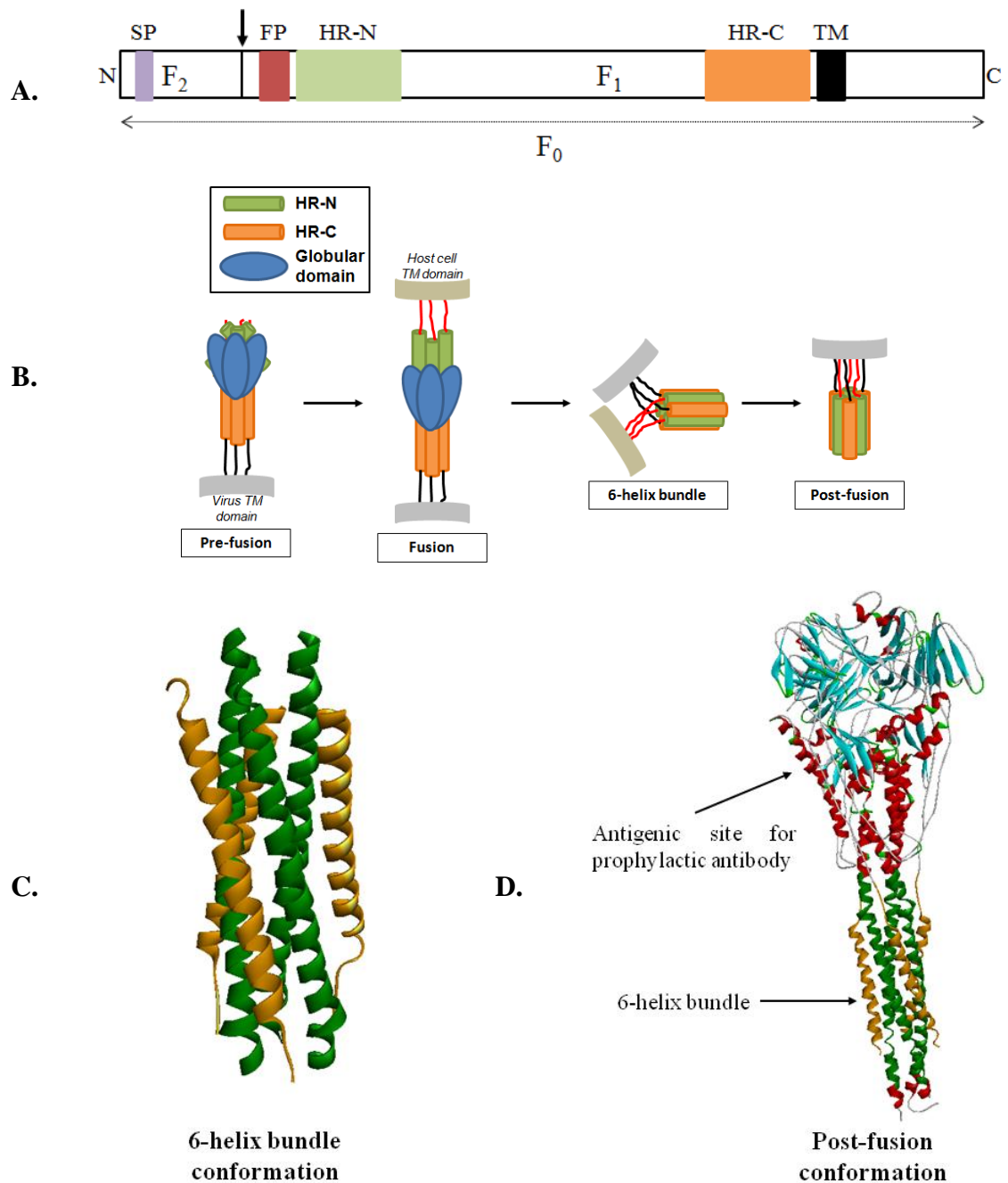


Figure 1.6 Fusion protein of hRSV. **A.** F_0 precursor: signal peptide (purple), furin-like proteolytic cleavage site (arrow), putative fusion peptide (red), HR-N (green), HR-C (orange) and a transmembrane anchor (black). **B.** Proposed intermediates involved in hRSV fusion. In the fusion-ready state, the putative fusion peptide (red) is directed towards the target cell. A series of conformational rearrangements lead HR-N and HR-C to form a 6-helix bundle. The final intermediate is the more stable post-fusion state. For ease of representation, the globular domain is only shown in the pre-fusion state. **C.** Crystal structure of the 6-helix bundle (PDB accession number 1G2C, 2.3 Å), shown in solid ribbon, reveals a homotrimer of antiparallel heterodimers⁶⁰. **D.** Crystal structure of the hRSV fusion protein in the post-fusion conformation (PDB accession number 3RRR, 2.8 Å) shown in solid ribbon⁶³. The fusion peptide is not shown. The presence of the 6-helix bundle suggests the protein might in the post-fusion state. The binding site of prophylactic antibodies (Section 1.3.2) is also shown^{63,65}. Picture generated with Discovery Studio (Accelrys).

The association of HR-C and HR-N is responsible for merging the viral and cellular membranes^{60,66}. From the crystal structure of the 6-helix bundle⁶⁰, it appears that the HR-C peptide binds inside a hydrophobic groove composed of two adjacent HR-N peptides (Figure 1.7). The resulting complex is held together by key hydrophobic interactions between residues L481, F483 and F488 of HR-C and the hydrophobic groove. Residues 480 to 520 of HR-C and 180 to 199 of HR-N are conserved between a range of hRSV strains (B1, B18537, A2, Long). By analogy with the HIV-1 gp41 crystal structure^{59,67}, the hydrophobic pocket occupied by F483 and F488 constitutes a potential target for small molecule inhibitors. The specific interactions observed in the complex between the F protein and a specific inhibitor will be described in Section 1.3.3.2.

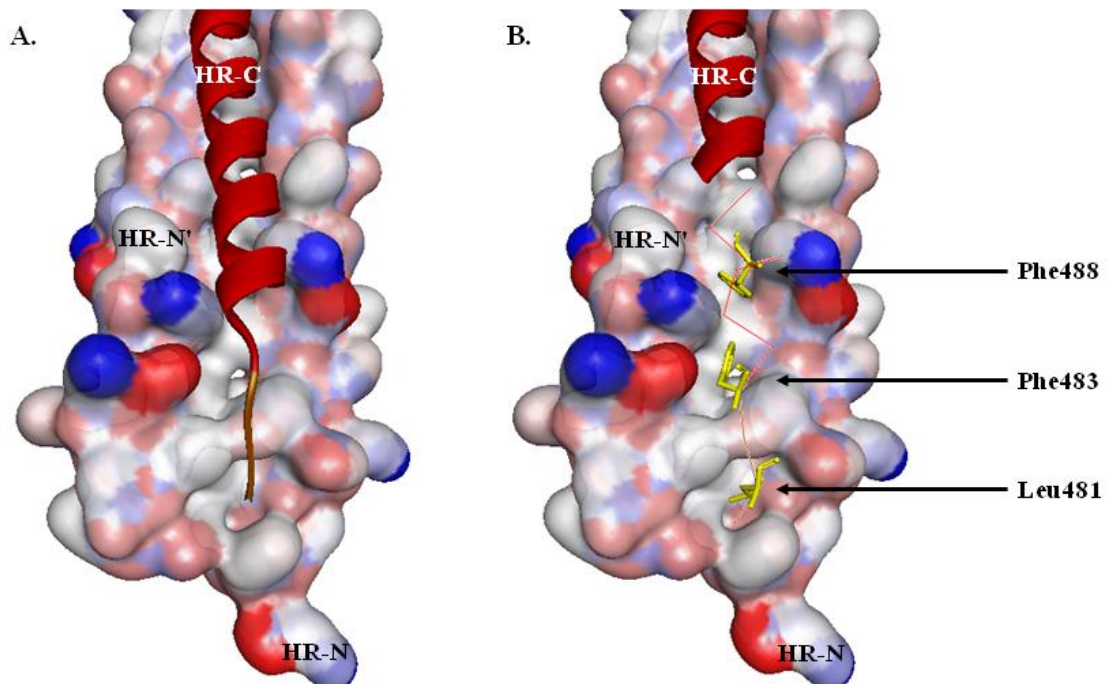


Figure 1.7. Hydrophobic groove of the 6-helix bundle. **A.** The formation of a 6-helix bundle (an intermediate in the pre-fusion to the post-fusion complex of the F protein) involves the formation of a hydrophobic groove formed by two adjacent HR-N peptides shown as a surface area (noted HR-N and HR-N'). HR-C, shown in solid ribbon, binds in the resulting hydrophobic groove, (1G2C, 2.3 Å). **B.** HR-C binds through three key hydrophobic interactions involving residues L481, F483 and F488. For ease of visualisation, only the residues that are involved in the interactions with the hydrophobic groove are shown (yellow sticks) and part of the α -helix is shown as a line, (1G2C, 2.3 Å). Picture generated with Discovery Studio (Accelrys).

1.2 General introduction to drug discovery

There are a range of complementary approaches that may be exploited in the discovery of small molecules with specific biological activity⁶⁸ including: i) modification a known drug or a natural product, ii) high-throughput screening (HTS), iii) structure-based drug design⁶⁹⁻⁷⁴ (SBDD), iv) fragment-based drug discovery^{68,75,76} (FBDD).

SBDD and, in general, FBDD rely on the availability of high-resolution structural data (X-ray or NMR). SBDD can follow *de novo* design approaches^{69,73} (e.g. SPROUT⁷⁰) or virtual high-throughput screening^{69,71,72,74} (vHTS). FBDD and *de novo* approaches were not used in the present study and are not discussed.

HTS has been widely used in the discovery of small molecule anti-virals against hRSV (see Section 1.3) and vHTS has been used against hRSV as part of the present study (see Chapter 3). Both HTS and vHTS allow for the screening of large compound collections, under different settings: in biological systems for the former and using *in silico* methods for the latter.

1.2.1 Physico-chemical properties of compound collections

A key characteristic to take into account in drug discovery is the interdependence between the absorption / permeation of a small molecule and its molecular weight, lipophilicity and hydrogen bond potential. This has been illustrated by the Lipinski “rule of five”, which is generally used to indicate the “drug-likeness” (good potency, good cell-wall penetration and rapid absorption) potential of a small molecule⁷⁷. An initial screening campaign generally aims at screening lead-like compounds, which are going to be optimised during later stages of development. In order to comply with the Lipinski parameters in a drug candidate, a different set of criteria has been defined for lead-like compounds (Table 1.1). The criteria are more stringent for “lead-likeness” as the lead optimisation process⁷⁸ is likely to add on key functionalities (to increase potency) which will usually increase lipophilicity and molecular weight (Figure 1.8).

Table 1.1: Specific parameters to take into account in the drug discovery process

	Lead-like ⁷⁸	Drug-like ^{a, 77}
Lipophilicity ^{77,78}	$-1 \leq \text{cLogP}^b \leq 3$	$\text{cLogP}^b \leq 5$
Molecular weight ⁷⁷⁻⁷⁹ (g/mol)	$200 \leq \text{M.W.} \leq 350$ (14 to 26 heavy atoms)	$\text{M.W.} \leq 500$
Hydrogen-bond donor ^{77,80}	≤ 3	≤ 5
Hydrogen-bond acceptor ^{77,80}	≤ 8	≤ 10
Polar surface area (PSA) ⁷⁸	$75 \text{ \AA}^2 \leq \text{PSA} \leq 120 \text{ \AA}^2$	$75 \text{ \AA}^2 \leq \text{PSA} \leq 150 \text{ \AA}^2$

a: Lipinski proposed that drug-like compounds generally complied with at least four of these criteria;
b: P is the partition coefficient between water and *n*-octanol.

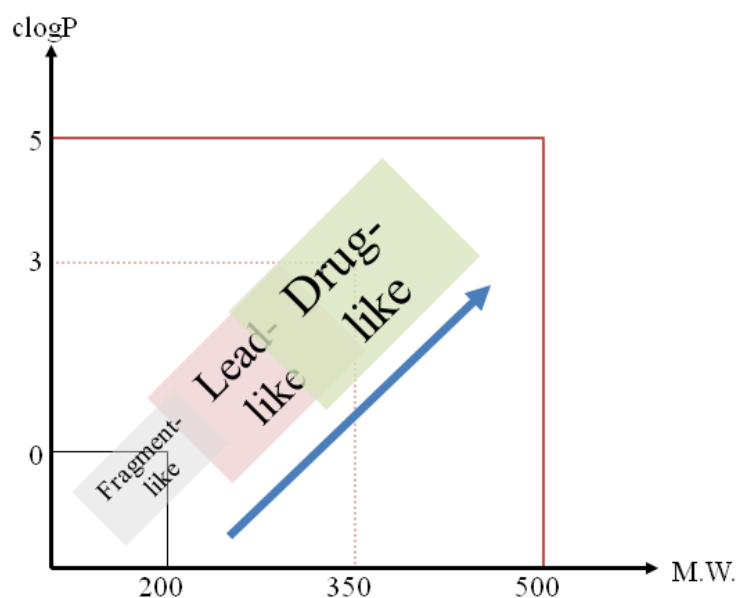


Figure 1.8. Chemical space relevant to small molecule drug discovery. The drug-like space is bounded by the Lipinski “rule of five” parameters (red line). The lead-like space is defined by the lead-like parameters (dotted line). The likely increase in lipophilicity and molecular weight as a result of optimisation is indicated by the blue arrow. Adapted from Nadin *et al.*⁷⁸.

1.2.2 HTS and vHTS as techniques towards the discovery of new biologically active small molecules

1.2.2.1 Summary of the discovery process

There are a number of steps⁸¹ required for the identification of new compounds with biological activity. A typical campaign would start by the selection of a target (HTS: protein, whole cell, virus; vHTS: protein with structural data available). The next step of the discovery process would be the identification of “hits” followed by the optimisation of validated “hits” using iterative rounds of synthesis and testing. As a final step of the discovery process, it is crucial to determine the mode of action of the optimised compound (*e.g.* knowing if it targets a specific protein or finding out at which stage of the virus life cycle the compound is active). The discovery process for the identification and optimisation of many new biologically active small molecules is represented in Figure 1.9.

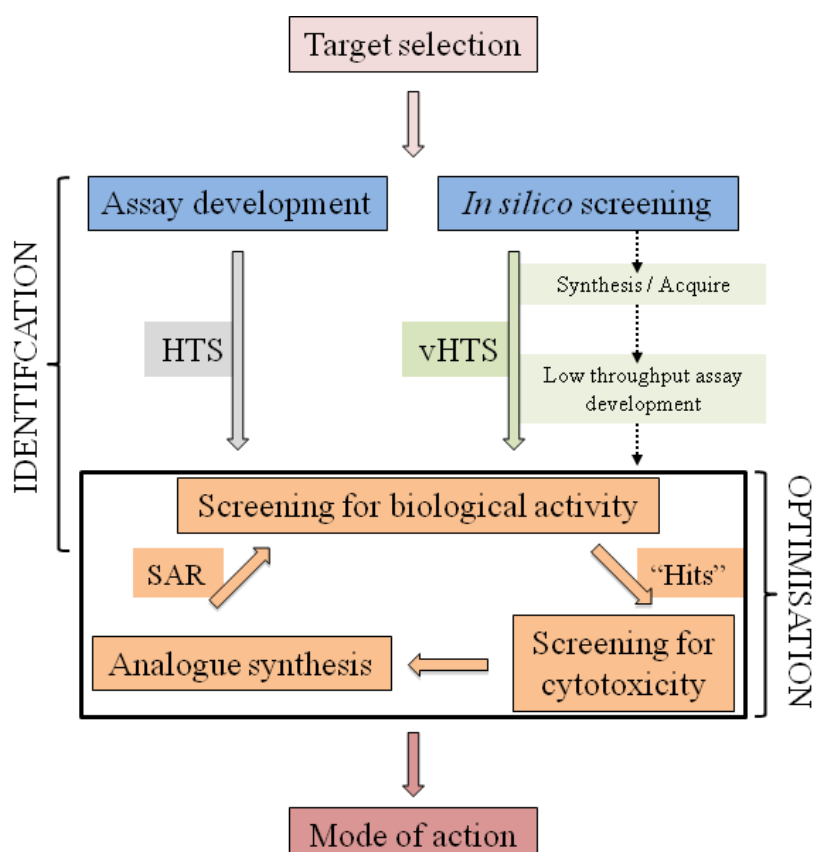


Figure 1.9. Step-wise discovery of new biologically active small molecules with activity against a chosen target. Once a target has been selected, HTS and vHTS “hits” are identified after screening for biological activity. Only the non-cytotoxic hits will undergo optimisation through analogue synthesis and the study of structure-activity relationships (SARs). The final step is the determination of the mode of action of the optimised hit(s).

1.2.2.2 High-throughput screening

In HTS, in order to screen large compound collections[†] against the chosen target, it is critical to use a robust screening assay. If the target is novel, the development of a new screening assay, according to robust statistical parameters, might be required. Inglese *et al.*⁸²⁻⁸⁴ have summarised which statistical parameters are important for the validation of an assay performed at a single concentration based on the results of both the internal positive and negative controls. A description of the statistics parameters that need to be considered is available in Appendix 1. Once “hits” have been identified, they must be validated (cytotoxic and secondary screening). The screening of large compound collections has the disadvantage of generating false positives and false negatives^{76,82}. In order to circumvent these two issues, the use of quantitative HTS, in which each compound is screened at a range of concentrations, has been reported⁸⁵.

1.2.2.3 Virtual high-throughput screening

In vHTS, an approach that relies on the availability of structural data (X-ray or NMR), the selection of the protein model that will form the basis of the *in silico* screening is important for the outcome of the campaign. Several parameters may influence the choice of the protein model for vHTS: single (X-ray crystallography) or multiple conformations (NMR spectroscopy), resolution with respect to side chain positioning, ionisation state of the residues, selection of the binding region, presence of tightly bound solvent molecules, flexibility. In order to screen compound collections[‡] against the chosen target, it is critical to have an *in silico* screening program available. Once the *in silico* screening process has been carried out, virtual “hits” may usually be purchased or synthesised in order to validate the predicted activity and verify that the hit is not cytotoxic.

[†] For HTS, compounds from a compound collection are compounds that are either commercially available or proprietary.

[‡] For vHTS, compounds from a compound collection are compounds that could be acquired from a commercial supplier (virtual library of commercially available compounds) or that could be prepared in the laboratory (virtual library of synthetically accessible compounds).

1.2.2.4 HTS and vHTS as complementary approaches.

There are some literature reports where both HTS and vHTS have been used in parallel to aid the identification of novel scaffolds against a chosen biological target. Shoichet *et al.*⁸⁶ used HTS and vHTS in parallel to target the tyrosine phosphatase-1B protein. Using HTS, they screened a proprietary library of 400,000 compounds and found 85 hits (hit-rate of 0.021%). Using vHTS, they screened a virtual library of 235,000 commercially available compounds and found 365 virtual hits. Upon biological testing, they could confirm 127 hits (hit-rate of 34.8% compared to the 365 virtual hits or 0.05% compared to the full library). In another experiment, Paiva *et al.*⁸⁷ screened a Merck proprietary collection against dihydrodipicolinate reductase using HTS (hit-rate < 0.2%) and vHTS (hit-rate *ca.* 6% for a diverse subset of the full collection after biological testing of the virtual hits). From these two studies, it seems that the hit-rate is higher for vHTS^{87,88} for those compounds that are actually assayed, circumventing the need for a high-throughput assay. It is also thought that when structural data is available vHTS could be used to identify common scaffolds predicted to be active (vHTS of small subsets of the full collection) that would then be screened using HTS methods⁸⁹, making the two methods complementary.

1.3 hRSV therapies: from proof-of-concept to clinical trials

There are no vaccines or potent small molecule anti-virals currently available for hRSV for use in the clinic. The effects of supportive treatments (*e.g.* bronchodilator, steroids) remain marginal or controversial⁹⁰. However, for children in hospitals, the preferred treatment remains the use of oxygen in order to prevent death^{90,91}.

Neither live attenuated vaccine, nor subunit vaccine has been reported to be effective in preventing hRSV⁹². Rather, the opposite effects are observed: ‘immunopotential’ and vaccine-enhanced disease^{91,93,94}. Two vaccines developed by MedImmune are currently in Phase I/II clinical trials⁹⁵.

1.3.1 Overview of the therapies available to tackle hRSV

A wide variety of small-molecule anti-virals have been developed against hRSV (Table 1.2 and Figures 1.10 and 1.11). They can be classified in three categories depending on their target: broad-spectrum *i.e.* active against non-viral proteins (Table 1.2, entries 1 to 3 and Figure 1.10), replication inhibitors (Table 1.2, entries 4 to 9 and Figure 1.10) and entry inhibitors (Table 1.2, entries 10 to 19 and Figure 1.11). An additional point of comparison has been added to describe the chemical genetics approach that was used to discover the compounds⁹⁶. Some small molecules were identified on the basis of their phenotype (forward chemical genetics approach), and other molecules were discovered on the basis of activity against a specific viral protein (reverse chemical genetics approach).

The discussion of the small molecules and biologics presented in Table 1.2 and Figures 1.10 and 1.11 will start with the presentation of the treatments that have been approved by the FDA for use against hRSV. The discussion will continue with the presentation of the small molecule anti-virals that have been identified in phenotypic assays and will end with the presentation of the biologics developed against hRSV.

Table 1.2: Summary of the target, activity, clinical trials status and chemical genetics approach for known anti-hRSV agents.

Entry	Active agent	Target	Activity ^a	Clinical trial	Chemical genetics
1	Ribavirin (Virazole®)	N/A	- ^b	Approved ⁹⁷	N/A ^e
2	1	DHODH ^c	EC ₅₀ = 7 nM ⁹⁸	N/A	N/A ^e
3	2	CADp ^d	EC ₅₀ = 86 nM ⁹⁸	N/A	N/A ^e
4	RSV604	N	EC ₅₀ = 500 nM ⁹⁹	PII	Forward
5	ALN-RSV01	N	IC ₅₀ = 0.7 nM ¹⁰⁰	PII	N/A ^e
6	P siRNA	P	IC ₅₀ = 18 nM ⁹³	N/A	N/A ^e
7	3	M2-1	Putative ⁹⁴	N/A	Reverse
8	Amantadine	SH	Putative ¹⁰¹	N/A	Reverse
9	YM-53404	L	EC ₅₀ = 200 nM ¹⁰²	N/A	Forward
10	T-118	F	EC ₅₀ = 51 nM ¹⁰³	N/A	N/A ^e
11	Constrained peptide	F	IC ₅₀ = 36 nM ¹⁰⁴	N/A	N/A ^e
12	Palivizumab (Synagis®)	F	K _d = 2.6 nM ¹⁰⁵	Approved ⁹⁷	N/A ^e
13	Motavizumab	F	K _d = 34.9 pM ¹⁰⁵	Rejected ¹⁰⁶	N/A ^e
14	JNJ-2408068	F	EC ₅₀ = 0.16 nM ¹⁰⁷	N/A	Forward
15	TMC353121	F	EC ₅₀ = 0.13 nM ¹⁰⁸	Pre-clinical evaluation	Forward
16	4	F	IC ₅₀ = 0.11 μM ¹⁰⁹	N/A	Forward
17	5	F	IC ₅₀ = 0.13 μM ¹⁰⁹	N/A	Forward
18	VP-14637	F	EC ₅₀ = 1.4 nM ¹¹⁰	Discontinued	Forward
19	BMS-433771	F	EC ₅₀ = 20 nM ¹¹¹	Discontinued	Forward

a: EC₅₀ / IC₅₀: 50% effective (or inhibitory) concentration. The data was reported as it was found in the literature. For virus inhibition, no distinction should be made between the EC₅₀ and IC₅₀; b: see Section 2.3.6.2, c: DHODH = dihydroorotate dehydrogenase; d: CAD carbamoyl-phosphate synthetase 2, aspartate transcarbamylase, and dihydroorotase; e: no chemical genetics data for biologics; f: SAR = structure-activity relationship.

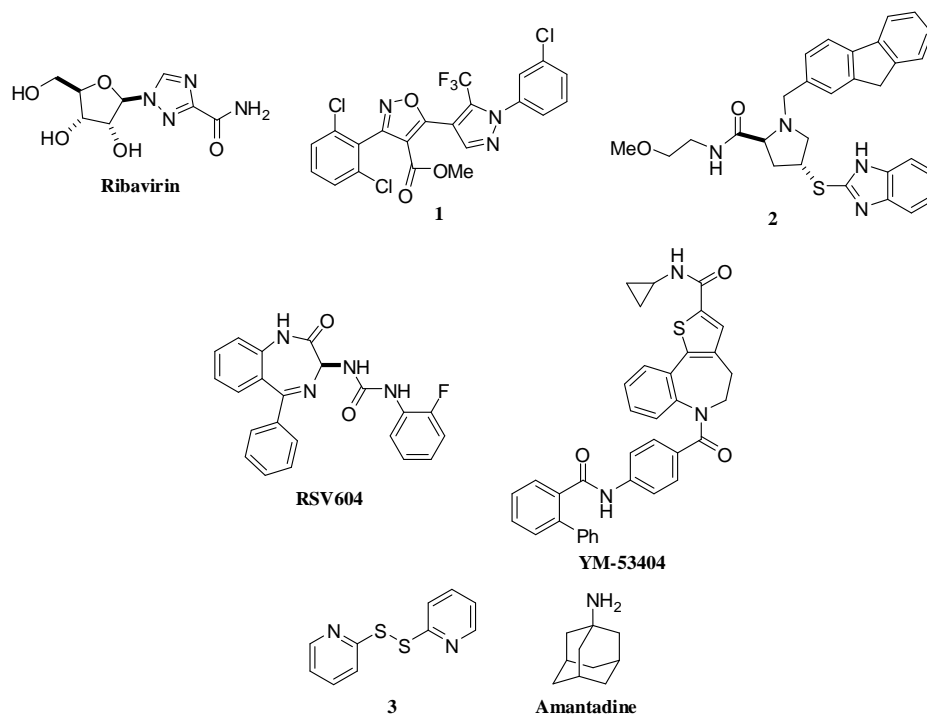


Figure 1.10. Small molecule anti-virals or inhibitors. Ribavirin, **1** and **2** are broad-spectrum anti-virals. RSV604 targets the N protein, YM-53404 targets the L protein, **3** and amantadine are putative inhibitors of the M2-1 and SH proteins, respectively. Biologics are not shown.

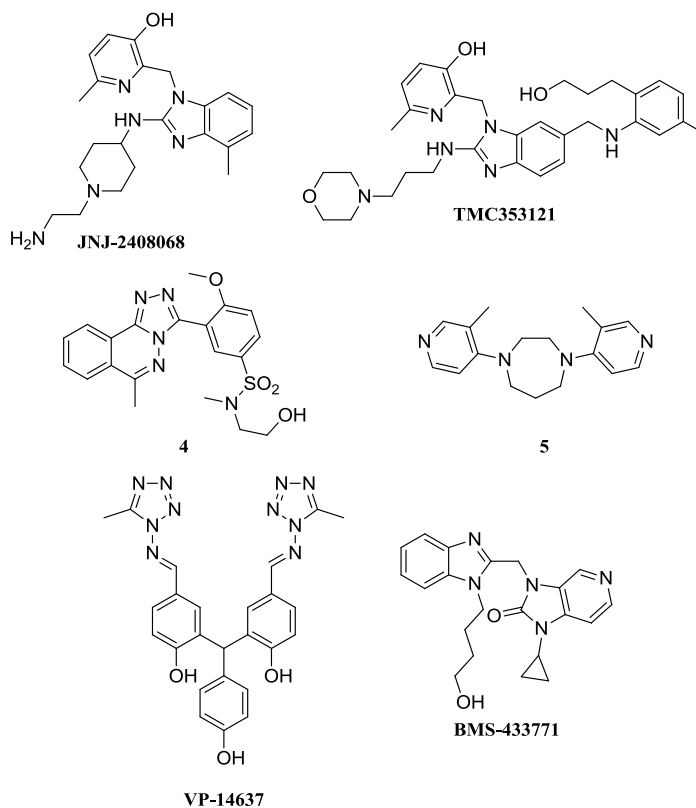


Figure 1.11. Small molecule inhibitors of the hRSV fusion protein. Biologics are not shown.

1.3.2 FDA-approved therapies

The treatments currently approved by the US Food and Drug Administration⁹⁷ are ribavirin (Table 1.2, entry 1) and palivizumab (Table 1.2, entry 12). Ribavirin (developed by Valeant) is a purine analogue whose mode of action is not well-defined¹¹². It is a broad-spectrum anti-viral with susceptibility varying between different cell lines¹¹². Additionally, it is not very efficient¹¹³ and it is a suspected teratogenic^{10,91}. Palivizumab (developed by MedImmune) is a humanised monoclonal antibody which targets the F protein^{10,91,114}. The next generation of humanised antibody (Motavizumab) has been discontinued by AstraZeneca / MedImmune at the end of 2010 after reaching phase III clinical trials¹⁰⁶.

1.3.3 High-throughput screening to discover new small molecules anti-virals

1.3.3.1 Small molecules identified in phenotypic assays

High-throughput screening has given rise to a variety of small-molecule inhibitors targeting either a host protein (broad-spectrum) or a viral protein. Recently, the discovery of two new small molecule inhibitors (from a commercially available screening collection by ChemBioNet) of the F protein has been reported by Lundin *et al.*¹⁰⁹ (Table 1.2, entries 16 and 17). After screening a National Institute of Health-wide screening collection, Bonavia *et al.* have reported the discovery of two new classes of compounds: the isoxazole-pyrazole **1** (Table 1.2, entry 2) and the proline derivative **2** (Table 1.2, entry 3). Both ligands targeted *de novo* pyrimidine biosynthesis pathways and showed nanomolar activity against different hRSV strains as well as HCV or HIV⁹⁸. The isoxazole-pyrazole compound **1** targeted dihydroorotate dehydrogenase⁹⁸ (DHODH) and the proline derivative **2** targeted carbamoyl-phosphate synthetase 2, aspartate transcarbamylase, and dihydroorotase⁹⁸ (also known as the CAD polypeptide). Both ligands displayed cytotoxicity in highly proliferating T and B lymphoid-derived cells which require more production of pyrimidine for proliferation¹¹⁵. The authors hypothesised that targeting cellular proteins / processes that have direct interactions with a viral protein might lead to less toxicity. VP-14367¹¹⁰ (Table 1.2, entry 18) and BMS-433771¹¹¹ (Table 1.2, entry 19), both F protein inhibitors, have been discontinued

because resistant strains arose rapidly in the laboratory⁹⁷. No data is currently available on the status of the polymerase inhibitor YM-53404 (Table 1.2, entry 9) developed by Sudo *et al.*¹⁰².

1.3.3.2 Small molecules optimised using a medicinal chemistry approach

TMC353121 (Table 1.2, entry 15), developed by Johnson & Johnson, is currently undergoing pre-clinical evaluations with Tibotec. TMC353121 targets the F protein^{108,116} and antiviral activity was observed in a mouse model¹¹⁷, as a prophylactic agent or even at 48 h post-infection¹¹⁸. TMC353121 was discovered following the optimisation of the pharmacokinetic properties¹¹⁹ (long tissue retention time) and activity¹⁰⁸ of JNJ-2408068¹⁰⁷ (Table 1.2, entry 14 and Figure 1.12.A) through iterative rounds of synthesis and assaying. JNJ-2408068 was the first such small molecule inhibitor reported in the literature¹⁰⁷. It was discovered by looking at the structure-activity relationships (SARs) of a lead (not disclosed in the literature). In dog, monkey and rat, JNJ-2408068 had long tissue retention times, which was addressed by another round of SARs which gave rise to **6** (Figure 1.12.A) with a loss of activity¹¹⁹. A final round of SARs coupled to molecular modelling gave rise to TMC353121¹⁰⁸ (Figure 1.12.A).

TMC353121 was successfully co-crystallised with the 6-helix bundle (1.5 Å) (Figure 1.12.B). Its mode of action was proposed to be through the stabilisation of a non-productive 6-helix bundle, rather than through the prevention of the formation of the 6-helix bundle. Both heptad repeats domains are required for TMC353121 binding to occur. TMC353121 makes key non-covalent interactions with the F protein (Figure 1.12.C). TMC353121 is involved in hydrogen-bond interactions between its OH group and pyridine ring and E487 (HR-C) through a water bridge, and in π - π stacking interactions between its pyridine ring and Y198 (HR-N) and F488 (HR-C). Mutations were observed in the F gene after exposure to the compound at *ca.* 1000 \times EC₅₀ for three passages¹⁰⁷ and were mapped in the 486-489^{108,116} region of HR-C (*e.g.* D486N) as well as in the globular domain¹¹⁶ (S398L, K394R). Mutations in the globular domains have been linked with effects on the fusion kinetics⁶⁴.

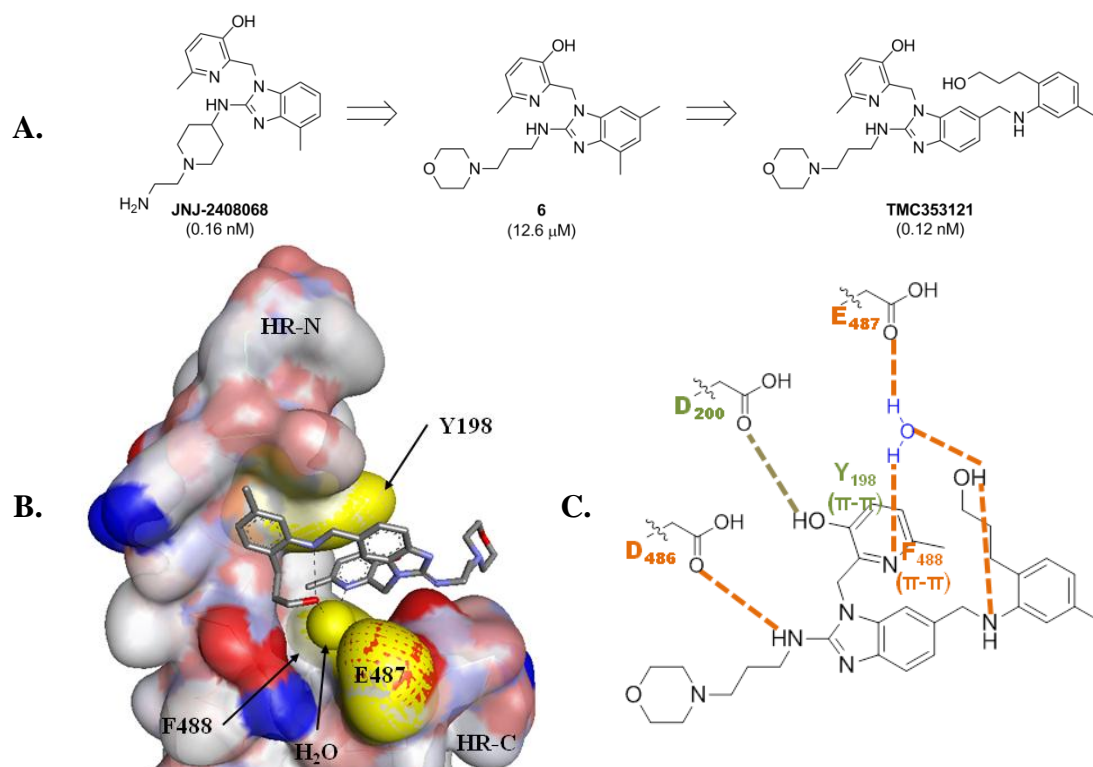


Figure 1.12 TMC353121, inhibitor of hRSV fusion protein. **A.** TMC353121 is the product of iterative rounds of synthesis and assaying from JNJ-2408068. EC_{50} values for anti-viral activity in a cell-based assay are given between brackets. **B.** The X-ray crystal structure of TMC353121 within its protein target (PDB accession number 3KPE, 1.5 Å) reveals key non-covalent interactions. Picture generated with Discovery Studio (Accelrys). **C.** 2D representation of the key non-covalent interactions TMC353121 makes with its protein target. The amino acids involved in non-covalent interactions have been coloured following the colour Scheme previously used: green for HR-N and orange for HR-C.

As can be seen from the discovery of TMC353121, the compounds to be taken forward for clinical trials are often quite different from the primary hits. In this case, the active core remained unchanged but appendages may be modified in order to determine structure-activity relationships and to optimise the compounds properties (*e.g.* physico-chemical, metabolism or bioavailability). This process is done by designing focused libraries which are libraries of compounds around active hits¹²⁰ and a chemical approach is used for the systematic variation of the initial active compounds.

1.3.3.3 Small molecule undergoing clinical trials

RSV604 (Table 1.2, entry 4), developed by Arrow Therapeutics (now AstraZeneca), is the most advanced small-molecule inhibitor project: it has passed phase II clinical trials. It was discovered from a high-throughput screen of an in-house library identifying a lead that was optimised through iterative rounds of synthesis and assaying. It targets the N protein⁹⁹ and inhibition was observed in a human airway epithelial model²³, even at 24 h post-infection. The exposure of the virus to increasing concentrations of RSV604 allowed the isolation of resistant strains after eight passages⁹⁹. Sequencing revealed that resistance arose at the proposed N-polymerase binding site⁵⁴ giving rise to the mutations N105D, K107N, I129L and L139I⁹⁹. Although RSV604 has not been co-crystallised with its protein target⁵⁴, the availability of the decameric N-RNA complex structure could suggest a proposed binding site for RSV604 (Figure 1.14). According to the protein structure, the N-RNA interaction is likely to be unaffected by RSV604.

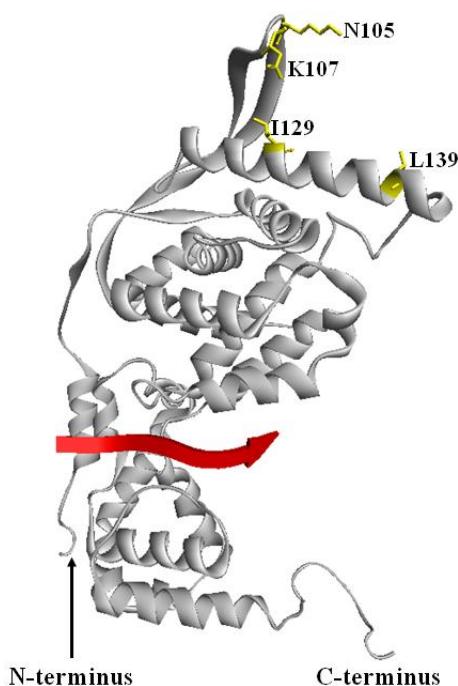


Figure 1.14. Mutations arising from exposure to RSV604. The four residues (Asn105, Lys107, Ile129, Leu139, shown in yellow and stick representation) that have been observed in RSV604 resistant strains have been located at a proposed interaction site between the N-RNA complex and the polymerase. RNA is shown in red. Adapted from Tawar *et al.*⁵⁴. Picture generated with Discovery Studio (Accelrys).

1.3.4 *The use of biologics to tackle hRSV*

A variety of biologics have been discovered with activity against hRSV. As reported in Section 1.1.6.4, both hRSV F protein and HIV-1 gp41 proteins are class I fusion proteins. For HIV-1, a 36-amino-acid synthetic peptide (T-20, derived from the HR-C of gp41) has been developed^{121,122}. A similar approach was used against hRSV, which led to the discovery of T-118 (Table 1.2, entry 10), a 35-amino-acid synthetic peptide corresponding to the HR-C of hRSV¹⁰³. Such peptides are proposed to bind to the hydrophobic groove formed by two adjacent HR-N peptides, preventing the conformational rearrangement leading to the 6-helix bundle formation¹²¹. Later, Shepherd *et al.* developed a 13-amino-acid constrained peptide (Table 1.2, entry 11) based on the HR-C of hRSV¹⁰⁴. Proof-of-concept studies have led to the discovery of double-stranded small interfering RNA (siRNA) targeting the N protein¹⁰⁰ (Table 1.2, entry 5) and the P protein⁹³ (Table 1.2, entry 6). Only the siRNA targeting the N protein (named ALN-RSV01 and developed by Alnylam Pharmaceuticals) has been taken into Phase II clinical trials¹²³.

1.3.5 *Conclusions and future perspectives*

ALN-RSV01, RSV-604 and TMC353121 are the only anti-viral projects known to be undergoing clinical trials. The work by Bonavia *et al.*⁹⁸ set methods for the discovery of new small molecules bioactives, while more mode of action studies are required for the work presented by Lundin *et al.*¹⁰⁹. Additional small molecules have also been proposed as putative hRSV inhibitors. The classification of the SH protein as a viroporin suggests it may be targeted in the same way the hepatitis C virus p7 protein, using viroporin inhibitors such as amantadine¹⁰¹ (Table 1.2, entry 8). M2-1 contains a zinc-finger motif and dithiodipyridine **3** (Table 1.2, entry 7) has shown zinc-finger motif activity in retroviruses⁹⁴.

There are a few explanations for the failure of hRSV treatments to date^{91,93}: hRSV is prone to the development of mutations as its RNA replication occurs without polymerase proofreading; cellular proteins found in purified hRSV virions and the intricacy of hRSV make the development of vaccine difficult; the discovery of palivizumab has resulted in a decrease of the research effort throughout the world leaving the field without a potent small molecule antiviral or a vaccine. The patent for palivizumab is set to expire in 2015 but there are doubts whether or not this will make it affordable for the developing world. The earliest expectations for the availability of an anti-viral is 2015 and for a vaccine is 2020⁹⁵.

1.4 Project outline

The project described herein was concerned with the use of complementary approaches to drug discovery, namely high-throughput screening and structure-based drug design, in order to discover new small molecule modulators of human respiratory syncytial virus.

Chapter 2 describes the development and optimisation of a phenotypic cell-based assay that satisfies recognised statistical parameters, for the identification of small molecules with anti-viral activity against hRSV. The use of fluorescence for the detection of virus inside cells conferred novelty to this assay. Additionally, it allowed for a quicker detection of anti-viral activity.

Chapter 3 describes the use of structure-based drug design (virtual high-throughput screening) in order to identify potential inhibitors to the fusion protein of hRSV. A novel approach, using virtual libraries based on synthetically accessible compounds has been used. A virtual library of commercially available compounds was also used. Chapter 4 describes the preparation of the potential inhibitors discovered in Chapter 3.

Chapter 5 describes the biological evaluation of proprietary compounds, using the robust screening assay reported in Chapter 2. The compounds prepared in Chapter 4 or identified from a commercial library and reported in Chapter 3 have also been evaluated for anti-viral activity against hRSV.

2 DEVELOPMENT OF A HIGH-THROUGHPUT SCREENING ASSAY

This Chapter describes the development of a novel high-throughput screening assay for the detection of anti-viral activity against hRSV. The selection of the detection method is outlined in Section 2.2; the optimisation of the assay for the internal negative control and the internal positive control is discussed in Section 2.3.

2.1 Introduction

2.1.1 *Virus-induced cytopathic effects*

The detection of anti-viral activity against hRSV has been achieved using HTS looking at the decrease in the display of virus-induced cytopathic effects (*e.g.* virus-induced cytotoxicity^{99,107,124} or virus-induced plaque formation^{102,125-127}). In the case of the discovery of RSV604⁹⁹ and JNJ-2408068¹⁰⁷ anti-viral activity was defined as a decrease of the virus-induced cytotoxicity over the course of four to seven days^{99,107}, using serial dilutions of compounds. However, the assays differed in the agent used for the evaluation of cell viability (XTT for RSV604, and MTT for JNJ-2408068). Mock- and virus-infected controls were also run. In living cells, tetrazolium salts such as MTT¹²⁸ (3-(4,5-dimethylthiazol-2-yl)-2,5-diphenyl tetrazolium bromide) or XTT¹²⁹ (2,3-bis[2-methoxy-4-nitro-5-sulfophenyl]-2H-tetrazolium-5-carboxyanilide, inner salt) are reduced to the corresponding formazan by mitochondria hydrogenase (Figure 2.1).

Rasmussen *et al.*¹²⁴ have commented on the instability of virus stocks and have proposed a small modification to the detection of hRSV cytopathic effects. They used frozen-infected cells and reported a coefficient of variation of 4% over a ten month period for the tissue culture infectious dose 50%. Cell viability was evaluated using a luminescent-based detection¹³⁰.

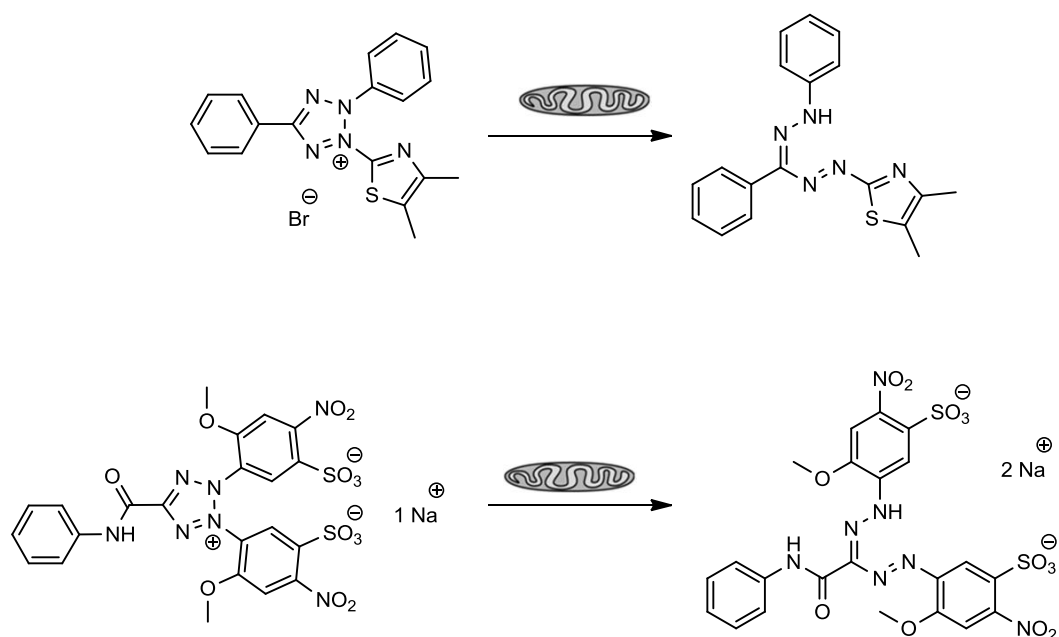


Figure 2.1. Non-radioactive cytotoxicity assay. Top: MTT assay, bottom: XTT assay. Absorbance at 450 nm (XTT) or 570 nm (MTT) is measured to calculate cell viability. An extra solubilisation step with DMSO is required for the MTT assay.

An alternative to the detection of virus-induced cytotoxicity is to look at virus-induced plaque formation. The discovery of YM-53403¹⁰² was done using a plaque reduction assay carried out three days post-infection in which the plaques were stained. Cannon¹²⁵ has reported a rapid (24 or 48 h) microplaque assay based on the detection of plaque using indirect antibody detection of hRSV and relying on the enzymatic activity of enzymes such as horseradish peroxidase (HRP). However, the use of microplaque assays has not been reported in an anti-viral screening assay.

2.1.2 Determination of the mode of action

In a phenotypic cell-based assay, the specific protein target is unknown. Therefore, it is crucial to determine the mode of action of a novel small molecule with anti-viral activity against hRSV. This can be done by isolating and characterising compound-resistant viruses. The development of drug resistance can be assayed through serial passages¹³¹ in the chosen cell line using increasing concentration (*e.g.* from EC₅₀) of the inhibitor. The resistant strain can also be used during drug-free passages to observe if resistance is maintained after drug-free passages. Using the reverse transcription polymerase chain reaction from total RNA extraction from infected cells, it can be identified if the resistance arose from a mutation in the viral genes. Such mutation(s) can be confirmed as being responsible for resistance by reverse genetics⁹⁹. The mutations would be introduced individually into the corresponding gene(s) of a plasmid expressing the viral anti-genome and the resulting recombinant virus exposed to the compounds to observe the effect on anti-viral activity.

Further understanding into the specific mode of action of a compound can be gained by carrying out time course analyses of the antiviral effect^{116,118}. The compound may also be tested against different strains of the same virus (within the A and B subgroups), and from the same family in order to demonstrate the specificity of the potential anti-viral or the general applicability of the strategy (*e.g.* broad-spectrum anti-viral).

2.1.3 Towards a robust HTS assay

In order to consider HTS as a means to discover new small molecules with anti-viral activity against hRSV, it is crucial to have a robust screening assay. The discovery of novel small molecules with anti-viral activity against hRSV relies on the reliable distinction between “hits” and inactive molecules using a HTS assay. This starts by the selection of a suitable detection method. Then it is important to establish the assay performance based on the selection of internal positive and internal negative controls, provided they can be tolerated (*e.g.* non-toxic) by the assay.

2.1.3.1 Overview of detection methods

Most high-throughput screening assays involve isolated proteins in cell-free systems⁸². Such cell-free systems have also been reported in anti-viral research with the use of liposome to find inhibitors to purified proteins of the hepatitis C virus¹⁰¹. However, when the protein target is not known, phenotypic cell-based assays are required^{99,107,132}.

Once the assay strategy has been defined, including the format (normally multi-well plates for HTS), the detection method should be chosen with respect to availability and cost of reagents, dynamic range[§], interference of compounds with the output signal and finally if it allows continuous or end-point detection^{82,133}. Typical detection methods include absorbance^{99,134}, chemiluminescence¹³⁵ and fluorescence¹³³. Absorbance and chemiluminescence both rely on the enzymatic activity of enzymes such as horseradish peroxidase (HRP) while fluorescence relies on the detection of a fluorophore such as fluorescein. Compounds activity is related to a decrease of the output signal.

The selection of the detection method chosen for the present study will be discussed in Section 2.2.

[§] The dynamic range is defined as the ratio between the highest and lowest values that can be detected.

2.1.3.2 Validation of the assay performance

A range of statistical parameters have been reported⁸²⁻⁸⁴ for the validation of an assay performed at a single concentration based on the results of both the internal positive and negative controls. They are: the coefficient of variation (assay variability)^{82,84}, signal-to-noise (signal quality) and signal-to-background (dynamic range) ratios^{82,84,136}, signal window (separation between the controls)¹³⁷, Z'-factor (assay quality¹³⁶). When possible, the assay should be run on a subset of compounds representing the whole library¹³⁶. In which case, a Z-factor^{**}, still indicative of assay quality, is calculated. In practical terms, a Z'-factor > 0.5 allows for distinction between hits and control. A visual description of the parameters described herein is given in Figure 2.2.

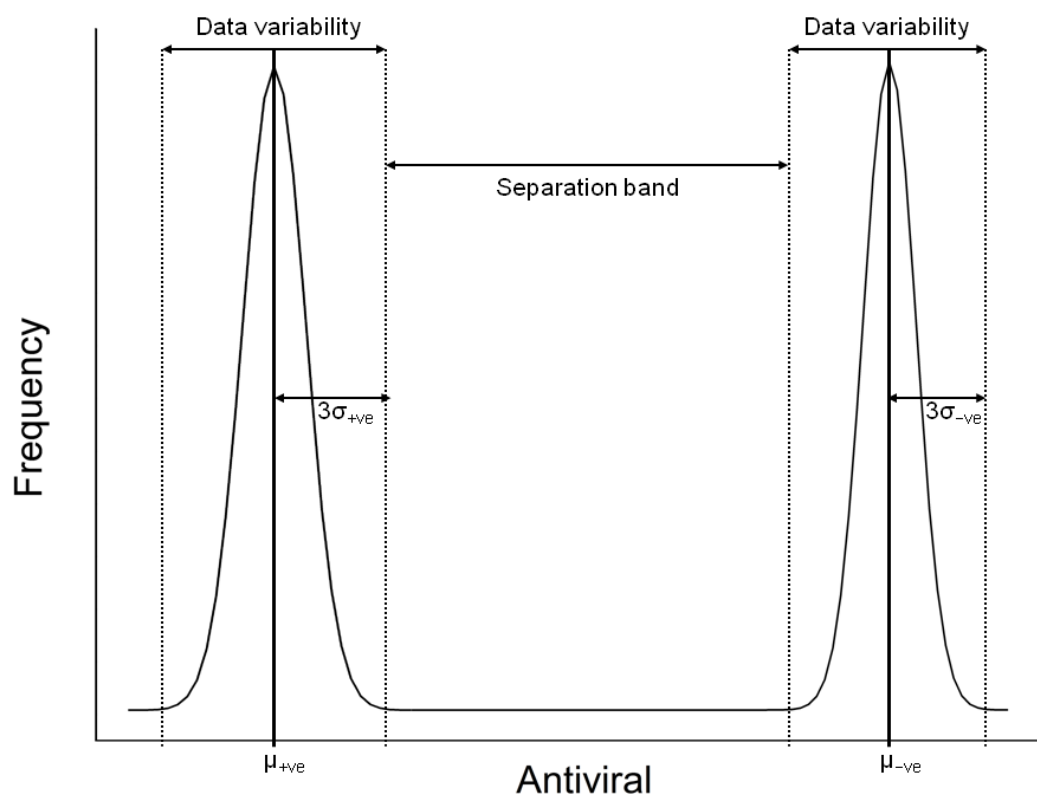


Figure 2.2. Normal distribution of the positive and negative controls. Idealised normal (Gaussian) distribution of the positive (+ve) and negative (-ve) controls. μ and σ refer to the mean and standard deviation, respectively. The data variability band corresponds to six times the mean of either sample. Adapted from Zhang *et al.*¹³⁶.

** The Z-factor is calculated for the control displaying the desired effect and the compounds tested while the Z'-factor is calculated for the positive and negative controls

2.2 Selectivity and range of antibody

In the present study, we have chosen to use antibodies to detect hRSV in human epithelial cells (HEp-2 or A549). The detection can be done directly, when the probe (HRP or fluorescence tag) is conjugated to the primary antibody, or indirectly, when the probe (HRP or fluorescence tag) is conjugated to the secondary antibody. First, we needed to make sure that the antibodies were selective for infected cells only (Section 2.2.1). Then we looked at two different detection methods: absorbance (Section 2.2.2) and fluorescence (Section 2.2.3).

2.2.1 *Western blot analysis*

The selectivity of the antibodies chosen to detect, directly or indirectly, hRSV in cells was analysed by Western blot, comparing mock- and hRSV- (A2 strain) infected samples.

2.2.1.1 Direct and indirect antibody detection

Western blot analyses of mock- and hRSV- (A2 strain) infected samples were carried out using a range of antibodies raised against hRSV. Direct antibody detection (with a goat anti-RSV polyclonal primary antibody conjugated to HRP) and indirect antibody detection (with a goat anti-RSV polyclonal primary antibody and a rabbit anti-goat polyclonal secondary antibody conjugated to HRP) were investigated (Figure 2.3).

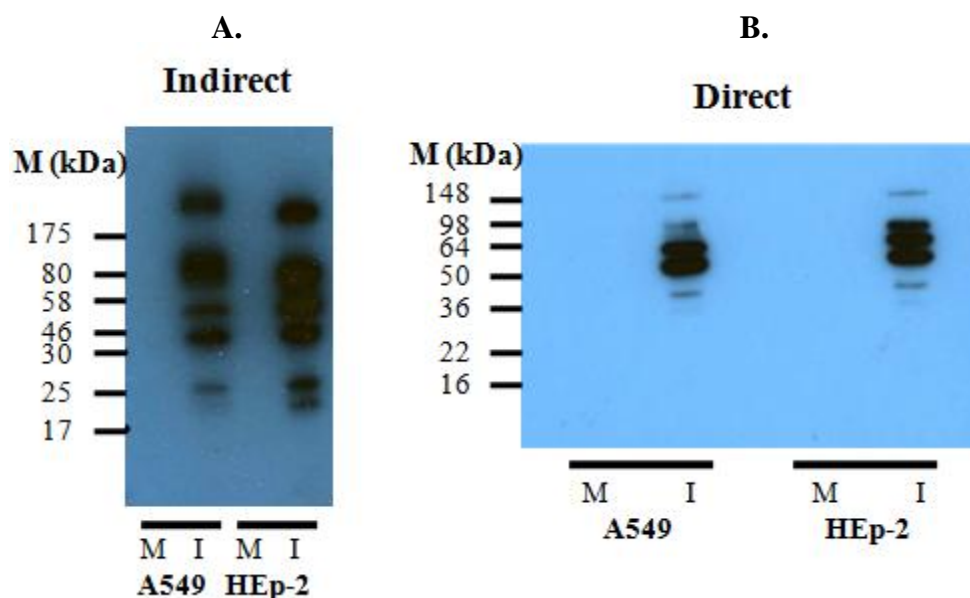


Figure 2.3. Determination of the selectivity of anti-hRSV antibodies using Western blot analyses. The indirect (A) and direct (B) detection methods were compared for mock-infected (M) and A2-infected (I) A549 and HEp-2 cell lysates. The films are slightly overexposed in order to ensure there was no background binding to the mock-infected samples. The antibodies were provided by Abcam.

According to the Western blot analyses presented above, both the indirect and direct methods could be used in an enzyme-linked immunosorbent assay (ELISA) as no background binding could be observed in the mock-infected samples. In the case of a fluorescence-based assay, both the direct and indirect detection methods were available. However, only the indirect virus detection was selected for sensitivity reasons: the FITC-conjugated secondary antibody, which is polyclonal, will amplify the signal as multiple secondary antibodies will be able to bind to the primary antibody.

2.2.1.2 Comparison of anti-RSV primary antibodies from different manufacturers

Primary antibodies raised against hRSV isolates were available from two different companies: Abcam and AbD Serotec. The Abcam antibody was *ca.* ten times more expensive than the AbD Serotec one. It was important to compare the detection quality offered by the two antibodies. Western blot analyses were carried out using both antibodies in an indirect detection setting (Figure 2.4).

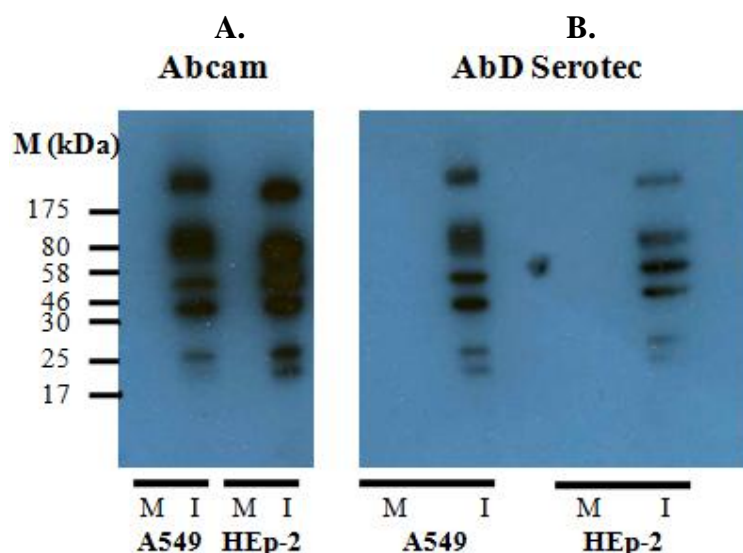


Figure 2.4. Comparison of anti-hRSV antibodies from different suppliers using Western blot analyses. The indirect detection method was tested using primary antibody manufactured by Abcam (**A**) and AbD Serotec (**B**) on mock-infected (M) and A2-infected (I) A549 and HEp-2 cell lysates. The two films have been aligned in order to match the molecular weight markers.

According to the Western blot analyses presented above, neither primary antibody gave rise to background detection in the mock-infected samples. The lower signal when the primary antibody from AbD Serotec was used is explained by the lower stock antibody concentration provided by the manufacturer (1 mg/mL as opposed to 4 mg/mL for Abcam). Also, the concentrations were not optimised for Western blot analyses as the experiment was carried out to assess the selectivity of the different antibodies.

2.2.1.3 Conclusion of the Western blot analyses

From the Western blot analyses, it was clear that all the antibodies tested were selective for the A2 strain of hRSV without any background binding detected on the mock-infected samples (all the membranes were over-exposed in the present study). The signal of lower intensity for the direct detection is probably due to the fact that there is no secondary antibody to amplify the signal, combined to the gradient in protein expression. Because these antibodies were raised against hRSV isolates, and not individual proteins, the bands were not labelled according to the molecular weights. Rather, the expected molecular weights of the eleven proteins are summarised in Table 2.1.

Table 2.1: The eleven viral proteins of hRSV and their expected molecular weights.

Protein	Molecular weight (kDa)	Protein	Molecular weight (kDa)
NS1	15.6	G	32.6
NS2	14.7	F	63.5
N	43.5	M2-1	22.2
P	27.1	M2-2	10.7
M	28.7	L	250.4
SH	7.5		

Western blot analyses revealed that both direct and indirect detection methods could be suitable for ELISA or fluorescent-based assays. The HEp-2 cell line was preferred to A549 cells due to easier tissue culture handling.

With the selectivity of a range of anti-hRSV antibodies now established, we started to analyse which detection method (absorbance or fluorescence) would be more suitable for the development of a new HTS assay for the detection of anti-viral activity against hRSV.

2.2.2 Enzyme-linked immunosorbent assay

For a direct ELISA detection, the manufacturer (Abcam) recommended using dilution ratios ranging from 1:200 to 1:1000. Unfortunately, the background for mock-infected cells was varying from medium (absorbance at 450 nm around 0.250) to high (absorbance at 450 nm around 0.7). Additionally, Canon¹²⁵ reported high background on virus-infected samples when the inocula had not been removed.

At this point, the decision was made to switch from ELISA assay to a cell-based fluorescence assay.

2.2.3 Fluorescence-based assay

2.2.3.1 Visualisation of hRSV into cells

Before any optimisation of the cell-based fluorescence assay could be done, it was important to verify that infection could be visualised in cells.

The A2 strain of hRSV was propagated in HEp-2 cells and infectivity of the stock was verified using confocal microscopy on fixed mock- and A2-infected HEp-2 cells (Figure 2.5). The comparison of mock- and A2-infected confocal images also confirmed the selectivity of the fluorescein isothiocyanate (FITC) conjugated primary antibody raised against hRSV towards infected cells.

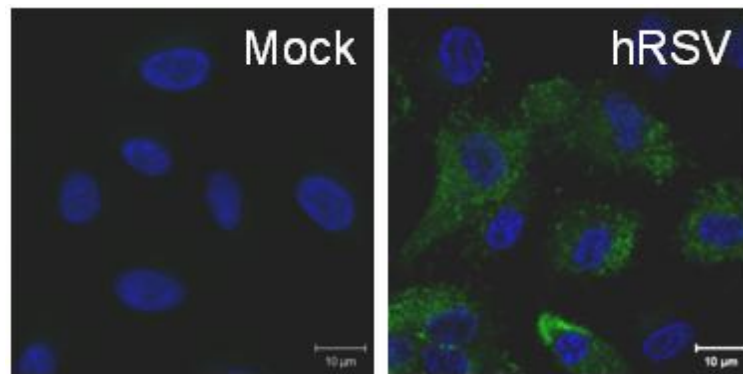


Figure 2.5. Confocal imaging of a freshly grown virus stock. Merged confocal images (63× lens) of mock- and A2-infected HEp-2 cells. The nuclei were stained with DAPI (blue) and hRSV was detected by indirect antibody detection (green). Cells were infected at a M.O.I. of 3. Scale bars are 10 µm. Images kindly provided by Diane Munday, a PhD student in the Hiscox–Barr group.

2.2.3.2 Working dilution ratios for the chosen antibodies

The working dilution ratios for the antibody manufactured by AbD Serotec were analysed in order to attain a signal-to-background ratio >2 . In the laboratory, the antibodies manufactured by Abcam would routinely be used at the following dilution ratios for confocal imaging: 1:50 (direct antibody detection) and 1:100 (indirect antibody detection). Such dilution would not have been sustainable with regards to cost management in a high-throughput screening campaign. Therefore, a range of dilution ratios were studied for the indirect detection of hRSV using the primary antibody manufactured by AbD Serotec and the secondary antibody conjugated to FITC. The results were compared to the working dilution ratios of the Abcam antibodies (primary: 1:200, secondary 1:200) and the appropriate controls (Figure 2.6).

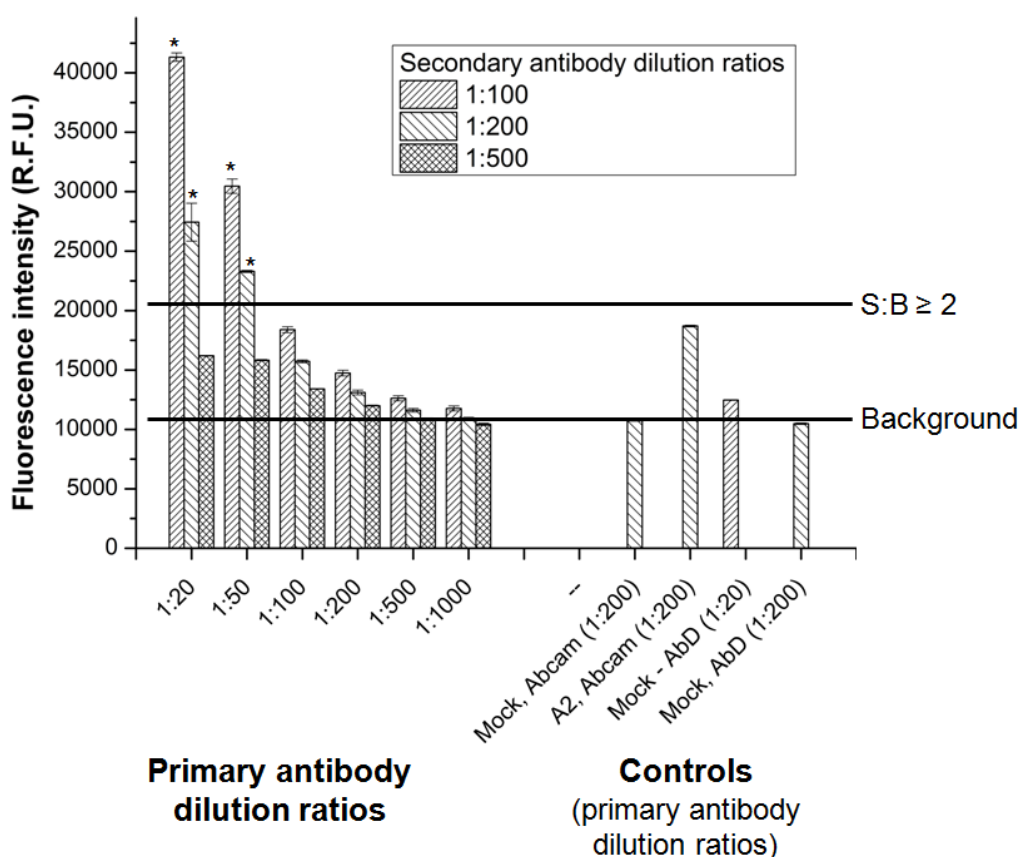


Figure 2.6 Working dilution ratios for the primary antibody manufactured by AbD Serotec. The effects of multiple dilution ratios of the primary antibody from AbD Serotec (1:20 to 1:1000) and the secondary antibody conjugated to FITC (1:100 to 1:500) on the fluorescence signal in relative fluorescence units (R.F.U.) were investigated. The results were compared to the appropriate mock- (Abcam and AbD Serotec) and A2-infected (Abcam) HEp-2 controls. The error bars refer to the standard deviation of two replicates. Dilution ratios that afforded a 2-fold signal-to-background (S:B) ratio are marked with a star (*).

According to the above bar chart, the primary/secondary antibody dilution ratios that afforded a 2-fold signal-to-background ratio (given in brackets) were: 1:20/1:100 (*ca.* 3.3), 1:20/1:200 (*ca.* 2.2), 1:50/1:100 (*ca.* 2.4), 1:50/1:200 (*ca.* 2.2). Cost-wise, the only sustainable dilution ratios would be 1:100/1:200. Under the present conditions (40 μ L and 2 hr incubation at 37 °C), the signal-to-background ratio was *ca.* 1.5. The signal-to-background ratio was increased to *ca.* 2.5 by increasing the antibody volumes from 40 μ L to 50 μ L and incubating the primary antibody overnight at 4 °C.

2.3 Optimisation of a fluorescence-based assay for hRSV growth

2.3.1 The different steps composing the assay

The library of compounds was added by a robot, which operates under non-sterile conditions. Therefore, the compounds, at the chosen assay concentration, had to be added first (25 μL), followed by the addition of cells (50 μL) and of hRSV (25 μL) 24 hrs after adding the cells. 24 hrs post-infection, the plate was worked-up and the raw results were obtained using a fluorescence plate reader. Finally, the data was processed and analysed thoroughly using suitable statistical tools (Figure 2.7).

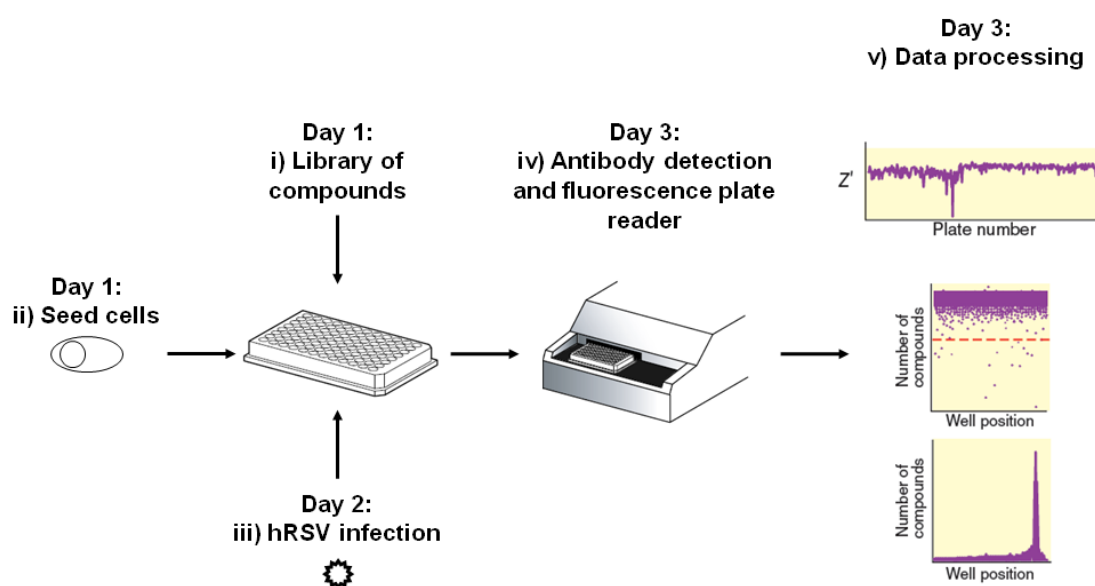


Figure 2.7. High-throughput screening assay setup. Day 1: HEp-2 cells are seeded into a 96-well plate containing compounds (columns 2 to 11) and appropriate controls (columns 1 and 12). Day 2: hRSV (A2 strain) is added to the plate. Day 3: the plate is fixed, treated with antibodies, and read on a plate reader. The data are then processed and statistical parameters are analysed. Statistics pictures are taken from Inglese *et al.*⁸³.

2.3.2 Signal variation across the plate

In a 96-well plate, reagents are added sequentially from column 1 to column 12. Therefore, it was important to investigate whether or not the fluorescence output varies across the plate in order to validate the assay. Mock-infected controls were added in column 1. Column 12 contained empty wells and was not incubated with any antibodies. The mean of the fluorescence intensity of column 10 and 11 is slightly lower than that of columns 2 to 9. However, it remains within standard error (Figure 2.8). Therefore, there is no significant signal variation across the plate. Additionally, the results show that it is easy to distinguish between infected wells and mock-infected wells.

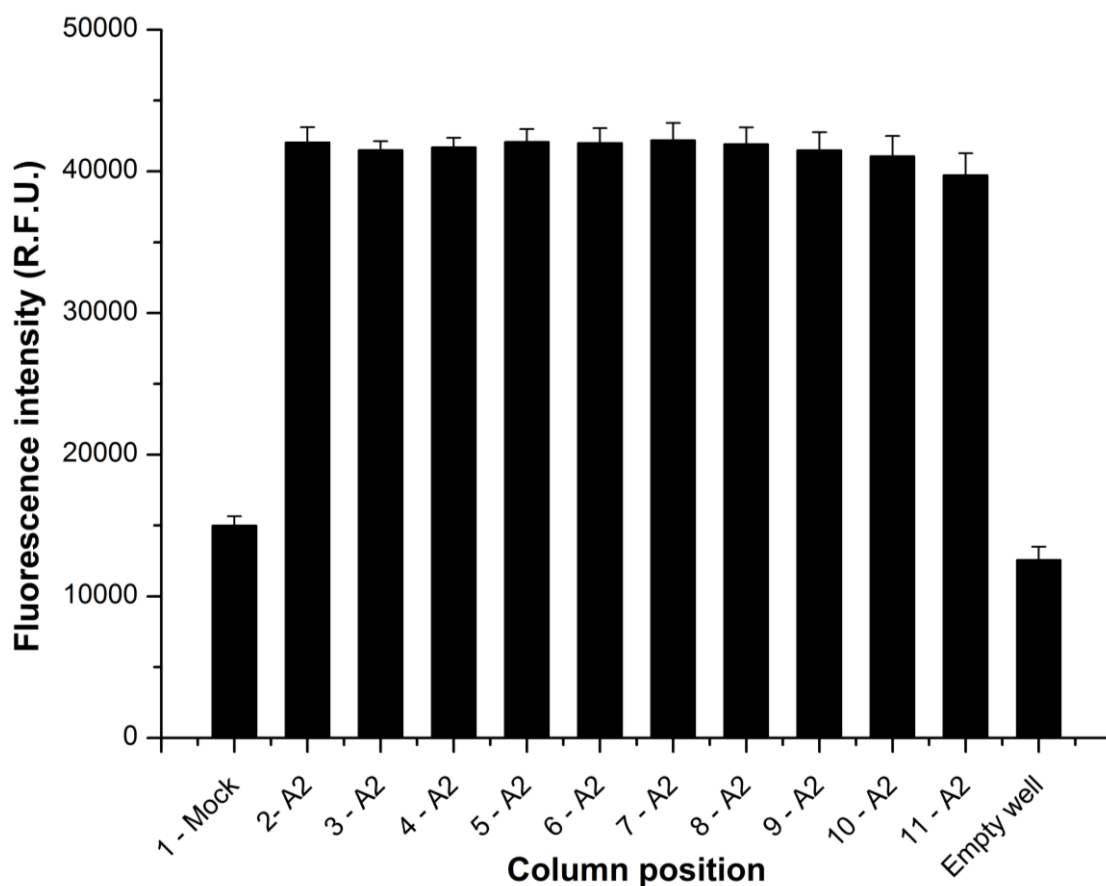


Figure 2.8 Signal variation across the plate. Mock and A2 refer to mock-infected and A2-infected HEp-2 cells, respectively. Numbers 1 to 11 refer to the column position in a 96-well plate. Mock-infected samples were in column 1, A2-infected samples were in columns 2 to 11, and column 12 was left empty. The error bars refer to the standard deviation of eight replicates.

2.3.3 Effect of the multiplicity of infection on the fluorescence signal

In order to attain an acceptable signal-to-background ratio, it was important to decide on the average number of infected particles per cell to be selected for the HTS assay. This number is given by the multiplicity of infection (M.O.I.) and we looked at whether or not the M.O.I. had an influence on the fluorescence output. For this, a total of ten different M.O.I. values, ranging from 17 to 1.7×10^{-4} , were assayed and the effect on the signal-to-background (> 2) ratios were compared (Figure 2.9). The fact that the signal increases upon dilution of the virus stock (up to a M.O.I. of 0.34) suggested that at a high M.O.I. (average of 17 virus particle per cell), the virus cytopathic effects were strong and were preventing the signal from being maximum. A lower M.O.I. (*ca.* 0.3) reduced the cytopathic effects associated with hRSV infection and the signal was maximum. In order to ensure a signal-to-background ≥ 2 and reduced viral cytopathic effects, the M.O.I. chosen for the HTS assay was between 0.5 and 1.

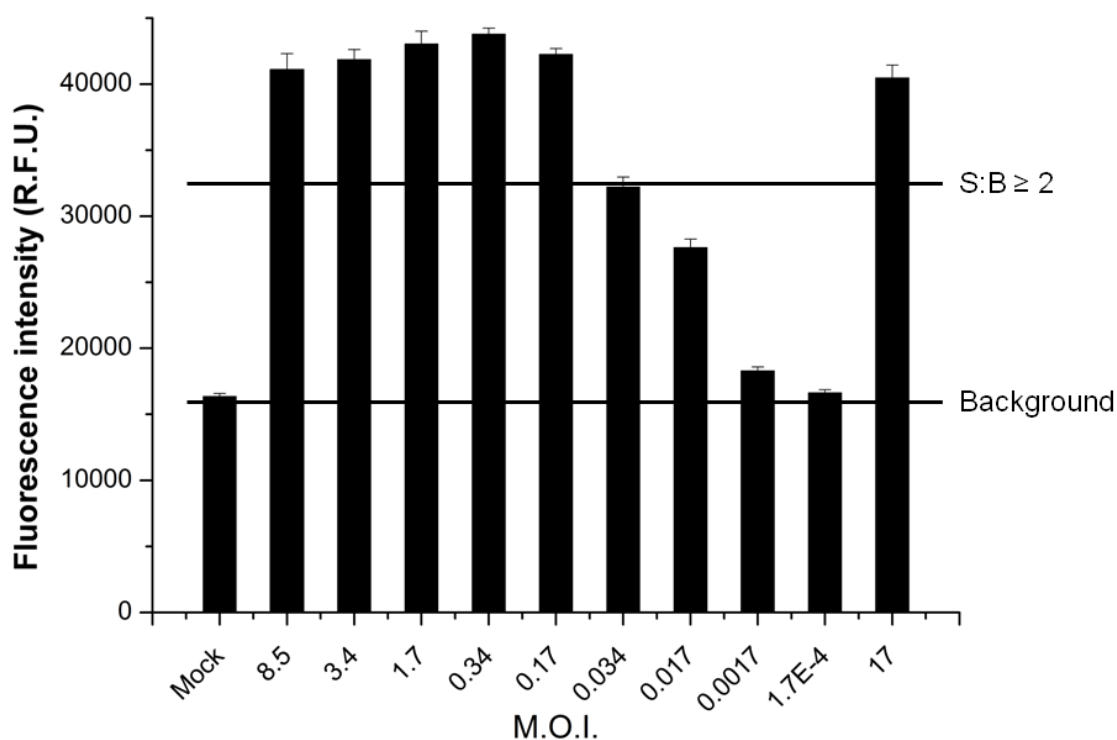


Figure 2.9. Effect of the multiplicity of infection on the normalised signal. Mock refers to mock-infected HEp-2 cells. M.O.I. values are for A2-infected HEp-2 cells and range from 17 to 1.7×10^{-4} . The serial dilution of virus added in columns. The results are expressed as the ratio to A2-infected cells at an M.O.I. of 17. S:B = signal-to-background. The error bars refer to the standard deviation of three replicates.

2.3.4 Study of the negative control (DMSO) effects

DMSO was chosen as the internal negative control for the HTS assay. In Leeds and as is common practice throughout the pharmaceutical industry¹³⁸, compounds are stored as 10 mM solution in DMSO. It was therefore important to establish the tolerance (cytotoxicity, Section 2.3.4.1 and influence on the fluorescence signal, Section 2.3.4.2) of the assay to DMSO.

2.3.4.1 Cytotoxicity of DMSO

The assay conditions (Section 2.3.1) imposed a 1:4 dilution of the DMSO concentration, meaning that the highest DMSO concentration that could be tested was 25%. A total of eight DMSO concentrations were assayed for cytotoxicity, ranging from 25% to 0.25%. The experiment was run on two different 96-well plates, each concentration in quadruplicate, on two different days and the results were combined (Figure 2.10).

Analyses of the results revealed that any concentrations above 1% DMSO had an effect on the mitochondrial dehydrogenase activity (which correlates to cell viability¹²⁸) with $\leq 40\%$ of cell viability. Over the two experiments, it appeared that only a final concentration of 0.25% DMSO afforded total cell viability.

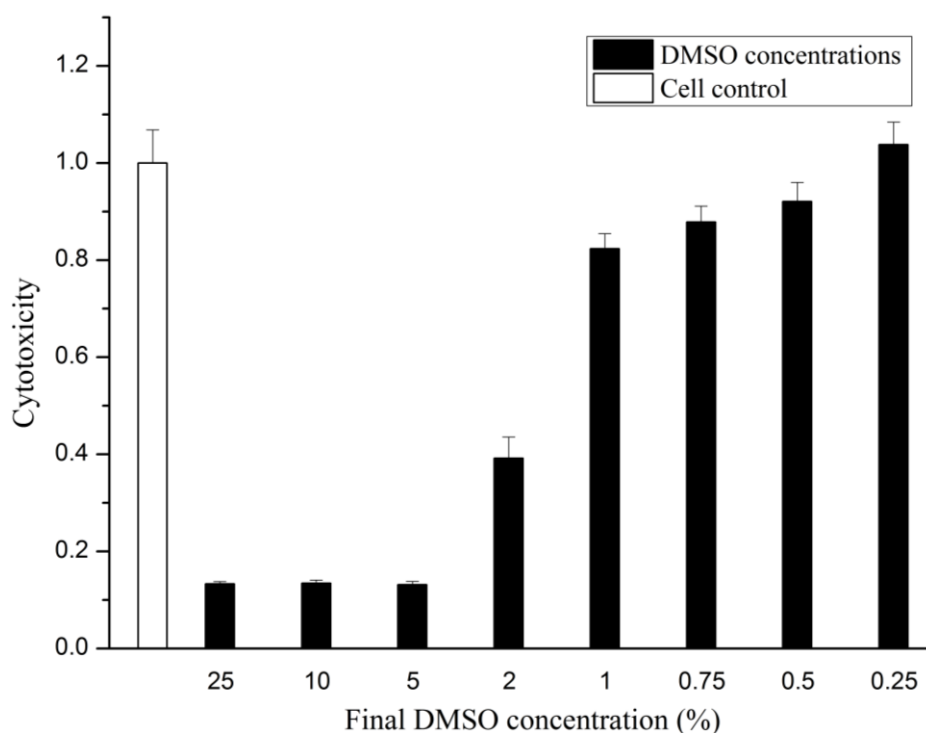


Figure 2.10. Effects of eight DMSO concentrations on cell viability. Cytotoxicity refers to the ratio of cells treated with DMSO to the cell control (*i.e.* 1.0 is not cytotoxic). Cell control refers to HEp-2 cells treated with growth media only. Absorbance was read at 570 nm. The error bars refer to the standard deviation of eight replicates (four on day 1, four on day 2).

The selection of 0.25% DMSO imposed that the maximum assay concentration for a given library compound would be 25 μ M (from a 10 mM stock in 100% DMSO). In order to validate the use of 0.25% of DMSO as the final internal negative control assay concentration, it was critical to look at the potential effects of DMSO on the fluorescence signal.

2.3.4.2 Comparison of the fluorescence signal with and without DMSO

The comparison of the fluorescence output in mock- and A2-infected HEp-2 cells treated with either media only or with a final concentration of 0.25% was carried out (Figure 2.11). This data validated the use of 0.25% of DMSO as the final internal negative control assay concentration as the differences observed between the datasets are within standard errors.

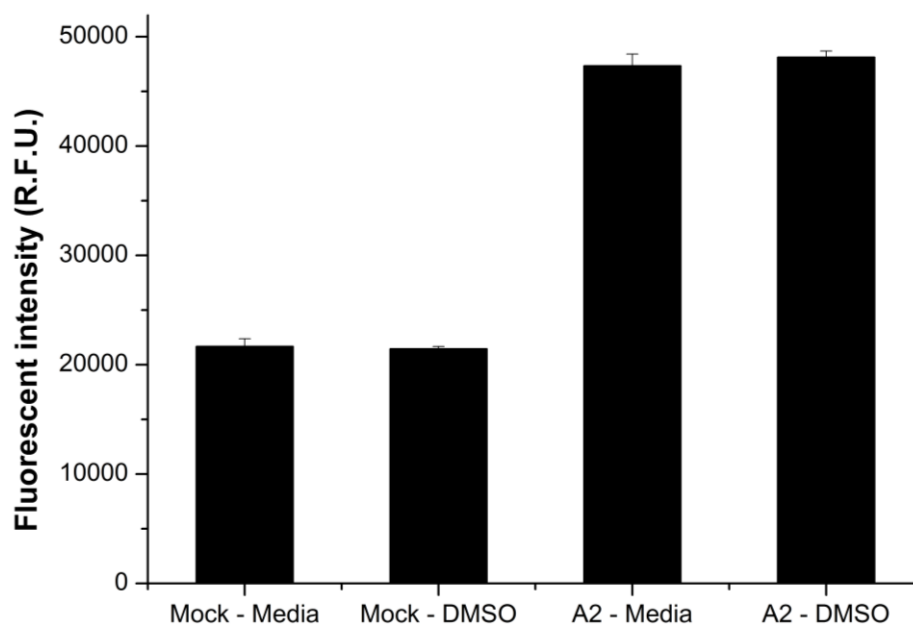


Figure 2.11 Effects of DMSO on the fluorescence output. Mock and A2 refers to mock- and A2-infected HEp-2 cells, respectively. The other two bars are the comparison of infection with the A2 strain without (media) and with 0.25% DMSO (DMSO). The error bars refer to the standard deviation of three replicates.

With the DMSO tolerance established, the assay response had to be tested with the internal positive and negative controls and attention should be paid to variability and reproducibility of the results^{82,83}.

2.3.5 *Study of the positive control (Ribavirin) effects*

Ribavirin is a known hRSV anti-viral (Section 1.3.2) and was chosen as the internal positive control for the HTS assay. Using Ribavirin, we established the robustness of the assay (Section 2.3.5.1). Because our assay conditions were different to what had previously been reported in the literature, it was crucial to estimate the EC₅₀ of Ribavirin and the 50% cytotoxic concentration (CC₅₀) under the new conditions (Section 2.3.5.2). The choice of the Ribavirin assay concentration will be discussed in Section 2.3.5.3. Finally, we looked at the influence of the M.O.I. on the EC₅₀ of Ribavirin (Section 2.3.5.4).

2.3.5.1 Establishing the robustness of the assay (between and within plates)

In order to assess the variability within and between plates, on three different days and at different cell passages, five plates were seeded (two on day 1, two on day 2 and one on day 3). A total of sixteen different Ribavirin concentrations, ranging from 2.5 mM to 10 nM, were assayed in a single 96-well plate with each concentration being assayed in triplicate (see Section 7.1 for the layout of the 96-well plate).

The following statistical parameters (Section 2.1.4 and Appendix 1) were looked at i) the coefficient of variation for each set of controls and Ribavirin dilutions, ii) the signal window, and iii) the Z'-factor.

As can be seen in Appendix 9^{††}, displaying the normalised values of each plate (labelled 1 to 5), the coefficient of variation (< 20% or < $\sigma_{\max \text{ signal}}$ when > 20%), the signal window (> 2) and the Z'-factor (> 0.5) criteria were all satisfied. Additionally, the remainder of the statistical parameters presented in Appendix 9 were also satisfied: signal-to-noise ratio (strong signal), signal-to-background (> 2). The intra-plate variability was therefore minimal, while the signal strength, the dynamic range and the separation between the controls were optimal.

^{††} Curve fitting for each plate is shown in Appendices 2 – 6.

There were two ways of looking at the variability between plates: either by combining the normalised values obtained in each plate and determine whether or not the statistical parameters were satisfied (Appendix 9 – overall), or by looking at plate 1 and plate 3 as being two runs for one compound and plate 2 and 4 as being two runs for another compound and looking at the minimum significant ratio¹³⁹ even though the two compounds are the same (Table 2.2).

For the former, every time the coefficient of variation is above 20%, due to low mean values, the standard deviation was smaller than that of the maximum signal, hence satisfying this criterion. Additionally, the signal window was > 2 (11.2). The Z'-factor, calculated for the positive (A2-infected) and negative (mock-infected) signals was > 0.5 (0.7). After combining the data for the five plates, the evolution of the Z'-factor with different concentrations of Ribavirin was also observed. This revealed that the cut-off concentration for a “good assay”¹³⁶ was 50 μ M (25 μ M for plate 2, 40 μ M for plate 3 and 4). For the latter, the data required for the minimum significant ratio (MSR, Appendix 1) and limits of agreements (LsA) calculations are summarised in Table 2.2.

Table 2.2: Determination of the minimum significant ratio and limits of agreements between two sets of two runs for Ribavirin

Plate #	Log(EC ₅₀)	Difference	σ_d	μ_d	MSR	LsA
1	-4.51	0.03	0.01	0.02	1.04	MR = 1.05
3	-4.48					
2	-4.51	0.01				MR/MSR = 1.00
4	-4.50					

Both the MSR (1.04) and the limits of agreement [1.00, 1.10] are satisfied. This concludes that the assay is reproducible.

2.3.5.2 Antiviral effect, cytotoxicity of Ribavirin

In order to look at the overall antiviral effect of Ribavirin, the data for the five plates used to validate the assay were combined (Figure 2.12). Additionally, the effect of Ribavirin on the fluorescence inside the wells was compared to the untreated A2- and mock-infected samples. In order to assess the cytotoxicity of Ribavirin, four plates were also seeded on four different days using cells at four different passages. Because no virus was used in the cytotoxicity assay, the virus control wells (Section 7, Figure 7.1) were replaced by cell controls. The results of the four experiments were combined and are shown in Figure 2.12.

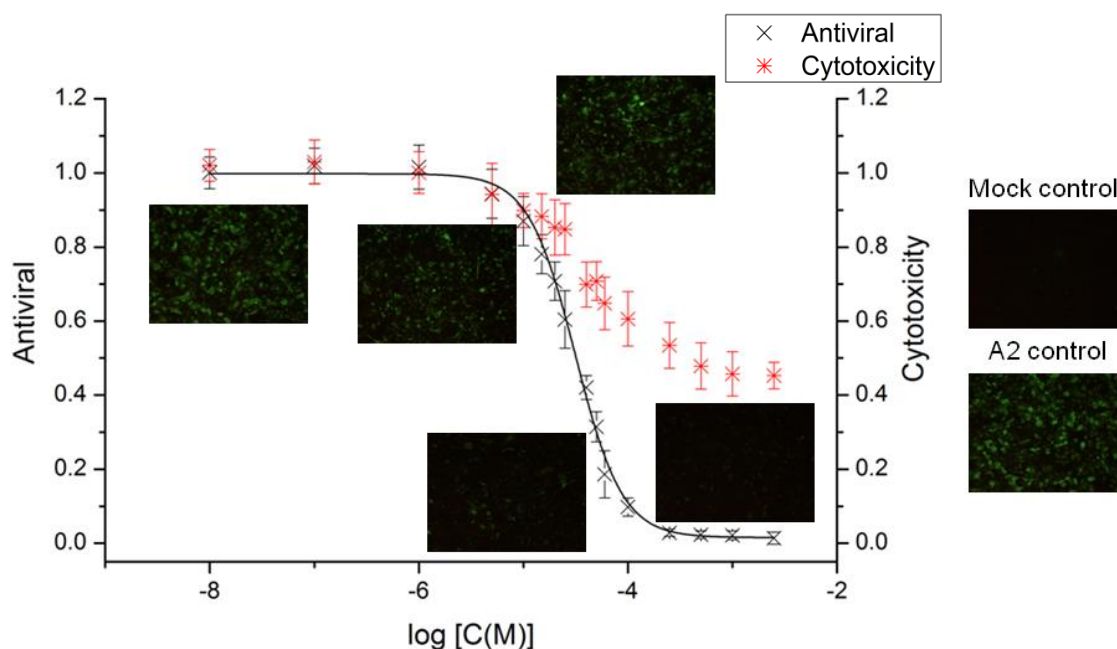


Figure 2.12 Overall antiviral effect of Ribavirin. The anti-viral dose-response to Ribavirin in HEp-2 cells describes a sigmoidal curve ($\chi^2/\text{degree of freedom}$: 0.23, R^2 : 0.998, A_1 : 0.02 ± 0.01 , A_2 : 1, $\log(\text{EC}_{50})$: -4.50 ± 0.02 , p : -1.93 ± 0.17). The results are expressed as the ratio to untreated A2-infected cells at an M.O.I. of 0.85. Microscope images at five different concentrations (2.5 mM, 60 μM , 40 μM , 25 μM , 15 μM , 10 nM) were compared to the A2-infected and mock-infected cell controls to observe variation in fluorescence intensity (magnification: 10 \times). The error bars refer to the standard deviation of fifteen replicates (three per plate) An additional y-axis has been added to show the cytotoxic dose-response of HEp-2 cells to Ribavirin. The results are expressed as the ratio of the Ribavirin-exposed cells to the unexposed cells against logarithm to base 10 of the Ribavirin concentrations (in molar). Absorbance was read at 570 nm. The error bars refer to the standard deviation of twelve replicates (three on days 1, 2, 3, and 4).

For this particular set of data, the EC_{50} was calculated to be $31.4 \mu\text{M}$ (Appendix 9 – overall). In the literature, for the A2 strain, it is possible to find a range of values for the reported EC_{50} of Ribavirin: $19 \mu\text{M}^{99}$, $23 \mu\text{M}^{102}$ (where the assay used are plaque reduction assay: lower multiplicity of infection and the cells are grown over the course of a few days), $36.7 \pm 1.8 \mu\text{M}^{124}$ (where frozen infected stocks were used and the endpoint was the observation of cytopathic effects), and *ca.* $41 \mu\text{M}^{140}$ (where all the components were added at the same time).

Regarding the cytotoxicity curve, it was only plotted as scattered points for the ease of visualisation. Further data points above 2.5 mM are required to describe the curve as fully sigmoidal. However, a CC_{50} was calculated at $40.6 \mu\text{M}$, diverging from previous reports in the literature, assuming they are referring to the final assay concentration: *ca.* 2 mM^{140} , $> 500 \mu\text{M}^{141}$, or $26 \mu\text{M}^{142}$. Overall, it is difficult to compare our results to those from the literature as it is unclear whether our assay conditions are the same (compounds added before or after the cells, incubation period in the presence of Ribavirin).

2.3.5.3 Normal distribution of the data

Another way to look at the above results is by plotting the normalised Gaussian function (normal distribution) for each of the Ribavirin concentrations along with the A2-infected control (Appendix 10).

Because the cut-off concentration for a “good assay”¹³⁶ was $50 \mu\text{M}$, the size of the data variation band (width of the Gaussian) was only calculated for concentrations above $50 \mu\text{M}$. The widths of the distribution are thin for the following concentrations: 2.5 mM , 1 mM , $500 \mu\text{M}$, and $250 \mu\text{M}$. The widths of distribution are adequate to detect the hits for the following concentrations: $100 \mu\text{M}$ and $50 \mu\text{M}$. The distribution width appeared wider for samples with a standard deviation greater than 0.06, especially the A2-infected control ($\sigma = 0.061$) and $50 \mu\text{M}$ of Ribavirin ($\sigma = 0.063$). The separation band for the A2-infected control is 0.8 when compared to the ideal sample with complete reduction of the fluorescence signal ($\mu = 0$) without any variation ($\sigma = 0$), and 0.75 when compared to the 2.5 mM , 1 mM , $500 \mu\text{M}$, and $250 \mu\text{M}$ Ribavirin samples (Appendix 10). The separation band decreases to values below 0.7 for concentrations of $100 \mu\text{M}$ and less.

The concentration of Ribavirin as the internal positive control was determined according to three criteria: i) a large separation band, *i.e.* concentration above 100 μM , ii) an acceptable Z'-factor, *i.e.* concentrations of 50 μM and above, iii) a complete reduction of the signal. An assay concentration of 2.5 mM was chosen, despite its toxicity to cells (only around 40% cell viability), in order to simulate compounds showing activity only because they are toxic to the cells (*i.e.* false positives).

2.3.5.4 Effects of the multiplicity of infection on Ribavirin

Further to the study on the effect of the M.O.I. on the fluorescence output in Section 2.3.3, the effects of the M.O.I on the EC_{50} were also investigated (Table 2.3).

Table 2.3: Evolution of the EC_{50} of Ribavirin with varying M.O.I.

M.O.I.	EC_{50}
17	> 250 μM
2	> 500 μM
0.85	<i>ca.</i> 31.4 μM ^a
0.5	14.9 μM
0.25	10.3 μM
0.1	8.5 μM

a: EC_{50} for a M.O.I. of 0.85 was combined over the results obtained for five plates.

The decrease in the effect of Ribavirin between an M.O.I. of 17 and 2 might also be explained by the cytopathic effects of hRSV at a high M.O.I., therefore reducing the effects of Ribavirin. As soon as the M.O.I. becomes lower than 1, *i.e.* less than one viral particle in each cell (on average), the EC_{50} reached the micro-molar range.

The final step was to assess the robustness of the assay by simulating how the robot was going to make the assay dilution of the library using a Ribavirin plate.

2.3.6 Robustness of the assay upon using a liquid-handling robot

A Hamilton liquid-handling robot was chosen to rapidly add the compounds to screen to assay plates, at the right concentration: 100 μM for a final assay concentration of 25 μM , after the 1:4 dilution imposed by the assay configuration (from a 10 mM solution in 100% DMSO). Therefore, it was crucial to determine the robustness of the assay when the robot was used.

The 1:100 dilution from the original stock is prepared in two steps by a liquid-handling robot: i) 1:20 followed by ii) 1:5. In order to simulate that process, a master plate of Ribavirin concentrations in 100% DMSO was prepared (see Section 7.12 for the layout of the 96-well plate).

One plate was prepared by the liquid-handling robot and one plate was prepared by hand. The two plates were then incubated, infected (M.O.I. of 0.5) and analysed in parallel. The resulting dose-response curves are presented in Figure 2.13 and Appendices 7 and 8.

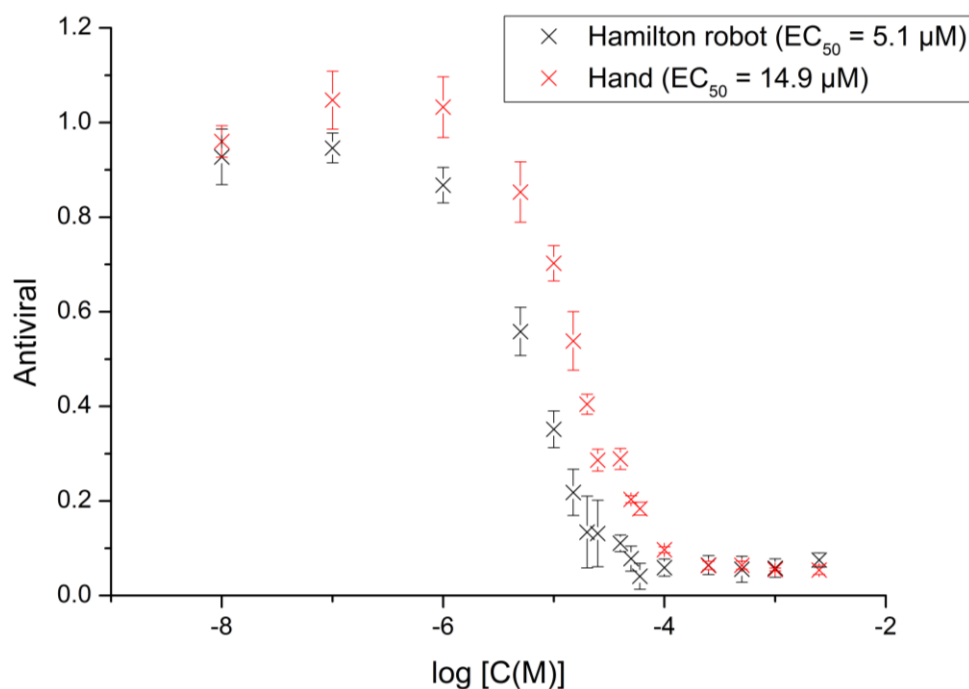


Figure 2.13 Comparison of Ribavirin EC_{50} when the plate is prepared by hand and by the Hamilton robot. The dose-response curve to Ribavirin in HEP-2 cells describes a sigmoidal curve. The results are expressed as the ratio to untreated A2-infected cells at an M.O.I. of 0.5. The error bars refer to the standard deviation of three replicates. A2 was set at 1 in the fitting function. In the case of the sigmoid for the robot curve, if this parameter is set at 0.93, the EC_{50} becomes 6.1 μM . Hamilton robot: $Z' = 0.74$, signal-to-background = 2.1; hand: $Z' = 0.83$, signal-to-background = 2.2.

When the Ribavirin concentrations were prepared using the liquid handling robot, the EC_{50} was calculated as 5.1 μM . The EC_{50} observed rose to 14.9 μM when the Ribavirin dilutions were prepared by hand. The potencies are different but remain in the same micromolar range. The difference can arise from multiple causes, which include inaccuracies when pipetting small volumes, working with low masses when preparing the Ribavirin stock, or variations in the titre of the virus stock¹²⁴.

The statistics of the two plates were then looked at (Appendix 9 – hand, robot): for the robot plate, two concentrations (25 and 20 μM) did not satisfy the coefficient of variation criteria but both Z' -factors were greater than 0.5. The plate prepared by hand had all its coefficients of variation below 20%, even for those concentrations with a low mean. For the robot plate, the cut-off concentration for a good assay was 10 μM (as opposed to 20 μM when prepared by hand). In order to validate the robustness of the assay, the raw data for the robot plate were analysed (Table 2.4).

Table 2.4: Raw data for the concentrations of Ribavirin that did not satisfy the coefficient of variation (%) when it was calculated on the normalised data (25 and 20 μ M).

	25 μM	20 μM
	24418	24500
Fluorescence intensity (R.F.U.)	22488	23242
	24047	23845
	20904	20551
μ	23651	23862
σ	1024	629
CV^a (%)	4.3	2.6

a: CV = coefficient of variation

The fact that the raw data satisfied the coefficient of variation criteria validated the study with respect to the coefficient of variation. On the normalised Gaussian function (normal distribution) for each of the Ribavirin concentrations along with the A2-infected control (Appendices 11 and 12), the widths of the distribution are thin, and probably ideal for 40 μ M and above. The separation band is around 0.7 only for the following concentrations: 2.5 mM, 1 mM, 500 μ M, 250 μ M, 100 μ M, and 60 μ M (Appendix 12). Taken together, these results confirm the robustness of the assay.

2.3.7 Further assay validation with a known specific sub-nanomolar inhibitor

As outlined in Section 1.4, the current project is also concerned with the discovery of a potential new fusion inhibitor. Therefore, it was critical to find out whether or not known fusion inhibitors could be detected using the assay described herein. Additionally, different assay conditions were tested in order to target virus-induced fusion more specifically.

2.3.7.1 The choice of a known specific inhibitor

The compound JNJ-2408068 has previously been reported¹⁰⁷ with sub-nanomolar activity ($EC_{50} = 0.16$ nM) against hRSV, and its synthesis has also been described in the literature¹⁴³. For ease of synthesis and because the difference in anti-viral activity was marginal, JNJ-4749914 ($EC_{50} = 0.40$ nM), a close analogue of JNJ-2408068, was prepared (Figure 2.14).

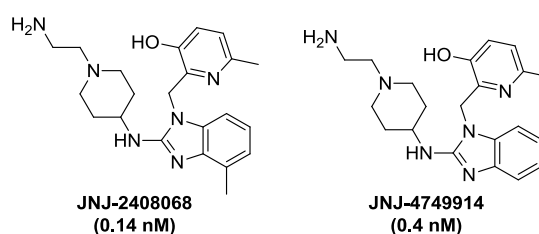
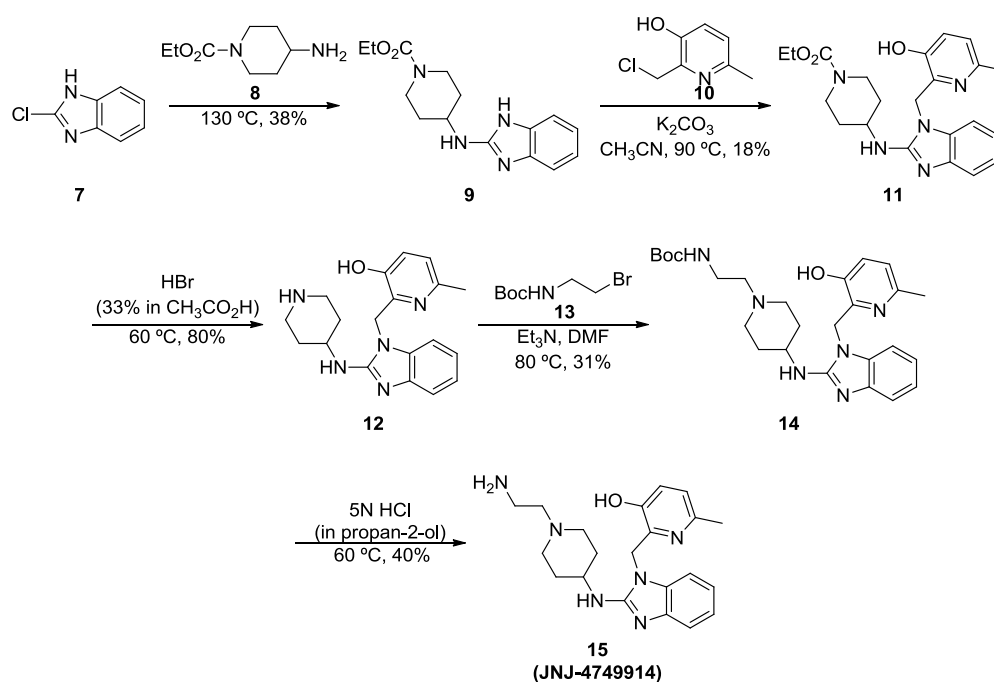


Figure 2.14. Chemical representations of JNJ-240868 and JNJ-4749914. The additional methyl group would lead to the formation of regioisomers upon introducing the hydroxypyridine moiety. EC_{50} values for anti-viral activity in a cell-based assay are given between brackets.

2.3.7.2 Synthesis of JNJ-4749914

JNJ-4749914 was prepared in five steps from commercially available 2-chlorobenzimidazole **7** following a literature route reported by Bonfanti *et al.*^{108,119,143} (Scheme 2.1). The synthesis started with the melting reaction of 2-chlorobenzimidazole **7** with ethyl-4-amino-1-piperidine **8** to give the benzimidazole **9** in 38% yield. Subsequent treatment of **9** with the chloride **10**^{††} and potassium carbonate yielded the *N*-alkylated benzimidazole **11** in 18% yield. Boc deprotection, by treatment with hydrobromic acid, furnished the secondary amine **12** in 80% yield. Nucleophilic substitution of *tert*-butyl *N*-(2-bromoethyl)carbamate **13** gave the carbamate **14**. Acid-mediated Boc deprotection of **14** by treatment with hydrochloric acid afforded JNJ-4749914 (**15**) in 0.7% overall yield.



Scheme 2.1. Preparation of JNJ-4749914 from 2-chlorobenzimidazole **7.**

JNJ-4749914 was subsequently used for the validation of the cell-based fluorescence assay developed with Ribavirin.

^{††} The chloride **10** was prepared in a single step from commercially available 2,6-lutidine- α ,3-diol 144 Gong, Y. & Kato, K. Facile synthesis of *o*- and *p*-(1-trifluoromethyl)-alkylated phenols via generation and reaction of quinone methides. *Synlett*. **2002**, 431-434 (2002).

2.3.7.3 Biological evaluation of JNJ-4749914

Following the verification of the assay suitability using the broad-spectrum anti-viral Ribavirin, the assay was tested on the known inhibitor JNJ-4749914. A total of twenty different JNJ-4749914 concentrations, ranging from 25 μM to 0.022 pM, were assayed in a single 96-well plate with each concentration being assayed in quadruplicates (Figure 2.15).

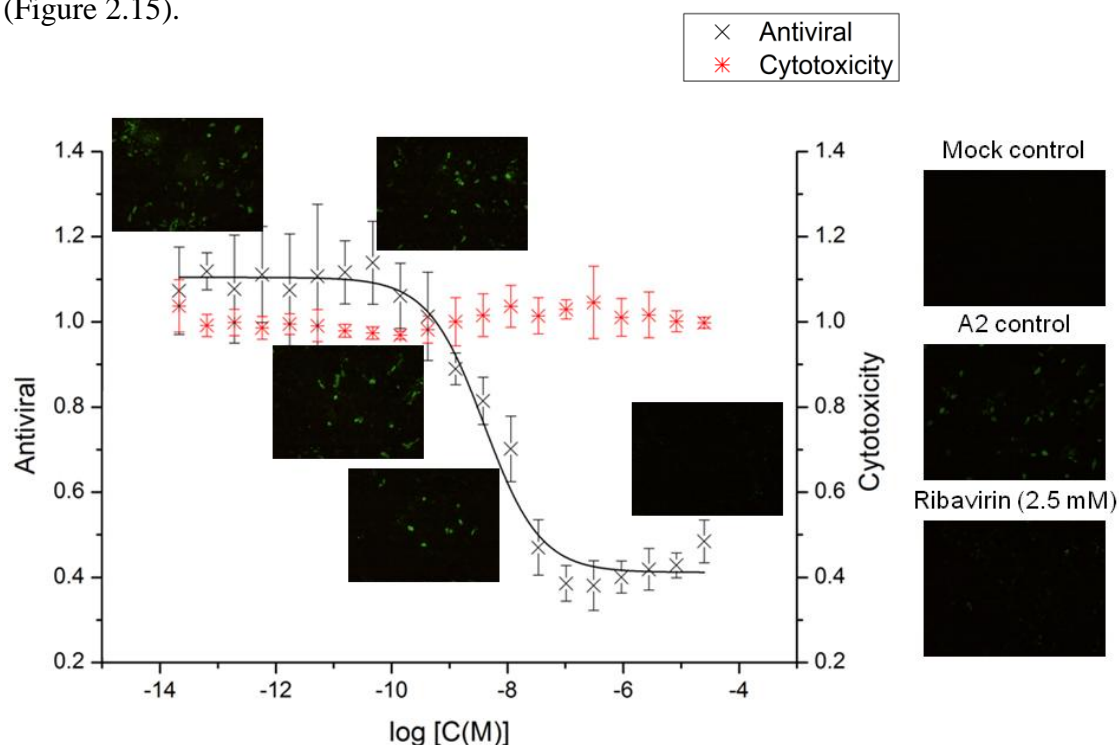


Figure 2.15. Overall antiviral effect of JNJ-4749914. The dose-response to JNJ-4749914 in HEp-2 cells describes a sigmoidal curve, $\log(\text{EC}_{50})$: -8.40 ± 0.09 , p : -0.90 ± 0.15). The results are expressed as the ratio to untreated A2-infected cells at an M.O.I. of 0.5. Microscope images at five different concentrations (25 μM , 11 nM, 1.3 nM, 0.4 nM, 0.022 pM) were compared to the A2- and mock-infected cell controls and 2.5 mM Ribavirin control to observe variation in fluorescence intensity (magnification: 10 \times). An additional y-axis has been added to show the cytotoxic dose-response of HEp-2 cells to Ribavirin. The results are expressed as the ratio of the JNJ-4749914-exposed cells to the unexposed cells against logarithm to base 10 of the JNJ-4749914 concentrations (in molar). Absorbance was read at 570 nm. The error bars refer to the standard deviation of four replicates.

For this particular set of data, the Z'-factor was 0.52 (> 0.5) and the EC₅₀ was calculated to be 4 nM. This compares to a reported EC₅₀ of 0.4 nM for a different assay of its activity¹⁰⁷. The CC₅₀ is $> 25 \mu\text{M}$. Although our EC₅₀ is ten times higher than the reported value, it remains in the nanomolar range. In the literature, the sub-nanomolar activity of JNJ-4749914 was calculated looking at the decrease in the display of virus-induced cytopathic effects after seven days. JNJ-2408068 was also assayed by Douglas *et al.*⁶⁴, looking at a reduction of the cytopathic effect four days post-infection, as opposed to seven days^{107,108,119}. They calculated an EC₅₀ of 2.1 nM. This is to compare to an EC₅₀ of 0.14 nM reported by Andries *et al.*¹⁰⁷ or 0.25 nM reported by Bonfanti *et al.*¹¹⁹. Here we are looking at a decrease in the number of virus particles inside cells upon exposure to JNJ-4749914 for 24 hours.

2.3.7.4 Alternative assay conditions to look at fusion directly

In order to make the assay more specific towards the detection of fusion inhibitors, three alternative conditions were investigated (Figures 2.16 to 2.18). In the first one, the M.O.I. was decreased to 0.05. In the second one, the compounds were added on the second day, immediately before the infection step. In the third one, the compounds were added on the second day, immediately before the infection, and after one hour incubation, the compound–virus solution was replaced by fresh media. The latter two conditions were designed to reduce any potential cytotoxicity as the time the cells have been exposed to compounds has been halved.

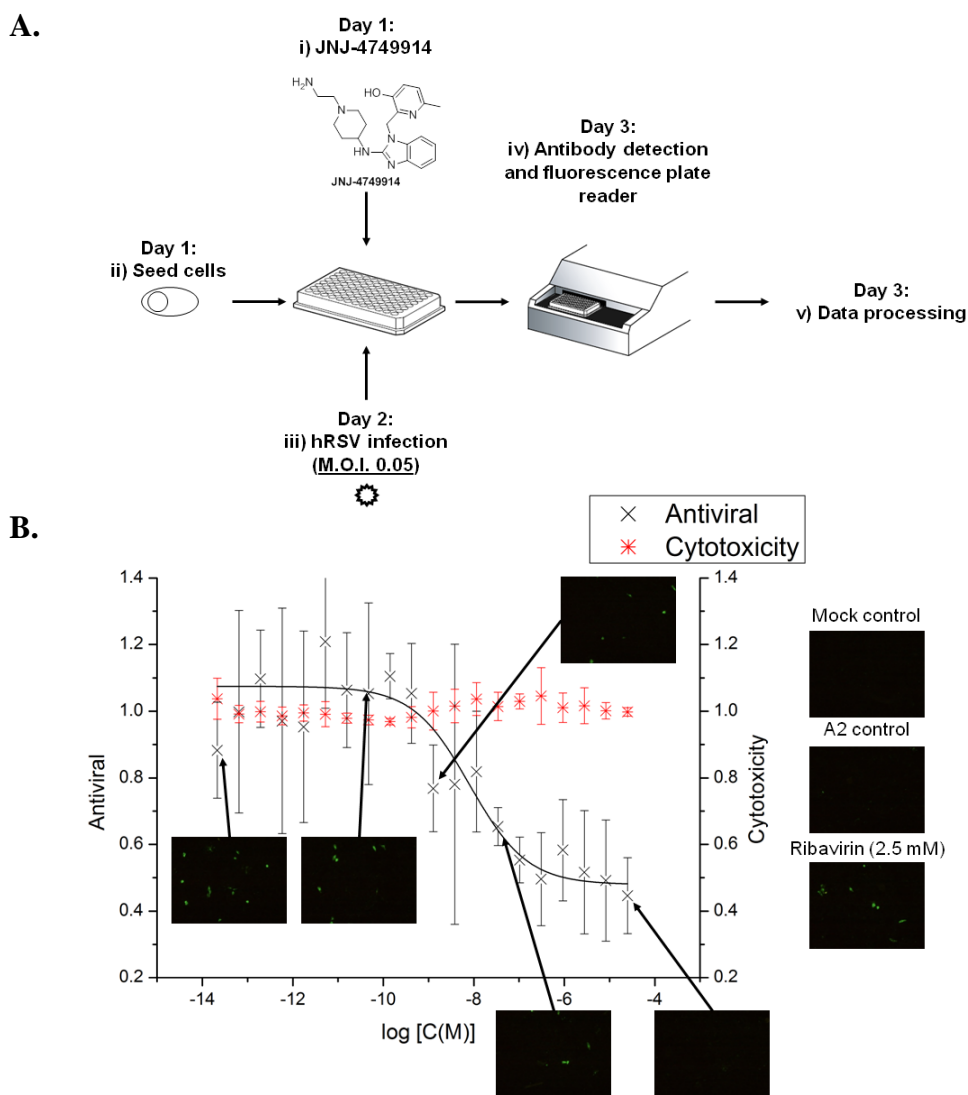


Figure 2.16. JNJ-4749914 assayed with a M.O.I. of 0.05. A. Assay setup. **B.** The dose-response to JNJ-4749914 in HEp-2 cells describes a sigmoidal curve, $\log(\text{EC}_{50})$: -8.08 . The results are expressed as the ratio to untreated A2-infected cells at an M.O.I. of 0.05. Microscope images at five different concentrations (25 μM , 34 nM, 1.3 nM, 40 pM, 0.022 pM) were compared to the A2- and mock-infected cell controls and 2.5 mM Ribavirin control to observe variation in fluorescence intensity (magnification: 10 \times). An additional y-axis has been added to show the cytotoxic dose-response of HEp-2 cells to Ribavirin. The results are expressed as the ratio of the JNJ-4749914-exposed cells to the unexposed cells against logarithm to base 10 of the JNJ-4749914 concentrations (in molar). Absorbance was read at 570 nm. The error bars refer to the standard deviation of four replicates.

For this particular set of data, the Z' -factor was < 0 . The explanation for the quality of the assay lies with a small proportion of cells that had been infected as a consequence of the low M.O.I. The EC_{50} was calculated to be 8.2 nM. However, the Z' -factor suggests that the assay setup is not suitable.

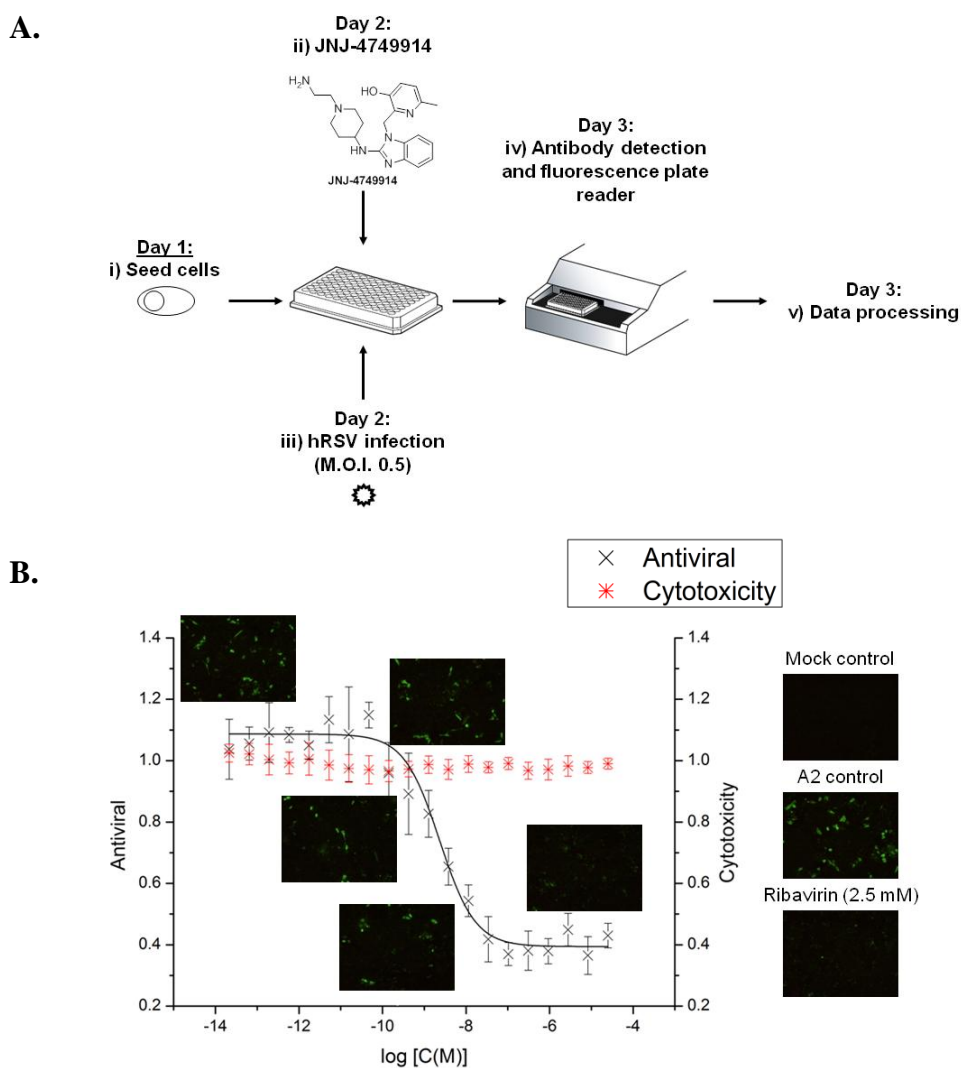
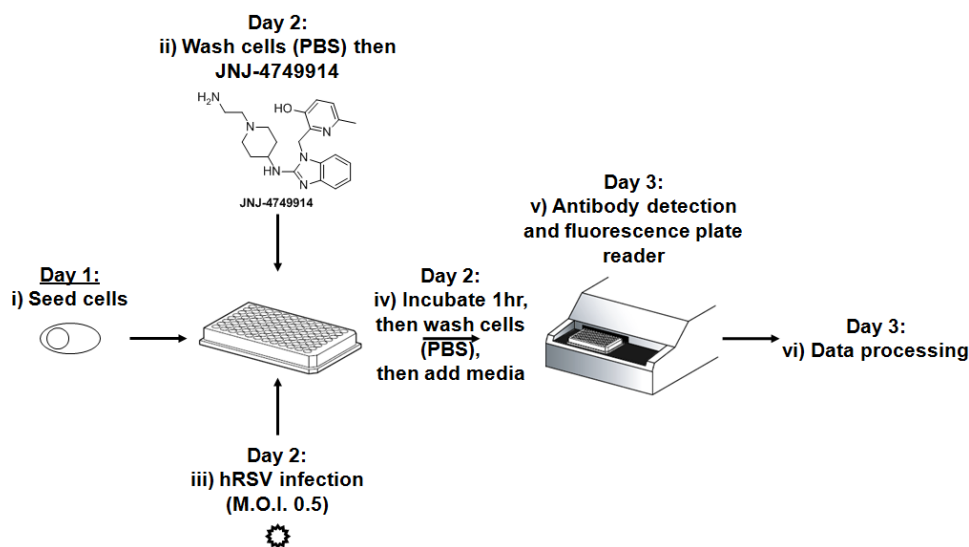


Figure 2.17. JNJ-4749914 assayed with addition immediately before infection on day 2. A. Assay setup. **B.** The dose-response to JNJ-4749914 in HEp-2 cells describes a sigmoidal curve, $\log(\text{EC}_{50})$: -8.63 . The results are expressed as the ratio to untreated A2-infected cells at an M.O.I. of 0.5. Microscope images at five different concentrations (25 μM , 3.8 nM, 1.3 nM, 0.4 nM, 0.022 pM) were compared to the A2- and mock-infected cell controls and 2.5 mM Ribavirin control to observe variation in fluorescence intensity (magnification: 10 \times). An additional y-axis has been added to show the cytotoxic dose-response of HEp-2 cells to Ribavirin. The results are expressed as the ratio of the JNJ-4749914-exposed cells to the unexposed cells against logarithm to base 10 of the JNJ-4749914 concentrations (in molar). Absorbance was read at 570 nm. The error bars refer to the standard deviation of four replicates.

For this particular set of data, the Z' -factor was 0.52 (> 0.5) and the EC_{50} was calculated to be 2.4 nM (higher than the reported 0.4 nM¹⁰⁷). Combined with a Z' -factor > 0.5 , these results suggest that the assay conditions are suitable.

A.



B.

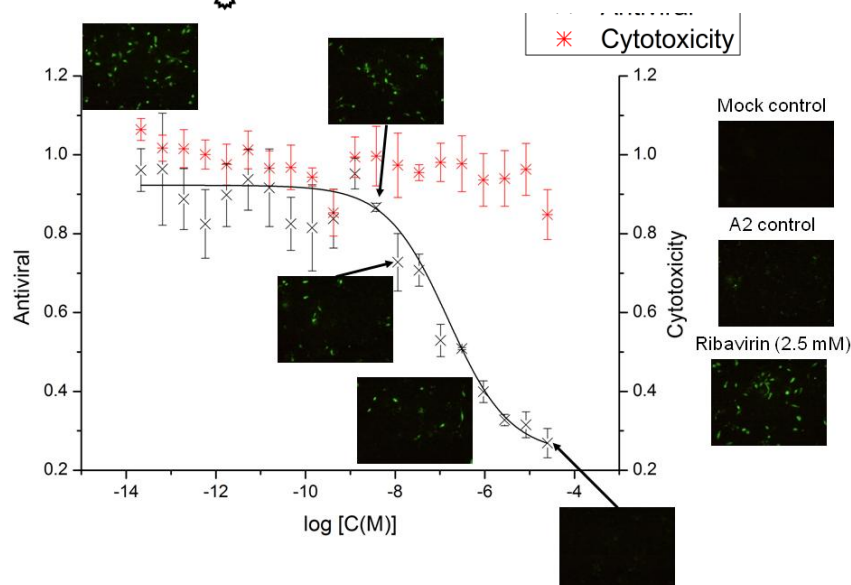


Figure 2.18. JNJ-4749914 assayed with addition immediately before infection on day 2 and subsequent PBS wash. A. Assay setup. B. The dose-response to JNJ-4749914 in HEp-2 cells describes a sigmoidal curve, log(EC₅₀): -6.82. The results are expressed as the ratio to untreated A2-infected cells at an M.O.I. of 0.5. Microscope images at five different concentrations (25 μ M, 926 nM, 11 nM, 1.3 nM, 0.022 pM) were compared to the A2- and mock-infected cell controls and 2.5 mM Ribavirin control to observe variation in fluorescence intensity (magnification: 10 \times). An additional y-axis has been added to show the cytotoxic dose-response of HEP-2 cells to Ribavirin. The results are expressed as the ratio of the JNJ-4749914-exposed cells to the unexposed cells against logarithm to base 10 of the JNJ-4749914 concentrations (in molar). Absorbance was read at 570 nm. The error bars refer to the standard deviation of four replicates.

For this particular set of data, the Z'-factor was 0.52 (> 0.5) and the EC₅₀ was calculated to be 152 nM. The values are not in the same nanomolar range as the reported literature value (0.4 nM¹⁰⁷). These conditions also detect fusion inhibitors.

2.4 Summary

The robustness of a high-throughput screening assay in HEp-2 cells and for the subgroup A of the human respiratory syncytial virus based on indirect fluorescence detection was established.

In short, antibody dilutions affording an acceptable signal-to-background ratio (> 2) for indirect fluorescence detection were chosen. The tolerance of the assay to DMSO was established (*ca.* 80% viability for 1% DMSO and lower) with a chosen assay concentration of 0.25% (no influence was observed on the fluorescence output). The variability (intra- and inter-plate or day-to-day) of the assay was investigated using a range of concentrations (2.5 mM to 10 nM) of Ribavirin (internal positive control) over the course of three days. The results were in agreement with recognised statistical parameters: signal-to-noise ratio (strong signal), signal-to-background ratio (>2 , good dynamic range), coefficient of variation ($<20\%$, low well-to-well variability), signal window (>2 , good separation between the controls). The Z'-factor > 0.5 coincides with a 'good' assay, with a cut-off concentration of 50 μM . In terms of reproducibility, both the MSR (<3) and the LsA (MR / MSR and $\text{MR} \times \text{MSR}$ were between 0.33 and 3) were within their respective acceptance criteria, concluding on the reproducibility and performance of the assay. The activity and cytotoxicity of Ribavirin with the present assay were established: $\text{CC}_{50} = 40.6 \mu\text{M}$ and $\text{EC}_{50} = 31.13 \pm 1.27 \mu\text{M}$ (at an M.O.I. of 0.85). The assay concentration for the internal positive control was set at 2.5 mM. The results presented for JNJ-4749914 suggests that the optimised assay conditions are suitable for the detection of known specific inhibitors which are not broad-spectrum.

Taken together, the results show that a robust high-throughput screening assay for the detection of small molecule inhibitors of hRSV was developed. Additionally, the detection of anti-viral activity was observed in three days, which is half the time required in all the previous assays published for hRSV drug discovery.

3 DESIGN OF POTENTIAL LIGANDS USING VIRTUAL HIGH-THROUGHPUT SCREENING

This Chapter describes the computational approach used to support the discovery of novel series of potential hRSV fusion inhibitors. The computational approach that was used is introduced in Section 3.1. The design and optimisation of a virtual library is discussed in Section 3.2. The results of the *in silico* screening campaign and the presentation of the novel series of potential hRSV fusion inhibitors are outlined in Sections 3.3 to 3.5.

3.1 vHTS approach to target hRSV

Our vHTS approach can be divided into four main parts (Figure 3.1). In order to start the virtual screening campaign, it is important to select a suitable protein target (*i.e.* structural data available ideally with a known small molecule binding cavity). A virtual library of molecules likely synthetically accessible¹⁴⁵ using methods developed within the Nelson group, as well as a virtual library of commercially available compounds, were used to identify potential hRSV inhibitors. The virtual library was optimised through iterative rounds of virtual screening and property evaluation. The approach enabled a range of molecules to be nominated for evaluation.

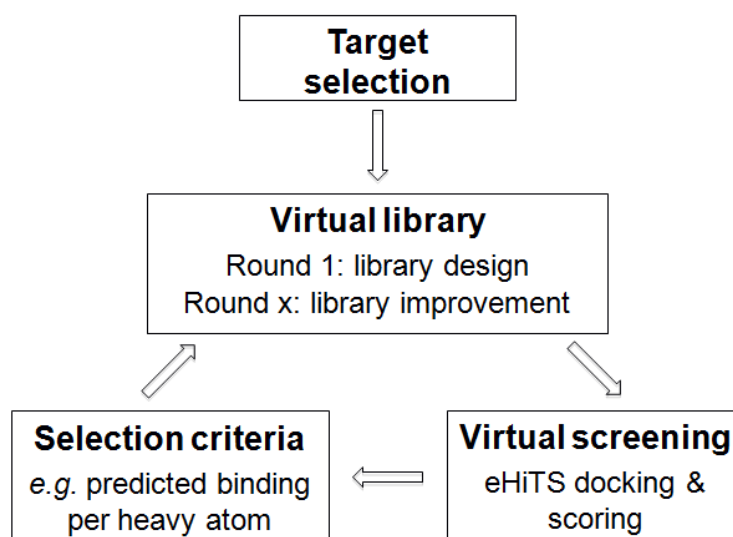


Figure 3.1. Virtual screening strategy.

3.1.1 Selection of a target

We based our vHTS approach on the availability of a crystal structure of a small molecule (TMC353121) in complex with the F protein (PDB accession number 3KPE, 1.5 Å). The binding cavity of TMC353121 has been described in Chapter 1. Key non-covalent interactions help explain the sub-nanomolar activity reported by Bonfanti *et al.*¹⁰⁸. One key interaction involved a water bridge between TMC353121, Glu487 and a water molecule¹¹⁶. The binding cavity with the water molecule was selected for the vHTS campaign. However, 3KPE is the only structure of a small molecule in complex with the F protein. Therefore, it is not possible to guarantee that the water molecule is tightly bound. As such, the binding cavity without the water molecule was chosen for further validation of the virtual hits identified (Figure 3.2).

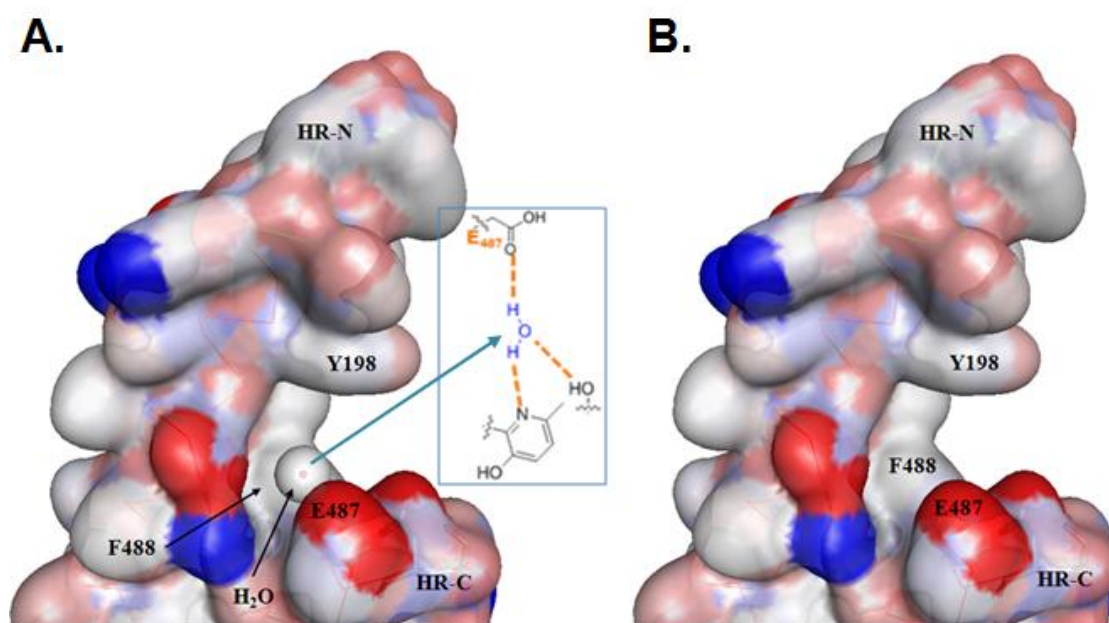


Figure 3.2. Protein targets for the vHTS campaign. **A.** Binding cavity of TMC353121 with the water bridge. The specific interactions that the water bridge makes with 3KPE are also shown. **B.** Binding cavity of TMC353121 without the water molecule. Pictures generated with Discovery Studio (Accelrys) from PDB accession number 3KPE.

3.1.2 Requirements for a virtual library

In Chapter 1, the concept of virtual libraries was introduced. There are two types of virtual libraries available: libraries containing commercially available compounds and libraries generated on the basis of reliable synthetic reactions. For the latter, a set of building blocks (or reactants), and reliable reactions, were imported into a software package (Pipeline Pilot) which generated a virtual library of likely synthetically accessible molecules (see Section 3.2.1). The virtual libraries were then converted into 3D using a 3D structure generator (CORINA).

3.1.3 Virtual screening package

Performing vHTS requires the use of virtual screening packages in order to perform the docking of molecules (*i.e.* the prediction of a binding pose inside the cavity) inside a protein target⁷¹. One such package is eHiTS from SymBioSys Inc.¹⁴⁶.

In short, eHiTS decomposes each ligand into small rigid fragments (and connecting chains), which are then docked inside the binding pocket covering the available 3D space, independently of each other. The fragments are then reassembled using the flexible connecting chains to match the original molecule while retaining the best possible binding pose in the target protein. The eHiTS package also takes into account all possible protonation states of the ligand and protein. Prior to performing the scoring function algorithm, a local energy minimisation step¹⁴⁶ (torsion angles, rotation and translation) for the ligand is performed.

3.1.4 Selection criteria

Using an empirical and statistical scoring function, the eHiTS package returns a score which correlates^{§§} to the binding affinity¹⁴⁷. Predicted scores may be normalised to the number of heavy atoms (C, N, O, S, halogens) in a molecule, to yield a predicted ligand efficiency¹⁴⁸ (cLE^{***}). cLE predicts how efficiently a molecule may bind to its target. It is likely that molecules with a high experimental ligand efficiency (LE > 0.3) might be developed into nanomolar ligands by maintaining LE during optimisation⁶⁸.

3.1.5 Free energy minimisation

Additional free energy minimisation steps, using force field-based methods (potential energy given as a function of distance and angle between atoms) may be required in order to minimise the conformational energy of the predicted binding pose. Two protocols may be followed: either the predicted binding conformation is minimised to the closest local energy minimum, not taking into account the protein environment, or the predicted binding conformation is minimised within the binding cavity residues in close proximity (up to 3 Å). The former is referred to as rigid minimisation; the latter is referred to as flexible minimisation. Such minimisation steps may be performed by the molecular modelling module MacroModel¹⁴⁹, from the Maestro suite (Schrödinger).

^{§§} eHiTS score $\sim -\log(K_i)$; *e.g.* a score of -9.0 corresponds to a predicted nanomolar affinity.

^{***} Predicted ligand efficiency is defined as:
$$\text{cLE} = -\frac{\text{eHiTS score}}{\text{Number of heavy atoms}}$$

3.2 vHTS campaign

A virtual library was designed to be based on diverse scaffolds and to provide appendages capable of non-covalent interactions (see Section 3.2.1). Common substructures found widely in the virtual hits would then be fed into the design of a refined substructure virtual library (see Section 3.2.2). The identification of common scaffolds allowed the design of a more focused library (Section 3.2.3) which led to the identification of novel series of potential hRSV fusion inhibitors (see Section 3.2.4). The overall approach is summarised in Figure 3.3.

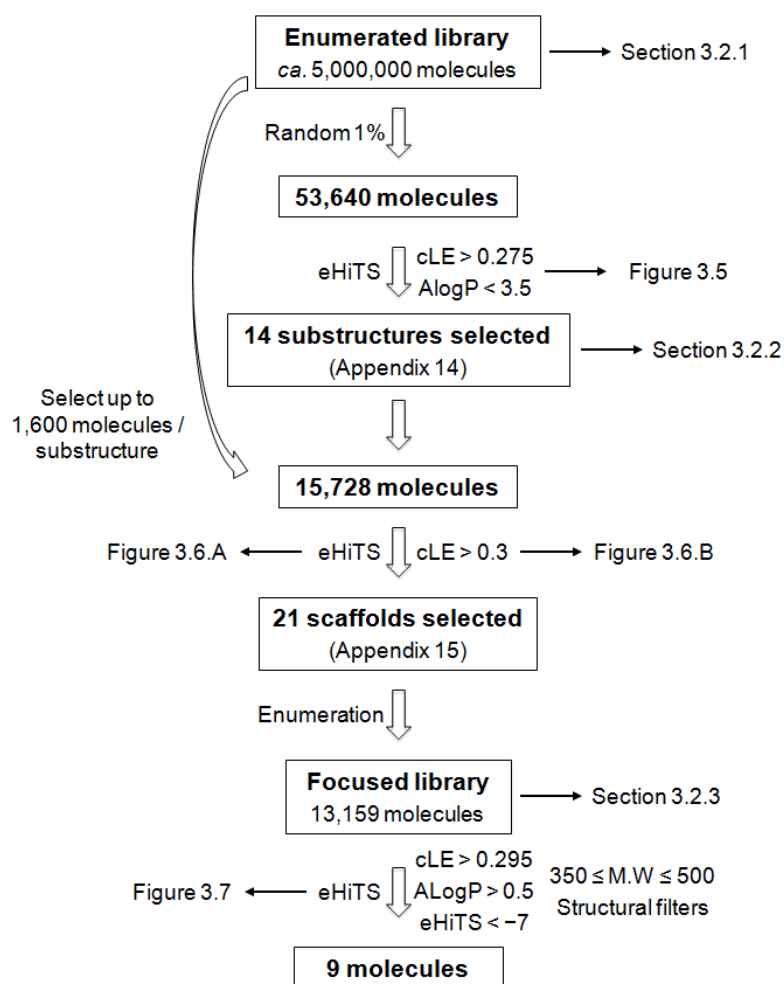


Figure 3.3. Overview of the virtual screening campaign adopted against hRSV. The steps leading to the identification of novel series of potential hRSV fusion inhibitors, from library enumeration to the final selection criteria, are highlighted.

3.2.1 Enumeration of a virtual library

At the start of the virtual screening campaign, a building-block based virtual library of likely synthetically accessible molecules was designed (*ca.* 5,000,000 molecules, Figure 3.4). The enumeration of this new virtual library was based on the diversity-oriented synthesis chemistry that was successfully developed within the Nelson group¹⁵⁰, and that had yielded natural product-like molecules of unprecedented scaffold diversity¹⁵¹⁻¹⁵³. Key to this approach was the use of a toolbox of available virtual reactions (*e.g.* amide bond formation, Mitsunobu) for the combination of building blocks (see Appendix 13 for the full set of building blocks used).

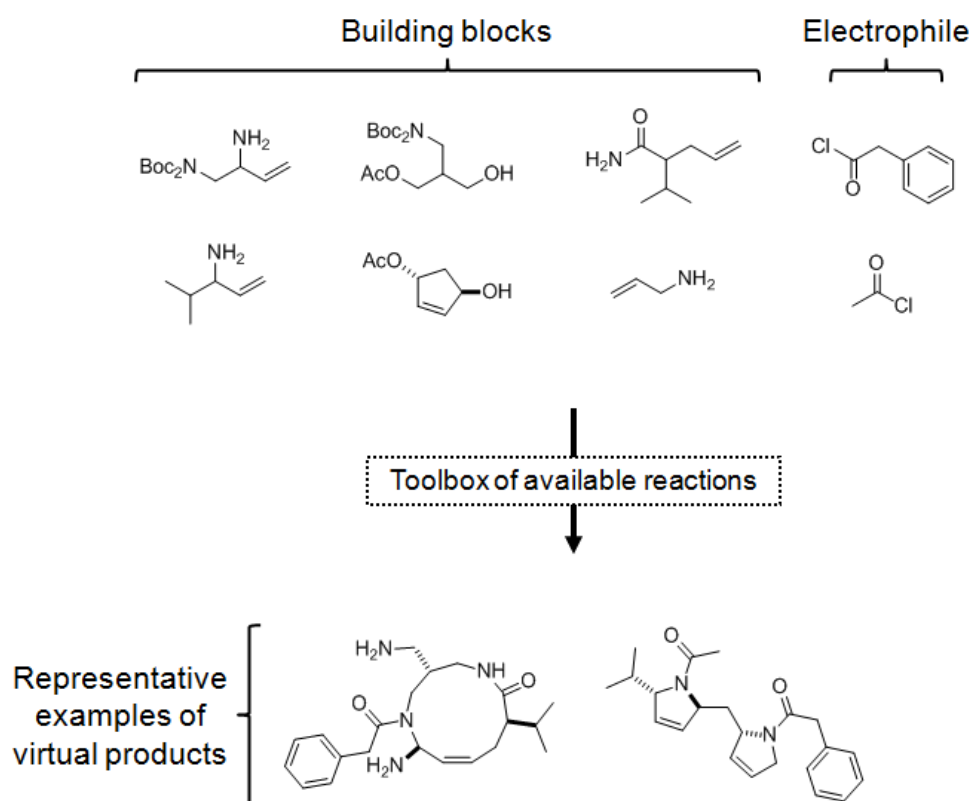


Figure 3.4. Enumeration of a virtual library. A building-block based approach was used for the generation of a virtual library of *ca.* 5,000,000 molecules. The examples of products shown stem from two possible combinations of the building blocks.

3.2.2 Identification of promising scaffolds for further development

With the newly generated virtual library, our initial objective was the identification of promising scaffolds for further development. The first step towards this objective was the identification of common substructures found in promising ligands. Therefore, a randomly selected 1% (53,640 molecules) subset of the full library was screened against 3KPE using eHiTS (the screening of *ca.* 5,000,000 molecules was too computationally demanding). The spread of the data, with respect to cLE and ALogP is shown in Figure 3.5. Molecules with $cLE > 0.275$ and $ALogP < 3.5$ were analysed and 14 common substructures (see Appendix 14) were identified.

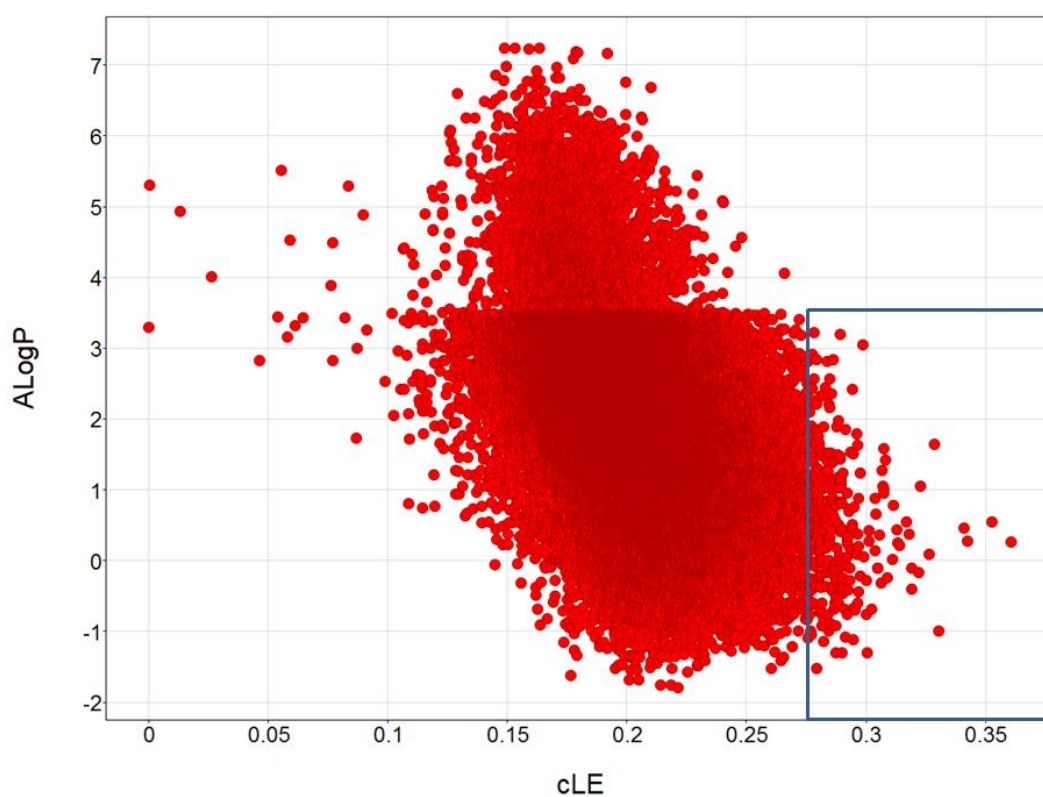


Figure 3.5. eHiTS results for a random 1% of the building-block based virtual library (53,640 molecules). Each molecule, shown by a red dot, is represented by its predicted ligand efficiency (cLE) and its predicted hydrophobicity (ALogP). The blue box represents those molecules with $cLE > 0.275$ and $ALogP < 3.5$. Graph generated using Vortex (Dotmatics).

This selection of substructures would then be used in the identification of promising scaffolds. Therefore, it was decided to extract additional molecules based on these substructures (up to 1,600 molecules / substructures) from the virtual library. 15,728 molecules were selected and screened against 3KPE using eHiTS (Figure 3.6.A). The molecules with $cLE > 0.275$ (675 molecules; 133 had $cLE > 0.3$) were also screened against the binding cavity without the bound water molecule. In that case, 135 molecules had $cLE > 0.3$, 65 of which were common to both datasets (Figure 3.6.B). These results were used for the identification of 21 promising scaffolds amongst those molecules with $cLE > 0.3$ (both with and without the bound water molecule) (see Appendix 15).

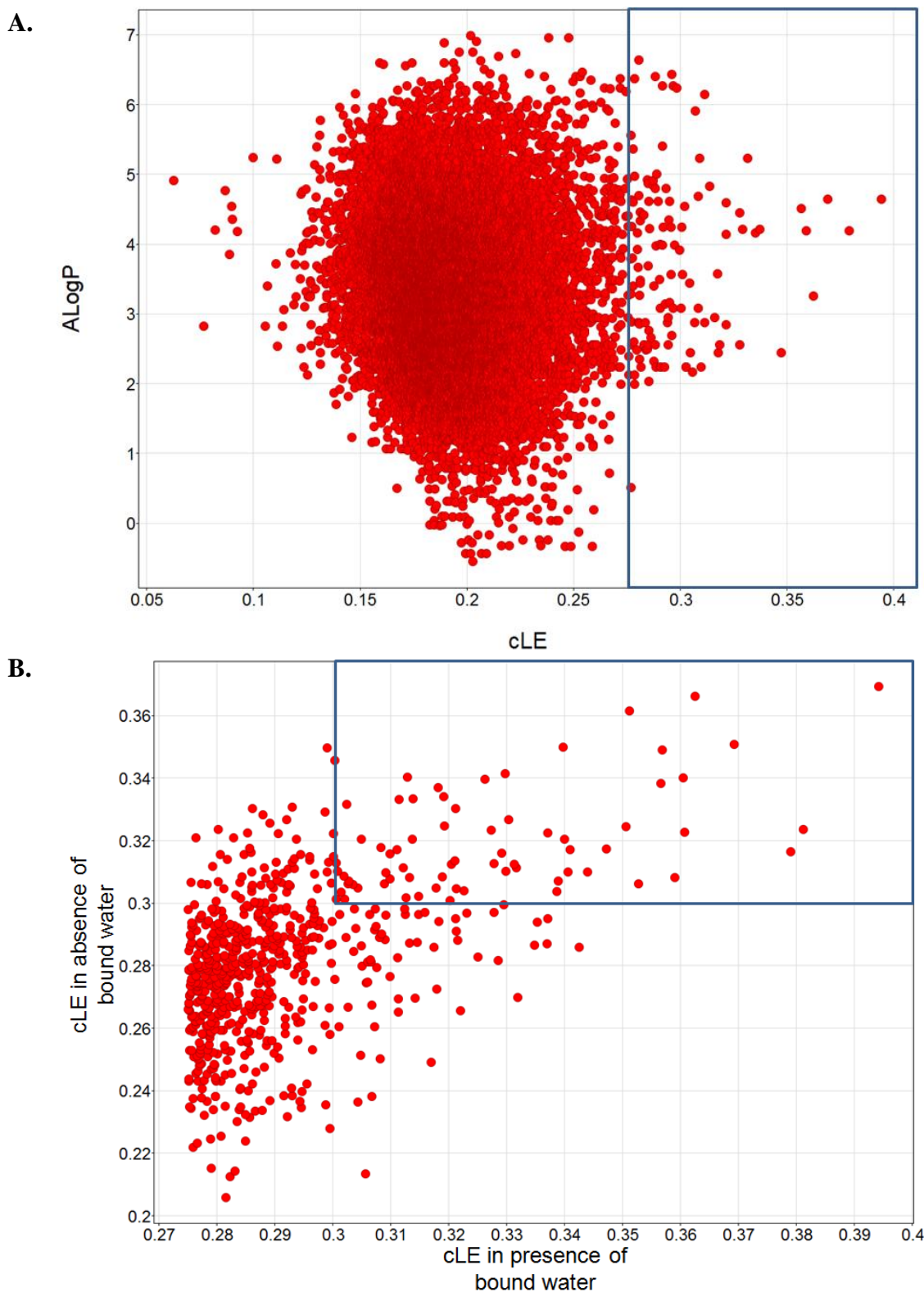


Figure 3.6. Identification of promising scaffolds. **A.** eHiTS results for the substructure virtual library (15,728 molecules). Each molecule, shown by a red dot, is represented by its predicted ligand efficiency (cLE) and its predicted hydrophobicity (ALogP). The blue box represents those molecules with $cLE > 0.275$. Graph generated using Vortex (Dotmatics). **B.** Influence of the water-bridge on the predicted results. 675 molecules with $cLE > 0.275$ in the presence of the bound water were screened against the cavity without the bound water. The blue box presents those molecules with $cLE > 0.3$ in both screens (65 molecules). Red dots represent individual molecules. Graph generated using Vortex (Dotmatics).

3.2.3 Identification of potential hRSV fusion inhibitors to be prepared

In order to identify potential hRSV fusion inhibitors to be prepared, we started by creating a more focused library based upon the 21 scaffolds (Figure 3.7.A). For this, the scaffolds were decorated virtually (Pipeline Pilot) with a range of groups corresponding to commercially available reagents. The reagents (acyl chloride, sulfonyl chloride and isocyanate) were selected on the basis of their diverse properties (size, hydrophobicity, basicity, hydrogen-bond character). The details are summarised in Appendix 16. The revised enumerated library (13,159 molecules) was screened against 3KPE with the bound water using eHiTS (Figure 3.7.B).

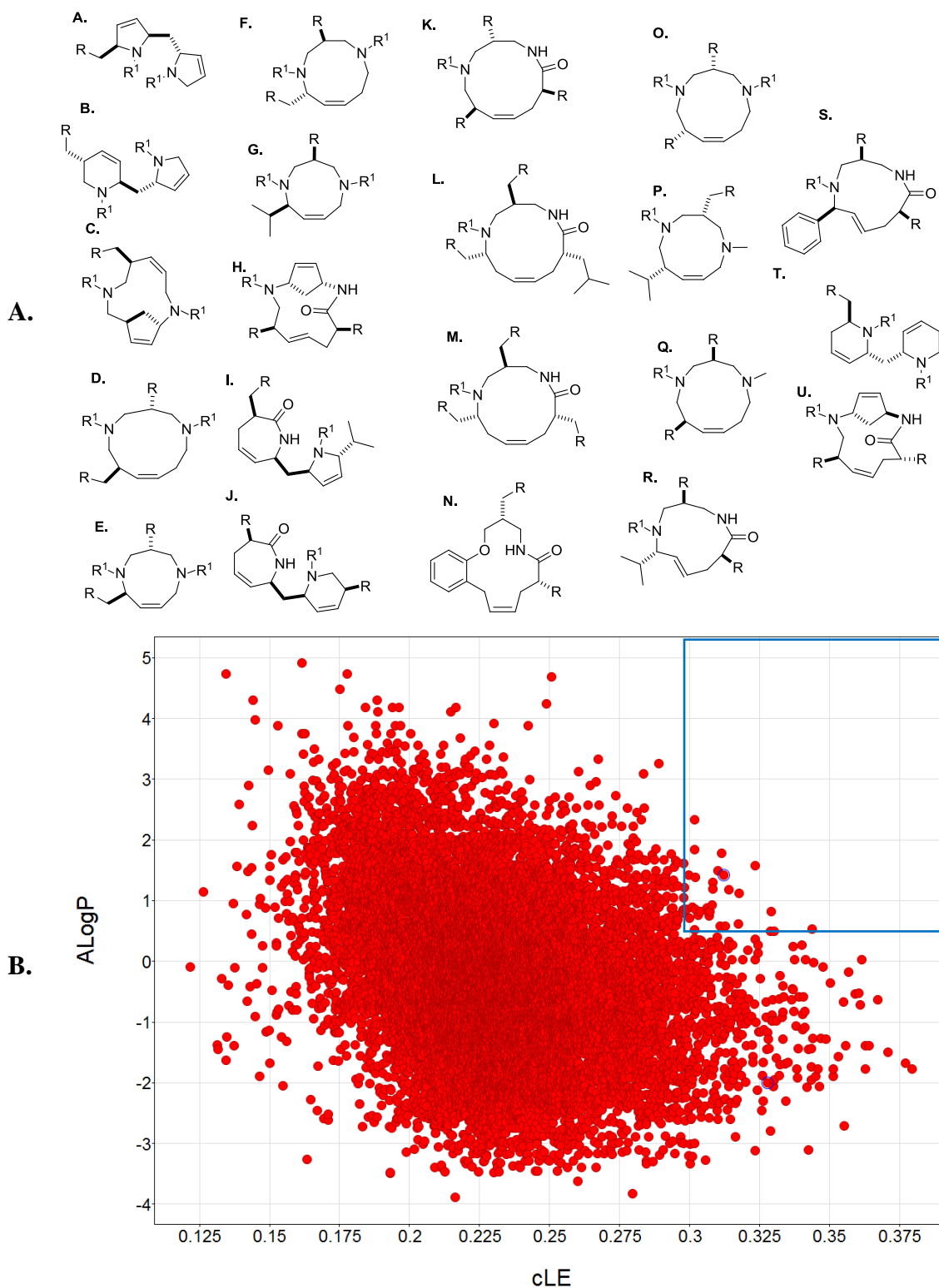


Figure 3.7. Characteristics of a focused library. **A.** Generic representation of the focused library. R and R¹ groups are shown in Appendix 16. **B.** Spread of the eHiTS results for a focused library of 13,159 molecules with respect to the predicted ligand efficiency (cLE) and the predicted hydrophobicity (ALogP). The box represents those molecules with cLE > 0.295 and ALogP > 0.5. Red dots represent individual molecules. Graph generated using Vortex (Dotmatics).

A range of selection criteria ($cLE > 0.295$, $A\text{Log}P > 0.5$, $e\text{HiTS} < -7$, $350 \leq \text{M.W.} \leq 500$, Figure 3.8.A) was applied to the focused library in order to ensure the predicted drug-likeness of the molecules. The criteria afforded the identification of 9 potential hRSV fusion inhibitors (Figure 3.8.B). A summary of the predicted non-covalent interactions that the 9 molecules are predicted to make with 3KPE is shown in Table 3.1.

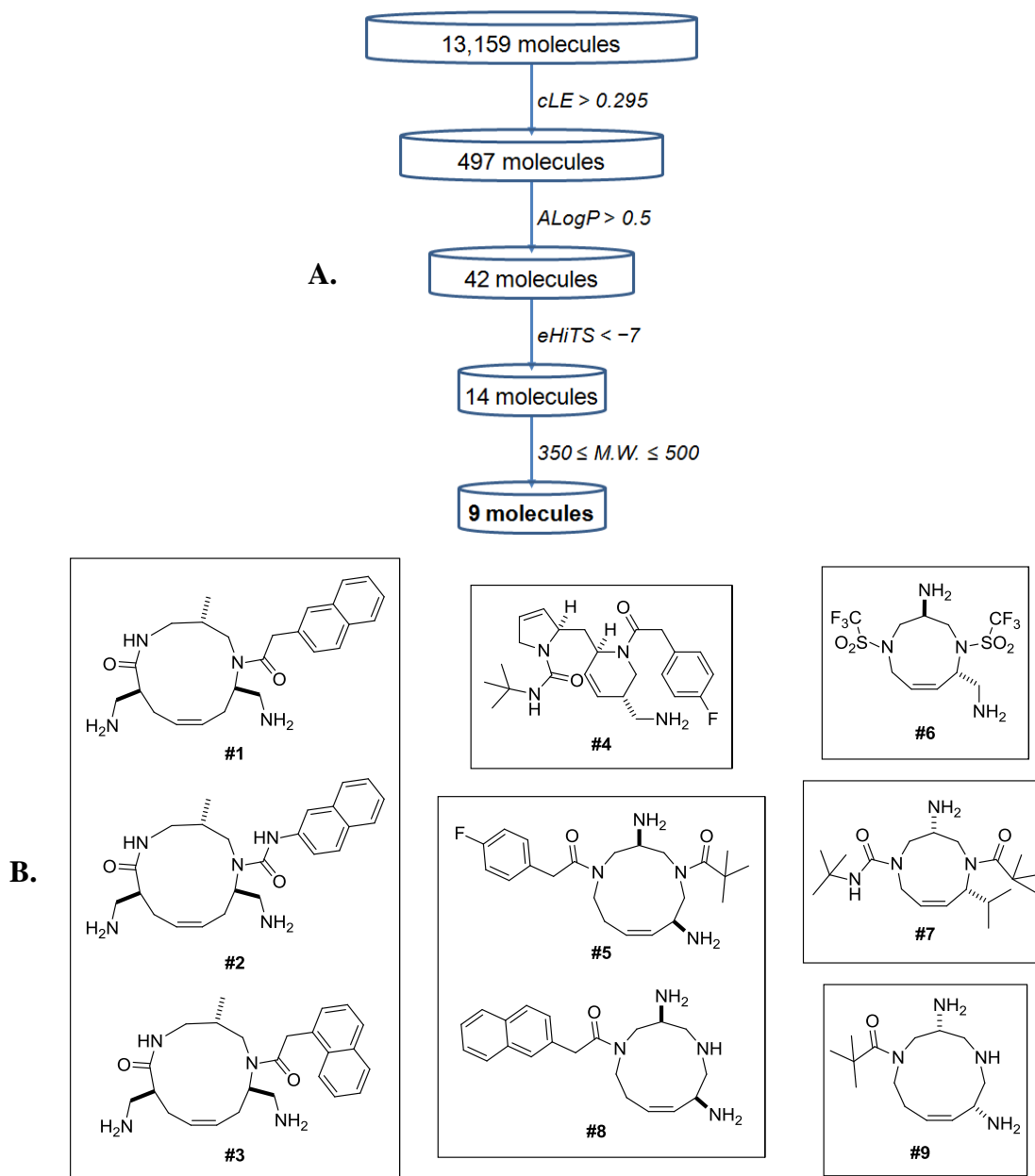
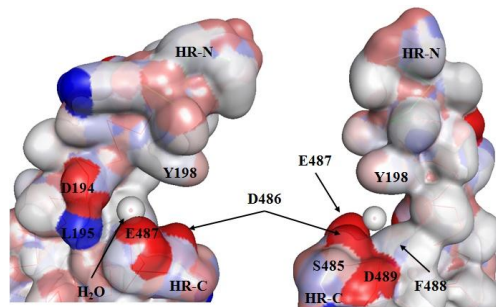


Figure 3.8. Novel series of proposed hRSV fusion inhibitors identified *via* vHTS. **A.** A range of selection criteria was applied in order to select 9 potential hRSV fusion inhibitors. **B.** Representation of the 9 selected molecules (split into 6 series). The numbers correspond to the entry numbers in Table 3.1.

Table 3.1: Summary of the predicted non-covalent interactions between the 9 selected molecules and 3KPE.



Entry	D ₁₉₄	L ₁₉₅	Y ₁₉₈	S ₄₈₅ (OH)	D ₄₈₆ (CO ₂ ⁻)	E ₄₈₇ (CO ₂ ⁻)	D ₄₈₉ (CO ₂ ⁻)	H ₂ O	eHiTS	cLE	ALogP	M.W.
1					√	√	√	√	-9.68	0.31	1.42	423
2				√	√	√	√	√	-9.62	0.31	1.49	424
3					√	√		√	-9.29	0.30	1.42	423
4	√ (CO ₂ ⁻)		√ (π-π)						-9.17	0.30	1.63	429
5				√	√	√			-8.64	0.30	1.61	405
6	√ (C=O backbone)	√				√		√	-7.98	0.31	0.75	434
7			√ (π-σ)					√	-7.85	0.30	2.33	366
8					√		√		-7.75	0.30	1.04	352
9				√	√				-7.69	0.30	1.24	400

√ indicates a predicted interaction with 3KPE.

3.2.4 Free energy minimisation

Two series of molecules (Figure 3.9) were chosen on the basis of the consistency of the binding pose. Members from series 1 are among the best scoring molecules and the virtual hit **16** also appeared as a virtual hit in the virtual screening without the bound water molecule. Series 2 was chosen on the basis of the novelty of the proposed binding pose. Both series underwent a round of rigid free energy minimisation (Section 3.1.5) to observe if the predicted non-covalent interactions would be retained once the molecule has been minimised. In contrast, flexible minimisation resulted in the removal of the bound water molecule from the binding site and was therefore not considered further.

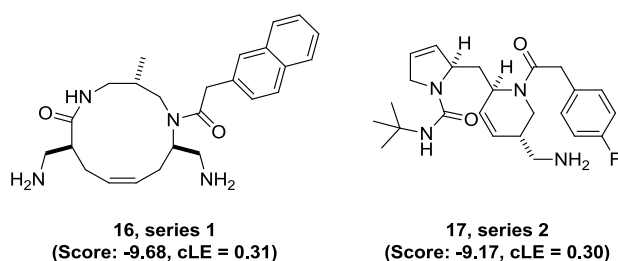


Figure 3.9. Novel series of potential hRSV fusion inhibitors.

3.2.4.1 Free energy minimisation for series 1 and series 2

In the raw predicted binding pose of the proposed inhibitor **16** (Figure 3.10.A), non-covalent interactions are predicted to be made with the bound water, directly with Glu487. Additionally, **16** is predicted to interact with Asp486 and Asp489 (eHiTS = -9.38, cLE = 0.31). After the rigid minimisation step (Figure 3.10.B), only the interaction with the bound water is predicted to be retained (eHiTS = -7.71, cLE = 0.25). The naphthalene group docks in a hydrophobic cavity formed by residues 197-202^{108,116}.

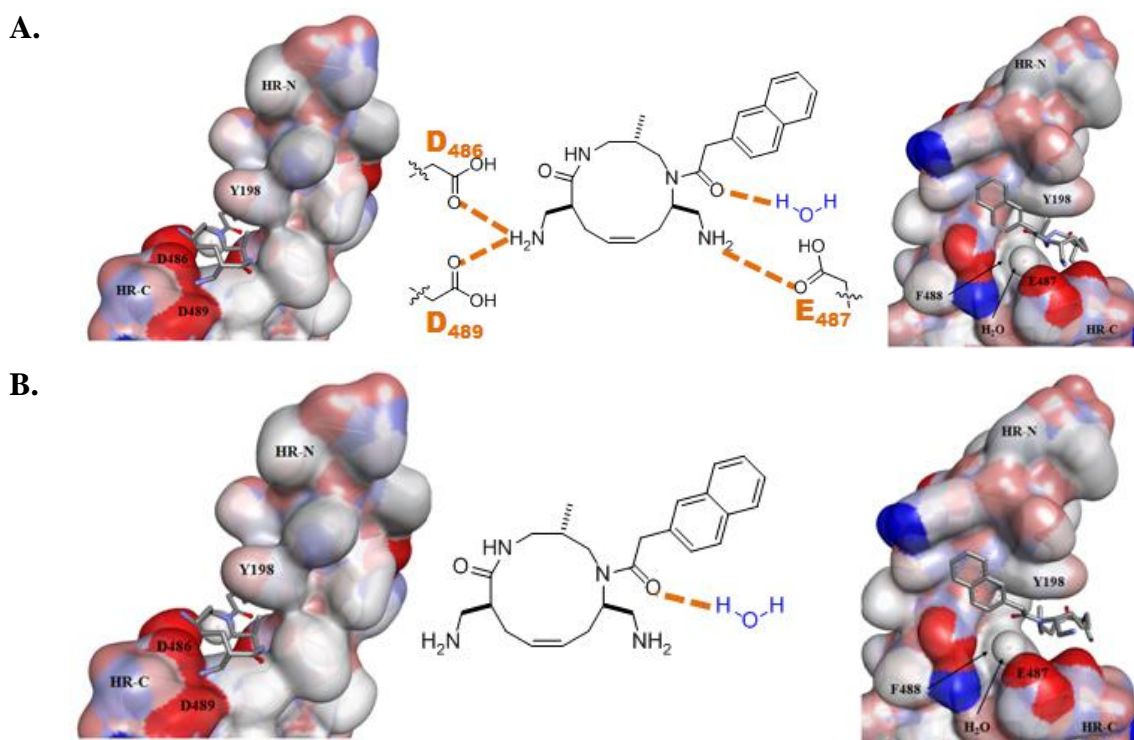


Figure 3.10. Predicted binding poses of the molecule representative of series 1. **A.** Raw binding poses (eHiTS = -9.38 , cLE = 0.31). **B.** Binding pose after rigid minimisation (eHiTS = -7.71 , cLE = 0.25). Pictures generated with Discovery Studio (Accelrys). Two faces of 3KPE are shown.

The raw predicted binding mode of the proposed inhibitor **17** is different to that of the proposed inhibitor **16** (Figure 3.11.A). A hydrogen-bond interaction is predicted with Asp194 (eHiTS = -9.17 , cLE = 0.30). Additionally, the *para*-fluorophenyl ring is predicted to be involved in π - π stacking interaction with Tyr198. After the rigid minimisation step (Figure 3.11B), only the π - π stacking interaction is retained (eHiTS = -8.18 , cLE = 0.26). The backbone of the proposed inhibitor **17** docks in the same hydrophobic cavity as the naphthalene group of the proposed inhibitor **16**.

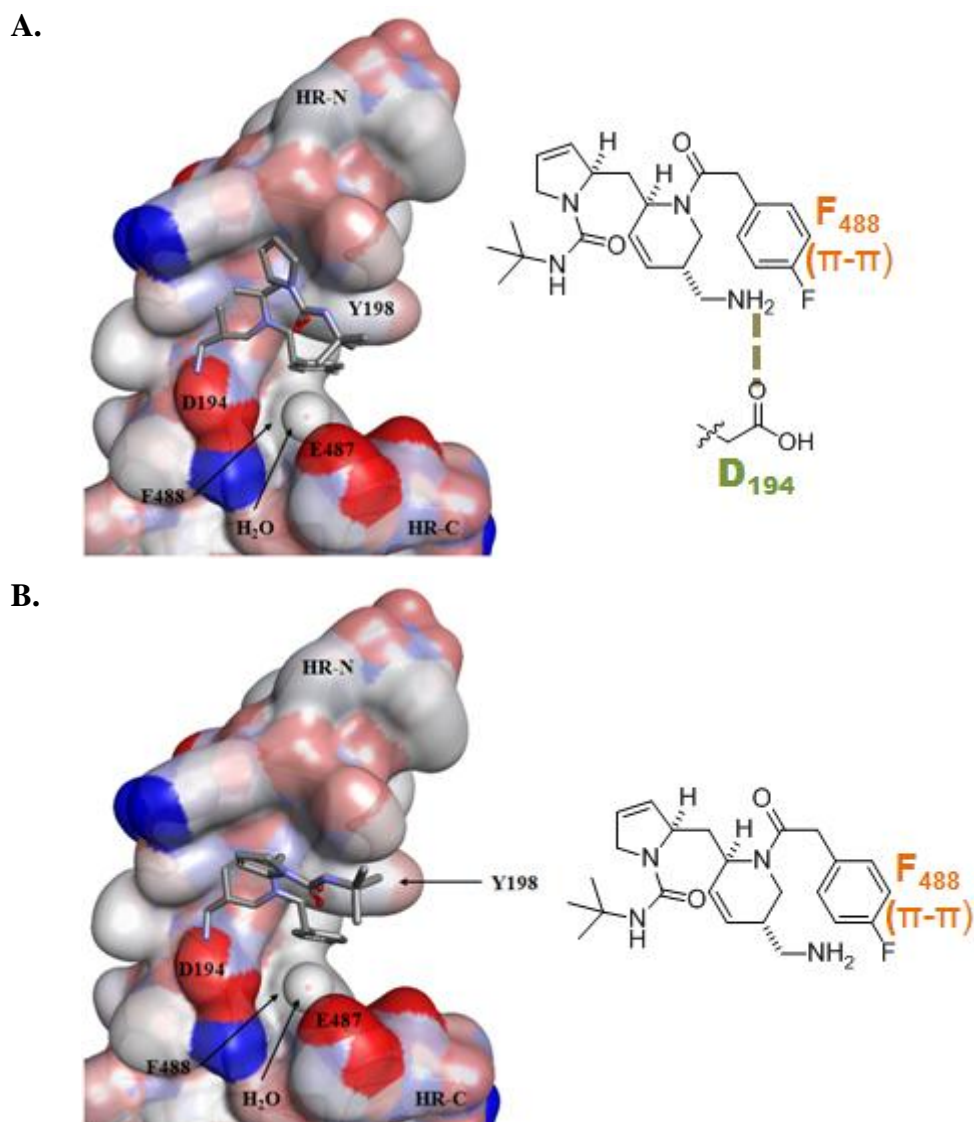
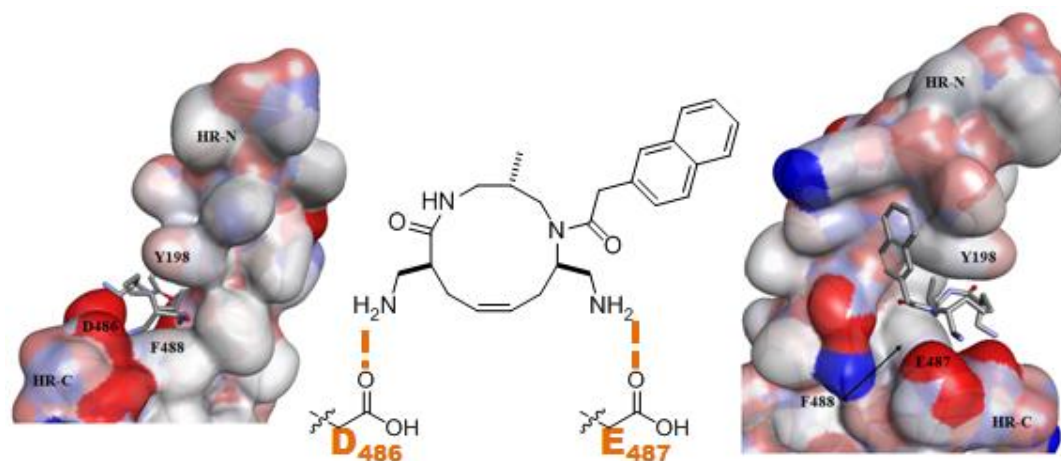


Figure 3.11. Predicted binding poses of the molecule representative of series 2. **A.** Raw binding poses (eHiTS = -9.17 , cLE = 0.30). **B.** Binding pose after rigid minimisation (eHiTS = -8.18 , cLE = 0.26). Pictures generated with Discovery Studio (Accelrys).

3.2.4.2 Free energy minimisation using the cavity without the bound water molecule

The representative member of series 1 was also screened virtually against the binding cavity without the bound water molecule and subsequently underwent rounds of free energy minimisation (Figure 3.12). When screened virtually against the binding cavity without the bound water, series 2 did not appear as a hit.

A.



B.

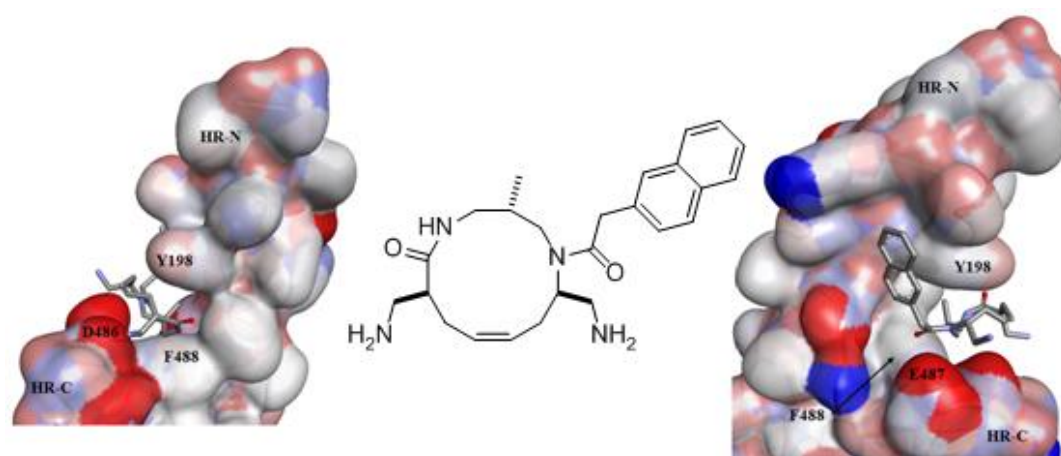


Figure 3.12. Predicted binding poses of the molecule representative of series 1, docked against the cavity without the bound water molecule. **A.** Raw binding poses (eHiTS = -9.35, cLE = 0.30). **B.** Binding pose after rigid minimisation (eHiTS = -7.65, cLE = 0.25). Two faces of 3KPE are shown.

3.3 *In silico* evaluation of a virtual library with lead-like properties

3.3.1 Identification of an additional series of potential hRSV fusion inhibitors

In order to increase the range of series of potential hRSV fusion inhibitors, a new virtual library was exploited. This virtual library had been enumerated by Giorgia Magnatti, a PhD student in the Nelson group, and contained 85,115 molecules that had been filtered for lead-like properties (Table 3.2). A similar approach to that outlined in Section 3.2.1 had been used to enumerate this library. A set of building blocks (see Appendix 17 for the full set of building blocks used) were used to yield a library based on 5-,6- and 7-membered heterocycles using a different toolbox of available virtual reactions (*e.g.* aminoarylation¹⁵⁴, allylic amination¹⁵⁵, metathesis). Representative examples of the virtual library are shown in Figure 3.13.

Table 3.2: Lead-like properties filters applied to a new virtual library

	Filter
Aromatic ring	≤ 2
Saturated ring	> 1
Hydrophobicity	$0.0 \leq A\text{LogP} \leq 3.5$
Heavy atoms	$16 \leq \# \leq 23$

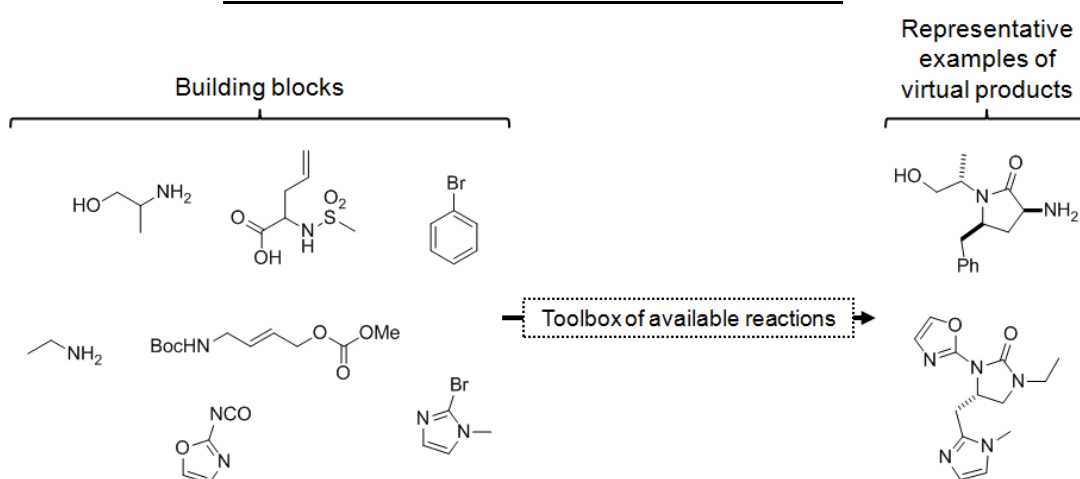


Figure 3.13. Enumeration of a virtual library. A building-block based approach was used for the generation of a virtual library of *ca.* 85,000 molecules. The examples of products shown stem from two possible combinations of the building blocks.

The overall virtual screening approach is summarised in Figure 3.14. George Karageorgis, an MSc student working in the Nelson group, screened *ca.* 13,000 diverse molecules selected from the virtual library against 3KPE with the bound water using eHiTS. This screening resulted in the selection of 7 common substructures amongst those molecules with $cLE > 0.275$. It was decided to extract additional molecules based on these substructures from the virtual library. An additional 13,872 molecules were selected and screened against 3KPE with the bound water using eHiTS. The molecules with $cLE > 0.275$ (141 molecules) were also screened against 3KPE without the bound water; 100 molecules had $cLE > 0.275$ against 3KPE with and without the bound water (Figure 3.15.A). Those molecules were used for the identification of 2 promising scaffolds amongst those molecules with $cLE > 0.30$ (both with and without the bound water): γ -lactams and 5-membered ring cyclic ureas.

Therefore, those scaffolds were targeted in a more focused library with a range of groups corresponding to commercially available reagents (101 aryl / heteroaryl and 80 benzyl bromides). The resulting virtual library of 2,644 molecules was screened against 3KPE with and without the bound water using eHiTS (Figure 3.15.B). The selection of an additional series of potential hRSV fusion inhibitors was carried out in two steps. First, molecules with $cLE > 0.29$ were extracted. Second, George Karageorgis observed that only γ -lactams had $cLE > 0.31$ against 3KPE with and without the bound water. This observation resulted in the selection of γ -lactams as an additional series of potential hRSV fusion inhibitors for further evaluation (virtual hit **18**, series 3, Figure 3.14).

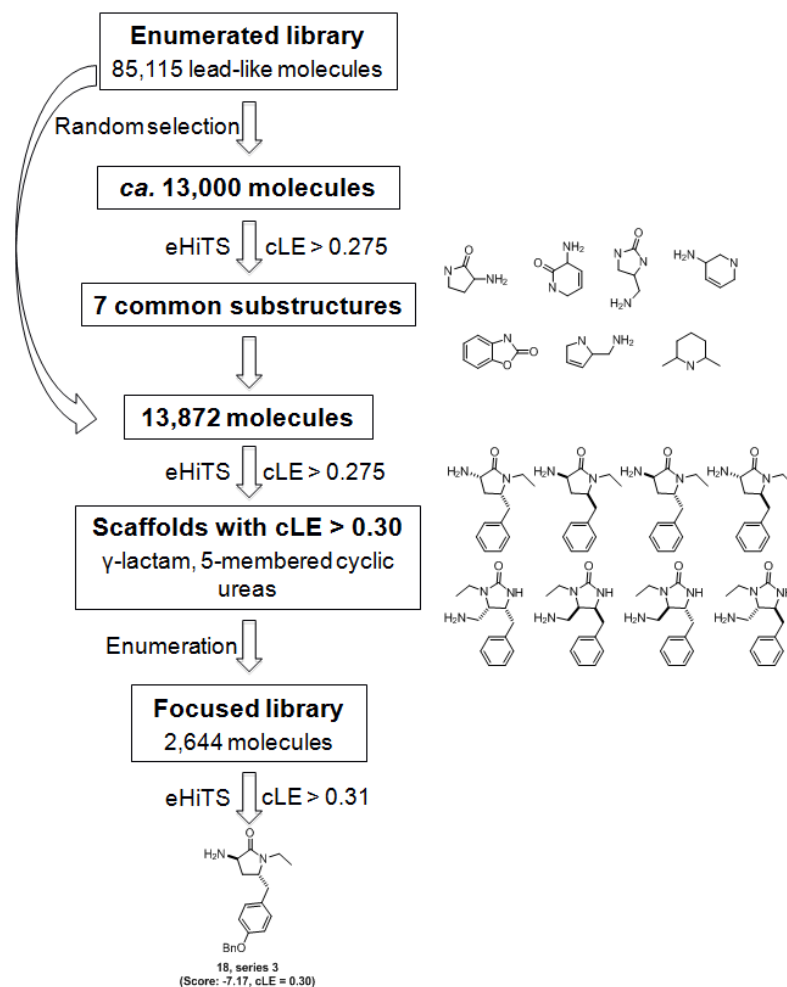


Figure 3.14. Overview of the virtual screening campaign carried out by George Karageorgis. The steps leading to the identification of novel series of potential hRSV fusion inhibitors, from library enumeration to the final selection criteria, are highlighted. A representative member of series 3, potential inhibitor **18** is shown.

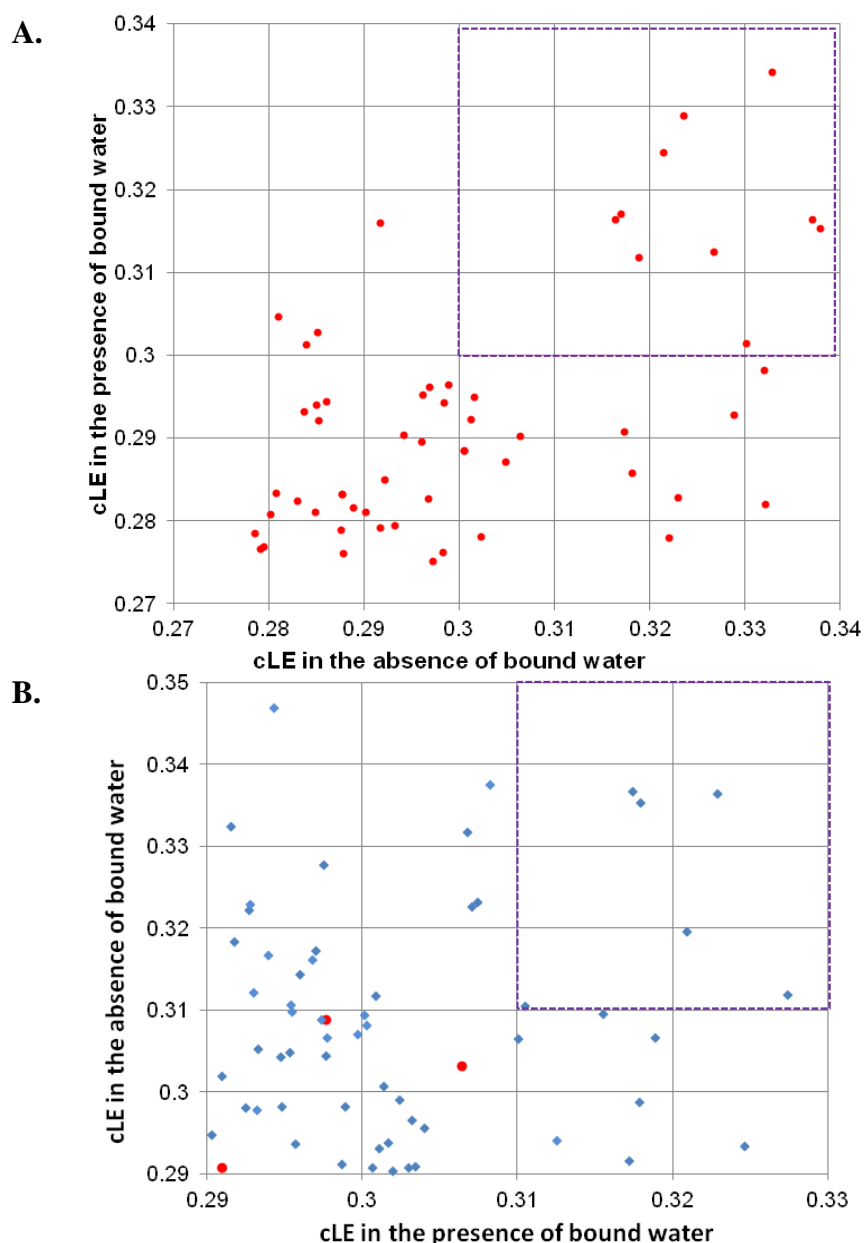


Figure 3.15 Identification of a new series of potential hRSV inhibitors. **A.** Virtual screening of substructure library (13,872 molecules) against 3KPE with the bound water. Molecules with $cLE > 0.275$ were also screened virtually against 3KPE without the water molecule. γ -Lactams and 5-membered ring cyclic ureas had $cLE > 0.3$ (both with and without the bound water). Red dots represent individual molecules. Diagram prepared by George Karageorgis. **B.** Virtual screening of more focused library (2,644 molecules) against 3KPE with and without the bound water. Molecules with $cLE > 0.29$ were extracted. Blue diamond: γ -lactam, red dots: 5-membered cyclic urea. Diagram prepared by George Karageorgis.

3.3.2 Predicted structure-activity relationships using eHiTS

Having identified a novel series of potential hRSV inhibitors, it was decided to understand the predicted structure-activity relationships. This analysis was expected to allow prioritisation of compounds for synthesis within this project.

First, we analysed the predicted binding pose of the virtual hit **18** in more detail (Figure 3.16) after screening **18** against 3KPE with the bound water using eHiTS. The virtual hit **18** was predicted to be involved in a range of non-covalent interactions (Figure 3.16.A): the phenyl ring of the *OBn* group was predicted to fit into a hydrophobic pocket; the phenyl ring at the 5-position was predicted to be involved in π - π stacking interactions with Tyr198 and Phe488; and the amine group at the 3-position was predicted to make ionic interactions with Asp486 and Asp489. Interestingly for **18**, cLE increased from 0.28 to 0.31 upon minimisation (Figure 3.16.B).

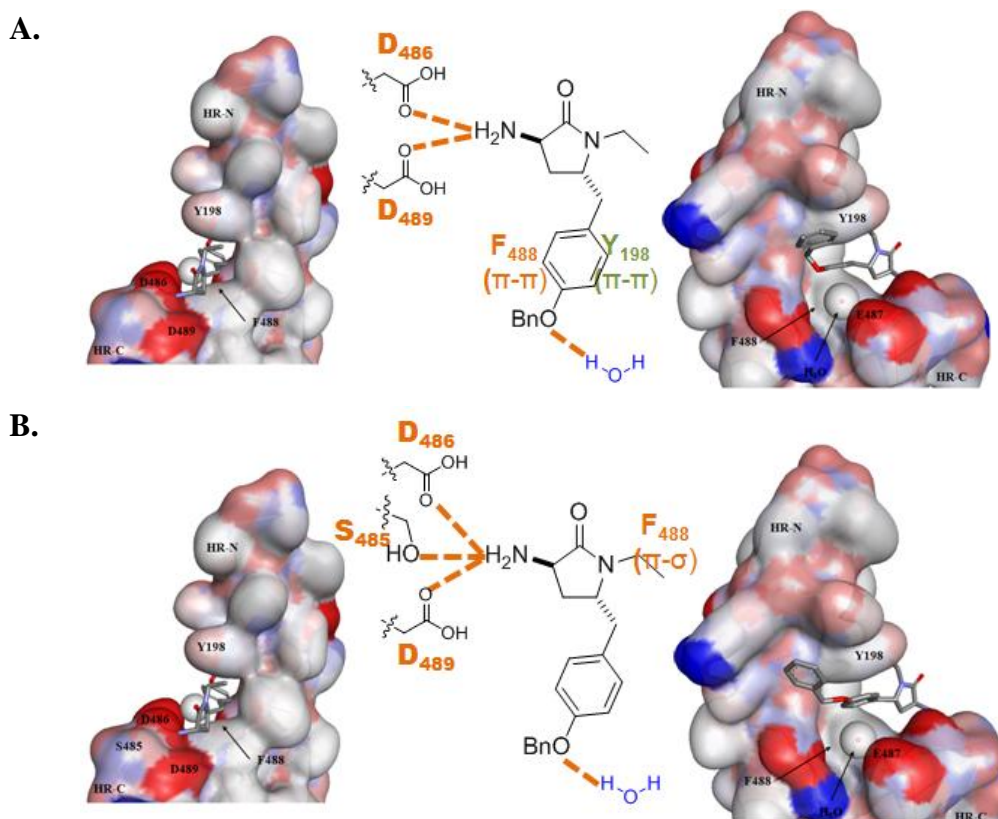


Figure 3.16. Predicted binding poses of virtual hit **18, a representative molecule of series **3**. A. Raw binding poses (eHiTS = -6.74, cLE = 0.28). B. Binding pose after rigid minimisation (eHiTS = -7.42, cLE = 0.31). Pictures generated with Discovery Studio (Accelrys). Two faces of 3KPE are shown.**

With the predicted binding pose of the potential hRSV fusion inhibitor **18** analysed, and accounting for synthetic accessibility, a focused library was designed for synthesis in this project (Figure 3.17.A). The resulting focused library of 48 members was screened against 3KPE with the bound water using eHiTS (Figure 3.17.B). The general conclusion was that the combination of $R = i\text{Pr}$, $R^1 = \text{OBn}$ and $R^2 = \text{NH}_2$ was predicted to yield the best potential inhibitor, with the *trans* diastereoisomer scoring better than the *cis*. The R group had little influence on the eHiTS score except when $R^1 = \text{OBn}$ and $R^2 = \text{NH}_2$. The predicted eHiTS score decreased from $R^2 = \text{NH}_2$ to $R^2 = \text{CO}_2\text{Et}$ (because of the loss of the predicted ionic interaction with the aspartate residues). As the molecules screened virtually become smaller (from $R^1 = \text{OBn}$ to $R^1 = \text{OPr}$ to $R^1 = \text{H}$), the predicted eHiTS score becomes less negative, yet the predicted ligand efficiency increases.

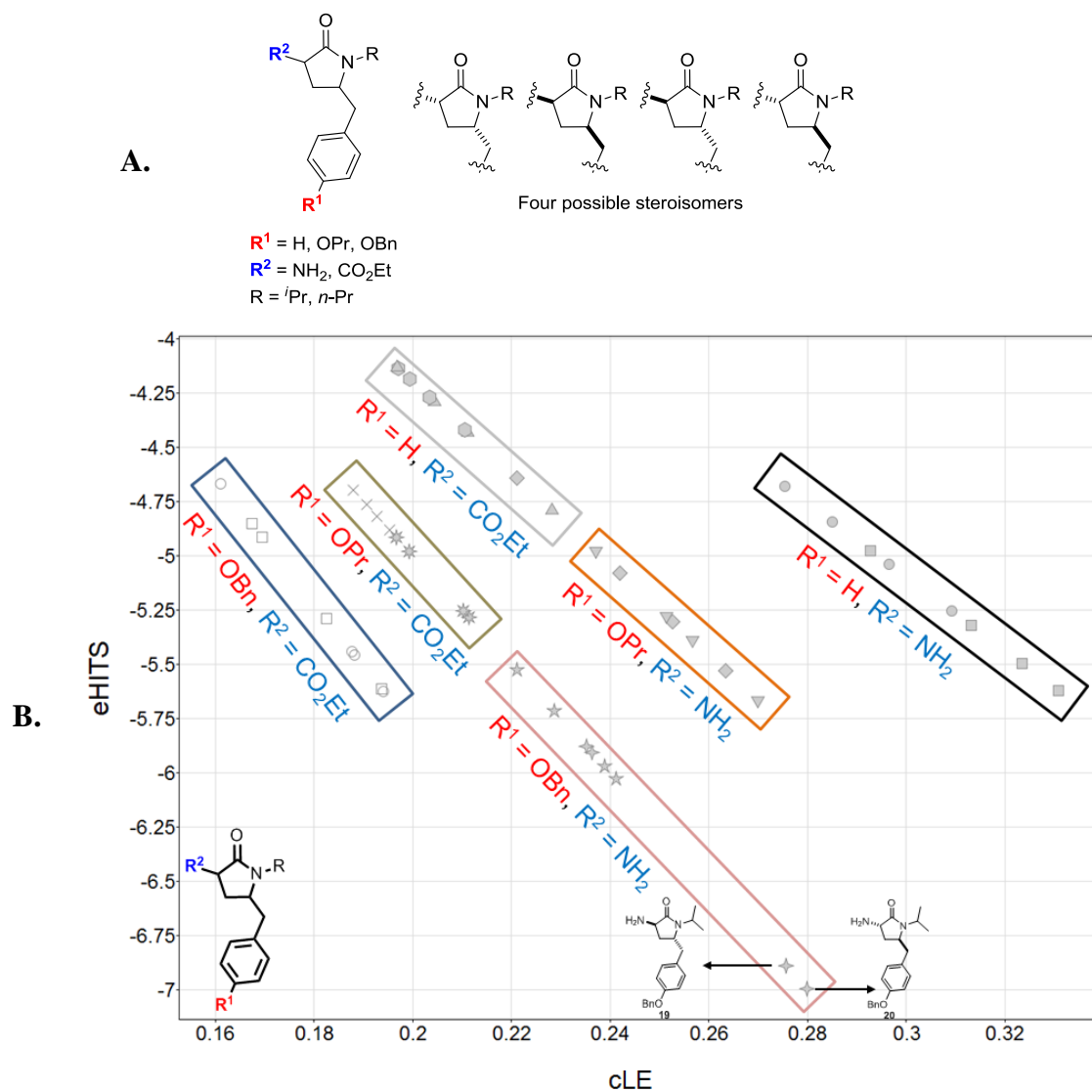


Figure 3.17. Focused library of γ -lactams. **A.** Generic representation of the members of the focused library of inhibitors generated based around the virtual hit **18**. **B.** Predicted structure activity relationships of a focused library of γ -lactams. The 48 compounds are split into 6 groups of 8 molecules: 4 stereoisomers, 2 possible R groups ($R = \text{}^i\text{Pr}$ and $R = n\text{-Pr}$), resulting in two different symbols per group. Graph generated using Vortex (Dotmatics).

The results from the virtual screening of the focused library against 3KPE with the bound water molecule have helped to prioritise which compounds to nominate for synthesis. The best scoring molecule from the focused library had $R = i\text{Pr}$. Therefore, this group was chosen as the R group. The predicted fitting into the hydrophobic pocket will be probed by preparing molecules with $R^1 = \text{OBn}$, OPr , H. The predicted ionic interactions with Asp486 and Asp489 will be probed by preparing molecules with $R^2 = \text{NH}_2$, CO_2Et . A summary of the molecules nominated for synthesis is shown in Figure 3.18.

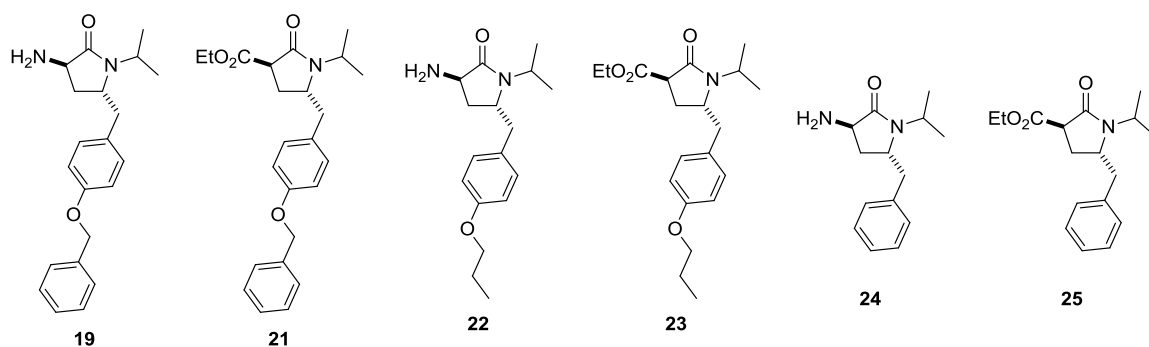


Figure 3.18. Molecules nominated for synthesis

3.4 vHTS on a virtual library of commercially available compounds

After exploring two different libraries of likely synthetically accessible compounds, we turned our attention to virtual libraries of commercially available compounds to identify alternative interesting scaffolds as potential hRSV fusion inhibitors. Thus, a virtual library of 26,493 diverse molecules, prepared by Dr. Richard Foster (School of Chemistry) on the basis that it contained a diverse set of molecules from a range of commercial suppliers (Asinex, ChemBridge, ChemDiv, AMRI, Peakdale Molecular) was used. The molecular properties of the library are shown in Table 3.3.

Table 3.3: Molecular properties for a virtual library of commercially available 26,493 molecules.

Property	Range [min, max]	μ	σ
M.W.	[136, 813]	362	65
logP	[-2.0, 7.2]	3.0	1.2
H-bond acceptors	[0, 9]	3.4	1.3
H-bond donors	[0, 5]	0.9	0.7

The virtual library of 26,493 molecules was screened against 3KPE with the bound water using eHiTS. 55 compounds had $cLE \geq 0.295$ (Figure 3.19.A). 82% of the molecules with $cLE > 0.295$ had a molecular weight below 250 and can be considered as fragments (Figure 3.19.B). The predicted binding poses of the highest scoring ligand with a $cLE \geq 0.295$ (eHiTS = -7.43, $cLE = 0.30$) is shown in Figure 3.19.C. The highest scoring ligand with $cLE \geq 0.3$ (virtual hit **26**) was predicted to make a hydrogen bond interaction with Asp194. Thus, 55 compounds were nominated for biological evaluation (Chapter 5).

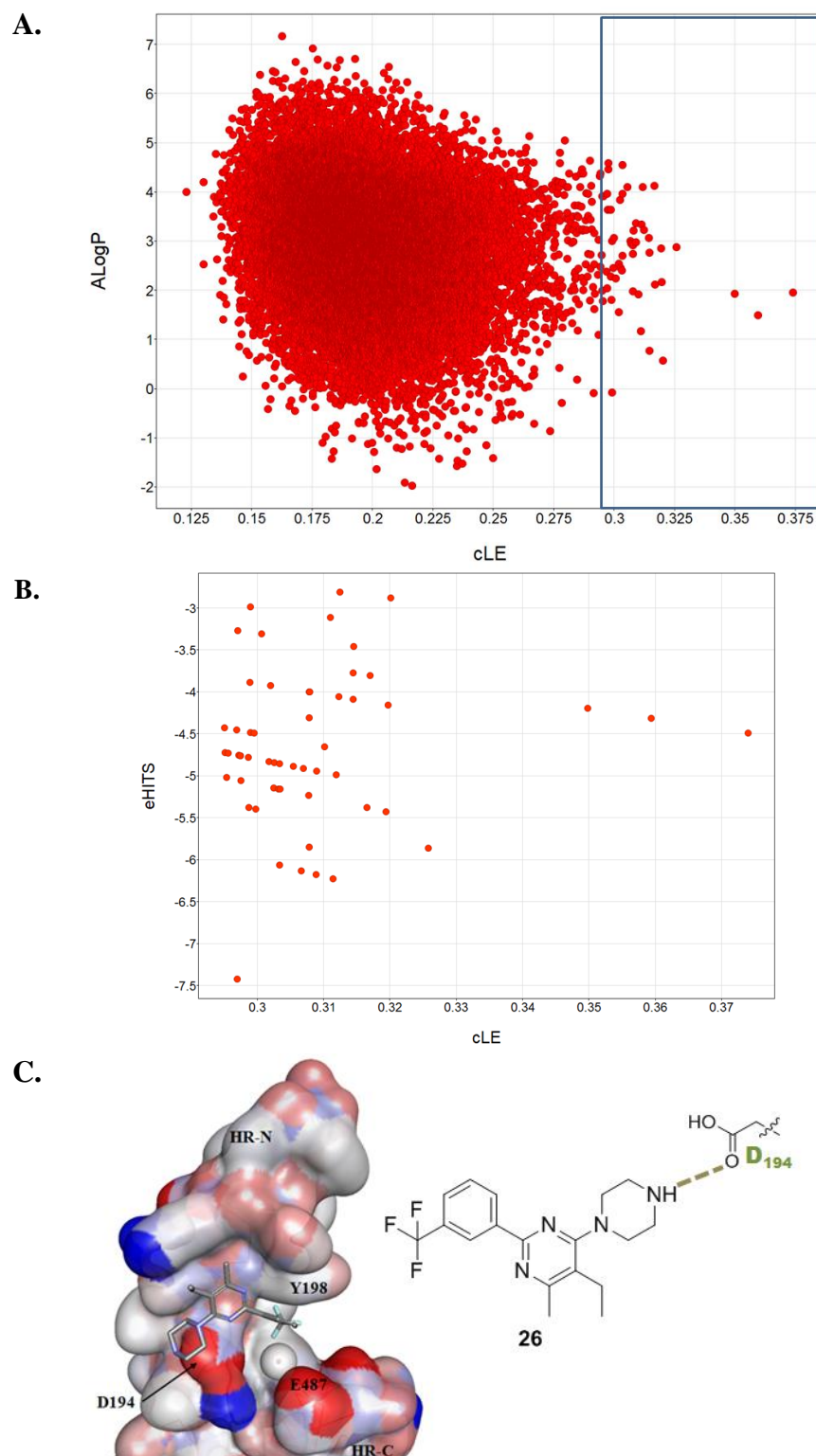


Figure 3.19. eHiTS results for a virtual library of commercially available compounds (26,493 molecules. A. Each molecule, shown by a red dot, is represented by its predicted ligand efficiency (cLE) and its predicted hydrophobicity (ALogP). The blue box represents those molecules with $cLE > 0.295$. Graph generated using Vortex (Dotmatics). **B.** Spread of the properties for the 55 molecules identified with $cLE > 0.295$. Red dots represent individual molecules. Graph generated using Vortex (Dotmatics). **C.** Predicted binding pose of the top-scoring molecule (virtual hit **26**) amongst the most ligand efficient molecule ($eHiTS = -7.43$, $cLE = 0.30$). Pictures generated with Discovery Studio (Accelrys).

3.5 Summary

The binding cavity of a known small molecule inhibitor to hRSV (TMC353121) was targeted using *in silico* methods and virtual libraries of likely synthetically accessible and commercially available compounds. The vHTS campaign described in the present Chapter has led to the discovery of three potential series of hRSV fusion inhibitors.

In order to achieve this, two different libraries of likely synthetically accessible compounds were enumerated. The virtual library enumeration was based on sets of building blocks and reliable synthetic reactions. After iterative rounds of virtual screening against 3KPE using eHiTS and property evaluation, three new series of potential hRSV fusion inhibitors were identified following this process.

Molecules from series 1-3 (Figure 3.20) were nominated for synthetic studies which will be discussed in Chapter 4. The 55 commercial compounds with cLE > 0.3 were purchased and nominated for biological testing which will be discussed in Chapter 5.

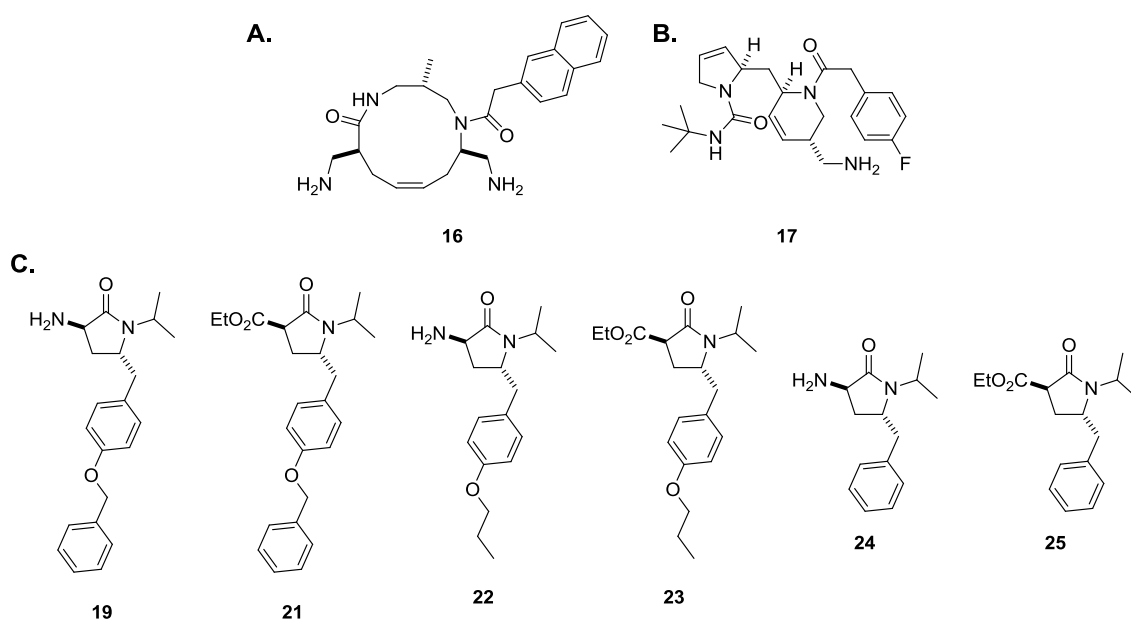


Figure 3.20. Series of molecules nominated for synthetic studies. **A.** Illustrative molecule from series 1. **B.** Illustrative molecule from series 2. **C.** Specific examples of molecules from series 3.

4 STUDIES TOWARDS THE SYNTHESIS OF POTENTIAL HRSV FUSION INHIBITORS

This Chapter describes the studies directed towards the synthesis of three series of potential hRSV fusion inhibitors (Figure 4.1). The common retrosynthetic analysis will be described in Section 4.1; the synthetic studies towards the preparation of the potential hRSV fusion inhibitors are outlined in Sections 4.2 and 4.3; and the synthesis of a focused library of potential inhibitors is discussed in Section 4.4.

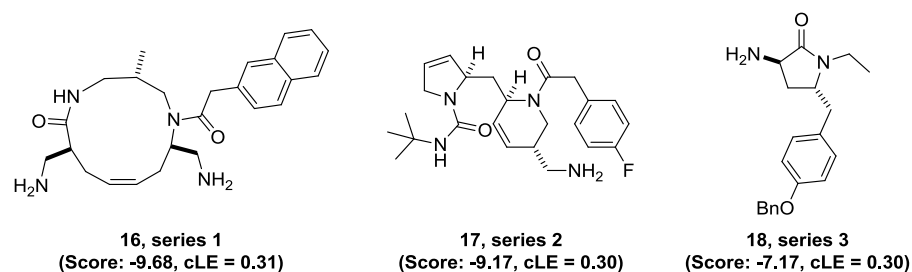
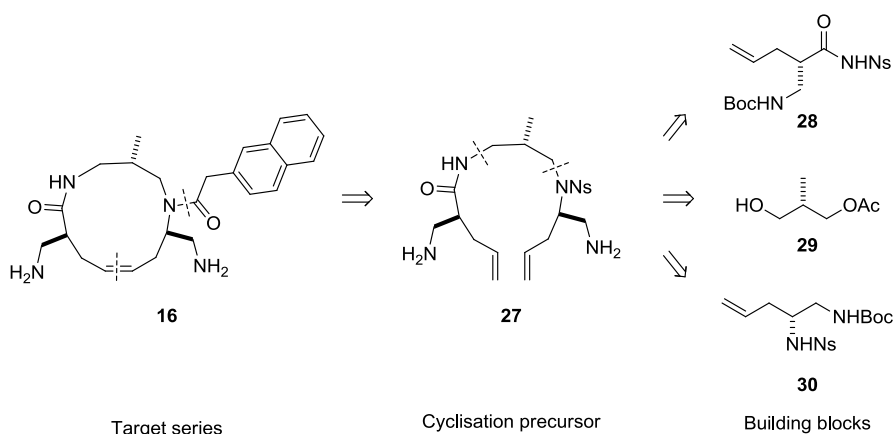


Figure 4.1. Examples of compounds from three series of potential hRSV F protein inhibitors.

4.1 Retrosynthetic analyses

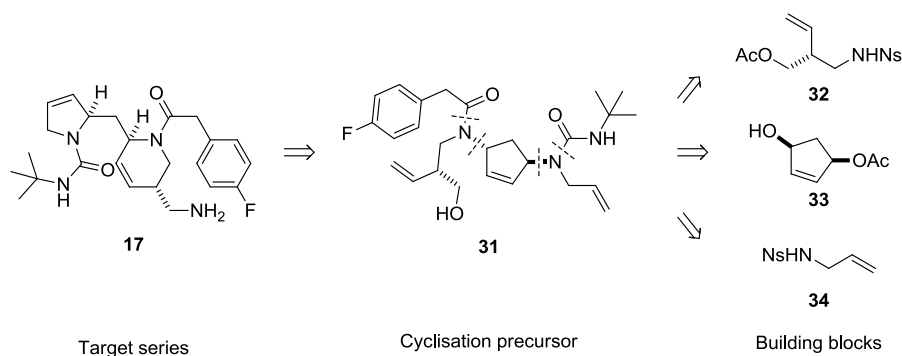
It was proposed that each of the series of molecules might be prepared using a building block-based approach. In each case, the retrosynthetic analysis yielded a cyclisation precursor which would be prepared from the appropriate building blocks.

It was envisaged that the proposed fusion inhibitor **16** might be prepared using the approach outlined in Scheme 4.1. It was proposed to exploit a ring-closing metathesis (RCM) reaction of the cyclisation precursor **27**. The RCM precursor **27** would be prepared by linking building blocks **28-30** using Fukuyama–Mitsunobu¹⁵⁶ reactions.



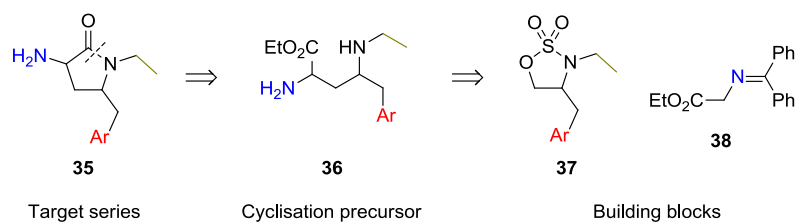
Scheme 4.1 Retrosynthetic analysis of ligand 16, a representative compound from vHTS series 1. Ns = 2-nitrobenzenesulfonyl, Boc = *tert*-butyloxycarbonyl.

It was envisaged that the proposed fusion inhibitor **17** might be prepared using the approach outlined in Scheme 4.2. It was proposed to exploit a metathesis cascade reaction of the precursor **31**. The precursor **31** would be prepared by linking building blocks **32-34** using a palladium catalysed allylic amination^{157,158} and a Fukuyama–Mitsunobu reaction. The combination of these reactions should yield a *trans*-substituted cyclopentene (**31**) from the *cis*-substituted building block (**33**).



Scheme 4.2 Retrosynthetic analysis of ligand 17, a representative compound from vHTS series 2.

It was envisaged that the proposed fusion inhibitor **18** might be prepared using the approach outlined in Scheme 4.3. It was proposed that the γ -lactam scaffold **35** could be prepared by cyclisation of the precursor **36**, itself prepared by opening of the cyclic sulfamidate **37** with the enolate derived from the glycine imine **38**.



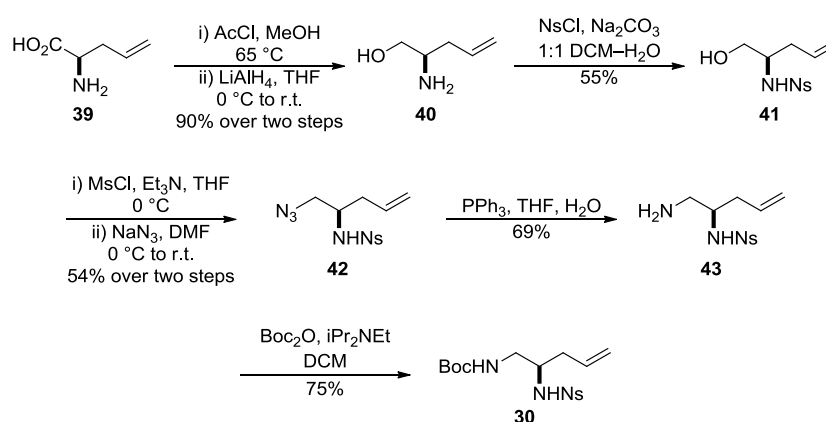
Scheme 4.3. Retrosynthetic analysis of the γ -lactam scaffold **35, a generic representation of series **3**.**

4.2 Synthesis of building blocks required for route development

For each series of ligands, a robust synthetic route was required. This Section describes the synthesis of the building blocks required for these synthetic studies.

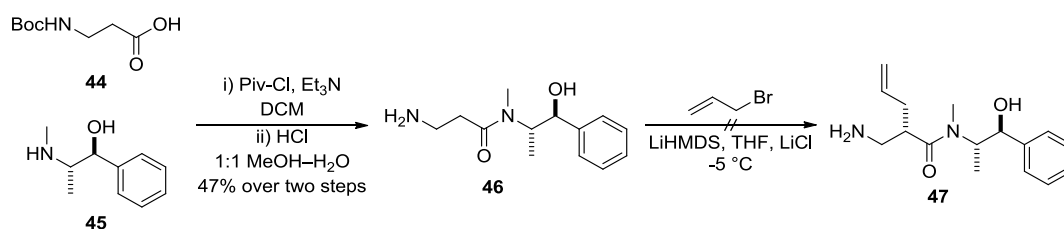
4.2.1 Synthesis of building blocks required for the synthetic studies towards series 1

A seven-step synthetic route was devised for the preparation of the building block **30**, starting from commercially available D-allylglycine **39** (Scheme 4.4) in 14% overall yield. The synthesis started with the formation of D-allylglycine methyl ester by treatment of **39** with methanolic hydrochloric acid; the resulting methyl ester was then immediately reduced with LiAlH_4 ¹⁵⁹ to give the corresponding amino alcohol **40** in 90% yield over two steps. Subsequent treatment of **40** with 2-nitrobenzenesulfonyl chloride furnished the sulfonamide¹⁵⁶ **41** in 55% yield. The sulfonamide **41** was then treated with methanesulfonyl chloride and triethylamine to provide a mesylate¹⁶⁰ that was immediately treated with sodium azide to give the azide **42** in 54% yield over two steps. The azide **42** was then reduced¹⁶¹ with PPh_3 to afford, after hydrolysis, the amine **43** in 69% yield. Finally, the amine **43** was protected by treatment with di-*tert*-butyl dicarbonate and Hünig's base¹⁶² to afford the building block **30** in 75% yield.



Scheme 4.4. Synthesis of the building block **30**.

It was envisaged that the synthesis of the building block **28** could start with the formation of the amide **46** (Scheme 4.5). First, a mixed anhydride¹⁶³ was formed between Boc- β -alanine **44** and pivaloyl chloride, which was treated with (+)-pseudoephedrine **45**¹⁶⁴; the resulting crude amide was immediately treated with hydrochloric acid in methanol–water to afford the amide **46** in 47% yield over two steps. Unfortunately, treatment¹⁶⁵ of the amide **46** with LiHMDS and subsequent allylation was unsuccessful. As a consequence, the synthesis of building block **28** was abandoned.

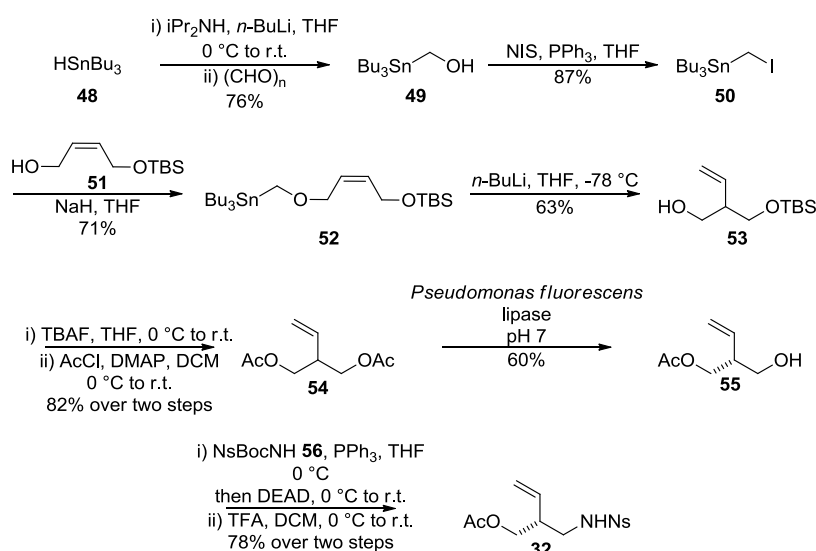


Scheme 4.5. Attempted synthesis of the building block 28. Piv = *tert*-butyl-CO, LiHMDS = lithium bis(trimethylsilyl)amide.

Only one of the three building blocks (**30**) required for the preparation of the RCM precursor **27** was successfully prepared. Accordingly, the synthesis of series 1 was discontinued.

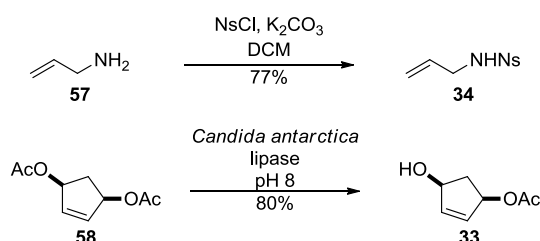
4.2.2 Synthesis of building blocks required for the studies towards series 2

The building block **32** was prepared in nine steps from *cis*-2-butene-1,4-diol in 11% overall yield. The synthesis involved the preparation of the alkene **53**, a key intermediate whose synthesis has previously been described by Carreira *et al.*¹⁶⁶ (Scheme 4.6). The synthesis started with the lithiation of tributyltin hydride **48**, by treatment with lithium diisopropylamide, and subsequent reaction with paraformaldehyde to give the alcohol **49** in 76% yield. The alcohol **49** was then treated with *N*-iodosuccinimide and PPh₃ to give the iodide **50**¹⁶⁷ in 87% yield. Subsequent nucleophilic substitution by a sodium anion of the alcohol **51** furnished the stannane **52** in 71% yield. The stannane **52** was then treated with *n*-butyllithium, leading to a [2,3]-sigmatropic rearrangement^{168,169} to yield the alkene **53** in 63% yield. Silyl ether deprotection, by treatment with tetra-*n*-butylammonium fluoride (TBAF), and immediate treatment with acetyl chloride, provided the diacetate **54** in 82% yield over two steps. The diacetate **54** was desymmetrised by treatment with *Pseudomonas fluorescens* lipase^{170,171} following a known literature procedure with established stereoselectivity (90% e.e.¹⁷¹) to give the hydroxyacetate **55** in 60% yield. Subsequent treatment of **55** with *N*sBocNH **56**, PPh₃, and diethyl azodicarboxylate (DEAD), followed by Boc deprotection, afforded the building block **32** in 78% over two steps.



Scheme 4.6. Synthesis of the building block 32. NIS = *N*-iodosuccinimide, DMAP = 4-dimethylaminopyridine, TFA = trifluoroacetic acid.

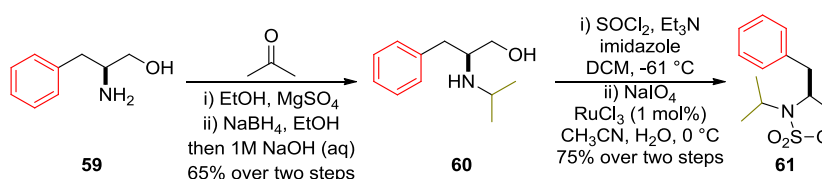
The other required building blocks were prepared in a single step from commercially available materials (Scheme 4.7). The preparation of the sulfonamide **34** was achieved from allylamine by treatment with¹⁷² 2-nitrobenzenesulfonamide and potassium carbonate in 77% yield. *cis*-3,5-Diacetoxy-1-cyclopentene was desymmetrised¹⁷³ by treatment with *Candida Antarctica* lipase following a known literature procedure with established stereoselectivity (>99% e.e.¹⁷³) to afford the hydroxyacetate **33** in 80% yield.



Scheme 4.7. Preparation of the sulfonamide **34** and the hydroxyacetate **33** building blocks.

4.2.3 Synthesis of building blocks required for the synthetic studies towards series 3

The building block **61** was prepared in four steps from L-phenylalaninol **59** in 48% overall yield (Scheme 4.8). The synthesis started with the reductive amination¹⁷⁴ of L-phenylalaninol using propan-2-one and MgSO₄. The resulting imine was then immediately reduced with NaBH₄ to give the corresponding *N*-isopropyl amino alcohol **60** in 65% yield over two steps. The amino alcohol **60** was then treated with thionyl chloride¹⁷⁵ in the presence of triethylamine and imidazole; the resulting cyclic sulfamidite, which was not isolated, was then oxidised by treatment with sodium periodate and 1 mol% RuCl₃¹⁷⁶ to give the corresponding cyclic sulfamidate **61**.



Scheme 4.8. Preparation of the cyclic sulfamidate building block **61** from L-phenylalaninol **59**.

4.3 Synthetic studies towards potential hRSV fusion inhibitors

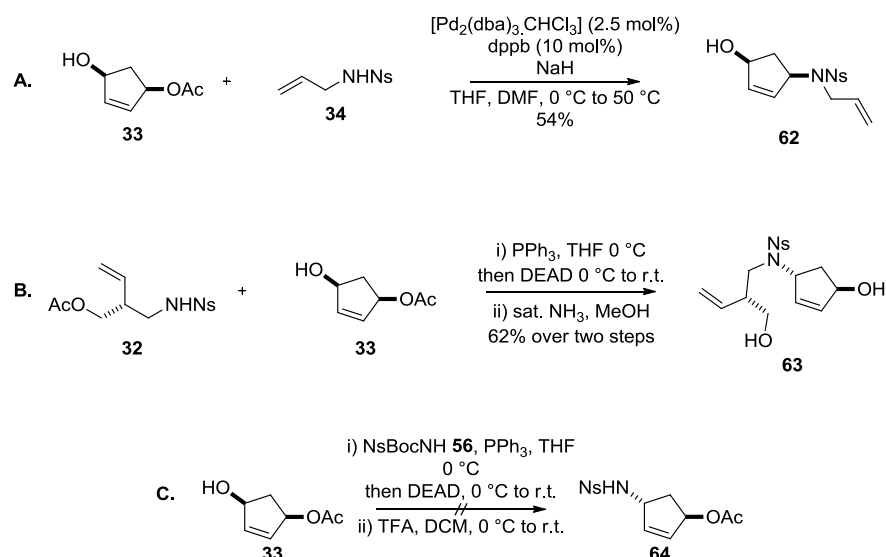
For each full set of building blocks, approaches for the preparation of potential hRSV fusion inhibitors were investigated. This Section describes reactions undertaken to link the requisite building blocks.

4.3.1 Synthetic studies towards series 2

Upon completion of the syntheses of the three key building blocks required for the preparation of the proposed inhibitor **17**, a representative compound from vHTS series 2, reactions to link the building blocks were investigated. Specifically, palladium-catalysed allylic amination and Fukuyama–Mitsunobu reactions were investigated.

4.3.1.1 Initial linking strategies

It was envisaged that the preparation of the cyclisation precursor **31** could start by the palladium-catalysed allylic amination between building blocks **33** and **34** (Scheme 4.9.A), leading to the formation of the diene **62** in 54% yield. Alternative synthetic pathways were also envisaged (Schemes 4.9.B and 4.9.C). First, the building blocks **32** and **33** were treated with PPh₃ and DEAD; the resulting sulfonamide was immediately treated with ammonia in methanol to give the sulfonamide **63** in 62% over two steps (Scheme 4.9.B). Second, the hydroxyacetate **33** was treated with NsBocNH **56**, PPh₃, and DEAD, followed by Boc deprotection (Scheme 4.9.C). Unfortunately, in this case the sulfonamide **64** was not isolated.

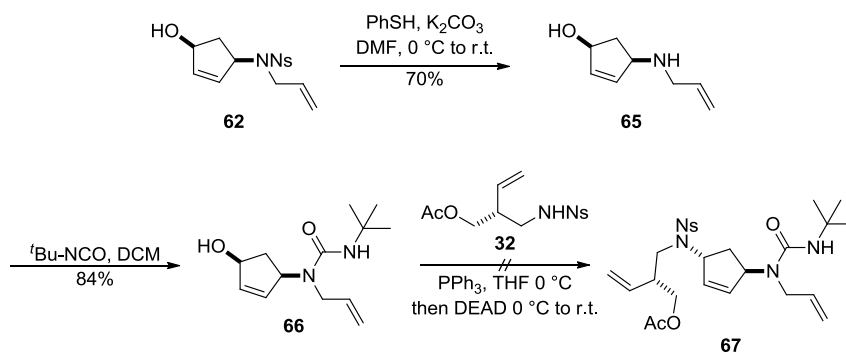


Scheme 4.9. Investigation into reactions for linking the required building blocks.

A. Palladium-catalysed allylic amination between building blocks **33** and **34**. dba = dibenzylideneacetone, dppb = 1,4-bis(diphenylphosphino)butane.
B. Fukuyama–Mitsunobu reaction between building blocks **32** and **33**.
C. Transformation of the building block **33** into a nucleophile for Fukuyama–Mitsunobu reaction.

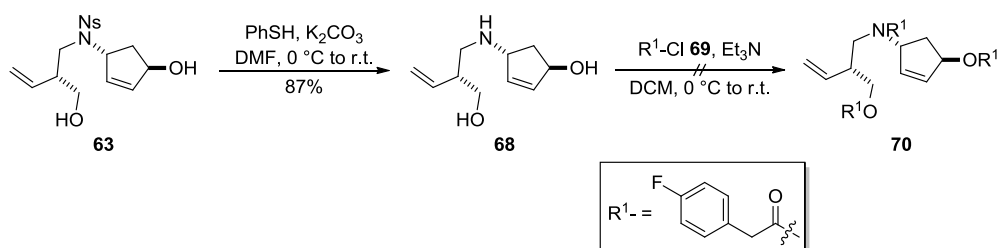
4.3.1.2 Synthetic studies towards the cyclisation precursor **31**

The adduct **62** was treated with thiophenol and potassium carbonate to give the amino alcohol **65** in 70% yield (Scheme 4.10). Treatment of the amino alcohol **65** with *tert*-butyl isocyanate afforded the allylic alcohol **66** in 84% yield. Unfortunately, the reaction between the allylic alcohol **66** and the sulfonamide **32** with PPh₃ and DEAD did not afford the triene **67**: instead, the building block **32** was recovered after purification.



Scheme 4.10. Investigation into a Fukuyama–Mitsunobu reaction to link the required building blocks.

In the case of the Fukuyama–Mitsunobu adduct, the resulting sulfonamide **63** underwent Ns deprotection¹⁵⁶, by treatment with thiophenol and potassium carbonate, to give the aminodiol **68** in 87% yield (Scheme 4.11). Unfortunately, treatment of the aminodiol **68** with an excess of 4-fluorophenylacetyl chloride **69** did not afford the diester **70**.

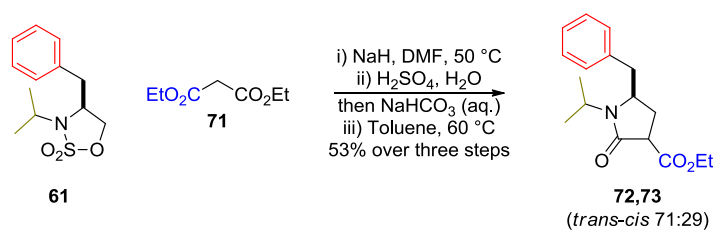


Scheme 4.11. Synthetic pathway involving the Fukuyama–Mitsunobu adduct **63**.

Two routes were investigated for the preparation of the cyclisation precursor **31**: palladium-catalysed allylic amination followed by Fukuyama–Mitsunobu reaction (Scheme 4.10) or Fukuyama–Mitsunobu reaction followed by palladium catalysed-allylic amination (Scheme 4.11). Unfortunately, neither synthetic route could be completed. Accordingly, the synthesis of series 2 was discontinued.

4.3.2 Synthetic studies towards series 3

Five-membered ring cyclic sulfamidates are prone to nucleophilic opening at the 5-position. Thus, diethyl malonate **71** was treated with sodium hydride and reacted with the cyclic sulfamidate **61** (Scheme 4.12). Acidification, neutralisation and subsequent heating in toluene yielded the γ -lactam **72,73** in 53% overall yield with the following configuration *trans-cis* 71:29 as assigned by nuclear Overhauser spectroscopy (Figure 4.2).



Scheme 4.12. Preparation of the γ -lactam scaffold derived from L-phenylalaninol.

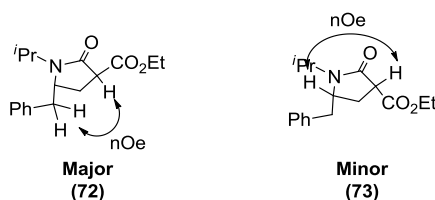


Figure 4.2. Assignment of the major and minor isomers by nuclear Overhauser spectroscopy.

4.4 Synthesis of building blocks required for a focused library of proposed inhibitors

The preparation of a focused library of γ -lactams (virtual hits **19**, **21-25**) was proposed to be possible from the cyclic sulfamidate building block **37** (Scheme 4.3). As outlined in Section 4.2.3, we proposed to derive cyclic sulfamidates from amino alcohols. First, we envisaged to prepare a focused library of proposed γ -lactam inhibitors, based on virtual hits **19**, **21-25**, starting from the racemic amino alcohols **74** and **75** (Figure 4.3).

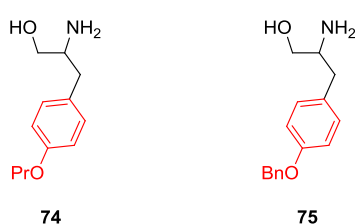
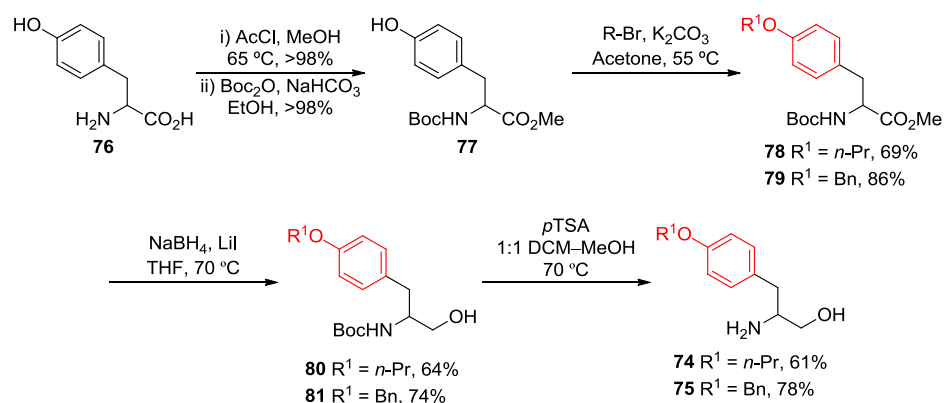


Figure 4.3. Amino alcohols required for the preparation of the cyclic sulfamidates **74** and **75**.

4.4.1 Preparation of DL-O-benzyloxytyrosinol and DL-O-n-propyltyrosinol

Baran *et al.*¹⁷⁷ have established a route for the preparation of L-O-benzyloxytyrosinol in five steps from commercially available L-tyrosine. This route was adapted (Scheme 4.13) for the preparation of DL-O-benzyloxytyrosinol **75** (50% overall yield) and DL-O-n-propyltyrosinol **74** (27% overall yield). The synthesis started with the stepwise protection of DL-tyrosine **76**. First, DL-tyrosine methyl ester (which was not characterised) was formed by treatment with methanolic hydrochloric acid, and was immediately treated with di-*tert*-butyl dicarbonate to yield the carbamate **77** in > 98% over two steps. *O*-Alkylation with benzyl bromide or propyl bromide in the presence of potassium carbonate gave the amino acid derivatives **79**¹⁷⁸ and **78** in 86% yield. The methyl ester of **79** and **78** was then reduced to the corresponding alcohols **81** and **80** by treatment with LiBH₄¹⁷⁹ (generated *in situ* from NaBH₄ and lithium iodide) in 74% yield. The Boc derivative was deprotected with *para*-toluenesulfonic acid^{†††} to afford the *O*-alkylated DL-tyrosinol **75** and **74**.

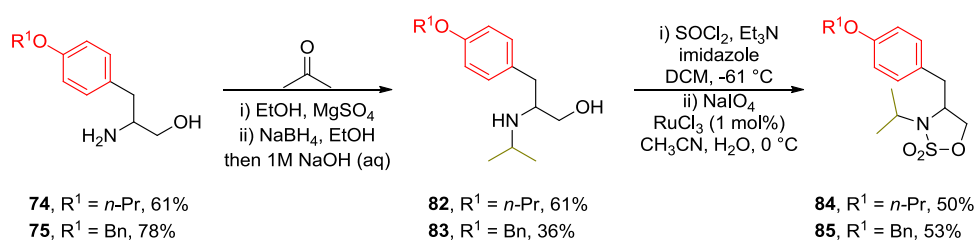
^{†††} When TFA is used, *O*-benzyl deprotection has been observed¹⁷⁹ Oila, M. J., Tois, J. E. & Koskinen, A. M. P. Ligand creation via linking a rapid and convenient method for construction of novel supported PyOX-ligands. *Tetrahedron* **61**, 10748-10756 (2005).



Scheme 4.13. Synthesis of DL-*O*-benzylytyrosinol **75** and DL-*O*-*n*-propyltyrosinol **74**. *p*TSA = *para*-toluenesulfonic acid.

4.4.2 Preparation of the cyclic sulfamidates derived from DL-*O*-benzylytyrosinol and DL-*O*-*n*-propyltyrosinol

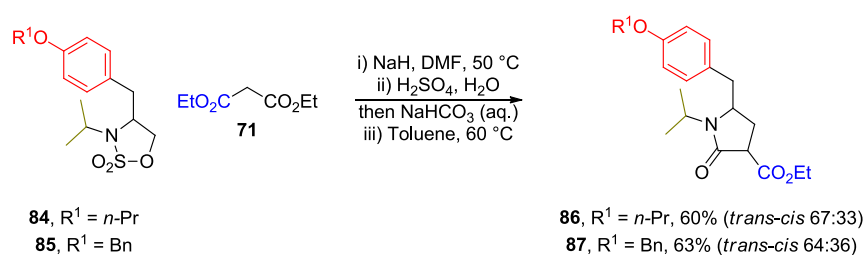
The cyclic sulfamidates **84** and **85** were prepared in three steps from the amino alcohols **74** and **75** (Scheme 4.14). Following the conditions reported in Section 4.2.3, the amino alcohols **74** and **75** successfully underwent reductive amination with propan-2-one and NaBH₄ to yield the corresponding *N*-isopropylated amino alcohols **82** and **83**. Subsequent treatment with thionyl chloride in the presence of triethylamine and imidazole afforded cyclic sulfamidites, which were immediately oxidised to the corresponding cyclic sulfamidates **84** and **85** by treatment with sodium periodate and 1mol% RuCl₃.



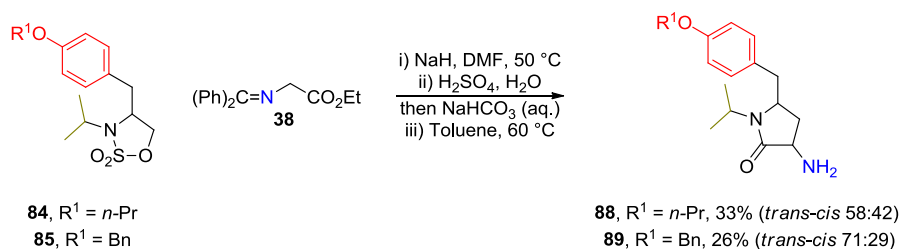
Scheme 4.14. Preparation of the cyclic sulfamidates **84** and **85**.

4.5 Synthesis of a focused library of proposed inhibitors

The γ -lactams were prepared by reaction between a cyclic sulfamidate and an enolate derived from either diethyl malonate **71** or the benzophenone-derived glycine imine **38**. In each case, the pronucleophile was treated with sodium hydride, and reacted with the required cyclic sulfamidate; acidification, neutralisation and subsequent heating in toluene yielded the γ -lactams **86-89**. The results are summarised in Schemes 4.15 and 4.16.



Scheme 4.15. Preparation of the γ -lactams by reaction of cyclic sulfamidates with diethyl malonate **71**.

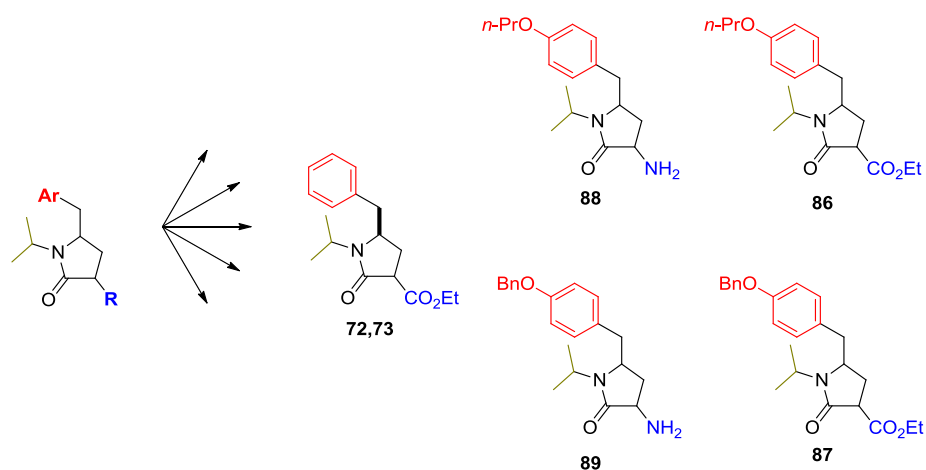


Scheme 4.16. Preparation of the γ -lactams by reaction of cyclic sulfamidates with the benzophenone-derived glycine imine **38**.

4.6 Summary

Retrosynthetic analyses revealed that the potential fusion inhibitors **16-18** might be prepared using a building block-based approach, involving a cyclisation precursor as a key intermediate. The syntheses of the proposed building blocks and the synthetic studies towards the cyclisation precursor, leading up to the proposed hRSV fusion inhibitor have been discussed. For series 1, it was only possible to prepare one of the three required building blocks. For series 2, all three required building blocks were successfully prepared. However, our synthetic studies directed towards linking the required building blocks were unsuccessful.

For series 3, the synthesis of a focused library of the proposed γ -lactams inhibitors was achieved (Scheme 4.17). Three cyclic sulfamidates (**61**, **84** and **85**) were prepared from commercially or synthetically accessible amino alcohols (**59**, **74** and **75**). The cyclic sulfamidates **61**, **84** and **85** successfully underwent nucleophilic opening leading to the corresponding γ -lactams **72,73** and **86-89** (Scheme 4.17). The evaluation of these compounds was expected to allow structure-activity relationships to be defined.



Scheme 4.17. Focused library of γ -lactams.

5 EVALUATION OF SELECTED COMPOUNDS AS INHIBITORS OF HRSV

This Chapter describes the biological evaluation of selected compounds as inhibitors of hRSV. The evaluation of compounds at a single concentration and dose-response analyses of selected hits is discussed in Section 5.1; and the evaluation of the intermediates leading up to JNJ-4749914 is discussed in Section 5.2.

5.1 Biological evaluation at a single concentration

5.1.1 *Choice of a compound collection for HTS*

Initially, we chose to use a HTS approach to find new small molecule inhibitors of hRSV. To date, the distribution of scaffolds amongst known organic compounds is remarkably uneven¹⁸⁰ and could potentially trap drug discovery into small regions of chemical space, that may not be biologically relevant¹⁸¹. One way of increasing the chances of finding actives through HTS would be to use a library that populates broad tracts of biologically-relevant chemical space. A synthetic approach that has been developed within the Nelson group¹⁵⁰ has yielded a library of natural product-like molecules of unprecedented scaffold diversity¹⁵¹⁻¹⁵³. Compounds from this library were screened for anti-hRSV activity (Figure 5.1).

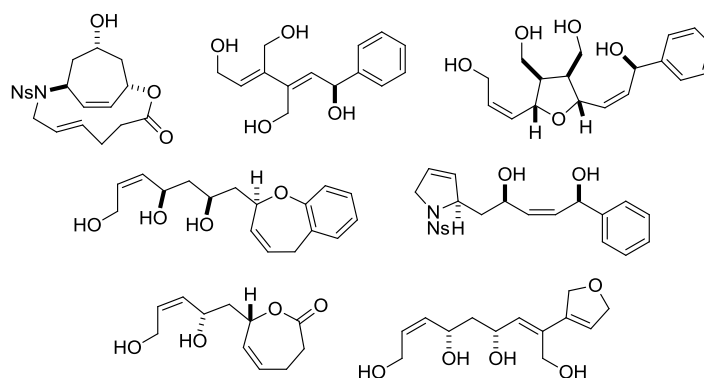


Figure 5.1 Representative examples of a natural product-like library with >80 distinct scaffolds prepared within the Nelson group.

The molecular properties of the library are shown in Table 5.1. Most molecules appear to adhere to the “rule-of-five”: the number of H-bond acceptors increased with the molecular weight and one molecule with molecular weight >500 also had $\log P > 5$. It has been reported¹⁸² that natural products libraries “largely adhere” to Lipinski's rule.

Table 5.1: Molecular property ranges for the natural product-like library screened against hRSV.

Property	Range [min, max]	μ	σ
M.W.	[164, 813]	410	148
logP	[-1.4 ^a , 5.7 ^b]	1.8	1.3
H-bond acceptor	[1, 12 ^c]	5.8	2.6
H-bond donor	[0, 5]	1.2	1.0

a: ten molecules had a negative logP; b: two molecules had $\log P > 5$; c: six molecules had more than 12 HBA groups.

5.1.2 High-throughput screening results

In the Leeds screening collection, compounds are stored as 10 mM solutions in DMSO. As described in Section 2.4.1, the assay setup required a final concentration of 0.25%, meaning that the highest concentration of assay compounds was 25 μ M. A selection of 160 compounds, from the diversity-oriented synthesis screening library was screened against hRSV at 25 μ M. The assay consisted of using a combination of antibodies raised against hRSV and fluorescent antibodies for the detection of virus in cells. Antiviral activity was defined as a decrease in the fluorescence intensity. Unfortunately, activity could be the result of the compounds targeting cellular mechanisms important for cell viability. It was crucial to make sure that activity was the result of the compounds interfering with the course of hRSV, rather than the compound being toxic to cells (*i.e.* false-positive). As such, the compounds were also tested in a cytotoxicity assay (MTT) in order to evaluate their potential toxicity. The results are presented in Figure 5.2. Four compounds are missing from Figure 5.2 as they suffered from ‘aberrant’^{†††} fluorescence. The detailed statistical parameters for each plate are shown in Table 5.2.

^{†††} When observed under the microscope, some wells contained auto-fluorescent particles. Each of these wells was observed under the microscope and, no significant decrease in fluorescence could be observed by eye.

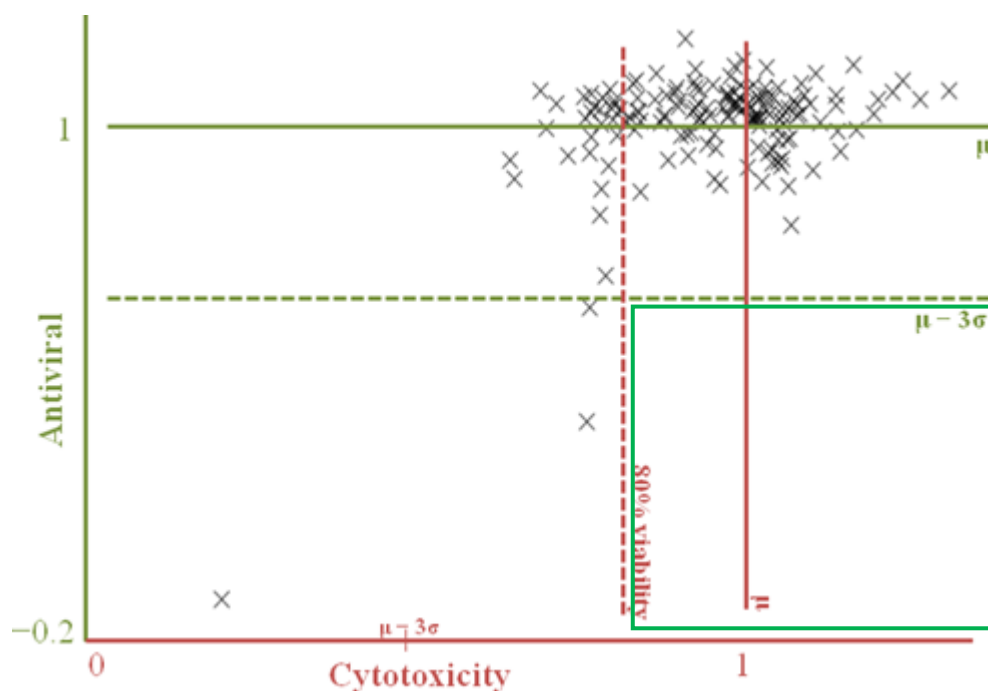


Figure 5.2. Antiviral activity and cytotoxic screen of 160 compounds from the diversity-oriented synthesis library. Each compound was screened at an assay concentration of 25 μM . On the x-axis (cytotoxic screen), the results are presented as a ratio to the untreated control (*i.e.* DMSO at 0.25%, the internal negative control). μ : mean of normalised activity of the 160 compounds ($\mu = 0.96$), σ : standard deviation of the normalised activity of the 160 compounds ($\sigma = 0.14$). Ribavirin was used at 2.5 mM and resulted in 45% cell viability. Also shown is a line representing 80% cell viability. On the y-axis, the results are presented as normalised to the A2 control. The cells were infected at an M.O.I. of 0.5. μ : mean of the normalised activity of the 160 compounds ($\mu = 1.01$), σ : standard deviation of the normalised activity of the 160 compounds ($\sigma = 0.13$). Highlighted by the green box is the ideal quadrant where activity from the screening is not associated with cytotoxicity.

Table 5.2: Statistical analysis for the screening of 160 compounds from Leeds collection carried out in two batches of 80 compounds.

	Plate 1		Plate 2
	Replicate 1 ^a	Replicate 2 ^a	
Signal-to-background	1.85	1.86	1.82
Signal-to-noise	24.23	12.19	14.79
Signal window	36.23	16.83	29.08
Z'-factor	0.81	0.64	0.72
Z-factor	0.59	0.44	0.49

a: the library was split into two batches of 80 compounds, only the first set was screened in duplicate.

The plates did not perform well in terms of Z-factor and signal-to-background ratio (both marginally below the recommended minimum values of 0.5 and 2, respectively). However the Z'-factor was within the acceptable range (> 0.5). The low value for the Z-factor could be explained by the small number of compounds screened, resulting in a high standard deviation when a few hits are observed. The low value for the signal-to-background could be explained by the higher background observed with the 2.5 mM Ribavirin control than with the mock-infected controls. Alternative explanations for the lower-than-expected statistical parameters include a poor batch of antibody or the inherent instability of virus stocks¹²⁴.

For the selection of potential hits, a hit threshold ($\mu - 3\sigma$) was defined and molecules with a normalised anti-viral activity below the hit threshold were marked as potential hits (Figure 5.3). The cytotoxic screen revealed that the three potential hits also had an effect on mitochondrial activity (<80% cell viability). The dose-response analyses of the three hits are discussed in Section 5.1.5.

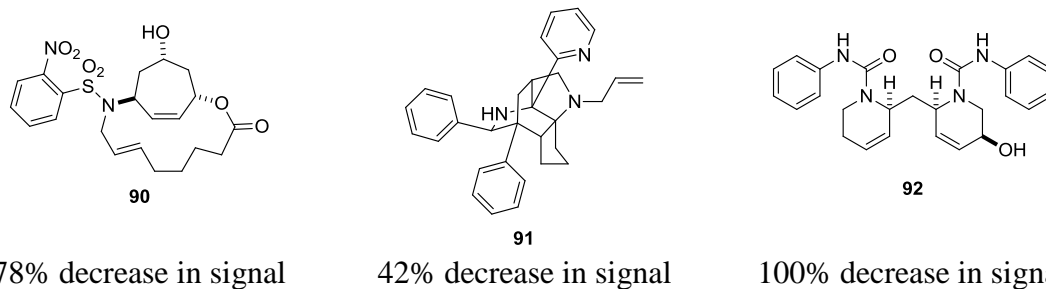


Figure 5.3 Compounds identified as potential ‘hits’ after screening for anti-viral activity against hRSV. The compounds were screened at 25 μM and anti-viral activity is reported as the influence on the normalised signal.

5.1.3 Evaluation of compounds identified through vHTS

A virtual screening campaign carried out against the fusion protein of hRSV identified potential hRSV fusion inhibitors (Chapter 3). The potential inhibitors of hRSV fusion could be split into two categories depending on whether they originated from a virtual library of synthetically accessible compounds or from a library of commercially accessible compounds. Both sets were screened for anti-viral activity against hRSV but also in a cytotoxicity assay (MTT) in order to evaluate toxicity of the molecules tested (Figure 5.5 and Appendix 18). The former set consisted of 8 molecules (Figure 5.4), whose synthesis was reported in Chapter 4, tested for anti-viral activity against hRSV at 80 and 20 μM (Figure 5.5.A). The latter consisted of commercially available compounds tested for anti-viral activity against hRSV at 20 μM (Figure 5.5.B).

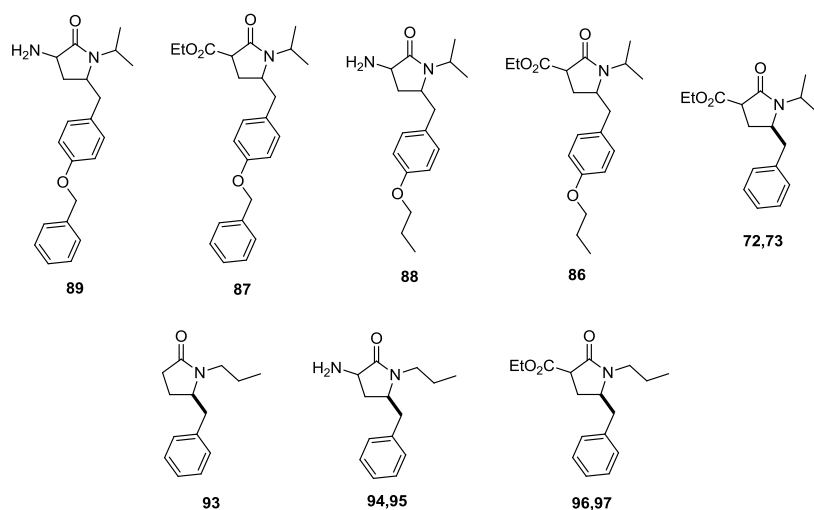


Figure 5.4 Focused library of potential γ -lactams inhibitors. The preparation of molecules **72,73-89** was described in Chapter 4. Molecules **93, 94,95** and **96,97** were prepared by George Karageorgis¹⁸³.

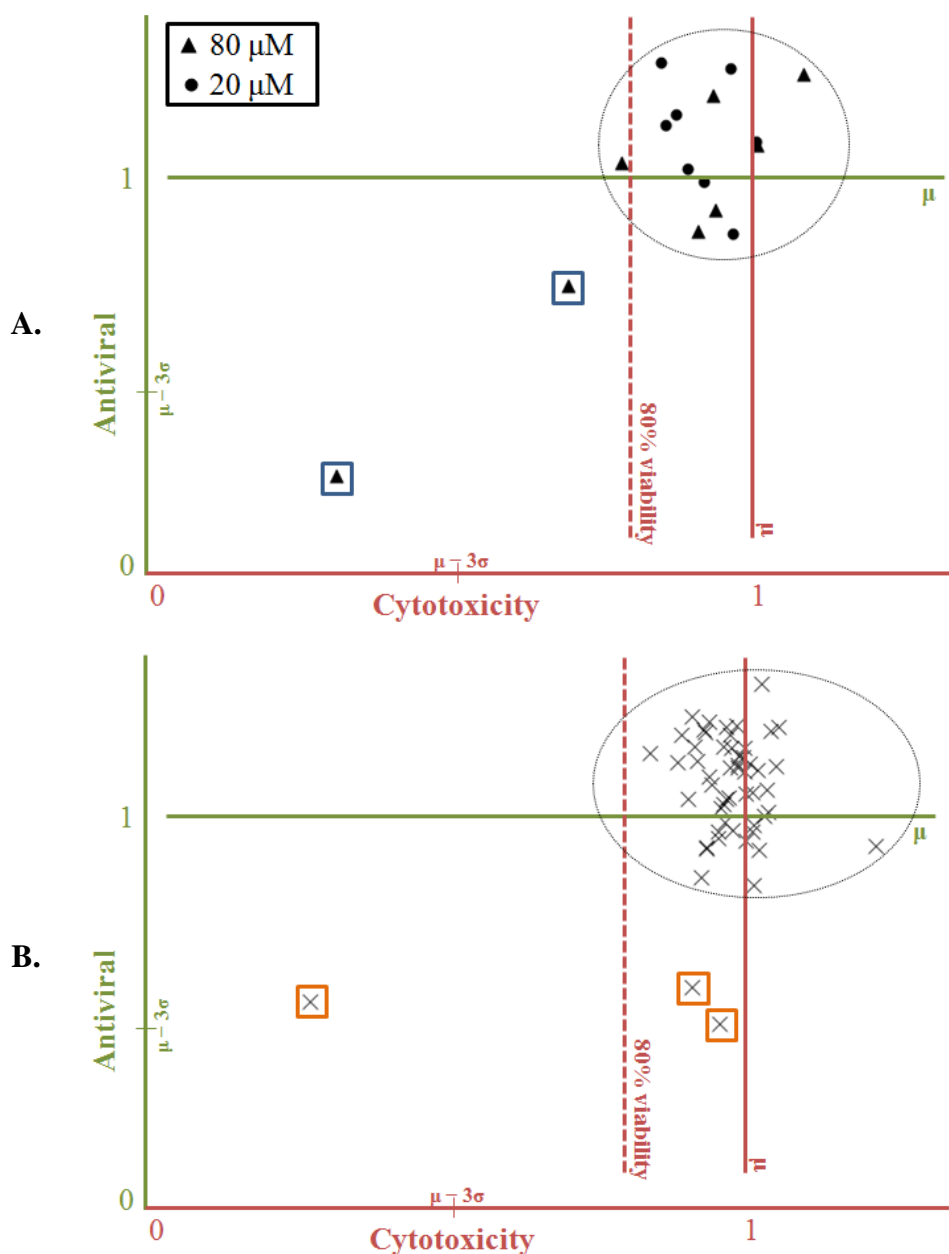


Figure 5.5. Antiviral activity and cytotoxic screen of 65 compounds screened following a vHTS campaign. **A.** Synthetically accessible compounds screened at 80 μM (black triangles) and 20 μM (black dots). **B.** Commercially accessible compounds tested at 20 μM . On the x-axis (cytotoxic screen), the results are presented as a ratio to the untreated control (*i.e.* DMSO at *ca.* 1%, the internal negative control). μ : mean of normalised activity of the compounds ($\mu = 0.95$), σ : standard deviation of the normalised activity of the compounds ($\sigma = 0.13$). Also shown is a bar representing 80% cell viability. On the y-axis, the results are presented as normalised. The cells were infected at an M.O.I. of 0.5. μ : mean of normalised activity of the compounds ($\mu = 1.06$), σ : standard deviation of the normalised activity of the compounds ($\sigma = 0.20$). The assay performed at a Z'-factor of 0.11 (feasible), with a signal-to-background ratio of 1.28 (< 2). Inactive molecules are in the oval. Both sets of compounds were screened on the same 96-well plate, therefore the statistical data have been combined.

Only a small number of compounds were assayed and a visual selection of hits for further evaluation was carried out (Figure 5.6). The potential hits **26**, **98**, **99** were selected for dose-response analyses (Section 5.1.5). The pyrrolidones **87** and **89** were found to have anti-viral activity at 80 μ M. However, this activity was lost as soon as the concentration was decreased to 20 μ M. Therefore, **87** and **89** were not considered further for dose-response analyses. The cytotoxicity screen revealed that the pyrrolidones hits and hit **26** were also cytotoxic (<80% cell viability). The dose-response analyses of the three hits are discussed in Section 5.1.5.

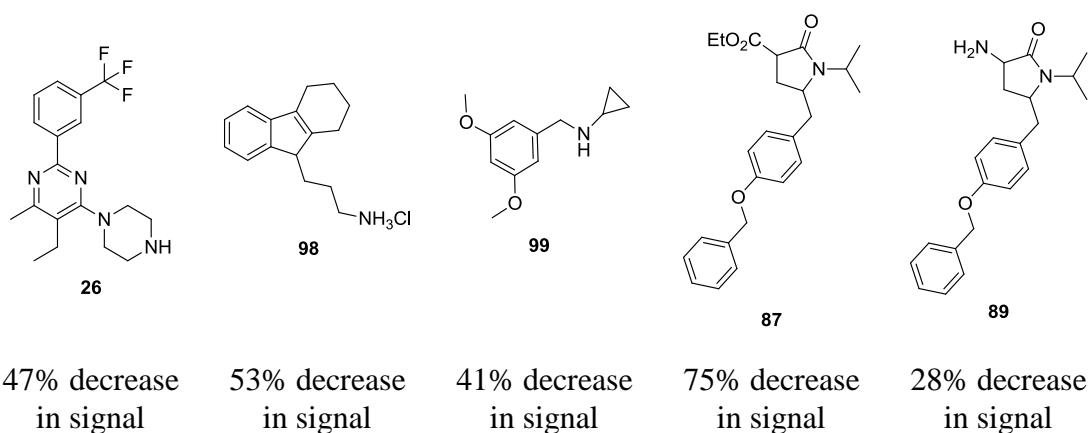


Figure 5.6 Compounds identified as potential ‘hits’ after screening for anti-viral activity against hRSV. Compounds **26**, **98**, **99** were seen as hits at 20 μ M and compounds **87** and **89** were seen as hits at 80 μ M. Anti-viral activity is reported as the influence on the normalised signal.

5.1.4 Therapeutic index

Anti-viral activity could also be a consequence of the compounds targeting cellular proteins and therefore being cytotoxic. Therefore, it was important to verify that the hits identified by HTS possess a “favourable” therapeutic index¹⁸⁴ (TI), which is a measure of the safety window of any given compound (Figure 5.7). There is no set value for an ideal TI but for hRSV, a favourable TI ($\frac{CC50}{EC50} > 1$) is desired¹⁸⁴.

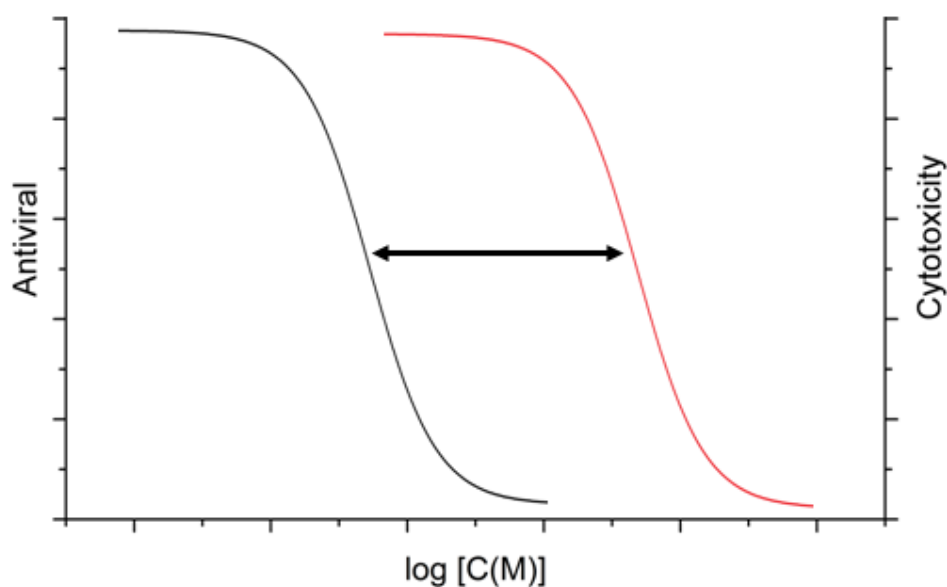
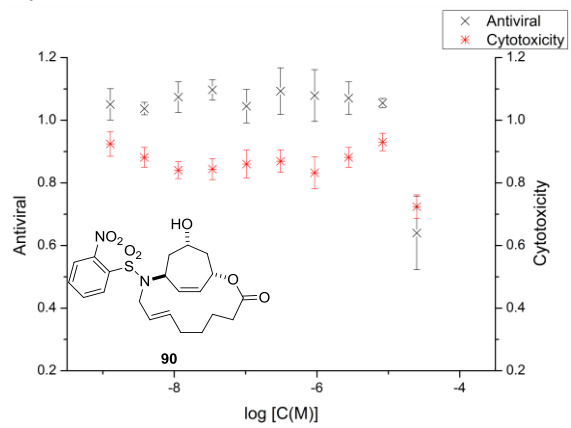
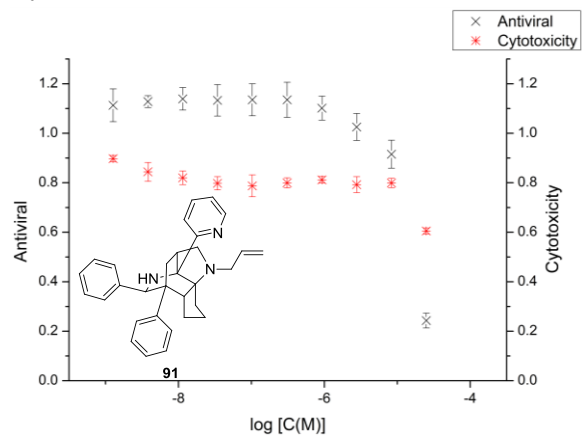
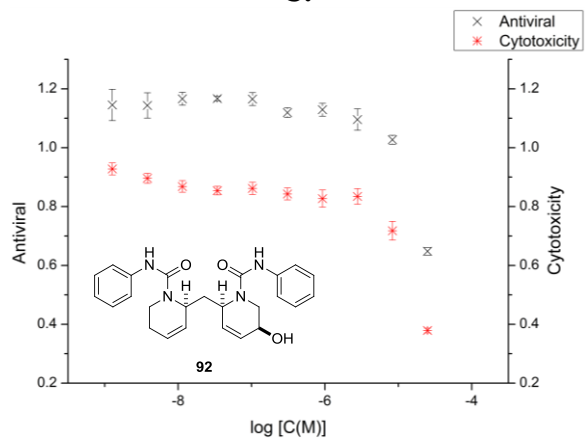


Figure 5.7. Representation of the therapeutic index. The efficacy curve (determination of the EC_{50} , black), and the safety curve (determination of the CC_{50} , red) are shown. The safety window is represented by the double-headed arrow. Adapted from Muller *et al.*¹⁸⁴.

5.1.5 Dose-response analyses on screening hits

In order to assess the TI of the hits identified following our screening campaign, dose-response analyses (25 μ M to 1.3 nM) were carried out on the following compound groups: i) three hits from the HTS campaign (Figures 5.8.A-5.8.C), ii) four cytotoxic compounds not identified as hits during the screening campaign (shown in Appendices 19-22), iii) one compound not identified as a hit and not classified as cytotoxic (negative compound, shown in Appendix 23), iv) three hits from the vHTS campaign (Figures 5.8.D-5.8.F).

A.**B.****C.**

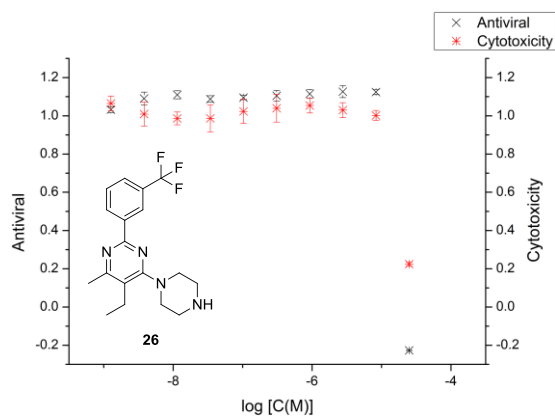
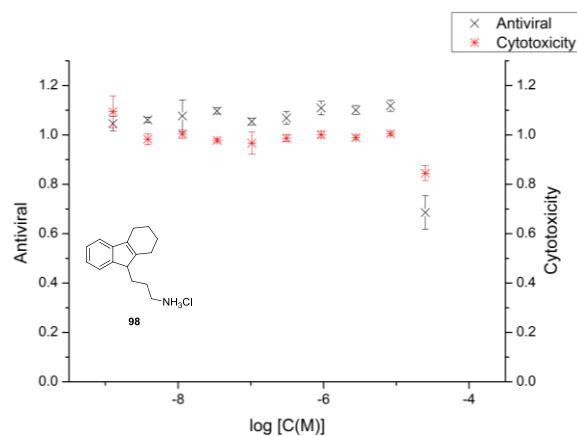
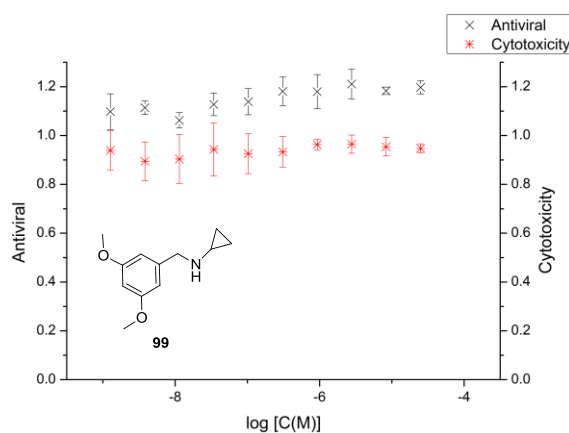
D.**E.****F.**

Figure 5.8 Dose-response analysis of the potential HTS and vHTS hits. The results are expressed as the ratio to untreated A2-infected cells at an M.O.I. of 0.5. An additional y-axis has been added to show the cytotoxic dose-response of HEP-2 cells to the hit. The results are expressed as the ratio of the hit-exposed cells to the unexposed cells against logarithm to base 10 of the hit concentrations (in molar). Absorbance was read at 570 nm. The error bars refer to the standard deviation of four replicates. **A.** Hit **90**, Z'-factor = 0.89, signal-to-background = 1.51. **B.** Hit **91**, Z'-factor = 0.61, signal-to-background = 1.62. **C.** Hit **92**, Z'-factor = 0.14, signal-to-background = 1.49. **D.** vHTS hit **26**, Z'-factor = 0.75, signal-to-background = 1.52. **E.** vHTS hit **98**, Z'-factor = 0.75, signal-to-background = 1.52. **F.** vHTS hit **99**, Z'-factor = 0.17, signal-to-background = 1.27.

For the potential HTS hits, the dose-response analyses revealed that the antiviral and cytotoxic profiles were similar for the potential hits **90-92** identified in the single-concentration screen. For the potential vHTS hits **26** and **98**, the observed activity at 20 μM was confirmed upon carrying out dose-response analyses. The dose-response analyses for the vHTS potential hits also revealed that the antiviral and cytotoxic profiles were similar. The activity of **99** observed at 20 μM was not reproduced in the dose-response analysis.

The TI does not appear to be favourable (≤ 1). Therefore, the hits are more likely to make cells unviable rather than genuinely targeting viral proteins.

5.1.6 Discussion

After two screening campaigns for anti-viral activity against hRSV, six compounds were identified as potential hits and were therefore selected for dose-response analyses. Unfortunately, the dose-response analyses revealed that the antiviral and cytotoxic profiles were similar (TI estimated^{§§§} at *ca.* 1), which was not considered sufficient to proceed with any of those hits. However, under the assay conditions reported in Section 2, the TI of Ribavirin is at best marginal ($EC_{50} = 31.4 \mu\text{M}$, $CC_{50} = 40.6 \mu\text{M}$; $TI = \frac{CC_{50}}{EC_{50}} = 1.4$). At $25 \mu\text{M}$, Ribavirin afforded a 40% decrease in the fluorescence signal for 84% cell viability. At $25 \mu\text{M}$, the hit **90** afforded a 78% decrease in the fluorescence signal for 60% cell viability. The extra activity is probably a consequence of the increased cytotoxicity of **90** at $25 \mu\text{M}$. However, the data suggest that Ribavirin and **90** appear to have similar activities, and that further development could lead to the compounds being used as probes, as has recently been reported by Moore *et al.*¹⁸⁵. Moore *et al.* discovered **100**, a novel hRSV small molecule probe (Figure 5.9) with a favourable TI of *ca.* 13 ($EC_{50} = 2.3 \mu\text{M}$, $CC_{50} = 30.9 \mu\text{M}$), starting from a hit with a TI of *ca.* 6 ($EC_{50} = 5.0 \mu\text{M}$, $CC_{50} = 31.5 \mu\text{M}$). In their assay, the TI for Ribavirin was *ca.* 4 ($EC_{50} = 28.4 \mu\text{M}$, $CC_{50} = 113.9 \mu\text{M}$).

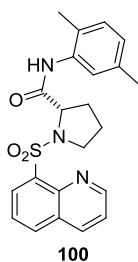


Figure 5.9. Novel small molecule inhibitor probe¹⁸⁵. $EC_{50} = 2.3 \mu\text{M}$, $CC_{50} = 30.9 \mu\text{M}$.

^{§§§} TI value given is only an estimation as the 10 mM stock solution did not allow screening at concentration $>25 \mu\text{M}$, which would have been required to obtain full sigmoidal curves.

5.2 Biological testing of the intermediates in the synthesis of JNJ-4749914

In order to gain more insight into the SAR of JNJ-4749914, we carried out dose-response analyses on the synthetic intermediates described in Section 2.3.7.2 (Figure 5.10).

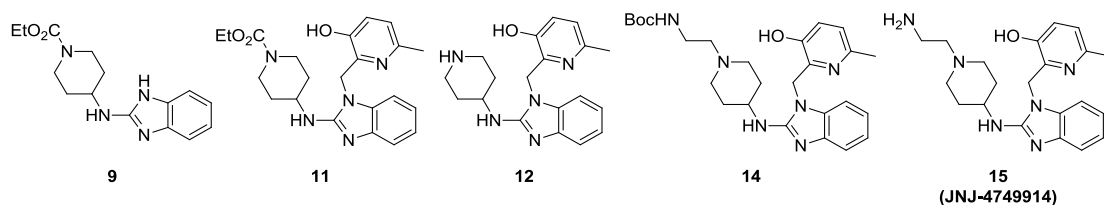


Figure 5.10. Focused library of benzimidazole derivatives.

5.2.1 Dose-response curves

A total of twenty different concentrations, ranging from 25 μM to 0.022 pM, were assayed in a single 96-well plate with each concentration being assayed in quadruplicates for the intermediates **9**, **11**, **12**, **14**, **15** (Figure 5.11).

At the concentration analysed, benzimidazole **9** displayed no antiviral activity ($\text{EC}_{50} > 25 \mu\text{M}$) and no cytotoxicity. The dose-response analysis for the *N*-alkylated benzimidazole **11** revealed that as soon the hydroxypyridine moiety was added, antiviral activity was detected at high concentrations ($\text{EC}_{50} > 1 \mu\text{M}$). However, the exact EC_{50} could not be determined due to the lack of data points at concentrations greater than 25 μM . No cytotoxicity was observed at the concentrations tested. Upon removal of the ester group, no changes in the antiviral and cytotoxic profiles were detected. The addition of the Boc ethylamine residue on the secondary amine **12** increased the antiviral activity: EC_{50} tentatively calculated at *ca.* 700 nM despite the missing data points at high concentrations ($C > 25 \mu\text{M}$). The cytotoxic profile remained unchanged. Removal of the Boc group resulted in a 100-fold increase in the antiviral activity without any modifications on the cytotoxicity profile.

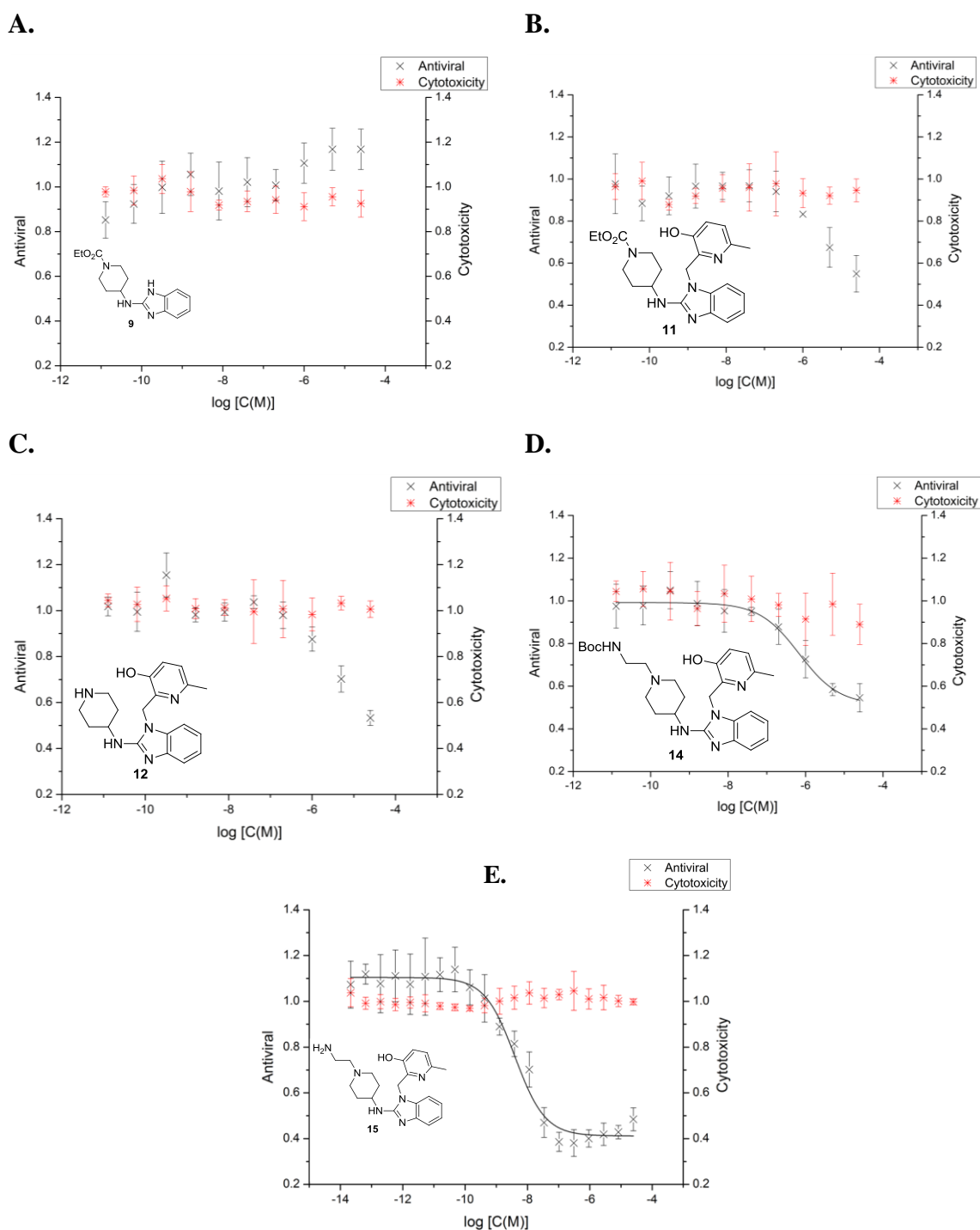


Figure 5.11. Dose-response analysis of benzimidazoles 9, 11, 12, 14, 15. The results are expressed as the ratio to untreated A2-infected cells at an M.O.I. of 0.5. An additional y-axis has been added to show the cytotoxic dose-response of HEP-2 cells to the compound tested. The results are expressed as the ratio of the compound-exposed cells to the unexposed cells against logarithm to base 10 of the compound concentrations (in molar). Absorbance was read at 570 nm. The error bars refer to the standard deviation of four replicates. **A.** Dose-response analysis of benzimidazole **9**, Z'-factor = 0.56, signal-to-background = 1.35. **B.** Dose-response analysis of the *N*-alkylated benzimidazole **11**, Z'-factor = 0.56, signal-to-background = 1.35. **C.** Dose-response analysis of the secondary amine **12**, Z'-factor = 0.76, signal-to-background = 1.38. **D.** Dose-response analysis of the carbamate **14**. Z'-factor = 0.76, signal-to-background = 1.38. **E.** Dose-response analysis of JNJ-4749914 (**15**), Z'-factor = 0.52, signal-to-background = 1.29.

5.2.2 Confocal imaging of the mode of action of JNJ-4749914

The JNJ compounds as well as the TMC compounds are all reported hRSV fusion inhibitors in the literature^{107,108,116,119}. However, to date, there has been no confocal imaging experiment visualising the inhibitory properties of the compounds such as that developed by Johnson & Johnson / Tibotec on cell fusion and cell-to-cell fusion¹⁸⁶. Therefore, we decided to look at the effects of JNJ-4749914 on A2-infected cells using confocal microscopy (Figure 5.12). The comparison between merged Panel B (A2-infected) and merged Panel C (A2-infected in the presence of JNJ-4749914) confirmed that JNJ-4749914 prevented virus entry, as shown by lack of fluorescence⁸. Closer analysis of the merged pictures in Panels B and C revealed that syncytia^{****} are observed in A2-infected cells whereas they are not present in A2-infected treated with JNJ-4749914, suggesting that JNJ-4749914 also prevents cell-to-cell fusion⁸.

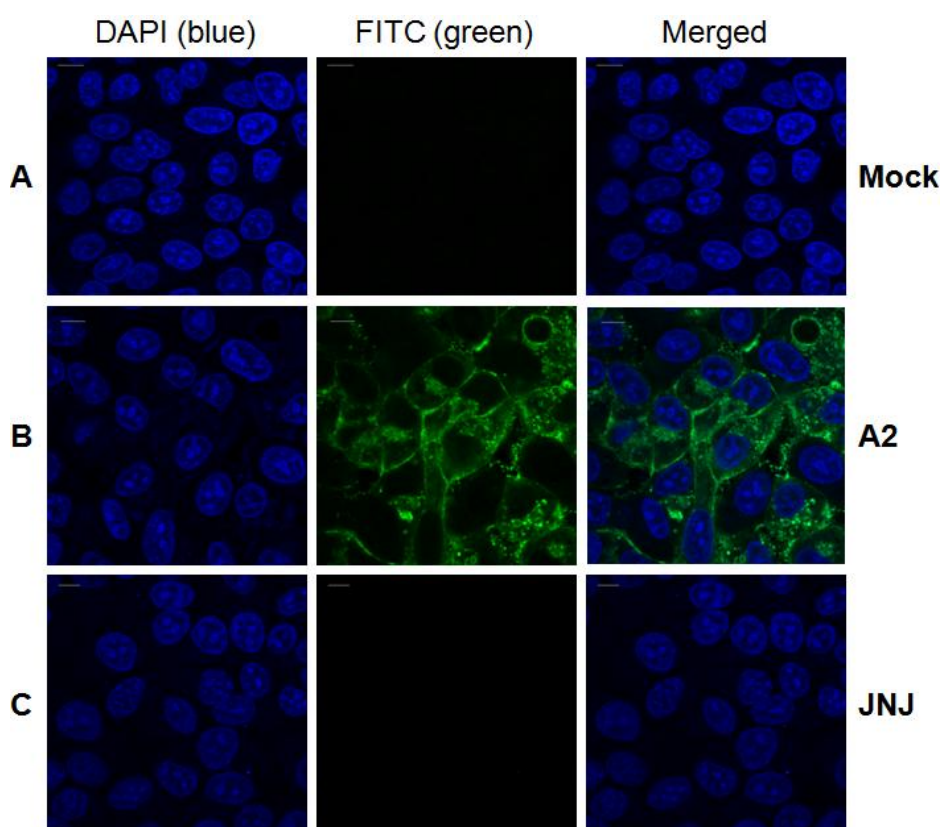


Figure 5.12. Analysis of the effect of JNJ-4749914 using confocal microscopy. **A.** Mock-infected HEp-2 cells. **B.** A2-infected HEp-2 cells, treated with media only. **C.** A2-infected HEp-2 cells, treated with JNJ-4749914 (JNJ). For all panel, the marker represents 10 μ m. Images acquired by Dr. Jamel Mankouri (University of Leeds).

**** In the case of hRSV, syncytia are a consequence of neighbouring cells merging their membranes. The consequence is the observation of cells with multiple nuclei.

5.2.3 Discussion

Bonfanti *et al.*¹⁰⁸ carried out molecular modelling experiments in order to better understand the binding of JNJ-2408068 (Figure 5.13). They predicted that the hydroxyl group of the hydroxypyridine moiety might be making hydrogen-bond interactions with Lys196 and Asp200. Assuming the binding mode of JNJ-2408068 (or JNJ-4749914) is similar to that of TMC353121, the key π - π stacking interaction could explain the anti-viral activity observed upon addition of the hydroxypyridyl moiety. The hydroxypyridyl moiety was not tested as a fragment alone and future work could involve its biological evaluation. The benzimidazole ring is also predicted to make σ - π interactions with Tyr198. The presence of the methyl group on JNJ-2408068, as opposed to hydrogen in JNJ-4749914, could explain the higher activity of JNJ-2408068. The σ - π interaction is not strong enough to observe anti-viral activity with the benzimidazole **9**. Finally, the ethylamine group of JNJ-4749914 is predicted to make hydrogen-bond interaction with either Gln202 or Asn208. The decreased anti-viral activity of the carbamate **14** could be explained by a lack of shape complementarity with the pocket where the ethylamine group of JNJ-4749914 is predicted to bind due to the bulk imposed by the Boc group.

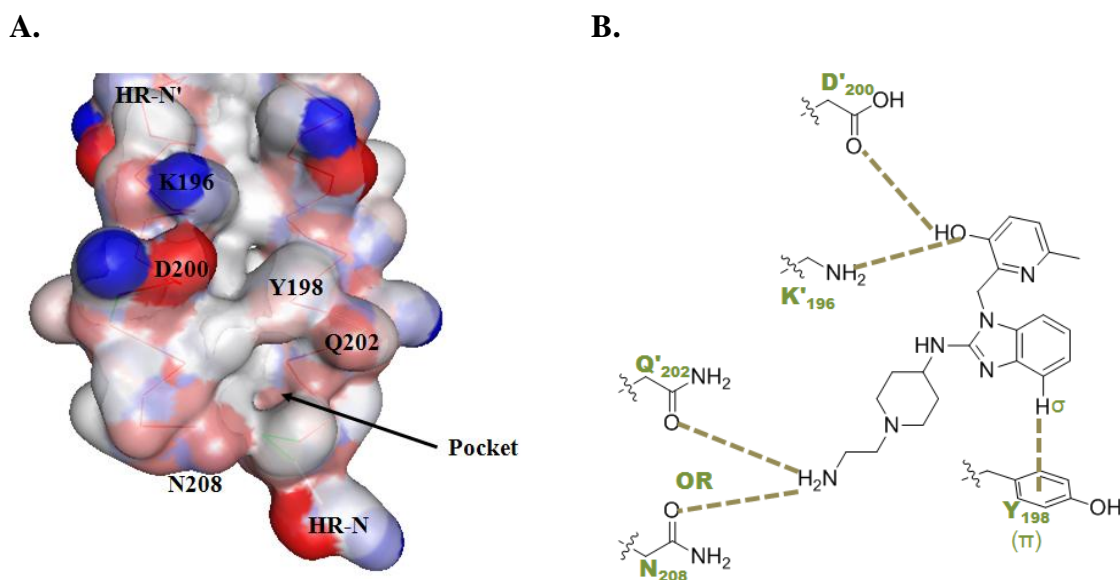


Figure 5.13. Prediction of the non-covalent interactions of JNJ-4749914. **A.** Part of the hydrophobic groove of hRSV F protein (PDB accession number 1G2C) JNJ-2408068 is predicted to make interactions with. N208 in HR-N' was not part of the crystal structure. Pocket refers to the pocket where the ethylamine group of JNJ-2408068 is predicted to dock. Picutre generated with Discovery Studio (Accelrys). **B.** 2-D representation of the key-non covalent interactions JNJ-4749914 is predicted to make with the hydrophobic groove of hRSV F protein. Adapted from Bonfanti *et al.*¹⁰⁸.

5.3 Summary

The biological evaluation of selected compounds as inhibitors of hRSV has been described. In the primary screen, three compounds from a natural product-like library were found with antiviral activity against hRSV at 25 μM (Figure 5.14.A). Three compounds from a commercially available library (identified by vHTS) were found with antiviral activity against hRSV at 20 μM (Figure 5.14.B). Unfortunately, upon dose-response analyses, none of the molecules displayed a sufficient TI to be taken forward as leads. Some of designed γ -lactams had anti-viral activity against hRSV at 80 μM (abolished upon testing at 20 μM).

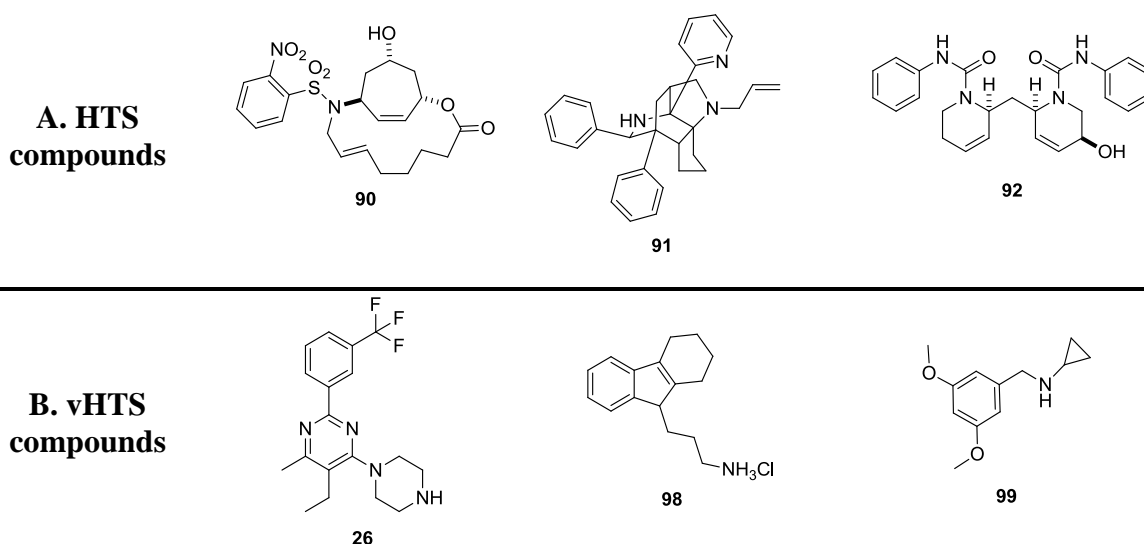


Figure 5.14. Compounds identified as potential ‘hits’ after primary screen screening for anti-viral activity against hRSV.

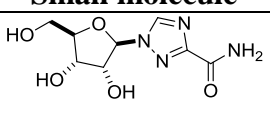
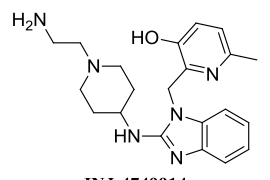
We also probed the structure-activity relationships of JNJ-4749914 by carrying out dose-response analyses on four isolated intermediates. Our conclusions were that the hydroxypyridyl moiety and the ethylamine chain proved critical for the display of nanomolar activity. Confocal imaging experiments confirmed that JNJ-4749914 acted as a cell entry inhibitor.

6 SUMMARY AND FUTURE WORK

The objective of the work described in this thesis was to discover new small molecule inhibitors of the human respiratory syncytial virus (hRSV). To do so, complementary approaches were used: high-throughput screening and virtual high-throughput screening.

In order to assess reliably activity against hRSV, it was crucial to develop a robust phenotypic high-throughput screening (HTS) assay. Thus, a novel fluorescence-based assay for the detection of hRSV in human epithelial cells (HEp-2) was developed which afforded the fast and reliable determination of anti-viral activity. The assay was validated for use in a high-throughput format using Ribavirin (an FDA-approved therapy for hRSV), JNJ-4749914 (a known hRSV fusion small molecule inhibitor) as reported in Table 6.1 and DMSO (negative control) as appropriate plate-based controls. Using the robust HTS assay, a library of natural product-like molecules was tested for anti-viral activity at 25 μM . Three compounds (out of 160) were selected as “hits” and nominated for dose-response analysis. Unfortunately, these analyses revealed that the therapeutic index was not sufficient in order to confirm the hits as active against hRSV.

Table 6.1: Summary of the activity (EC_{50}) and cytotoxicity (CC_{50}) of known hRSV inhibitors

Small molecule	Assay	Literature
 Ribavirin	EC_{50} <i>ca.</i> 30 μM CC_{50} <i>ca.</i> 40 μM	EC_{50} from 19 μM ⁹⁹ to 41 μM ¹⁴⁰ CC_{50} from 26 μM ¹⁴² to 2 mM ¹⁴⁰
 JNJ-4749914	EC_{50} <i>ca.</i> 0.4 nM CC_{50} > 25 μM	EC_{50} <i>ca.</i> 0.4 nM ¹⁰⁷ CC_{50} N/A

The results of the biological testing for anti-viral activity highlighted some of the challenges faced by drug discovery carried out in academia¹⁸⁷: the small size of the proprietary compound collection and the lack of diversity of commercially available compounds¹⁸⁸⁻¹⁹⁰. The natural product-like library tested was rich in diversity, offered novel coverage of the natural product chemical space, but only 160 molecules were screened for anti-viral activity against hRSV. Therefore, it is possible that the areas covered were not overlapping with the hRSV-relevant chemical space. In order to bypass the lack of diversity from commercial vendors, a novel approach to vHTS was devised, relying on the use of virtual library of likely synthetically accessible compounds¹⁴⁵. Two virtual libraries of likely synthetically accessible compounds, which identified three new series of potential hRSV fusion inhibitors, and a virtual library of commercially available compounds were used.

The *in silico* method used to generate the proposed inhibitors from series 1 and 2 was based on the diversity-oriented synthesis building block approach. This building block based approach has previously yielded molecules with unprecedented scaffold diversity¹⁵¹⁻¹⁵³ using synthetically accessible building blocks and robust linking strategies. The present report highlighted the difficulties behind the prediction of synthetic accessibility, even for established robust methodologies. Pfizer have designed their own virtual library of likely synthetically accessible compounds (Pfizer Global Virtual Library¹⁴⁵, *ca.* 10¹⁴ compounds) based on twelve years of parallel synthesis data collection. In the present report, some of the building blocks required for the preparation of the proposed inhibitors could not be prepared, despite being closely related to known building blocks. Additionally, the linking strategies were similar to what had been reported previously but were unsuccessful in the present work. A different outcome was observed for series 3 suggesting that careful synthetic planning could afford the synthesis of compounds from a library of likely synthetically accessible compounds. A total of 63 compounds, identified by vHTS were screened for anti-viral activity against hRSV at 20 μ M; three compounds were selected as “hits” and nominated for dose-response analysis. Unfortunately, these analyses revealed that the therapeutic index was not sufficient in order to confirm the hits as active against hRSV.

The results obtained for the compounds identified by vHTS highlighted the problems associated with the prediction of affinity using scoring functions. The scoring function used by eHiTS is empirical in nature¹⁴⁶, *i.e.* the score is a function of weighted parameters such as hydrogen bond or ionic interactions, π - π stacking or non-compatible interactions. The scoring functions are refined using datasets of known high-affinity protein-ligand complexes: PDBbind¹⁹¹ with a set of 1,300 complexes or Astex Diverse Set¹⁹² with 85 complexes, both dating from 2007. eHiTS was refined using a set of 133 complexes¹⁴⁶, and was reported as one of the best *in silico* pose prediction software with the PDBbind dataset¹⁹³. However, problems may arise in translating the results to lower affinity ligands or to novel protein-ligand complexes. The 3D conformation generation software has also been reported to influence the outcome of the docking software¹⁹⁴. Finally, the displacement of water molecule in the binding site was not taken into account by eHiTS, and could also account for the lack of correlation between the predicted score and the observed affinity. Computational methods such as WaterMap¹⁹⁵ are available to estimate the free energy of hydration but are not included in the eHiTS package.

Finally, the work described in the present report allowed gaining more insight into the key groups (hydroxypyridyl and aminoethyl groups) responsible for the nanomolar activity of JNJ-4749914. Additionally, we provided additional data regarding the mode of action of JNJ-4749914, using confocal images to show that JNJ-4749914 inhibited cell entry. The work carried out of JNJ-4749914 highlights two avenues that could be explored in the future. First, there are reports that TMC353121 acts as a cell-to-cell fusion inhibitor¹¹⁶. However, there are no reported confocal microscopy evidence to support that claim. It could be possible to verify those claims using JNJ-4749914 by adding it at a given time after infection (up to 48 h post-infection¹¹⁸) and observe whether or not syncytia are formed. Second, the hydroxypyridyl fragment itself was not tested for anti-viral activity against hRSV. More generally, fragment-based drug discovery could be used to target the small molecule binding cavity of 3KPE.

The discovery of a ligand efficient fragment with a well-defined binding mode could provide a valuable starting point for structure-based drug design. Fragments could be docked *in silico* and the most ligand efficient fragments screened for anti-viral activity or a diverse subset of available fragment libraries could be screened for anti-viral activity in a high-throughput format. Follow up experiment would be the connection of promising fragments and the analysis of the evolution of anti-viral activity. Both avenues could be explored using methods reported in the present thesis.

7 MATERIALS AND METHODS

7.1 Buffers and solutions

PBS (10 × stock): NaCl (137 mM), KCl (2.7 mM), Na₂HPO₄ (10 mM), KH₂PO₄ (2 mM) pH 7.4 upon dilution to 1×PBS, referred to as PBS.

Cell permeabilisation & non-specific antibody binding washing: PBS-Tween: 5% Tween® 20 (Merck) in 1×PBS, referred to as PBST.

Table 7.1: cell lysates and Western Blot buffers and solutions:

<i>Lysis buffer (referred to as RIPA buffer):</i>	<i>5× Loading buffer:</i>
- 50 mM Tris (pH 7.5)	- 600 µL 1M Tris.HCl (pH 6.8)
- 150 mL NaCl	- 5 mL 50% Glycerol
- 1% NP40	- 2 mL 10% SDS
- 0.5% sodium deoxycholate	- 500 µL β-mercaptoethanol
- 0.1% SDS	- 1 mL 1% bromophenol blue (filtered)
- 1× protease inhibitor (Roche)	- 900 µL water

<i>12% resolving gel:</i>	<i>5% stacking gel:</i>
- 4 mL 30% acrylamide	- 830 µL 30% acrylamide
- 2.5 mL 1.5M Tris-HCl (pH 8.8)	- 630 µL 1M Tris-HCl (pH 6.8)
- 3.3 mL water	- 3.4 mL water
- 100 µL 10% SDS	- 50 µL 10% SDS
- 100 µL 10% ammonium persulphate	- 50 µL 10% ammonium persulphate

50 µL (25 µL for the stacking gel) of *N,N,N',N'*-tetramethylethylenediamine

Dry transfer buffer (also known as Towbin buffer): Tris (25 mM), glycine (1.92 M), methanol (20%).

Chemiluminescence (reagents provided by Sigma–Aldrich):

- Solution 1: 200 µL luminol (250 mM, in DMSO), 88 µL p-coumaric acid (90 mM, in DMSO), 2 mL 1M Tris-HCl (pH 8.5), up to 20 mL with water
- Solution 2: 12 µL 30% (w/w) H₂O₂, 2 mL 1M Tris-HCl (pH 8.5), up to 20 mL with water

7.2 Tissue culture techniques

7.2.1 Tissue culture plasticware

T25, T75, and T175 tissue culture flasks (Corning) were used. The number refers to the growth area in cm². 6-well plate (Corning, 9.5 cm²), 24-well plate (Corning, 1.9 cm²) and 96-well plate (Greiner, 0.34 cm²) were also used.

7.2.2 Maintaining cells

HEp-2 (Human cervix carcinoma epithelial cell²⁵, Health Protection Agency culture collections), A549 (Human lung carcinoma epithelial cell¹⁹⁶, Health protection agency culture collections) cells were grown at 37°C with 5% CO₂ in Dulbecco's Modified Eagle's Media (DMEM) supplemented with 10% foetal bovine serum (FBS) and 1% penicillin/streptomycin, referred to as DMEM. At 70-80% confluency in a T175 tissue culture flask, cells were washed with PBS, trypsinised for 5-10 min at 37 °C, and fresh DMEM was added to neutralise trypsin. At which point, cells were either counted or split 1:10 in a T175 tissue culture flask. HEp-2 cells were used from a frozen stock at passage 11 and were discarded at passage 25. Cells were routinely checked for mycoplasma infection by Carsten Zothner using the MycoAlert Mycoplasma detection kit (Lonza).

7.2.3 Freezing cells down

From a confluent T175 tissue culture flask, cells were washed with PBS, trypsinised and centrifuged at 1,500 rpm for 5 min at room temperature. Cells were then washed once with PBS, centrifuged and 5 mL of the cryopreservation mix (9:1 FBS–DMSO) was added. It was then split into five cryogenic vials (1 mL).

7.2.4 Using cells from a frozen stock

The cryogenic vial, which was stored either in liquid nitrogen or in a -80°C freezer, was thawed in a water bath at 37°C . The cells were centrifuged at 1,500 rpm for 5 min at room temperature. The cryopreservation mix was discarded and the cells were washed three times with PBS (with a centrifugation step in-between each wash), and once with DMEM. The cells were then transferred to a T25 tissue culture flask. Once confluent, the cells were trypsinised and transferred a T75 tissue culture flask. Once confluent, the cells were trypsinised and transferred to a T175 tissue culture flask to be used for further experiments.

7.2.5 Counting cells

The cell suspension obtained after trypsin neutralisation was transferred into a new 15 mL universal. In duplicates, 100 μL of this suspension was added to 100 μL of Trypan Blue Stain (GIBCO), in order to count viable cells only. 10 μL of each replicate was then loaded on a haemocytometer for cell counting. A total of 10 counting areas were used to count cells. The number of cells per millilitre of suspension was calculated as follow:

$$\frac{\text{Total number of cells (excluding)}}{10 (\# \text{ calculated grids})} \times 2 (\text{dilution}) \times 10^4 (\text{area of grids})$$

7.2.6 Virus propagation

The laboratory adapted A2 strain of hRSV, previously passaged through Vero cells (Monkey African green kidney epithelial cell), was obtained from labelled passage number 2 and used up to passage number 4 (for this report). HEp-2 cells (2×10^6) were incubated for 24 hrs in a T175 tissue culture flask. The growth media was discarded and replaced by fresh DMEM (5 mL). 500 μL of the previous A2 stock was added to the T175 and incubated for 2 hrs on a rocker at 37°C . DMEM (15 mL) was then added to the T175 and it was incubated for 4 to 5 days.

7.3 Confocal imaging

In a 6-well plate, glass coverslips (\varnothing 19 mm, VWR) were added to the bottom of the wells, and A549 cells (2×10^5) were added to DMEM (2 mL) and incubated until 60% confluent (normally 24 hrs). When ready, DMEM was removed and the monolayer was washed carefully three times with PBS, and freshly prepared virus was added (400 μ L) to the wells (one well was kept for the mock-infected control), and the plate was incubated for 2 hrs on a rocker at 37 °C. After which the inocula were removed and replaced by fresh DMEM (2 mL). The plate was then incubated for 24 hrs, and the cells were:

- i) Washed three times with PBS (2 mL) and fixed with methanol (1 mL) for 10 min at -20 °C
- ii) Washed three times with PBS (2 mL) and were permeabilised with PBST (1 mL) for 15 min at room temperature, and washed three times with PBST (2 mL)
- iii) Blocked with PBST with 5% skimmed milk (Fluka) (1 mL) for 1 hr at room temperature, and washed three times with PBST (1 mL)
- iv) Incubated with a goat anti-RSV polyclonal primary antibody conjugated to fluorescein isothiocyanate (ab20391, Abcam) in PBST with 5% skimmed milk (1:50, 50 μ L), applied directly onto the coverslips, for 1 hr at room temperature, and washed three times with PBST (150 μ L)
- v) Were washed twice in PBS (1 mL) and the coverslips were mounted onto glass slides (Agar Scientific) using VECTASHIELD Mounting Medium with DAPI (VECTOR Laboratories). The slides were stored in the dark at 4 °C until confocal imaging.
- vi) Confocal sections of fixed samples were captured on the laser scanning microscope 510 META Microscope (Carl Zeiss Ltd) equipped with a 40 \times and 63 \times , NA 1.4, oil immersion lens.

7.4 Plaque assay

The virus titres were evaluated in HEp-2 cells using a plaque assay method based on antibody detection^{126,127}.

- i) In a 24-well plate, HEp-2 cells (1×10^5) were added to DMEM (1 mL) and incubated until confluent (normally 24 hrs). When ready, DMEM was removed and the monolayer was washed once with PBS.
- ii) Virus dilutions (mock, $1:10^3$, $1:10^4$, $1:10^5$, $1:10^6$, $1:10^7$) were prepared in DMEM and added (200 μ L) in triplicate. The plate was then incubated for 2 hrs on a rocker at 37 °C.
- iii) The inocula were removed and replaced by DMEM–methylcellulose (1:1, 1 mL) and the plate was incubated for 4 to 5 days. The overlay was removed using an aspirator and cells were fixed with methanol (1 mL) for 1 hr at 4 °C
- iv) The cells were permeabilised with PBST (1 mL) for 15 min at room temperature, and washed three times with PBST (1 mL)
- v) The plate was blocked with PBST with 5% skimmed milk (1 mL) for 1 hr at room temperature, and washed three times with PBST (1 mL)
- vi) The cells were incubated with a goat anti-RSV polyclonal primary antibody (7950-0004, AbD Serotec) in PBST with 5% Skimmed milk (1:100, 200 μ L) for 1 hr at room temperature, and washed three times with PBST (1 mL)
- vii) The cells were incubated with a rabbit anti-goat polyclonal secondary antibody conjugated to horseradish peroxidase (ab6741, Abcam) in PBST with 5% Skimmed milk (1:1000, 200 μ L) for 1 hr at room temperature, and washed three times with PBST (1 mL), and washed two times in PBS (1 mL)
- viii) The cells were incubated with 4-Chloro-1-naphtol (Pierce) substrate (200 μ L) for 10 min, and the reaction was neutralised by washing once with water (1mL) for 5 min. Preparation of the 4-chloro-1-naphtol substrate: 1 mL of a 3 mg/mL stock solution (prepared in methanol) was added to 10 mL of PBS. 10 μ L of 30% (w/w) H₂O₂ (Sigma) was added prior to incubation.

- ix) Plaques were counted for wells which only had between 10 and 100 plaques, and were averaged over the replicates. The titre, expressed in plaque forming unit per millilitre (p.f.u./mL) is calculated as follow:

$$\frac{\text{average of the number of plaques}}{\text{volume of virus added (mL)} \times \text{dilution considered}}$$

7.5 Preparation of cell lysates and western blot analyses

For each cell line, two T25 tissue culture flasks were seeded (3×10^6), and incubated for 24 hr. The flasks were then used for mock-infection and for infection with the A2 strain (M.O.I. = 1), and incubated for 1 hr on a rocker at 37 °C. Then, the inocula were removed and replaced by fresh DMEM. The cells were incubated for 24 hr. After which, the media was removed, the cells washed with PBS and trypsinised (1 mL). Once detached, the cells were pipetted into a 1.5 mL Eppendorf tube and centrifuged at 1,500 rpm for 3 min. The cells were then washed with PBS (1 mL) and centrifuged at 1,500 rpm for 2 min. The cell pellets were re-suspended in RIPA buffer (1 mL) and incubated on ice for 30 min. The mixture was then centrifuged at 13,000 rpm for 2 min and the supernatants collected in fresh Eppendorf tubes.

Total protein was quantified by BCA assay (Pierce), where the concentrations are compared to bovine serum albumin standards as per the manufacturer's instruction. 2 µg of total protein from each sample in 1×loading buffer were denatured at 95 °C for 5 min. In order to estimate the molecular weight of the proteins, protein markers (P7708S from NEB or LC5925 from Invitrogen) were loaded alongside total proteins. These samples were separated by sodium dodecyl sulphate polyacrylamide gel electrophoresis (15 mA for 5% stacking gel and 25 mA for the 12% resolving gel) and electrophoretically transferred to Immobilon™ transfer membranes (Millipore) at 15V for 1hr using a semi-dry blotter.

The membrane was:

- i) blocked overnight at 4 °C in PBST with 5% skimmed milk
- ii) incubated for 1 hr with either a goat anti-RSV polyclonal primary antibody (ab20745, Abcam) in PBST with 5% skimmed milk (1:1000), or a goat anti-RSV polyclonal primary antibody (7950-0004, AbD Serotec) in PBST with 5% skimmed milk (1:500), both for 1 hr at room temperature.
- iii) washed three times with PBST, and incubated with a rabbit anti-goat polyclonal secondary antibody conjugated to horseradish peroxidase (ab6741, Abcam) in PBST with 5% skimmed milk (1:1000) for 1 hr at room temperature, and washed three times with PBST with 5% Skimmed milk
- iv) washed three times with PBST, followed by a final water wash.
- v) Reactive bands were detected by chemiluminescence (1:1, Solution 1 – Solution 2).
- vi) Films (x-ray, Kodak) were exposed to the membranes at various exposure times and developed using x-ray film developer (Konica).

A goat anti-RSV polyclonal primary antibody conjugated to horseradish peroxidase (ab20686, Abcam) in PBST with 5% Skimmed milk (1:500) was also used for direct detection: it did not require the use of a secondary antibody. The final washing steps were identical.

7.6 Spinoculation

Spinoculation, or the centrifugation of the multi-well plate just after infection, has been reported to increase the efficiency of virus infection (hRSV¹⁹⁷: 1,750g for 15 min at 4 °C in HeLa cells; human immunodeficiency virus type 1¹⁹⁸: 1,500g for 60 min at room temperature in human primary monocytes; Kaposi's sarcoma-associated herpesvirus¹⁹⁹: in human umbilical vein endothelial cells). The purpose of the current research was not to further study the effects of spinoculation on hRSV. However, it was assumed that spinoculation at low speed and below room temperature (15 °C) would ensure that all cells would be infected at the same time (hRSV binds to its cellular target at 4 °C but fusion only occurs at temperature >18 °C in HEp-2 cells²⁰⁰).

7.7 Antiviral assay

All liquids were dispensed using the 10-100 μL or 30-300 μL Research® multi-channel pipettes (Eppendorf). 25 μL of DMEM containing either i) 1% DMSO, or ii) Ribavirin concentration (in quadruplicate), or iii) 25 μL of compounds library (100 μM) were added to a black 96-well plate (μClear ®, Greiner). HEp-2 cells were then seeded (50 μL at 8.4×10^3) and incubated for 24 hrs. At which point, the cells were infected with hRSV (A2 strain) at a M.O.I. of 0.5 (25 μL), unless otherwise stated, and were centrifuged at 1,000g at 15 °C for 30 min, and were incubated for 24 hrs, giving a final 1:4 dilution of DMSO or any compound used.

24 hr post infection, the cells were:

- i) Washed three times with PBS (100 μL)
- ii) Fixed with methanol (100 μL) for 10 min at -20 °C, and washed three times with PBST (150 μL)
- iii) Permeabilised with PBST (100 μL) for 15 min at room temperature, and washed three times with PBST (150 μL)
- iv) Blocked with PBST with 5% skimmed milk (100 μL) for 8 hrs at 4 °C, and washed three times with PBST (150 μL)

The virus was detected by indirect fluorescence. The cells were:

- i) Incubated with a goat anti-RSV polyclonal primary antibody (7950-0004, AbD Serotec) in PBST with 5% skimmed milk (1:100, 50 μL) overnight at 4 °C, and washed three times with PBST (150 μL)
- ii) Incubated with a donkey anti-goat polyclonal secondary antibody conjugated to fluorescein isothiocyanate (ab6881, Abcam) in PBST with 5% skimmed milk (1:200, 50 μL) for 2 hrs at 37 °C, and washed three times with PBST (150 μL)
- iii) Washed two times in PBS (150 μL) prior to the final addition of PBS (50 μL)

- iv) The plate was either stored at 4 °C, or read on a plate reader (Fluostar, BMG LABTECH) or was also observed under a benchtop inverted fluorescent microscope attached to an imaging computer (Nikon) equipped with 4×, 10×, 20×, 40× lenses.
- v) The data from the plate reader are expressed in relative fluorescent units (R.F.U.).

7.8 Plate reader parameters

The program used to read the plate was as follow:

- i) The bottom optics of the plate reader were used
- ii) The excitation and emission filters were set at 485 nm and 520 nm respectively
- iii) The gain was calculated automatically for every plate, relatively to the brightest well
- iv) The plate was read using the well scanning mode with a scan matrix of 8 × 8, a number of flashes per scan point of 10 and a position delay of 0.5 s.

7.9 Cytotoxicity assay

All liquids were dispensed using the 10-100 μL or 30-300 μL Research® multi-channel pipettes (Eppendorf). 25 μL of DMEM containing i) 1% DMSO, or ii) Ribavirin concentration (in triplicate), or iii) 25 μL of compounds library (100 μM) were added to a clear 96-well plate (Greiner). HEp-2 cells were then seeded (50 μL 8.4×10^3) and incubated for 24 hrs. At which point, 25 μL of DMEM was added and the plate was centrifuged at 1,000g at 15 °C for 30 min, and were incubated for 24 hrs, giving a final 1:4 dilution of DMSO or any compound used. 48 hrs post seeding, the cells were washed twice with PBS (150 μL). The plate was then incubated with an MTT solution (M2128, Sigma) (1 mg/L made in serum-free DMEM, 100 μL) for 30 min at 37 °C. The MTT mixture was discarded and replaced by 100% DMSO, in order to dissolve the cells, and was incubated in the dark, at room temperature for 15 min on an orbital shaker (200 rpm). Absorbance was read at 570 nm (DYNEX Technologies).

7.10 Data analysis

The study of the antiviral effects of the internal positive control or the compounds library was carried out as follow:

- i) The first step is only for compounds with enough replicate wells, *i.e.* the internal positive (Ribavirin and the internal negative (DMSO) controls. For each individual data series (*i.e.* Ribavirin concentrations or controls i) in triplicate for the study of the antiviral effects of Ribavirin, or ii) in quadruplicate for the assay plate), an outlier detection was performed using the Grubbs' test^{201,202} (<http://www.graphpad.com/quickcalcs/Grubbs1.cfm>). When the test came back positive, the highlighted outliers were discarded.

- ii) The data was then normalised as follow:

$$N(i, j) = \frac{x(i, j) - L}{H - L}$$

N(i,j): normalised values for each sample loaded on the plate in row i, column j; x(i,j): samples loaded on the plate in row i, column j, H: high, average of maximum signal (virus control for the Ribavirin plate, DMSO control for the assay plate), L: low, average of the minimum signal (mock-infected for the Ribavirin plate, 2.5 mM Ribavirin for the assay plate).

- iii) When serial dilutions were used, average and standard deviation of the normalised data series were then plotted using OriginPro 7.5 (OriginLab) and fitted to a sigmoid using the Pharmacology-Dose Response fitting function with instrumental weighting to take the standard deviation into account. The fitting equation is given as:

$$y = A_1 + \frac{A_2 - A_1}{1 + 10^{[\log(EC_{50}) - x]p}}, A_2 \text{ was set to } 1$$

- iv) When serial dilutions were used, data variability band: for this, we used normalised Gaussian (normal distribution):

$$f(x) = \frac{1}{\sqrt{2\pi\sigma^2}} \times \exp \left[-\frac{(x - \mu)^2}{2\sigma^2} \right]$$

μ and σ are the mean and standard deviation of the normalised N(i,j), respectively. x is between 0 and 1 with 0.01 increments.

- v) Alternatively, we determined hits as follow: normalised value greater than three standard deviation of the plate (without including the controls).

The study of the cytotoxic effects of the internal positive control or the compounds library was carried out as follow:

- i) The first step is only for compounds with enough replicate wells, *i.e.* the internal positive (Ribavirin and the internal negative (DMSO) controls. For each individual data series (*i.e.* Ribavirin concentrations or controls i) in triplicate for the study of the antiviral effects of Ribavirin, or ii) in quadruplicate for the assay plate), an outlier detection was performed using the Grubbs' test^{201,202} (<http://www.graphpad.com/quickcalcs/Grubbs1.cfm>). When the test came back positive, the highlighted outliers were discarded.
- ii) The data was expressed as the ratio of the compounds (*i.e.* average of Ribavirin concentrations for the Ribavirin plate, or single value for the assay plate) to the average of the untreated cells
- iii) Average and standard deviations of the expressed data were then plotted using Origin 7.5 (OriginLab).

7.11 Ribavirin stock and preparation of dilution series

Ribavirin (R9644, Sigma) was prepared as a 1M stock in DMSO and stored at -20°C . Ribavirin antiviral and cytotoxic studies were carried out using sixteen different Ribavirin concentrations, ranging from 2.5 mM to 10 nM (assay concentration). These concentrations were prepared as described in Table 7.2.

The plate layout was as follows (Figure 7.1): the mock-infected cell controls and the A2-infected cell controls were added in column 1 with their respective positioning swapped in column 12. Additionally, twelve A2-infected cell controls were dispensed between column 2 and 11 in order to correct for potential tailing off of the fluorescence signal.

	1	2	3	4	5	6	7	8	9	10	11	12
A												
B												
C	Mock	2.5 mM	1 mM	A2	500 μM	250 μM	A2	100 μM	60 μM	50 μM	40 μM	A2
D												
E												
F	A2	25 μM	20 μM	15 μM	10 μM	A2	5 μM	1 μM	100 nM	A2	10 nM	Mock
G												
H												

Figure 7.1 Typical layout of the 96-well plate to study the cytotoxic and antiviral effects of Ribavirin. The top and bottom rows were never used and are shown in black. Mock refers to non-infected HEp-2 cells treated with growth media only, A2 refers to the A2-infected HEp-2 cells. The concentrations are the final assay concentrations.

Table 7.2: Preparation of the sixteen serial dilutions of Ribavirin (dispensed by hand):

Reference number	Ribavirin concentration	Volume of diluents	Volume and source of Ribavirin	Ribavirin assay concentration
1	10 mM	495 μ L of DMEM	5 μ L of stock	2.5 mM
2	4 mM	150 μ L of DMEM (1% DMSO)	100 μ L of 1	1 mM
3	2 mM	200 μ L of DMEM (1% DMSO)	50 μ L of 1	500 μ M
4	1 mM	270 μ L of DMEM (1% DMSO)	30 μ L of 1	250 μ M
5	400 μ M	180 μ L of DMEM (1% DMSO)	20 of 2	100 μ M
6	240 μ M	220 μ L of DMEM (1% DMSO)	30 of 3	60 μ M
7	200 μ M	360 μ L of DMEM (1% DMSO)	40 of 3	50 μ M
8	160 μ M	230 μ L of DMEM (1% DMSO)	20 of 3	40 μ M
9	100 μ M	180 μ L of DMEM (1% DMSO)	20 of 4	25 μ M
10	80 μ M	230 μ L of DMEM (1% DMSO)	20 of 4	20 μ M
11	60 μ M	170 μ L of DMEM (1% DMSO)	30 of 5	15 μ M
12	40 μ M	160 μ L of DMEM (1% DMSO)	40 μ L of 7	10 μ M
13	20 μ M	990 μ L of DMEM (1% DMSO)	10 μ L of 3	5 μ M
14	4 μ M	180 μ L of DMEM (1% DMSO)	20 μ L of 12	1 μ M
15	400 nM	180 μ L of DMEM (1% DMSO)	20 μ L of 14	100 nM
16	40 nM	180 μ L of DMEM (1% DMSO)	20 μ L of 15	10 nM

7.12 Ribavirin master plate to test the robustness of the assay upon using the robot

Ribavirin (R9644, Sigma) was prepared as a 1M stock in DMSO and stored at -20°C . The robustness of the assay upon using the robot (Hamilton) was assessed using sixteen different Ribavirin concentrations ranging from 2.5 mM to 10 nM (assay concentration). These concentrations were prepared as described in Table 7.3. 15 μL was required for each replicate. The robot would do a 1:100 dilution as follow, as it would do for the compound library: 1 μL from the master plate to 19 μL of DMEM (this would constitute the dilution plate). 5 μL of dilution plate to 20 μL of DMEM (this would constitute the assay plate). The same procedure was used (10 mM to 100 μM for a final assay concentration of 25 μM) to prepare the assay plate from the master plate of the library of compounds.

The master plate layout was as follows (Figure 7.2): the mock-infected cell controls and the A2-infected cell controls were added in column 1 with their respective positioning swapped in column 12. Additionally, sixteen A2-infected cell controls were dispensed between column 2 and 11 in order to correct for potential tailing off of the fluorescence signal.

	1	2	3	4	5	6	7	8	9	10	11	12
A	Mock	1 M (to 2.5 mM)	400 mM (to 1 mM)	A2	200 mM (to 500 μM)	100 mM (to 250 μM)	A2	40 mM (to 100 μM)	24 mM (to 60 μM)	20 mM (to 50 μM)	16 mM (to 40 μM)	A2
B												
C												
D												
E	A2	10 mM (to 25 μM)	8 mM (to 20 μM)	6 mM (to 15 μM)	4 mM (to 10 μM)	A2	2 mM (to 5 μM)	400 μM (to 1 μM)	40 μM (100 nM)	A2	4 μM (to 10 nM)	Mock
F												
G												
H												

Figure 7.2 Layout of the Ribavirin master plate. Mock refers to non-infected HEp-2 cells treated with growth media only, A2 refers to the A2-infected HEp-2 cells. The concentrations are made in 100% DMSO. Shown in brackets are the final assay concentrations.

Table 7.3: Preparation of the sixteen serial dilutions of Ribavirin (dispensed with the robot):

Reference number	Ribavirin concentration	Volume of DMSO	Volume and source of Ribavirin	Ribavirin assay concentration
1	1 M	N/A	Stock	2.5 mM
2	400 mM	60 μ L	40 μ L of 1	1 mM
3	200 mM	100 μ L	25 μ L of 1	500 μ M
4	100 mM	90 μ L	10 μ L of 1	250 μ M
5	40 mM	90 μ L	10 μ L of 2	100 μ M
6	24 mM	88 μ L	12 μ L of 3	60 μ M
7	20 mM	90 μ L	10 μ L of 3	50 μ M
8	16 mM	92 μ L	8 μ L of 3	40 μ M
9	10 mM	90 μ L	10 μ L of 4	25 μ M
10	8 mM	92 μ L	8 μ L of 4	20 μ M
11	6 mM	85 μ L	15 μ L of 5	15 μ M
12	4 mM	90 μ L	10 μ L of 5	10 μ M
13	2 mM	90 μ L	10 μ L of 7	5 μ M
14	400 μ M	90 μ L	10 μ L of 12	1 μ M
15	40 μ M	90 μ L	10 μ L of 14	100 nM
16	4 μ M	90 μ L	10 μ L of 15	10 nM

7.13 Mode of action of JNJ-4749914

In a 6-well plate, glass coverslips (ø19 mm, VWR) were added to the bottom of the wells, and:

- Mock- and virus-infected wells: 500 µL of DMEM (1% DMSO) were added to the corresponding wells or,
- Virus-infected and treated with JNJ-4749914: 500 µL of a solution of JNJ-4749914 in DMEM (100 µM, 1% DMSO) were added to the corresponding well

HEp-2 cells (1.5 mL / well, 2×10^5) were then added to the 6-well plate and incubated for 24 hr at 37 °C. 500 µL of DMEM (mock-infected control) or 500 µL of virus at a M.O.I. = 0.5 (virus-infected control and virus-infected treated with JNJ-4749914) were added and the plate was incubated for 24 hr at 37 °C. The media was then removed and the cells washed three times with PBS (2 mL), and replaced by:

- Mock- and virus-infected wells: 2 mL DMEM (0.25% DMSO)
- Virus-infected treated with JNJ-4749914: 2 mL of a solution of JNJ-4749914 in DMEM (25 µM, 0.25% DMSO)

The plate was then incubated until syncytia could be observed (at least 3 days), and the cells were:

- i) Washed three times with PBS (2 mL) and fixed with methanol (1 mL) for 10 min at -20 °C
- ii) Washed three times with PBS (2 mL) and were permeabilised with PBST (1 mL) for 15 min at room temperature, and washed three times with PBST (2 mL)
- iii) Blocked with PBST with 5% skimmed milk (Fluka) (1 mL) overnight at 4 °C, and washed three times with PBST (1 mL)
- iv) Incubated with a goat anti-RSV polyclonal primary antibody (7950-0004, AbD Serotec) in PBST with 5% skimmed milk (1:100, 1 mL) for 1 hr at 37 °C, and washed three times with PBST (150 µL)

- v) Incubated with a donkey anti-goat polyclonal secondary antibody conjugated to fluorescein isothiocyanate (ab6881, Abcam) in PBST with 5% skimmed milk (1:200, 1 mL) for 1 hrs at 37 °C, and washed three times with PBST (150 µL)
- vi) Were washed twice in PBS (1 mL) and the coverslips were mounted onto glass slides (Agar Scientific) using VECTASHIELD Mounting Medium with DAPI (VECTOR Laboratories). The slides were stored in the dark at 4 °C until confocal imaging.
- vii) Confocal sections of fixed samples were captured on the laser scanning microscope 510 META Microscope (Carl Zeiss Ltd) equipped with a 40× and 63×, NA 1.4, oil immersion lens.

Each condition was tested in duplicate.

7.14 High-throughput screening

The results were stored within a Laboratory Information Management System (LIMS). The LIMS tracks the location of compounds in bar-coded plates and integrates biological (assay) and chemical (structural) data. The screening data were then rigorously analysed⁸¹⁻⁸³ (*e.g.* Z-factor, as a measurement of the assay quality¹³⁶) and active compounds are selected as having an activity greater than three standard deviations from the normalised mean^{81,83,136,203}.

7.15 Compounds characterisation

All reactions were carried out in oven-dried glassware under an atmosphere of N₂ from a Schlenk line fitted with a nitrogen bubbler, using dry techniques. Tetrahydrofuran, dichloromethane, toluene, acetonitrile were dried and purified by means of a Pure Solv MD solvent Purification System (Innovative Technology Inc.) or obtained from Oxford sure/seal™ bottles from Sigma-Aldrich. All other solvents used were chromatography or analytical grade. Chemicals used were supplied by Sigma–Aldrich, Alfa-Aesar, Fluka, and TCI Europe.

Thin layer chromatography was carried out on aluminium backed silica (Merck silica gel 60 F₂₅₄) plates supplied by Merck. Visualisation of the plates was achieved using an ultraviolet lamp ($\lambda_{\text{max}} = 254 \text{ nm}$), KMnO₄ and anisaldehyde. Flash chromatography was carried out using silica gel 60 (35-70 μm particles) according to the method of Still, Kahn and Mitra²⁰⁴.

Optical rotation measurements were carried out at room temperature either on a Perkin-Elmer AA-1000 with a path length of 0.5 dm or on a Schmidt+Haensch Polartronic H 532 with a path length of 1 dm; concentrations are g/100mL and the optical rotations are given in $10^{-1} \text{ deg cm}^2\text{g}^{-1}$ (omitted). Infrared spectra were recorded on a Perkin-Elmer one FT-IR spectrometer and the wavenumbers (ν_{max}) are given in cm^{-1} (omitted).

Proton and carbon NMR data were collected on an Avance 500, DPX500 and Bruker DPX 300. All shifts were recorded against an internal standard of tetramethylsilane (TMS). Solvents (CDCl₃, C₆D₆, DMSO-*d*₆ and MeOD) used for NMR experiments were obtained from Sigma-Aldrich. Splitting patterns in this report have been recorded in an abbreviated manner, s (singlet), d (doublet), t (triplet), q (quartet) and m (multiplet). See the abbreviations section for additional splitting pattern abbreviation. NMR data was recorded in the following format, PPM (*splitting pattern, number of protons, coupling constant (Hz), proton ID*). Signal assignments were made by the aid of COSY, DEPT 90 and 135, HMQC, HMBC, and NOESY.

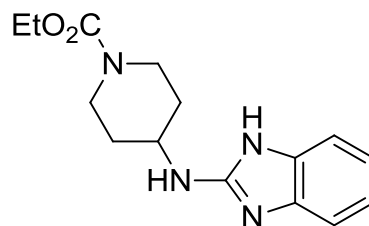
Low resolution mass spectra data were recorded on a Agilent 1200 series LC system comprising a Bruker HCT Ultra ion trap mass spectrometer, a high vacuum degasser, a binary pump, a high performance autosampler, an autosampler thermostat, a thermostated column compartment a diode array detector. The system used two solvent systems: MeCN/H₂O + 0.1% formic acid with a Phenomenex Luna C18 50 × 2mm 5 micron column or MeCN/H₂O with a Phenomenex Luna C18 50 × 2mm 5 micron column

Nominal and high resolution mass spectrometry using electrospray ionization was recorded by Mrs Tanya Marinko-Covell on a Micromass LCT-KA11 or a Bruker Daltronics micrOTOF spectrometer. Field Desorption Ionisation mass spectra were acquired on a Water-Micromass GCT premier spectrometer equipped with a Linden LIFDI probe.

Method A: Synthesis of γ -lactams from cyclic sulfamidates

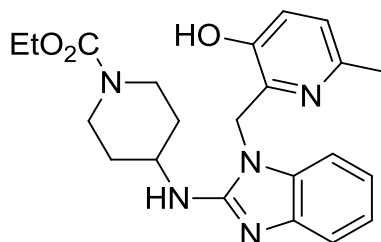
Diethyl malonate or *N*-(diphenylmethylene)glycine ethyl ester (2.0 eq.) was added to a suspension of sodium hydride (2.0 eq.) in DMF (0.25 M). The resulting mixture was stirred at room temperature for 20 min and the cyclic sulfamidate (1.0 eq.) was added in one portion. The reaction mixture was heated to 50 °C for 24 h, cooled to room temperature and treated with concentrated sulfuric acid (6 drops / mmol) and water (6 drops / mmol) (pH < 2) and stirred at room temperature for a further 48 hrs. The reaction mixture was neutralised with saturated aqueous NaHCO₃ (pH 7-8), diluted with EtOAc and dried (Na₂SO₄). The solvent was removed under reduced pressure to give the crude product which was dissolved in toluene (0.05 M) and heated to 60 °C overnight and the solvent removed under reduced pressure to give the crude product.

Ethyl 4-[(1H-1,3-benzodiazol-2-yl)amino]piperidine-1-carboxylate **9**



2-Chlorobenzimidazole **7** (3.2 g, 21 mmol) and ethyl-4-amino-1-piperidinecarboxylate **8** (14.5 mL, 84 mmol) were stirred overnight at 130 °C after which the reaction was cooled to room temperature and acetone (30 mL) was added. The resulting precipitate was filtered and the filtrate was removed under reduced pressure to give the crude which was purified by flash chromatography, eluting with 95:5:0.1 DCM–MeOH–NH₄OH, to give the *benzimidazole* **9** (2.3 g, 38%) as a light yellow solid, $R_f = 0.25$ (95:5:0.1 DCM–MeOH–NH₄OH); ¹H NMR (500 MHz; MeOD) δ 7.26-7.22 (m, 2H, Ar 2-H & 5-H or 3-H & 4-H), 7.03-6.99 (m, H, Ar 2-H & 5-H or 3-H & 4-H), 4.17 (q, $J = 7.1$ Hz, 2H, Et 1-H₂), 4.19-4.11 (m, 2H, 2-H or 6-H), 3.86 (tt, $J = 10.6, 4.0$ Hz, 1H, 4-H), 3.08 (br, 2H, 2-H or 6-H), 2.15-2.06 (m, 2H, 3-H or 5-H), 1.55-1.44 (m, 2H, 3-H or 5-H), 1.31 (t, $J = 7.1$ Hz, 3H, Et 2-H₃); ¹³C NMR (125 MHz, CDCl₃) δ 157.3, 155.9, 121.4, 112.8, 62.8, 50.9, 44.0, 33.4, 15.0; HRMS-ES m/z 289.1655 (M+H calculated for C₁₅H₂₀N₄O₂ requires 289.1659).

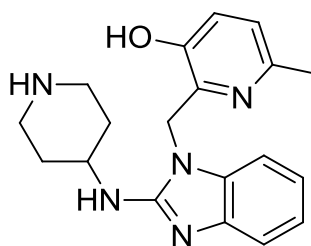
Ethyl 4-({1-[(3-hydroxy-6-methylpyridin-2-yl)methyl]-1H-1,3-benzodiazol-2-yl}amino)piperidine-1-carboxylate **11**



2-(chloromethyl)-6-methylpyridin-3-ol **10**^{††††} (1.2 g, 6.2 mmol) and K_2CO_3 (2.3 g, 16.4 mmol) were added to a solution of benzimidazole **9** (1.2 g, 4.1 mmol) in acetonitrile (19 mL). The resulting mixture was stirred overnight at 90 °C after which the reaction was cooled to room temperature. The solvent was removed under reduced pressure to give the crude which was dissolved in 9:1 DCM–MeOH (30 mL). The organic phase was washed with a 10% aqueous solution of K_2CO_3 (15 mL), dried ($MgSO_4$) and the solvent was removed under reduced pressure. Acetone was added and the precipitate filtered to afford the *N*-alkylated benzimidazole **11** (370 mg, 18%) as a light yellow solid, $R_f = 0.57$ (9:1 DCM–MeOH); 1H NMR (500 MHz; MeOD) δ 7.47-7.44 (m, 1H, Ar H), 7.33-7.29 (m, 1H, Ar H), 7.19 (d, $J = 8.3$ Hz, 1H, Py 4-H or 5-H), 7.10 (d, $J = 8.4$ Hz, 1H, Py 4-H or 5-H), 7.09-7.02 (m, 2H, Ar H), 5.23 (s, 2H, Bn CH_2), 4.20 (q, 2H, Et 1- H_2), 4.13 (br dt, $J = 13.7, 3.7$ Hz, 2H, 2-H or 6-H), 4.00 (tt, $J = 10.1, 3.9$ Hz, 1H, 4-H), 3.18 (br, 2H, 2-H or 6-H), 2.47 (s, 3H, Me), 2.23-2.15 (m, 2H, 3-H or 5-H), 1.64-1.53 (m, 2H, 3-H or 5-H), 1.33 (t, $J = 7.1$ Hz, 3H, Et 2- H_3); ^{13}C NMR (125 MHz, $CDCl_3$) δ 157.4, 155.9, 151.1, 149.6, 143.6, 142.5, 135.6, 125.4, 125.2, 122.2, 120.8, 115.9, 109.7, 62.8, 50.9, 44.0, 43.8, 33.4, 23.2, 15.0; HRMS-ES m/z 410.2202 (M+H calculated for $C_{22}H_{27}N_5O_3$ requires 410.2187).

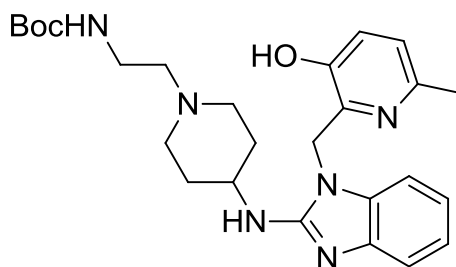
^{††††} 2-(chloromethyl)-6-methylpyridin-3-ol was prepared in a single step from 2,6-lutidine- α ,2,3-diol and was used crude.

6-Methyl-2-({2-[(piperidin-4-yl)amino]-1H-1,3-benzodiazol-1-yl}methyl)pyridin-3-ol **12**



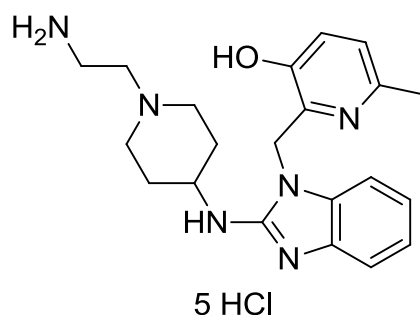
A 33% solution of HBr in acetic acid (8 mL) was added to the *N*-alkylated benzimidazole **11** (300 mg, 0.7 mmol). The resulting mixture was stirred overnight at 60 °C after which the reaction was cooled to room temperature. A 10% aqueous solution of K₂CO₃ (10 mL) followed by K₂CO₃ (powder) were added to neutralise the acid. The solvent was removed under reduced pressure to give the crude which was dissolved in 9:1 DCM–MeOH (30 mL). The organic phase was washed with water (10 mL) and the aqueous layer was saturated with K₂CO₃ (powder). The organic layer was dried (MgSO₄) and the solvent was removed under reduced pressure to give the *secondary amine* **12** (198 mg, 80 %) as a light brown solid, ¹H NMR (500 MHz; MeOD) δ 7.44-7.39 (m, 1H, Ar H), 7.25-7.21 (m, 1H, Ar H), 7.08 (d, *J* = 8.3 Hz, 1H, Py 4-H or 5-H), 7.02-6.93 (m, 3H, Ar H, Py 4-H or 5-H), 5.14 (s, 2H, Bn CH₂), 3.93 (tt, *J* = 10.3, 3.9 Hz, 1H, Piperidine 1-H), 3.34-3.25 (m, 2H, Piperidine 3-H or 5-H), 3.00-2.92 (m, 2H, Piperidine 3-H or 5-H), 2.39 (s, 3H, Me), 2.23 (m, 2H, Piperidine 2-H or 6-H), 1.70 (m, 2H, Piperidine 2-H or 6-H); ¹³C NMR (125 MHz, MeOD) δ 156.0, 147.7, 144.1, 142.7, 135.8, 126.4, 125.5, 122.1, 120.7, 115.8, 109.7, 45.3, 44.3, 32.9, 24.2, 23.1; HRMS-ES *m/z* 338.1982 (M+H calculated for C₁₉H₂₃N₅O requires 338.1975). No *R_f* was recorded as the compound stayed on the baseline in 50:8:1 DCM–MeOH–NH₄OH.

tert-Butyl *N*-{2-[4'-({1-[(3-hydroxy-6-methylpyridin-2-yl)methyl]-1H-1,3-benzodiazol-2-yl}amino)piperidin-1'-yl]ethyl}carbamate **14**



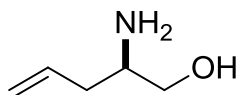
tert-Butyl *N*-(2-bromoethyl)carbamate **13** (159 mg, 0.7 mmol) and Et₃N (123 μ L, 0.9 mmol) were added to a solution of the secondary amine **12** (198 mg, 0.6 mmol) in DMF (4.5 mL). The resulting mixture was stirred overnight at 80 °C and the solvent was evaporated. The residue was dissolved in 4:1 DCM–water (30 mL) and the organic phase was dried (MgSO₄) and the solvent was removed under reduced pressure to the crude product which was purified by flash chromatography, eluting with 9:1 DCM–MeOH, to give the *carbamate* **14** (88 mg, 31 %) a yellow solid, $R_f = 0.25$ (9:1 DCM–MeOH); ¹H NMR (500 MHz; MeOD) δ 7.43–7.39 (m, 1H, Ar H), 7.28–7.24 (m, 1H, Ar H), 7.14 (d, $J = 8.3$ Hz, 1H, Py 4-H or 5-H), 7.05–6.97 (m, 3H, Ar H, Py 4-H or 5-H), 5.16 (s, 2H, Bn CH₂), 3.81–3.73 (m, 1H, 4'-H), 3.23 (br t, $J = 6.7$ Hz, 2H, 1-H or 2-H), 3.00 (br dd, $J = 11.5$ Hz, 2H, 2'-H or 6'-H), 2.54 (t, $J = 6.8$ Hz, 2H, 1-H or 2-H), 2.44 (s, 3H, Me), 2.33 (t, $J = 10.7$ Hz, 2H, 2'-H or 6'-H), 2.18–2.11 (m, 2H, 3'-H or 5'-H), 1.69 (td, $J = 13.8, 3.4$ Hz, 2H, 3'-H or 5'-H), 1.45 (s, 9H, ^{*t*}Bu); ¹³C NMR (125 MHz, MeOD) δ 158.4 (C=O), 155.8 (Ar C), 151.1 (Ar C), 149.7 (Ar C), 143.5 (Ar C), 142.0 (Ar C), 135.5 (Ar C), 125.4 (Ar C), 125.2 (Ar C), 122.3 (Ar C), 121.0 (Ar C), 115.8 (Ar C), 109.7 (Ar C), 80.2 (C(CH₃)₃), 58.7 (C-1 or C-2), 53.5 (C-2' and C-6'), 49.9 (C-4'), 44.1 (C-1 or C-2), 38.5 (Bn CH₂), 33.1 (C-3' and C-5'), 28.9 (C(CH₃)₃), 23.4 (Me); HRMS-ES m/z 481.2943 (M+H calculated for C₂₆H₃₆N₆O₃ requires 481.2922). IR spectrum could not be recorded.

2-[(2-[[1-(2-Aminoethyl)piperidin-4-yl]amino]-1H-1,3-benzodiazol-1-yl)methyl]-6-methylpyridin-3-ol 15



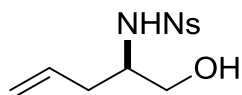
5N HCl in propan-2-ol (570 μ L) was added to a solution of the carbamate **14** (45 mg, 94 μ mol) in propan-2-ol (5.6 mL). The resulting mixture was stirred at 60 $^{\circ}$ C for 4 hrs and the resulting precipitate was filtered, washed with propan-2-ol and diisopropylether to give JNJ-4749914 **15** (21 mg, 40%) as a light brown solid, ^1H NMR (500 MHz; CDCl_3) δ 7.80 (d, 1H, $J = 8.2$ Hz, Py 4-H or 5-H), 7.67 (d, $J = 8.6$ Hz, 1H, Py 4-H or 5-H), 7.57 (d, $J = 7.5$ Hz, 1H, Ar-H), 7.45 (d, $J = 7.9$ Hz, 1H, Ar-H), 7.42-7.31 (m, 2H, Ar-H), 5.83 (s, 2H, Bn CH_2), 4.26 (br s, 1H, 1-H), 3.91 (br d, $J = 12.3$ Hz, 2H, 3-H or 5-H), 3.68-3.55 (m, 4H, Et 1- H_2 and 2- H_2), 3.49 (br t, $J = 11.9$ Hz, 2H, 3-H or 5-H), 2.76 (s, 3H, Me), 2.51 (br d, $J = 13.5$ Hz, 2H, 2-H or 6-H), 2.45-2.32 (m, 2H, 2-H or 6-H); ^{13}C NMR (125 MHz, CDCl_3) δ 153.8, 151.3, 147.8, 137.2, 132.0, 131.5, 130.5, 129.0, 125.8, 125.4, 113.1, 111.5, 54.7, 53.5, 50.6, 43.2, 35.4, 30.3, 20.2; IR (film): 3368, 3043, 2890, 1644, 1618, 1550, 1481; HRMS-ES m/z 381.241 ($\text{M}+\text{H}$ calculated for $\text{C}_{22}\text{H}_{29}\text{N}_5\text{O}$ requires 381.2397). R_f was not recorded. IR spectrum could not be recorded.

(2R)-2-Aminopent-4-en-1-ol 40



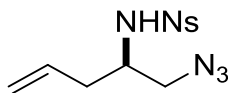
Acetyl chloride (4.2 mL, 59.4 mmol) was added to a solution of D-allylglycine hydrochloride **39** (1.0 g, 6.6 mmol) in MeOH (14 mL) cooled to 0 °C. The resulting mixture was then heated to reflux for 4 h before being cooled to room temperature. The solvent was removed under reduced pressure and the yellow oil obtained was dried overnight to give the crude *methyl ester* as a colourless solid. Lithium aluminium hydride (531 mg, 14.0 mmol) was added to a solution of the crude methyl ester in THF (20 mL) cooled to 0 °C. The resulting mixture was then warmed to room temperature and stirred overnight, before being diluted with ether (25 mL). It was then quenched by the addition of water (1 mL) and 15% NaOH (1 mL), filtered through a pad of Celite, which was washed with ether (50 mL), and dried (Na₂SO₄). The solvent was removed under reduced pressure to give the crude product which was purified by flash chromatography, eluting with 50:8:1 DCM–EtOH–NH₄OH, to give the *amino alcohol* **40**¹⁵⁹ (600 mg, 90%) as a brown oil, *R*_f = 0.21 (50:8:1 DCM–EtOH–NH₄OH); [α]_D: –22.0 (c. 1.2, CHCl₃); ¹H NMR (500 MHz; CDCl₃) δ 5.78 (dddd, 1H, *J* = 16.9, 10.4, 7.9, 6.5 Hz, 4-H), 5.11 (m, 2H, 5-H₂), 3.60 (dd, *J* = 10.7, 3.9 Hz, 1H, 1-H_A), 3.35 (dd, *J* = 10.8, 7.4 Hz, 1H, 1-H_B), 2.93 (m, 1H, 2-H), 2.40 (s, 3H, NH₂, OH), 2.23 (app dddt, *J* = 14.3, 6.5, 5.2, 1.3 Hz, 1H, 3-H_A), 2.04 (app dtt, *J* = 13.9, 8.0, 1.0 Hz, 1H, 3-H_B); ¹³C NMR (125 MHz, CDCl₃) δ 134.9, 117.8, 66.3, 52.1, 38.8; IR (film): 3354, 3071, 2910, 1641, 1593, 1441, 1360; HRMS-EI *m/z* 102.0916 (M+H calculated for C₅H₁₁NO requires 102.0919).

N*-[(2*R*)-1-hydroxypent-4-en-2-yl]-2-nitrobenzene-1-sulfonamide **41*



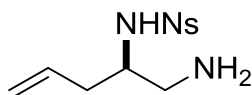
2-Nitrobenzenesulfonyl chloride (1.0 g, 4.7 mmol) was added to a solution of amino alcohol **40** (500 mg, 5.0 mmol) and sodium carbonate (525 mg, 5.0 mmol) in 50:50 DCM–H₂O (6 mL). The resulting mixture was stirred at room temperature overnight before being diluted with water and acidified (pH < 2) with 5M aqueous HCl. The aqueous phase was extracted with DCM (3 × 20 mL) and the organic washings were washed with brine (20 mL) and dried (Na₂SO₄). The solvent was removed under reduced pressure to give the crude product which was purified by flash chromatography, eluting with 50:50 petrol–EtOAc to give the *sulfonamide* **41** (750 mg, 55%) as a viscous light yellow oil, *R*_f = 0.25 (50:50 Petrol–EtOAc); [α]_D: –108.3 (c. 1.3, CHCl₃); ¹H NMR (500 MHz; CDCl₃) δ 8.18–8.12 (m, 1H, Ns), 7.91–7.85 (m, 1H, Ns), 7.78–7.70 (m, 2H, Ns), 5.64–5.50 (m, 2H, NH, 4-H), 5.06–4.92 (m, 2H, 5-H₂), 3.69–3.52 (m, 3H, 2-H, 1-H₂), 2.35–2.23 (m, 2H, 3-H₂), 1.97 (br s, 1H, OH); ¹³C NMR (75 MHz, CDCl₃) δ 147.8 (Ns), 134.6 (Ns), 133.6 (Ns), 132.9 (Ns), 132.8 (Ns), 130.7 (Ns), 125.4 (C-4), 119.1 (C-5), 64.5 (C-1), 56.2 (C-2), 36.3 (C-3); IR (film): 3547, 3340, 3097, 2939, 1594, 1542, 1362; HRMS-EI *m/z* 287.0700 (M+H calculated for C₁₁H₁₄N₂O₅S requires 287.0702).

N*-[(2*R*)-1-Azidopent-4-en-2-yl]-2-nitrobenzene-1-sulfonamide **42*



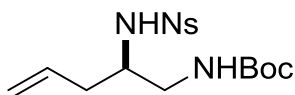
Mesyl chloride (100 μ L, 1.3 mmols) was added to a solution of the sulfonamide **41** (338 mg, 1.18 mmols), triethylamine (247 μ L, 1.77 mmols) in THF (4 mL) cooled to -5 $^{\circ}$ C. The resulting mixture was stirred at this temperature for 5 min and was filtered prior to the solvent being removed under reduced pressure. The resulting liquid was dissolved in EtOAc–H₂O (67:33, 15 mL) and the organic phase was dried (MgSO₄) and the solvent was removed under reduced pressure to give the crude mesylate which was used immediately in the next step. Sodium azide (115 mg, 1.8 mmols) was added portion-wise to a solution of the crude mesylate (330 mg, 0.91 mmol) in DMF (7 mL) at 0 $^{\circ}$ C. The reaction was warmed to and stirred at room temperature for 2 h. Ether (10 mL) was added to the reaction mixture and DMF was extracted with brine (3 \times 10 mL). The organic phase was dried (MgSO₄), filtered and the solvent was removed under reduced pressure to give the crude product which was purified by flash chromatography, eluting with 75:25 petrol–EtOAc to give the *azide* **42** (200 mg, 54%) as a viscous yellow oil, R_f = 0.73 (50:50 Petrol–EtOAc); $[\alpha]_D$: +6.4 (c. 1.2, CHCl₃); ¹H NMR (500 MHz; CDCl₃) δ 8.17-8.13 (m, 1H, Ns), 7.93-7.88 (m, 1H, Ns), 7.79-7.72 (m, 2H, Ns), 5.61-5.48 (m, 2H, 4-H and NH), 5.08 (dq, J = 17.1, 1.4 Hz, 1H, 5-H_A), 5.02 (ddt, J = 10.1, 1.8, 1.0 Hz, 1H, 5-H_B), 3.66-3.60 (m, 1H, 2-H), 3.42 (dd, J = 5.1, 2.3 Hz, 2H, 1-H_A and 1-H_B), 2.33-2.27 (m, 2H, 3-H_A and H_B); ¹³C NMR (125 MHz, CDCl₃) δ 147.7 (Ns), 134.8 (Ns), 133.6 (Ns), 133.0 (Ns), 132.0 (Ns), 130.5 (Ns), 125.6 (C-4), 119.8 (C-5), 54.5 (C-1), 53.9 (C-2), 36.3 (C-3), 36.3 (C-3); IR (film): 3340, 3097, 2934, 2105, 1643, 1594, 1539; HRMS-ES m/z 334.0583 (M+Na calculated for C₁₁H₁₃N₅O₄S requires 334.058).

N*-[(2*R*)-1-Aminopent-4-en-2-yl]-2-nitrobenzene-1-sulfonamide **43*



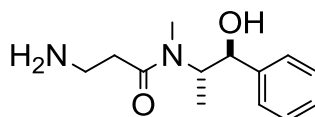
Triphenylphosphine (233 mg, 0.9 mmol) and water (0.3 mL) were added to a solution of the azide **42** (184 mg, 0.59 mmol) in THF (6 mL). The resulting mixture was stirred overnight at room temperature and the solvent was removed under reduced pressure to give the product which was purified by flash chromatography eluting with 90:10 Petrol–EtOAc followed by 50:8:1 DCM–EtOH–NH₄OH to give the *amine* **43** (117 mg, 69%) as a yellow oil, $R_f = 0.5$ (50:8:1 DCM–EtOH–NH₄OH); $[\alpha]_D^{25}$: -100.2 (c. 0.9, CHCl₃); ¹H NMR (500 MHz; CDCl₃) δ 8.18–8.11 (m, 1H, Ns), 7.90–7.83 (m, 1H, Ns), 7.76–7.68 (m, 2H, Ns), 5.55 (ddt, $J = 17.3, 10.1, 7.2$ Hz, 1H, 4-H), 4.95 (m, 2H, 5-H₂), 3.48–3.42 (m, 1H, 2-H), 2.79–2.70 (m, 2H, 1-H), 2.68–2.28 (br, 3H, NH), 2.23 (app t, $J = 6.9$ Hz, 2H, 3-H₂); ¹³C NMR (75 MHz, CDCl₃) δ 147.8 (Ns), 135.0 (Ns), 133.4 (Ns), 133.1 (Ns), 132.8 (C-4), 130.6 (Ns), 125.3 (Ns), 118.7 (C-5), 56.8 (C-2), 45.1 (C-1), 37.3 (C-3); IR (film): 3426, 3064, 2956, 1648, 1594, 1539; HRMS-ES m/z 286.0857 (M+H calculated for C₁₁H₁₅N₃O₄S requires 286.0856).

tert*-Butyl *N*-[(2*R*)-2-[(2-nitrobenzene)sulfonamido]pent-4-en-1-yl]carbamate **30*



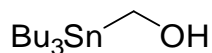
Di-*tert*-butyl dicarbonate (104 mg, 0.48 mmol) was added to a solution of diisopropylethylamine (91 μ L, 0.52 mmol) and the amine **43** (117 mg, 0.41 mmol) in DCM (7 mL). The reaction mixture was stirred overnight and the organic phase was washed with an aqueous solution of 0.5 M citric acid (10 mL), a saturated aqueous solution of NaHCO₃ (10 mL), brine (10 mL), dried (Na₂SO₄). The organic phase was filtered and the solvent was removed under reduced pressure to give the crude product which was purified by flash chromatography, eluting with 67:33 Petrol–EtOAc, to give the *building block* **30** (120 mg, 75%) as an orange oil, $R_f = 0.24$ (2:1 Petrol–EtOAc); $[\alpha]_D^{25} = -37.2$ (c. 1.1, CHCl₃); ¹H NMR (500 MHz; CDCl₃) δ 8.15-8.11 (m, 1H, Ns), 7.89-7.85 (m, 1H, Ns), 7.76-7.71 (m, 2H, Ns), 5.57-5.46 (m, 2H, 4-H and NH(Ns)), 5.03-4.90 (m, 2H, 5-H₂), 4.84 (br s, 1H, NH(Boc)), 3.64-3.55 (m, 1H, 2-H), 3.38-3.29 (m, 1H, 1-H_A), 3.11 (ddd, $J = 14.2, 7.3, 6.1$ Hz, 1H, 1-H_B), 2.29-2.15 (m, 2H, 3-H₂), 1.42 (9H, C(CH₃)₃); ¹³C NMR (125 MHz, CDCl₃) δ 156.3 (C=O), 147.8 (Ns), 134.7 (Ns), 133.5 (Ns), 132.9 (Ns), 132.4 (Ns), 130.7 (Ns), 125.4 (C-4), 119.3 (C-5), 79.8 (C(CH₃)₃), 55.0 (C-2), 44.4 (C-1), 37.4 (C-3), 28.3 (C(CH₃)₃); IR (film): 3346, 3096, 2980, 1699, 1643, 1593, 1539; HRMS-ES m/z 408.1211 (M+Na calculated for C₁₆H₂₃N₃O₆S requires 408.12).

3-Amino-N-[(1*S*,2*S*)-1-hydroxy-1-phenylpropan-2-yl]-*N*-methylpropanamide **46**



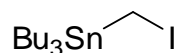
Pivaloyl chloride (2.2 mL, 18 mmols) was added to a solution of β -Boc-alanine **44** (3.03 g, 16 mmols) and triethylamine (2.6 mL, 18.7 mmol) in DCM (25 mL) cooled to 0 °C. The resulting mixture was stirred at 0 °C for 1h. Triethylamine (2.5 mL, 18 mmols) and a solution of (+)-*S,S*-pseudoephedrine **45** (2.64 g, 18 mmols) in DCM (10 mL) were added and the resulting mixture was stirred at room temperature overnight. The solvent was removed under reduced pressure and MeOH–water (50:50, 18 mL) was added followed by the addition of concentrated HCl (14 mL) at 0 °C. The resulting mixture was stirred for 4 hr, the solvent was removed under reduced pressure and water (20 mL) was added. The aqueous phase was washed with EtOAc–hexane (50:50, 2 \times 20 mL) and basified with 50% aqueous NaOH (pH > 12). The aqueous phase was then extracted with DCM (5 \times 25 mL). The organic extracts were combined, dried (Na₂SO₄), and dried further (K₂CO₃, overnight). The residue was recrystallised from toluene to give the *amide* **46**¹⁶⁴ (1.8 g, 47%) as a colourless solid, [α]_D: +107.1 (c. 2.0, CHCl₃); ¹H NMR (500 MHz; CDCl₃) δ 7.39-7.24 (m, 8H, Ar H^{rotA,rotB}), 4.62-4.55 (m, 1.8H, 2'-H^{rotA}, 1'-H^{rotA}), 4.53 (d, *J* = 9 Hz, 0.7H, 1'-H^{rotB}), 4.08-4.00 (m, 0.6H, 2'-H^{rotB}), 3.11-3.03 (m, 0.6H, 2-H^{rotB} or 3-H^{rotB}), 3.03-2.94 (m, 2.6H, 2-H^{rotA} or 2-H^{rotB} or 3-H^{rotA} or 3-H^{rotB}), 2.92 (s, 1.9H, NMe^{rotB}), 2.86 (s, 3H, NMe^{rotA}), 2.84-2.76 (m, 0.9H, 2-H^{rotA} or 3-H^{rotA}), 2.73-2.55 (br, 5.5H, OH and NH₂), 2.55-2.47 (m, 1.3H, 2-H^{rotA} or 2-H^{rotB} or 3-H^{rotA} or 3-H^{rotB}), 2.44-2.34 (m, 1.8H, 2-H^{rotA} or 2-H^{rotB} or 3-H^{rotA} or 3-H^{rotB}), 1.04 (d, *J* = 6.6 Hz, 3H, Me^{rotA}), 0.96 (d, *J* = 6.8 Hz, 1.9H, Me^{rotB}); ¹³C NMR (75 MHz, CDCl₃) δ 173.8 (C=O^{rotA}), 172.9 (C=O^{rotB}), 142.3 (Ar C-1^{rotA}), 142.0 (Ar C-1^{rotB}), 128.6 (Ar^{rotA,rotB}), 128.4 (Ar^{rotA,rotB}), 128.1 (Ar^{rotA,rotB}), 127.8 (Ar^{rotA,rotB}), 127.0 (Ar^{rotA,rotB}), 126.6 (Ar^{rotA,rotB}), 76.1 (C-1^{rotA} or C-2^{rotA}), 75.4 (C-1^{rotB}), 58.5 (C-2^{rotB}), 57.5 (C-1^{rotA} or C-2^{rotA}), 38.2 (C-2^{rotB} or C-3^{rotB}), 37.8 (C-2^{rotB} or C-3^{rotB}), 36.9 (C-2^{rotB} or C-3^{rotB}), 35.8 (C-2^{rotB} or C-3^{rotB}), 31.9 (NMe^{rotA}), 26.5 (NMe^{rotB}), 15.6 (Me^{rotB}), 14.4 (Me^{rotA}); IR (film): 3357, 3142, 2931, 1621, 1454, 1416; HRMS-ES *m/z* 237.16 (M+H calculated for C₁₃H₂₀N₂O₂ requires 237.1598). No *R_f* was recorded. Mixtures of rotamers A (rotA) and B (rotB).

(Tributylstannyl)methanol 49

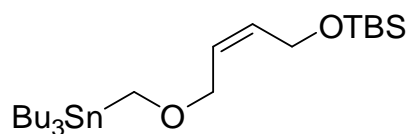


n-Butyllithium (2.5 M in hexanes, 15.2 mL, 38.0 mmol) was added to a solution of diisopropylamine (722 μL , 40.0 mmol) in THF (140 mL) cooled to 0 °C. The resulting mixture was stirred at 0 °C for 30 min, before tributyltin hydride **48** (9.2 mL, 34 mmol) was added dropwise. The resulting mixture was stirred at 0 °C for 20 min, before paraformaldehyde (1.5 g, 48 mmol) was added as a suspension in THF (20 mL). The reaction mixture was warmed to room temperature, stirred for 3 h, and poured into water–ether (50:50, 300 mL). The aqueous layer was extracted with ether (150 mL), and the organic extracts were combined, washed with water (250 mL), brine (250 mL), dried (Na_2SO_4), and the solvent removed under reduced pressure to give the crude product which was purified by flash chromatography, eluting with 83:17 pentane–EtOAc, to give the *alcohol* **49**¹⁶⁶ (8.4 g, 76%) as a colourless oil, $R_f = 0.62$ (83:17 Pentane–EtOAc); ^1H (500 MHz; CDCl_3) δ 4.04 (d, $J = 4.7$ Hz, 2H, CH_2OH), 1.63–1.44 (m, 6H, CH_2Bu), 1.37–1.23 (m, 6H, CH_2Bu), 0.96–0.81 (m, 15H, CH_3Bu and CH_2Bu); ^{13}C (125 MHz, CDCl_3) δ 55.6, 29.1, 27.3, 13.7, 8.9; IR (film): 3325, 2926, 2730, 1745, 1727, 1463, 1376; Mass spectra were unobtainable.

Tributyl(iodomethane)stannane **50**

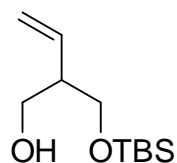


A solution of *N*-iodosuccinimide (8.8 g, 39.2 mmol) in THF (80 mL) was added dropwise to solution of triphenylphosphine (10.3 g, 39.2 mmol) in THF (80 mL). The resulting mixture was stirred at room temperature for 10 min, before a solution of the alcohol **49** (8.4 g, 26.2 mmol) in THF (45 mL) was added. The reaction mixture was stirred overnight at room temperature, before being poured into pentane–H₂O (50:50, 200 mL), and the aqueous phase was extracted with pentane (3 × 100 mL). The organic extracts were combined, dried (Na₂SO₄), and the solvent removed under reduced pressure to give the crude product which was purified by flash chromatography, eluting with neat pentane, to give the *iodide* **50**¹⁶⁶ (9.9 g, 87%) as a colourless oil, *R*_f = 0.78 (100:0 Pentane); ¹H (500 MHz; CDCl₃) δ 1.95 (t, *J* = 9 Hz, 2H, CH₂I), 1.58-1.49 (m, 6H, CH₂Bu), 1.37-1.28 (m, 6H, CH₂Bu), 1.01-0.95 (m, 6H, CH₂Bu), 0.91 (dd, 9H, *J* = 9.4, 5.3 Hz, CH₃Bu); ¹³C (125 MHz, CDCl₃) δ 28.8, 27.3, 13.7, 10.7; IR (film): 3018, 2957, 2871, 2853, 1463, 1417, 1291; Mass spectra were unobtainable.



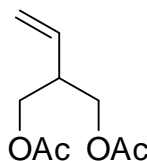
A solution of the alcohol **51** (8.0 g, 39.5 mmol) in THF (110 mL) was added to a suspension of sodium hydride (60 % dispersion in oil, 1.6 g, 40.0 mmol) in THF (140 mL) at room temperature, before a solution of the iodide **50** (8.5 g, 19.7 mmol) in THF (110 mL) was added. The resulting mixture was stirred overnight at room temperature, before being quenched with water (200 mL), and brine (60 mL). The aqueous phase was extracted with ether (3 × 200 mL). The organic extracts were combined, washed with brine (200 mL), dried (Na₂SO₄), and the solvent removed under reduced pressure to give the crude product which was purified by flash chromatography, eluting with 100:0 to 90:10 pentane–EtOAc, to give the *stannane* **52**¹⁶⁶ (7.2 g, 71%, mixture) as a colourless oil, *R*_f = 0.8 (100:0 Pentane); ¹H (500 MHz; CDCl₃) δ 5.62-5.55 (m, 1H, 6-H or 7-H), 5.50-5.44 (m, 1H, 6-H or 7-H), 4.20-4.14 (m, 2H, 5-H₂ or 8-H₂), 3.87-3.82 (m, 2H, 5-H₂ or 8-H₂), 3.67-3.58 (t, *J* = 7.5 Hz, 2H, 10-H₂), 1.50-1.35 (m, 6H, CH₂Bu), 1.27-1.16 (m, 6H, CH₂Bu), 0.90-0.74 (m, 24H, ^tBuSi, CH₃Bu, CH₂Bu), 0.00 (s, 3H, MeSi), -0.01 (s, 3H, MeSi); ¹³C (125 MHz, CDCl₃) δ 131.9, 127.8, 71.1, 61.5, 59.6, 29.1, 27.2, 25.9, 18.3, 13.7, 8.9, -5.2; IR (film): 3025, 2928, 2857, 2463, 1406, 1253, 1082; *m/z* (ES) 507.3 [M+H]⁺; HRMS-ES *m/z* 507.2672 (M+H calculated for C₂₃H₅₀O₂SiSn requires 507.2675).

2-(*tert*-Butyldimethylsilyloxymethyl)but-3-en-1-ol 53



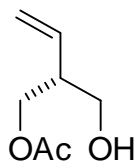
n-Butyllithium (2.5 M in hexanes, 17 mL, 41.5 mmol) was added to a solution of the stannane **52** (7.0 g, 13.9 mmol) in THF (170 mL) cooled to -78 °C. The resulting mixture was stirred at this temperature for 2 h, before being quenched with water (80 mL), and the aqueous phase was extracted with ether (3×80 mL). The organic extracts were combined, washed with brine (80 mL), dried (Na_2SO_4), and the solvent removed under reduced pressure to give the crude product which was purified by flash chromatography, eluting with neat DCM, to give the *alkene* **53**¹⁶⁶ (1.9 g, 63%) as a colourless oil, $R_f = 0.20$ (100:0 DCM); ^1H (500 MHz; CDCl_3) δ 5.71-5.62 (m, 1H, 3-H), 5.16-5.09 (m, 2H, 4-H₂), 3.80-3.63 (m, 4H, 1-H₂, CH_2OSi), 2.55-2.44 (m, 2H, 2-H, OH), 0.88 (s, 9H, $^t\text{BuSi}$), 0.05 (s, 6H, MeSi); ^{13}C (125 MHz, CDCl_3) δ 135.8, 117.3, 66.1, 65.5, 47.4, 30.9, 25.7, 18.2, -5.5 ; IR (film): 3478, 2955, 2930, 2858, 1640, 1471, 1390; m/z (ES) 217.2 $[\text{M}+\text{H}]^+$.

2-[(Acetyloxy)methyl]but-3-en-1-yl acetate **54**



Tetrabutylammonium fluoride (1.0 M in THF, 27 mL, 26.8 mmol) was added dropwise to a solution of the alkene **53** (1.9 g, 8.8 mmol) in THF (90 mL) cooled to 0 °C. The resulting mixture was stirred at this temperature for 45 min, before being warmed to room temperature and stirred for 1 h. The solvent was removed under reduced pressure to give the crude diol. Triethylamine (3.8 mL, 26.8 mmol), 4-(dimethylamino)pyridine (110 mg, 0.9 mmol) were added to a solution of the crude diol in DCM (20 mL). The resulting mixture was cooled to 0 °C, before acetyl chloride (2 mL, 26.8 mmol) was added dropwise. The resulting mixture was stirred overnight before being poured into ice-water (100 mL), and the aqueous phase was extracted with DCM (3 × 100 mL). The organic extracts were combined, washed with cold saturated aqueous NaHCO₃ (2 × 60 mL), water (60 mL), 1M HCl (2 × 60 mL), water (60 mL), brine (60 mL), and dried (Na₂SO₄), and the solvent removed under reduced pressure to give the crude product which was purified by flash chromatography, eluting with 80:20 hexane–EtOAc, to give the *diacetate* **54**¹⁷¹ (1.4 g, 85%) as a colourless oil, *R*_f = 0.42 (80:20 Hexane–EtOAc); ¹H (500 MHz; CDCl₃) δ 5.76-5.67 (m, 1H, 3-H), 5.20 (ddd, *J* = 11.6, 6.4, 1.1 Hz, 2H, 4-H₂), 4.12 (m, 4H, 1-H₂, CH₂OAc), 2.75 (m, 1H, 2-H), 2.05 (s, 6H, Me); ¹³C (125 MHz, CDCl₃) δ 170.9, 134.7, 118.2, 63.9, 20.8; IR (film): 3155, 2984, 1793, 1735, 1643, 1469, 1380; *m/z* (ES) 209.1 [M+Na]⁺.

(R)-2-(Hydroxymethyl)but-3-enyl acetate 55



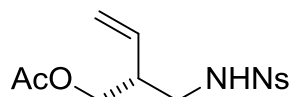
Pseudomonas fluorescens lipase AK (213 mg) was added to a suspension of the diacetate **54** (850 mg, 4.6 mmol) in 0.5 M, pH 7.0 phosphate buffer (KH₂PO₄/K₂HPO₄). The resulting mixture was stirred at room temperature for 1 h, before being filtered through a pad of celite. The filtrate was saturated with sodium chloride, and extracted with EtOAc (3 × 20 mL). The organic extracts were combined, dried (MgSO₄), and the solvent removed under reduced pressure to give the crude product which was purified by flash chromatography, eluting with 67:33 hexane–EtOAc to give, the *hydroxy acetate* **55**^{170,171} (400 mg, 60%) as a colourless oil, $R_f = 0.23$ (67:33 Hexane–EtOAc); $[\alpha]_D^{25} +24.6$ (c. 2.1, CHCl₃), (lit.¹⁷¹: +24.0 (c. 1.0, CHCl₃)); ¹H (500 MHz; CDCl₃) δ 5.76–5.66 (m, 1H, 3-H), 5.24–5.14 (m, 2H, 4-H₂), 4.23–4.09 (ddd, $J = 17.7, 11.1, 6.2$ Hz, 2H, CH₂OAc), 3.65–3.56 (m, 2H, 1-H₂), 2.62–2.53 (m, 1H, 2-H), 2.04 (s, 6H, Me), 2.00 (s, 1H, OH); ¹³C (125 MHz, CDCl₃) δ 171.4, 135.3, 118.3, 64.0, 62.5, 45.4, 20.9; IR (neat): 3445, 3080, 2954, 2890, 1739, 1643, 1468; m/z (ES) 167.1 [M+Na]⁺.

tert*-Butyl-*N*-[(2-nitrobenzene)sulfonyl]carbamate **56*

NsNHBoc

Di-*tert*-butyl dicarbonate (5.2 mL, 22.6 mmol) was added to solution of 2-nitrobenzenesulfonamide (3.8 g, 18.8 mmol), triethylamine (3.9 mL, 28.1 mmol), and 4-dimethylaminopyridine (216 mg, 1.8 mmol) in DCM (36 mL). The resulting mixture was stirred for 1 h at room temperature before being poured in 1N HCl (40 mL), and the aqueous phase was extracted with ether (4 × 20 mL). The organic extracts were combined washed with brine (2 × 50 mL), dried (Na₂SO₄), and the solvent removed under reduced pressure to give the crude product which was recrystallised from toluene to give the *sulfonamide* **56** (2.4 g, 41%) as yellow plates, *R*_f = 0.3 (60:40 Hexane–EtOAc); mp 138.5-139.4 °C (toluene); ¹H (500 MHz; CDCl₃) δ 8.38-8.32 (m, 1H, Ns), 7.91-7.74 (m, 3H, Ns), 7.49-7.35 (br s, 1H, NH), 1.43 (s, 9H, ^tBu); ¹³C (75 MHz, CDCl₃) δ 148.8, 148.1, 134.6, 133.2, 132.4, 132.1, 125.0, 84.7, 27.9; IR (film): 3335, 3249, 3009, 2981, 1746, 1595; *m/z* (ES) 325 [M+Na]⁺.

(2R)-2-[(2-Nitrobenzene)sulfonamidomethyl]but-3-en-1-yl acetate 32

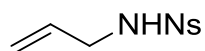


Diethylazodicarboxylate (437 μ L, 2.8 mmol) was added to a solution of the hydroxyacetate **55** (400 mg, 2.8 mmol), NsBocNH **56** (763 mg, 2.5 mmol), and triphenylphosphine (795 mg, 3.0 mmol) in THF (23 mL) cooled to 0 °C. The resulting mixture was stirred for 30 min at this temperature, before being warmed to room temperature and stirred for 2 h. The solvent was removed under reduced pressure to give the crude product which was purified by flash chromatography, eluting with 60:40 hexane–EtOAc, to give a *sulfonamide* (1.1 g, 95%) as a yellow oil, $R_f = 0.31$ (60:40 Hexane–EtOAc); $[\alpha]_D^{25} +9.0$ (c. 2.1, CHCl₃); ¹H (500 MHz; CDCl₃) δ 8.33–8.30 (m, 1H, Ns), 7.77–7.71 (m, 3H, Ns), 5.77–5.68 (m, 1H, 3-H), 5.29–5.20 (m, 2H, 4-H₂), 4.20 (dd, $J = 11.2, 5.7$ Hz, 1H, 1-H_A), 4.08 (dd, $J = 11.2, 6.2$ Hz, 1H, 1-H_B), 3.86 (ddd, $J = 23.1, 14.8, 7.5$ Hz, 2H, 2-CH₂), 2.93 (m, 1H, 2-H), 2.08 (s, 3H, Me), 1.36 (s, 9H, ^tBu); ¹³C (125 MHz, CDCl₃) δ 171.0 (C=O Ac), 150.3 (C=O Boc), 147.6 (Ns), 135.1 (C-3), 134.2 (Ns), 133.7 (Ns), 133.5 (Ns), 131.7 (Ns), 124.4 (Ns), 119.2 (C-4), 85.2 (C(Me)₃), 65.0 (C-1), 49.2 (2-CH₂), 43.8 (C-2), 27.8 (C(Me)₃), 20.9 (Me); IR (film): 3452, 3083, 2982, 1737, 1643, 1591, 1543; HRMS-ES m/z 451.1146 (M+Na calculated for C₁₈H₂₄O₈N₂S requires 451.1154).

Trifluoroacetic acid (3.0 mL, 39.2 mmol) was added to a solution of the sulfonamide (1.1 g, 2.6 mmol) in DCM (15 mL) cooled to 0 °C. The resulting mixture was stirred at this temperature for 1 h before being warmed to room temperature and stirred overnight. The reaction was quenched with saturated NaHCO₃ (45 mL), and the aqueous phase was extracted with ether (3 \times 30 mL). The organic extracts were combined, dried (Na₂SO₄), and the solvent removed under reduced pressure to give the crude product which was purified by flash chromatography, eluting with 60:40 hexane–EtOAc, to give the *building block 32* (690 mg, 80%) as a yellow oil, $R_f = 0.25$ (60:40 hexane–EtOAc); $[\alpha]_D^{25} -13.0$ (c. 2.0, CHCl₃); ¹H (500 MHz; CDCl₃) δ 8.19–8.13 (m, 1H, Ns), 7.93–7.87 (m, 1H, Ns), 7.81–7.75 (m, 2H, Ns), 5.67–5.55 (m, 2H, 3-H and NH), 5.26–5.13 (m, 2H, 4-H₂), 4.14 (dd, $J = 11.3, 5.3$ Hz, 1H, 1-H_A), 3.98 (dd, $J = 11.3, 7.2$ Hz, 1H, 1-H_B), 3.27 (ddd, $J = 12.8, 6.9, 6.0$, 1H, 2-CH_A), 3.08 (ddd, $J = 12.8, 7.3, 5.5$ Hz, 1H, 2-CH_B), 2.69–2.60 (m, 1H, 2-H), 2.08 (s, 3H, Me); ¹³C (125 MHz, CDCl₃) δ 170.9 (C=O),

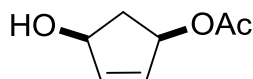
148.1 (Ns), 134.4 (Ns), 133.7 (C-3), 132.8 (Ns), 131.0 (Ns), 131.0 (Ns), 125.5 (Ns), 119.4 (C-4), 64.6 (C-1), 44.7 (2-CH₂), 42.9 (C-2), 20.8 (Me); IR (film): 3337, 3096, 2978, 2897, 1851, 1737, 1643; HRMS-ES *m/z* 351.0634 (M+Na calculated for C₁₃H₁₆O₆N₂S requires 351.0621).

2-Nitro-*N*-(prop-2-en-1-yl)benzene-1-sulfonamide **34**



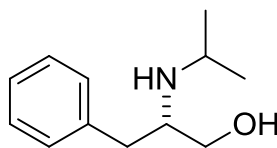
Allylamine **57** (3.5 mL, 46.7 mmol) was added dropwise to a solution of 2-nitrobenzenesulfonamide (9.8 g, 44.4 mmol) and potassium carbonate (6.5 g, 46.7 mmol) in DCM (70 mL). The resulting mixture was stirred overnight at room temperature before being quenched with water (20 mL) and 10% HCl in water (100 mL). The biphasic mixture was stirred until the organic phase became clear. The layers were separated, and the organic layer was washed with saturated aqueous NaHCO₃ (100 mL), water (110 mL), dried (MgSO₄), and the solvent removed under reduced pressure to give the crude product which was recrystallised from toluene–hexane to give the *sulfonamide* **34**¹⁷² (8.3 g, 77%) as yellow prisms, *R*_f = 0.6 (50:50 Petrol–EtOAc); mp 72.2–74.0 °C (toluene–hexane), (lit.¹⁷²: 74.0–75.0 °C (toluene–petrol)); ¹H (300 MHz; CDCl₃) δ 8.16–8.06 (m, 1H, Ns), 7.90–7.81 (m, 1H, Ns), 7.79–7.69 (m, 2H, Ns), 5.72 (ddt, *J* = 17.1, 10.2, 5.8 Hz, 1H, 2-H), 5.47–5.31 (br t, *J* = 4.9 Hz, 1H, NH), 5.19 (dd, *J* = 17.1, 2.6, 1H, 3-H_A), 5.09 (dd, *J* = 10.2, 2.6 Hz, 1H, 3-H_B), 3.76 (app tt, *J* = 5.8, 1.6 Hz, 2H, 1-H₂); ¹³C (75 MHz, CDCl₃) δ 148.0, 134.0, 133.7, 132.9, 132.5, 131.1, 125.4, 118.2, 46.32; IR (solid): 3330, 3100, 3032, 2943, 2897, 1671, 1546; *m/z* (ES) 265.0 [M+Na]⁺.

(1*R*,4*S*)-4-Hydroxycyclopent-2-en-1-yl acetate **33**



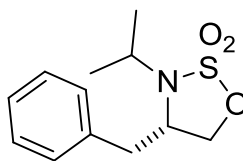
Candida antarctica lipase (Novozyme 435, 250 mg) was added to a suspension of *cis*-3,5-diacetoxy-1-cyclopentene **58** (1.5 g, 8.1 mmol) in 0.1 M, pH 8.0 phosphate buffer (NaH₂PO₄/Na₂HPO₄). The resulting mixture was stirred at room temperature for 18 h, before being filtered through a pad of celite, which was washed with water (50 mL), and EtOAc (100 mL). The aqueous layer was extracted with EtOAc (3 × 50 mL), and the organic extracts were combined, washed with brine (50 mL), dried (MgSO₄), and the solvent removed under reduced pressure to give the crude product which was purified by flash chromatography, eluting with 50:50 petrol–EtOAc, to give the *hydroxyacetate* **33**¹⁷³ (600 mg, 80%) as a colourless solid, $R_f = 0.21$ (50:50 Petrol–EtOAc); $[\alpha]_D$: +66.8 (c. 2.0, CHCl₃), (lit.¹⁷³: +66.0 (c. 1.0, CHCl₃)); ¹H (500 MHz; CDCl₃) δ 6.12 (ddd, $J = 5.6, 1.9, 1.2$ Hz, 1H, 3-H), 5.99 (ddd, $J = 5.6, 2.0, 1.1$ Hz, 1H, 2-H), 5.53–5.46 (m, 1H, 4-H), 4.75–4.68 (m, 1H, 1-H), 2.80 (dt, $J = 14.7, 7.4$ Hz, 1H, 5-H_A), 2.05 (s, 3H, Me), 1.66 (dt, 1H, $J = 14.7, 3.8$ Hz, 5-H_B); ¹³C (75 MHz, CDCl₃) δ 170.8, 138.5, 132.7, 76.7, 74.9, 40.5, 21.2; IR (film): 3379, 3077, 2949, 1823, 1722, 1577; Mass spectra were unobtainable.

(2S)-3-Phenyl-2-[(propan-2-yl)amino]propan-1-ol 60



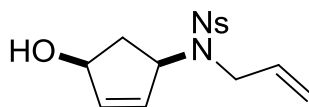
Acetone (2.7 mL, 37.2 mmol) was added to a solution of L-phenylalaninol **59** (2.8 g, 18.6 mmol), MgSO₄ (300 mg) in EtOH (23 mL). The resulting mixture was stirred at room temperature overnight and diluted with EtOH (23 mL). Sodium borohydride (2.0 g, 54.5 mmol) was added portionwise and the resulting mixture was stirred at room temperature overnight before being quenched with 1M aqueous NaOH (34 mL) and dissolved with EtOAc (10 mL). The resulting suspension was dried (Na₂SO₄), and the solvent removed under reduced pressure to give the crude product which was purified by flash chromatography, eluting with 90:10 DCM–MeOH, to give the *amino alcohol* **60**¹⁷⁴ (2.3 g, 65%) as a colourless solid, *R*_f = 0.26 (90:10 DCM–MeOH); [α]_D: +16.2 (c. 1.0, CHCl₃); ¹H (500 MHz; CDCl₃) δ 7.35-7.14 (m, 5H, Ar H), 3.54 (dd, *J* = 10.5, 4.1 Hz, 1H, 1-H_A), 3.23 (dd, *J* = 10.5, 5.9 Hz, 1H, 1-H_B), 2.96 (m, 1H, 2-H), 2.85 (hept, *J* = 6.2 Hz, 1H, iPr *CH*), 2.76 (dd, *J* = 13.6, 6.4 Hz, 1H, 3-H_A), 2.70 (dd, *J* = 13.6, 7.2 Hz, 1H, 3-H_B), 1.02 (d, *J* = 6.2 Hz, 3H, iPr *CH*₃), 0.97 (d, *J* = 6.2 Hz, 3H, iPr *CH*₃); ¹³C (75 MHz, CDCl₃) δ 138.4, 129.2, 128.6, 126.4, 62.9, 57.3, 46.0, 38.5, 23.3; IR (film): 3291, 3026, 2964, 1479, 1382, 1177, 1039; HRMS-ES *m/z* 194.1545 (M+H calculated for C₁₂H₁₉NO requires 194.1539).

(4S)-3-(Propan-2-yl)-4-benzyl-[1,2,3]oxathiazolidine-2,2-dioxide **61**



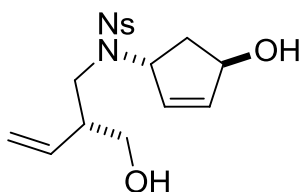
Thionyl chloride (950 μ L, 13.0 mmol) was added to a solution of triethylamine (3.5 mL, 25.3 mmol) and imidazole (3.1 g, 46.0 mmol) in DCM (200 mL) cooled to -60 $^{\circ}$ C. The amino alcohol **60** (2.2 g, 11.5 mmol) was added dropwise over 30 min as solution in DCM (30 mL). The resulting mixture was stirred at -60 $^{\circ}$ C for 2 h before being warmed to and stirred at room temperature overnight. The reaction was quenched by the addition of water (130 mL) and the aqueous phase was washed with DCM (3×80 mL). The organic extracts were combined, washed with water (80 mL), brine (2×80 mL), dried (MgSO_4), and the solvent removed under reduced pressure to give the crude sulfamidite which was used without further purification. The crude sulfamidite was then dissolved in acetonitrile (57 mL) and cooled to 0 $^{\circ}$ C. Sodium periodate (3.7 g, 17.3 mmol), ruthenium (III) chloride (30.1 mg, 1 mol%) and water (57 mL) were added sequentially and the resulting mixture was stirred at 0 $^{\circ}$ C for 1 h. The reaction was quenched by the addition of water (40 mL) and the aqueous phase was washed with EtOAc (4×50 mL). The organic extracts were combined, washed with saturated aqueous NaHCO_3 (50 mL), brine (2×50 mL), dried (MgSO_4), and the solvent removed under reduced pressure to give the crude which was purified by flash chromatography, eluting with 83:17 petrol–EtOAc, to give the *cyclic sulfamidate* **61** (2.2 g, 75%) as a colourless solid, $R_f = 0.19$ (83:17 Petrol–EtOAc); $[\alpha]_D$: -42.5 (c. 1.1, CHCl_3); ^1H (500 MHz; CDCl_3) δ 7.36–7.18 (m, 5H, Ar), 4.30 (dd, $J = 8.7, 6.5$ Hz, 1H, 5- H_A), 4.21 (dd, $J = 8.7, 3.8$ Hz, 1H, 5- H_B), 3.90 (dtd, $J = 9.0, 6.4, 3.8$ Hz, 1H, 4-H), 3.70 (hept, $J = 6.7$ Hz, 1H, iPr CH), 3.18 (dd, $J = 13.6, 6.2$ Hz, 1H, 4- CH_A), 2.90 (dd, $J = 13.6, 9.0$ Hz, 1H, 4- CH_B), 1.34 (d, $J = 6.7$ Hz, 3H, iPr CH_3), 1.18 (d, $J = 6.7$ Hz, 3H, iPr CH_3); ^{13}C (75 MHz, CDCl_3) δ 135.9 (Ar-C), 129.3 (Ar-C), 128.9 (Ar-C), 127.3 (Ar-C), 70.3 (C-3), 57.3 (C-4), 50.0 (iPrCH), 39.9 (4- CH_2), 20.9 (Me), 19.4 (Me); IR (film): 3088, 3032, 2936, 1604, 1499, 1390, 1229; HRMS-ES m/z 278.0824 (M+Na calculated for $\text{C}_{12}\text{H}_{17}\text{NO}_3\text{S}$ requires 278.0821).

N*-[(1*R*,4*S*)-4-Hydroxycyclopent-2-en-1-yl]-2-nitro-*N*-(prop-2-en-1-yl)benzene-1-sulfonamide **62*



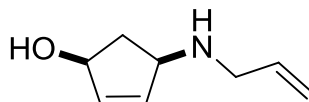
Sodium hydride (90 mg, 2.3 mmols) was added to a solution of the hydroxyacetate **33** (300 mg, 2.1 mmols) and the sulfonamide **34** (614 mg, 2.5 mmols) in THF (12 mL) cooled to 0 °C. The resulting mixture was stirred at 0 °C for 30 min and tris(dibenzylideneacetone)dipalladium(0)-chloroform adduct (55 mg, 50 μmol), 1,4-bis(diphenylphosphino)butane (90 mg, 0.2 mmol) and DMF (3 mL) were added. The reaction was heated to 50 °C overnight, quenched by the addition of water (30 mL) and the aqueous phase was extracted with ether (3 × 60 mL). The organic extracts were combined, dried (MgSO₄) and the solvent removed under reduced pressure to give the crude product which was purified by flash chromatography eluting with 50:50 petrol–EtOAc to give the *diene* **62** (370 mg, 54%) as a light yellow oil, *R*_f = 0.20 (50:50 petrol–EtOAc); [α]_D: +2.0 (c. 1.1, CHCl₃); ¹H (500 MHz; CDCl₃) δ 8.08-8.04 (m, 1H, Ns), 7.72-7.61 (m, 3H, Ns), 5.98 (dt, *J* = 5.6, 2.1 Hz, 1H, 2-H or 3-H), 5.81-5.72 (m, 2H, 2-H or 3-H and allyl 2-H), 5.18 (dq, *J* = 17.1, 1.5 Hz, 1H, allyl 3-H_A), 5.07 (dq, *J* = 10.2, 1.4 Hz, 1H, allyl 3-H_B), 4.91 (br, 1H, 4-H), 4.70 (br, 1H, 1-H), 3.95 (ddt, *J* = 16.7, 6.1, 1.2 Hz, 1H, allyl 1-H_A), 3.88 (ddt, *J* = 16.7, 5.7, 1.5 Hz, 1H, allyl 1-H_B), 2.70 (ddd, *J* = 14.7, 8.5, 7.7 Hz, 1H, 5-H_A), 1.91 (d, *J* = 6.3 Hz, 1H, OH), 1.62 (dt, *J* = 14.6, 4.5 Hz, 1H, 5-H_B); ¹³C (125 MHz, CDCl₃) δ 148.0, 137.5, 135.3, 134.1, 133.6, 133.1, 131.7, 131.4, 124.2, 118.0, 74.7, 62.5, 47.0, 38.9; IR (film): 3539, 3401, 3094, 2982, 1643, 1543, 1439; HRMS-ES *m/z* 347.0677 (M+Na calculated for C₁₄H₁₆N₂O₅S requires 347.0672).

N*-{(1*R*,4*S*)-*N'*-[(2'*R*)-2'-Ethenyl-3'-hydroxypropyl]-1-hydroxycyclopent-2-en-1-yl}-2-nitro-*N*-(prop-2-en-1-yl)benzene-1-sulfonamide **63*



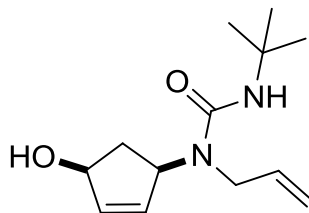
Diethylazodicarboxylate (361 μ L, 2.1 mmol) was added to a solution of the hydroxyacetate **33** (250 mg, 1.8 mmol), the building block **32** (693 mg, 2.1 mmol), and triphenylphosphine (647 mg, 2.5 mmol) in THF (35 mL) cooled to 0 °C. The resulting mixture was stirred for 30 min at this temperature, before being warmed to room temperature and stirred for a further 2 h. The solvent was removed under reduced pressure to give the crude product which was purified by flash chromatography eluting with 83:17 to 50:50 petrol–EtOAc to give a *sulfonamide* which was subsequently dissolved in saturated ammonia in methanol (18 mL) and stirred overnight at room temperature. The solvent was removed under reduced pressure to give the crude product which was purified by flash chromatography eluting with 83:17 to 50:50 petrol–EtOAc to give the *sulfonamide* **63** (400, 62%) as a light yellow oil, $R_f = 0.43$ (100:0 EtOAc); $[\alpha]_D^{25} +26.7$ (c. 2.0, CHCl_3); ^1H (500 MHz; CDCl_3) δ 8.07-7.61 (m, 4H, Ns), 6.05 (dt, $J = 5.6, 2.1$ Hz, 1H, 2-H or 3-H), 5.81 (ddd, $J = 5.6, 2.3, 1.1$ Hz, 1H, 2-H or 3-H), 5.69 (ddd, $J = 17.3, 10.4, 8.5$ Hz, 1H, ethenyl CH), 5.21-5.10 (m, 3H, 1-H, ethenyl CH_2), 4.97 (br s, 1H, 4-H), 3.69-3.57 (m, 2H, CH_2O), 3.22 (ddd, $J = 34.3, 15.1, 7.6$ Hz, 2H, CH_2N), 2.52-2.43 (m, 1H, 2'H), 2.12 (ddd, $J = 15.0, 7.3, 4.3$ Hz, 1H, 5- H_A), 1.97 (ddd, $J = 15.1, 8.3, 3.1$ Hz, 1H, 5- H_B), 1.91 (s, 1H, OH), 1.76 (s, 1H, 1-OH); ^{13}C (125 MHz, CDCl_3) δ 148.2 (Ns), 138.5 (C-2 or C-3), 136.7 (ethenyl CH), 133.8 (Ns), 133.4 (Ns), 133.2 (C-2 or C-3), 131.7 (Ns), 131.4 (Ns), 124.3 (Ns), 118.6 (ethenyl CH_2), 75.7 (C-1), 63.9 (C-4), 62.9 (CH_2O), 46.7 (C-2'), 46.2 (CH_2N), 38.7 (C-5); IR (film): 3532, 3369, 2942, 2884, 1542, 1373, 1163; HRMS-ES m/z 391.0945 ($\text{M}+\text{Na}$ calculated for $\text{C}_{16}\text{H}_{20}\text{N}_2\text{O}_6\text{S}$ requires 391.0934).

(1*S*,4*R*)-4-[(Prop-2-en-1-yl)amino]cyclopent-2-en-1-ol **65**



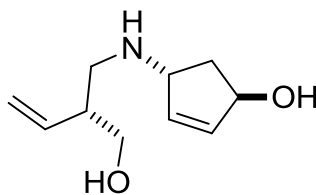
Thiophenol (144 μ L, 1.4 mmol) and potassium carbonate (256 mg, 1.9 mmol) were added to a solution of sulfonamide **62** (300 mg, 0.9 mmol) in DMF (3 mL) cooled to 0 $^{\circ}$ C. The resulting mixture was warmed to room temperature and stirred overnight. The solvent was removed under reduced pressure to give the crude product which was purified by flash chromatography eluting with 50:8:1 DCM–EtOH–NH₄OH to give the *amino alcohol* **65** (90 mg, 70%) as a brown oil, $R_f = 0.37$ (50:8:1 DCM–EtOH–NH₄OH); $[\alpha]_D$: +16.8 (c. 1.0, CHCl₃); ¹H (500 MHz; CDCl₃) δ 5.98–5.84 (m, 3H, 2-H, 3-H and allyl 2-H), 5.17 (dq, $J = 17.2, 1.6$ Hz, 1H, allyl 3-H_A), 5.08 (ddd, $J = 10.2, 2.9, 1.3$ Hz, 1H, allyl 3-H_B), 4.66 (dddd, $J = 8.1, 3.9, 1.9, 0.9$ Hz, 1H, 1-H), 3.68–3.63 (m, 1H, 4-H), 3.29–3.25 (m, 2H, allyl 1-H), 2.56 (dt, $J = 13.8, 7.3$ Hz, 1H, 5-H_A), 2.31 (br s, 2H, NH, OH), 1.42 (dt, $J = 13.8, 4.2$ Hz, 1H, 5-H_B); ¹³C (75 MHz, CDCl₃) δ 136.4 (C-2 or C-3 or allyl C-3), 136.0 (C-2 or C-3 or allyl C-3), 135.3 (C-2 or C-3 or allyl C-3), 116.3 (allyl C-2), 75.3 (C-1), 61.7 (C-4), 50.4 (allyl C-1), 41.4 (C-5); IR (film): 3272, 3077, 2966, 1852, 1644, 1450, 1362; HRMS-EI m/z 120.0820 (Fragment calculated for C₈H₁₀N requires 120.0813).

3-*tert*-Butyl-1-[(1*R*,4*S*)-4-hydroxycyclopent-2-en-1-yl]-1-(prop-2-en-1-yl)urea 66



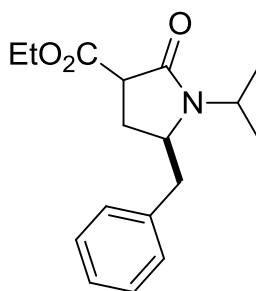
tert-Butyl isocyanate (74 μ L, 0.6 mmol) was added to a solution of the amino alcohol **65** (90 mg, 0.6 mmol) in DCM (3 mL). The resulting was stirred overnight at room temperature and the solvent was removed under reduced pressure to give the crude product which was purified by flash chromatography eluting with 75:25 EtOAc–petrol to give the *allylic alcohol* **66** (130 mg, 84%) as a colourless oil, $R_f = 0.28$ (75:25 EtOAc–petrol); $[\alpha]_D^{25}$: +51.5 (c. 1.0, CHCl_3); ^1H (500 MHz; CDCl_3) δ 5.96 (dt, 1H, $J = 5.5, 2.1$ Hz, 2-H or 3-H), 5.82 (ddd, $J = 17.3, 10.3, 4.9$, 1H, allyl 2-H), 5.80–5.77 (m, 1H, 2-H or 3-H), 5.28–5.21 (m, 2H, allyl 3-H₂), 5.16–5.10 (m, 1H, 4-H), 4.74–4.69 (m, 1H, 1-H), 4.45 (br s, 1H, NH), 3.78–3.71 (m, 1H, allyl 1-H_A), 3.67 (ddt, $J = 18.0, 5.0, 1.8$ Hz, 1H, allyl 1-H_B), 2.76–2.69 (m, 2H, 5-H_A, OH), 1.49–1.42 (m, 1H, 5-H_B), 1.30 (s, 9H, *t*Bu); ^{13}C (125 MHz, CDCl_3) δ 157.5 (C=O), 136.2 (C-2 or C-3 or allyl C-2), 135.9 (C-2 or C-3 or allyl C-2), 134.7 (C-2 or C-3 or allyl C-2), 116.4 (allyl C-3), 75.0 (C-1), 59.5 (C-4), 50.8 ($\text{C}(\text{CH}_3)_3$), 46.8 (allyl C-1), 39.1 (C-5), 29.4 ($\text{C}(\text{CH}_3)_3$); IR (film): 3424, 3061, 2967, 1633, 1529, 1455, 1392; HRMS-ES m/z 261.1572(M+Na calculated for $\text{C}_{13}\text{H}_{22}\text{N}_2\text{O}_2$ requires 261.1573).

(1*R*,4*R*)-4-[(2'*R*)-2'-Ethenyl-3'-hydroxypropyl]amino)cyclopent-2-en-1-ol **68**



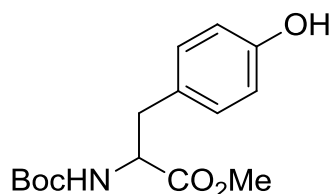
Thiophenol (163 μ L, 1.6 mmol) and potassium carbonate (293 mg, 2.1 mmol) were added to a solution of sulfonamide **63** (390 mg, 1.1 mmol) in DMF (3.5 mL) cooled to 0 °C. The resulting mixture was warmed to room temperature and stirred overnight. The solvent was removed under reduced pressure to give the crude product which was purified by flash chromatography eluting with 50:8:1 DCM–EtOH–NH₄OH to give the *aminodiol* **68** (170 mg, 87%, mixture of diastereoisomers: 83:17) as a yellow oil, $R_f = 0.13$ (50:8:1 DCM–EtOH–NH₄OH); ¹H (500 MHz; CDCl₃) δ 6.03 (ddd, 1H, $J = 5.6, 2.0, 0.9$ Hz, 2-H or 3-H), 5.99–5.96 (m, 1H, 2-H or 3-H), 5.69–5.61 (m, 1H, ethenyl CH), 5.16–5.10 (m, 2H, ethenyl CH₂), 4.96 (dq, $J = 3.8, 2.1, 0.9$ Hz, 1H, 1-H or 4-H), 4.08–4.04 (m, 1H, 1-H or 4-H), 3.75 (ddd, $J = 10.6, 4.5, 1.4$ Hz, 1H, 1'-H_A or 3'-H_A), 3.69 (dd, $J = 10.6, 8.0$ Hz, 1H, 1'-H_B or 3'-H_B), 2.96 (ddd, $J = 11.6, 4.5, 1.4$ Hz, 1H, 1'-H_A or 3'-H_A), 2.75 (dd, $J = 11.7, 8.8$ Hz, 1H, 1'-H_B or 3'-H_B), 2.52–2.44 (m, 1H, 2'-H), 2.06 (ddd, $J = 14.2, 7.1, 2.8$ Hz, 1H, 5-H_A), 1.94 (ddd, $J = 14.2, 7.0, 4.3$ Hz, 1H, 5-H_B); ¹³C (125 MHz, CDCl₃) δ 136.7 (ethenyl CH), 136.6 (C-2 or C-3), 135.8 (C-2 or C-3), 116.9 (ethenyl CH₂), 76.2 (C-1 or C-4), 67.8 (C-1' or C-3'), 63.1 (C-1 or C-4), 52.0 (C-1' or C-3'), 44.4 (C-2'), 41.4 (C-5); IR (film): 3291, 3076, 2921, 1640, 1444, 1356; HRMS-EI m/z 184.1342 (M+H calculated for C₁₀H₁₇NO₂ requires 184.1338); no optical rotation recorded.

(2*R*,5*R*)- and (2*S*,5*R*)-Ethyl 5-benzyl-2-oxo-1-(propan-2-yl)pyrrolidine-3-carboxylate **72,73**



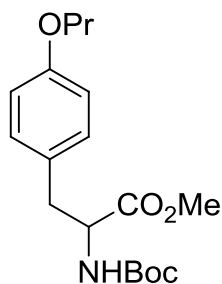
By method A, diethyl malonate **71** (304 μ L, 2.0 mmols) and the cyclic sulfamidate **61** (255 mg, 1.0 mmol) gave a crude product which was purified by flash chromatography eluting with 75:25 petrol–EtOAc to give the γ -lactam **72,73** (154 mg, 53%); *trans*–*cis* (71:29), $R_f = 0.15$ (75:25 Petrol–EtOAc); ^1H (500 MHz; CDCl_3) δ 7.35–7.16 (m, 10H, Ar^{maj,min}), 4.18 (q, $J = 7.1$ Hz, 2H, Et 1- H_2^{min}), 4.24–4.06 (m, 4H, Et 1- H_2^{maj} , iPr $\text{CH}^{\text{maj,min}}$), 3.96 (m, 1H, 5- H^{maj}), 3.85 (ddt, $J = 11.2, 8.0, 4.0$ Hz, 1H, 5- H^{min}), 3.36 (dd, $J = 9.3, 8.8$ Hz, 1H, 3- H^{maj}), 3.33 (dd, $J = 10.2, 5.4$ Hz, 1H, 3- H^{min}), 3.27 (dd, $J = 13.0, 3.8$ Hz, 1H, 5- CH_A^{min}), 3.16 (dd, $J = 13.5, 3.8$ Hz, 1H, 5- CH_A^{maj}), 2.72 (dd, $J = 13.0, 11.1$ Hz, 1H, 5- CH_B^{min}), 2.52 (dd, $J = 13.5, 10.0$ Hz, 1H, 5- CH_B^{maj}), 2.32–2.23 (m, 1H, 4- H_A^{maj}), 2.13 (ddd, $J = 13.6, 5.4, 4.2$ Hz, 1H, 4- H_A^{min}), 2.04 (m, 1H, 4- H_B^{min}), 1.98 (m, 1H, 4- H_B^{maj}), 1.43–1.35 (m, 12H, $\text{CH}_3^{\text{maj,min}}$), 1.33 (t, $J = 7.1$ Hz, 3H, Et 2- H_3^{min}), 1.27 (t, $J = 7.1$ Hz, 3H, Et 2- H_3^{maj}); ^{13}C (125 MHz, CDCl_3) δ 170.8 ($\text{C}=\text{O}^{\text{min}}$), 170.4 ($\text{C}=\text{O}^{\text{maj}}$), 169.8 (C-2^{maj}), 169.5 (C-2^{min}), 137.4 (Ar C-1^{min}), 137.0 (Ar C-1^{maj}), 129.2 (Ar), 129.1 (Ar), 128.8 (Ar), 128.7 (Ar), 126.9 (Ar), 126.7 (Ar), 61.6 (Et C-1^{min}), 61.4 (Et C-1^{maj}), 58.1 (C-5^{min}), 57.1 (C-5^{maj}), 48.5 (C-3^{min}), 47.8 (C-3^{maj}), 45.7 (iPr CH^{maj}), 45.6 (iPr CH^{min}), 41.9 (5- CH_2^{min}), 41.3 (5- CH_2^{maj}), 28.0 (C-4^{maj}), 27.0 (C-4^{min}), 21.4 (iPr CH_3), 19.8 (iPr CH_3), 19.6 (iPr CH_3), 14.2 (Et C-2^{min}), 14.2 (Et C-2^{maj}); IR (film): 3027, 2976, 1736, 1692, 1603, 1495, 1454; HRMS-ES m/z 312.1575 (M+Na calculated for $\text{C}_{17}\text{H}_{23}\text{NO}_3$ requires 312.1570). Maj and min refer to the major and minor diastereomer, assigned by observation of NOESY correlations between 5- CH_2 and 3-H (major) or 5-H and 3-H (minor).

DL-Methyl 2-[[*tert*-butoxy]carbonyl]amino]-3-(4-hydroxyphenyl)propanoate **77**



Acetyl chloride (19.4 mL, 270 mmol) was added to a solution of DL-tyrosine **76** (7.0 g, 39 mmol) in MeOH (160 mL) cooled to 0 °C. The resulting mixture was then heated to reflux overnight before being cooled to room temperature. The solvent was removed under reduced pressure to give the crude *methyl ester* as a colourless solid (7.5 g, 100%), which was dissolved in EtOH (160 mL). NaHCO₃ (32.5 g, 386 mmol) and di-*tert*-butyl dicarbonate (8.4 g, 39 mmol) were added to the resulting suspension, which was stirred overnight at room temperature. The reaction mixture was filtered through a pad of celite, and the solvent was removed under reduced pressure to give the crude *carbamate* **77**¹⁷⁷ (11.4 g, 100%) as a colourless solid, $R_f = 0.6$ (50:50 Petrol–EtOAc); ¹H (500 MHz; CDCl₃) δ 6.98 (d, 2H, $J = 8.4$ Hz, Ar 2-H), 6.74 (d, $J = 8.4$ Hz, 2H, Ar 3-H), 5.02-4.92 (m, 2H, NH, OH), 4.54 (dd, $J = 13.4, 6.1$ Hz, 1H, 2-H), 3.71 (s, 3H, Me), 3.01 (ddd, $J = 33.6, 14.0, 6.1$ Hz, 2H, 3-H₂), 1.42 (s, 9H, ^tBu); ¹³C (75 MHz, CDCl₃) δ 172.5, 155.2, 154.8, 130.4, 127.9, 115.5, 80.0, 54.6, 52.2, 37.6, 28.3; IR (film): 3356, 2986, 1906, 1731, 1683, 1611, 1591; HRMS-ES m/z 318.1337 (M+Na calculated for C₁₅H₂₁NO₅ requires 318.1312).

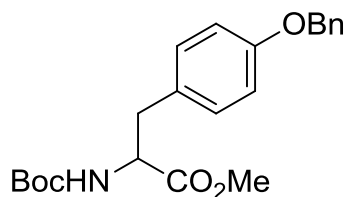
DL-Methyl 2-[[(*tert*-butoxy)carbonyl]amino]-3-(4-propoxyphenyl)propanoate **78**



Potassium carbonate (6.4 g, 46.0 mmol), and propyl bromide (5.3 mL, 58.5 mmol) were added to a solution of the crude carbamate **77** (11.4 g, 39.0 mmol) in acetonitrile (39 mL). The resulting mixture was heated to reflux overnight, and the solvent was removed under reduced pressure. The resulting solid was dissolved with water (200 mL) and the aqueous phase was extracted with DCM (5×125 mL). The organic extracts were combined, and dried (Na_2SO_4). The solvent was removed under reduced pressure to give the crude product which was purified by flash chromatography, eluting with 92:8 to 86:14 hexane–EtOAc, to give the *propyl carbamate* **78** (9.0 g, 69%) as a colourless solid, $R_f = 0.54$ (67:33 Petrol–EtOAc); ^1H (500 MHz; CDCl_3) δ 7.02 (d, 2H, $J = 8.5$ Hz, Ar 2-H), 6.82 (d, $J = 8.7$ Hz, 2H, Ar 3-H), 4.94 (br d, $J = 7.7$ Hz, 1H, NH), 4.53 (br dd, $J = 7.8$ Hz, 1H, 2-H), 3.89 (t, $J = 6.6$ Hz, 2H, Pr 1-H₂), 3.71 (s, 3H, OMe), 3.02 (qd, $J = 14.2, 6.0$ Hz, 2H, 3-H₂), 1.83–1.75 (m, 2H, Pr 2-H₂), 1.42 (s, 9H, ^tBu), 1.03 (t, $J = 7.4$ Hz, 3H, Pr 3-H₃); ^{13}C (125 MHz, CDCl_3) δ 172.5 (CO_2Me), 158.3 (CO_2^tBu), 155.1 (Ar), 130.3 (Ar), 127.7 (Ar), 114.6 (Ar), 79.9 ($\text{C}(\text{CH}_3)_3$), 69.5 (Pr 1-C), 54.6 (C-2), 52.2 (OMe), 37.5 (C-3), 28.3 ($\text{C}(\text{CH}_3)_3$), 22.6 (Pr 2-C), 10.5 (Pr 3-C); IR (film): 3357, 2960, 1698, 1614, 1583, 1505, 1391; HRMS-ES m/z 360.1785 ($\text{M}+\text{Na}$ calculated for $\text{C}_{18}\text{H}_{27}\text{NO}_5$ requires 360.1781).

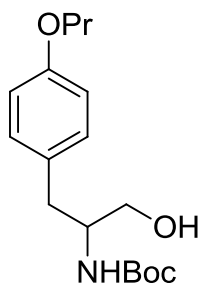
DL-Methyl 3-[4-(benzyloxy)phenyl]-2-[[*tert*-butoxy]carbonyl]amino}propanoate

79



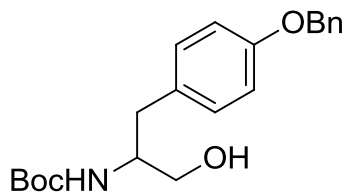
Potassium carbonate (5.9 g, 42.9 mmol), and benzyl bromide (5.3 mL, 44.5 mmol) were added to a solution of the crude carbamate **77** (11.4 g, 39 mmol) in acetone (39 mL). The resulting mixture was heated to reflux overnight, before being dissolved with water (200 mL). The aqueous phase was extracted with DCM (5 × 125 mL), and the organic extracts were combined, and dried (Na₂SO₄). The solvent was removed under reduced pressure to give the crude product which was purified by flash chromatography, eluting with 67:33 to 86:14 hexane–EtOAc, to give the *benzyl carbamate* **79**¹⁷⁸ (13.0 g, 86%) as a colourless solid, R_f = 0.42 (67:33 hexane–EtOAc); ¹H (500 MHz; CDCl₃) δ 7.44–7.29 (m, 5H, Bn), 7.03 (m, 2H, Ar 2-H), 6.90 (m, 2H, Ar 3-H), 5.04 (s, 2H, Bn CH₂), 4.95 (d, *J* = 7.2 Hz, 1H, NH), 4.54 (dd, *J* = 13.9, 6.3 Hz, 1H, 2-H), 3.70 (s, 3H, Me), 3.02 (qd, *J* = 13.9, 5.8 Hz, 2H, 3-H₂), 0.42 (s, 9H, ^tBu); ¹³C (75 MHz, CDCl₃) δ 172.4, 157.9, 155.1, 137.0, 130.3, 128.6, 128.3, 128.0, 127.5, 114.9, 79.9, 70.0, 54.5, 52.2, 37.5, 28.3; IR (film): 3355, 2976, 1954, 1742, 1704, 1613, 1585; HRMS-ES *m/z* 408.1791 (M+Na calculated for C₂₂H₂₇NO₅ requires 408.1781).

DL-*tert*-Butyl *N*-[1-hydroxy-3-(4-propoxyphenyl)propan-2-yl]carbamate **80**



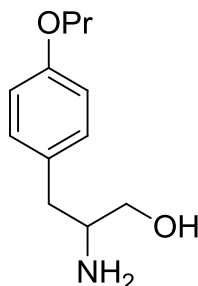
Lithium iodide (3.9 g, 29.4 mmol) and sodium borohydride (1.1 g, 29.4 mmol) were added to a solution of the propyl carbamate **78** (9 g, 26.7 mmol) in THF (100 mL). The resulting mixture was heated to reflux overnight, before being cooled to room temperature and quenched with a saturated aqueous solution of ammonium chloride (145 mL). The aqueous phase was extracted with EtOAc (3 × 200 mL), and the organic extracts were combined, and dried (Na₂SO₄). The solvent was removed under reduced pressure to give the crude product which was purified by flash chromatography, eluting with 67:33 petrol–EtOAc, to give the *alcohol* **80** (5.3 g, 64%) as a colourless solid, *R*_f = 0.21 (67:33 Petrol–EtOAc); ¹H (500 MHz; CDCl₃) δ 7.11 (d, 2H, *J* = 8.6 Hz, Ar 2-H), 6.83 (d, *J* = 8.7 Hz, 2H, Ar 3-H), 4.71 (br s, 1H, NH), 3.90 (t, *J* = 6.6 Hz, 2H, Pr 1-H₂), 3.81 (br s, 1H, 2-H), 3.66 (dd, *J* = 11.0, 3.2 Hz, 1H, 1-H_A), 3.54 (dd, *J* = 10.9, 5.3 Hz, 1H, 1-H_B), 2.77 (d, *J* = 7.1 Hz, 2H, 3-H₂), 2.36 (br s, 1H, OH), 1.84–1.75 (m, 2H, Pr 2-H₂), 1.42 (s, 9H, ^tBu), 1.03 (t, 3H, Pr 3-H₃); ¹³C (125 MHz, CDCl₃) δ 157.91 (C=O), 156.2 (Ar), 130.2 (Ar), 129.5 (Ar), 114.6 (Ar), 79.7 (C(CH₃)₃), 69.5 (Pr 1-C), 64.5 (C-1), 53.9 (C-2), 36.6 (C-3), 28.4 (C(CH₃)₃), 22.7 (Pr 2-C), 10.5 (Pr 3-C); IR (film): 3381, 3063, 2888, 1672, 1611, 1580; HRMS-ES *m/z* 332.1827 (M+Na calculated for C₁₇H₂₇NO₄ requires 332.1832).

DL-*tert*-Butyl *N*-{1-[4-(benzyloxy)phenyl]-3-hydroxypropan-2-yl}carbamate **81**



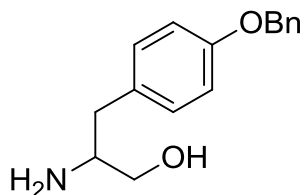
Lithium iodide (3.8 g, 28.6 mmol) and sodium borohydride (1.1 g, 28.6 mmol) were added to a solution of the benzyl carbamate **79** (9.0 g, 26.0 mmol) in THF (135 mL). The resulting mixture was heated to reflux for 4 h, before being cooled to room temperature and quenched with a saturated aqueous solution of ammonium chloride (150 mL). The aqueous phase was extracted with EtOAc (3 × 200 mL), and the organic extracts were combined, and dried (Na₂SO₄). The solvent was removed under reduced pressure to give the crude product which was purified by flash chromatography, eluting with 80:20 to 67:33 petrol–EtOAc, to give the *alcohol* **81**¹⁷⁹ (9.0 g, 74%) as a colourless solid, *R_f* = 0.43 (50:50 Petrol–EtOAc); ¹H (500 MHz; CDCl₃) δ 7.44–7.28 (m, 5H, Bn), 7.12 (d, *J* = 8.5 Hz, 2H, Ar 2-H), 6.91 (d, *J* = 8.4 Hz, 2H, Ar 3-H), 5.03 (s, 2H, Bn CH₂), 4.77 (d, *J* = 8 Hz, 1H, NH), 3.81 (br, 1H, 2-H), 3.64 (dd, *J* = 11.0, 3.6 Hz, 1H, 3-H_A), 3.53 (dd, *J* = 11.0, 5.2 Hz, 1H, 3-H_B), 2.77 (app d, *J* = 7.1 Hz, 2H, 1-H₂), 2.51 (br s, 1H, OH), 1.41 (s, 9H, ^{*t*}Bu); ¹³C (125 MHz, CDCl₃) δ 157.6, 156.2, 137.1, 130.3, 130.1, 128.6, 127.9, 127.5, 115.0, 79.7, 70.1, 64.3, 53.8, 36.7, 28.4; IR (film): 3532, 3357, 3027, 2932, 1680, 1610, 1583; HRMS-ES *m/z* 380.1834 (M+Na calculated for C₂₁H₂₇NO₄ requires 380.1832).

DL-2-Amino-3-(4-propoxyphenyl)propan-1-ol 74



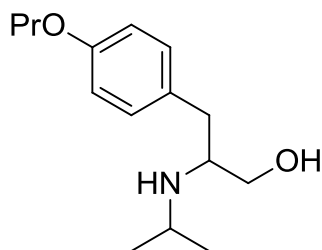
p-Toluenesulfonic acid (6.5 g, 34.3 mmol) was added to a solution of the alcohol **80** in 50:50 THF–DCM (172 mL). The resulting mixture was heated to reflux overnight, before being cooled to room temperature and diluted with 1M NaOH (170 mL). The aqueous phase was extracted with EtOAc (4 × 125 mL), and the organic extracts were combined, washed with brine (100 mL), and dried (Na₂SO₄). The solvent was removed under reduced pressure to give the crude product which was purified by flash chromatography, eluting with 50:50 petrol–EtOAc followed by 50:8:1 DCM–EtOH–NH₄OH, to give the *amino alcohol* **74** (2.2 g, 61%) as a colourless solid, *R*_f = 0.3 (50:8:1 DCM–EtOH–NH₄OH); ¹H (500 MHz; CDCl₃) δ 7.09 (d, 2H, *J* = 8.5 Hz, Ar 2-H), 6.84 (d, *J* = 8.6 Hz, 2H, Ar 3-H), 3.90 (t, *J* = 6.6 Hz, 2H, Pr 1-H₂), 3.62 (dd, *J* = 10.6, 3.9 Hz, 1H, 1-H_A), 3.36 (dd, *J* = 10.6, 7.2 Hz, 1H, 1-H_B), 3.07 (m, 1H, 2-H), 2.72 (dd, *J* = 13.7, 5.3 Hz, 1H, 3-H_A), 2.46 (dd, *J* = 13.7, 8.5 Hz, 1H, 3-H_B), 1.93–1.71 (m, 5H, Pr 2-H₂, NH₂, OH), 1.03 (t, *J* = 7.4 Hz, 3H, Pr 3-H₃); ¹³C (125 MHz, CDCl₃) δ 157.8 (Ar), 130.4 (Ar), 130.1 (Ar), 114.6 (Ar), 69.6 (Pr C-1), 66.4 (C-1), 54.3 (C-2), 40.0 (C-3), 22.6 (Pr C-2), 10.5 (Pr C-3); IR (film): 3713, 3359, 2741, 1607, 1578, 1507, 1469; HRMS-ES *m/z* 210.1495 (M+H calculated for C₁₂H₁₉NO₂ requires 210.1489).

DL-2-Amino-3-[4-(benzyloxy)phenyl]propan-1-ol 75



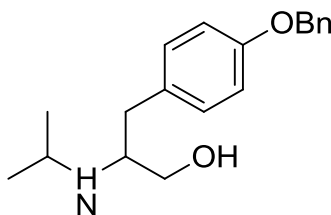
p-Toluenesulfonic acid (9.5 g, 50 mmol) was added to a solution of the alcohol **81** in 50:50 THF–DCM (250 mL). The resulting mixture was heated to reflux for 6 h, before being cooled to room temperature and diluted with 1M NaOH (300 mL). The aqueous phase was extracted with EtOAc (4 × 250 mL), and the organic extracts were combined, washed with brine (300 mL), and dried (Na₂SO₄). The solvent was removed under reduced pressure to give the crude product which was purified by flash chromatography, eluting with 50:50 petrol–EtOAc followed by 50:8:1 DCM–EtOH–NH₄OH, to give the *amino alcohol* **75**¹⁷⁷ (5.0 g, 78%) as a colourless solid, *R*_f = 0.25 (50:8:1 DCM–EtOH–NH₄OH); ¹H (500 MHz; CDCl₃) δ 7.45–7.29 (m, 5H, Bn), 7.09 (m, 2H, Ar 2-H), 6.91 (m, 2H, Ar 3-H), 5.03 (s, 2H, Bn CH₂), 3.61 (dd, *J* = 10.6, 3.7 Hz, 1H, 1-H_A), 3.36 (dd, *J* = 10.6, 7.2 Hz, 1H, 1-H_B), 3.06 (m, 1H, 2-H), 2.72 (dd, *J* = 13.6, 5.2 Hz, 1H, 3-H_A), 2.45 (dd, *J* = 13.6, 8.6 Hz, 1H, 3-H_B), 1.98 (br, 3H, NH₂, OH); ¹³C (125 MHz, CDCl₃) δ 157.5, 137.1, 131.0, 130.2, 128.6, 128.0, 127.5, 115.0, 70.1, 66.3, 54.3, 40.0; IR (film): 3335, 2905, 2758, 1610, 1581, 1514, 1470; HRMS-ES *m/z* 258.1476 (M+H calculated for C₁₆H₁₉NO₂ requires 258.1489).

DL-2-[(Propan-2-yl)amino]-3-(4-propoxyphenyl)propan-1-ol 82



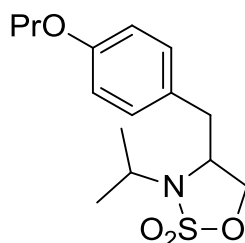
Acetone (352 μL , 4.8 mmol) was added to a solution of the amino alcohol **74** (500 mg, 2.4 mmol), and MgSO_4 (30 mg) in EtOH (3 mL). The resulting mixture was stirred at room temperature overnight and diluted with EtOH (3 mL). Sodium borohydride (266 mg, 7.0 mmol) was added portion-wise and the resulting mixture was stirred at room temperature overnight before being quenched with 1M NaOH (4 mL) and dissolved with EtOAc (10 mL). The resulting suspension was dried (Na_2SO_4), and the solvent removed under reduced pressure to give the crude product which was purified by flash chromatography, eluting with 90:10 DCM–MeOH, to give the *amino alcohol* **82** (370 mg, 61%) as a colourless solid, $R_f = 0.32$ (90:10 DCM–MeOH); ^1H (500 MHz; CDCl_3) δ 7.07 (d, 2H, $J = 8.5$ Hz, Ar 2-H), 6.83 (d, $J = 8.6$ Hz, 2H, Ar 3-H), 3.90 (t, $J = 6.6$ Hz, 2H, Pr 1- H_2), 3.56 (dd, $J = 10.6, 4.0$ Hz, 1H, 1- H_A), 3.26 (dd, $J = 10.6, 6.0$ Hz, 1H, 1- H_B), 2.95 (m, 1H, 2-H), 2.8 (hept, $J = 6.3$ Hz, 1H, iPr CH), 2.69 (qd, $J = 13.8, 6.9$ Hz, 2H, 3- H_2), 2.55-2.00 (br s, 2H, NH, OH), 1.84-1.76 (m, 2H, Pr 2- H_2), 1.07-0.99 (m, 9H, iPr CH_3 , Pr 3- H_3); ^{13}C (125 MHz, CDCl_3) δ 157.8 (Ar), 130.1 (Ar), 130.0 (Ar), 114.6 (Ar), 69.6 (Pr C-1), 62.8 (C-1), 57.6 (C-2), 46.2 (iPr CH), 37.4 (C-3), 23.2 (iPr CH_3), 23.2 (iPr CH_3), 22.6 (Pr C-2), 10.5 (Pr C-3); IR (film): 3714, 3271, 2729, 1614, 1583, 1476, 1380; HRMS-ES m/z 252.1962 (M+H calculated for $\text{C}_{15}\text{H}_{25}\text{NO}_2$ requires 252.1958).

DL-3-[4-(Benzyloxy)phenyl]-2-[(propan-2-yl)amino]propan-1-ol **83**



Acetone (287 μ L, 3.9 mmol) was added to a solution of the amino alcohol **75** (500 mg, 2.0 mmol), and MgSO_4 (40 mg) in EtOH (3 mL). The resulting mixture was stirred at room temperature overnight and diluted with EtOH (3 mL). Sodium borohydride (220 mg, 5.8 mmol) was added portionwise and the resulting mixture was stirred at room temperature overnight before being quenched with 1M NaOH (3.5 mL) and dissolved with EtOAc (10 mL). The resulting suspension was dried (Na_2SO_4), and the solvent removed under reduced pressure to give the crude product which was purified by flash chromatography, eluting with 90:10 DCM–MeOH, to give the *amino alcohol* **83** (210 mg, 36%) as a colourless solid, $R_f = 0.25$ (90:10 DCM–MeOH); ^1H (500 MHz; CDCl_3) δ 7.45–7.29 (m, 5H, Bn), 7.09 (d, $J = 8.6$ Hz, 2H, Ar 2-H), 6.91 (d, $J = 8.6$ Hz, 2H, Ar 3-H), 5.05 (s, 2H, Bn CH_2), 3.56 (dd, $J = 10.7, 4.0$ Hz, 1H, 1- H_A), 3.27 (dd, $J = 10.7, 6.0$ Hz, 1H, 1- H_B), 2.95 (m, 1H, 2-H), 2.88 (hept, $J = 6.3$ Hz, 1H, iPr CH), 2.73 (dd, $J = 13.7, 7.3$ Hz, 1H, 3- H_A), 2.68 (dd, $J = 13.7, 7.3$ Hz, 1H, 3- H_B), 2.51 (br s, 2H, NH, OH), 1.05 (d, $J = 6.2$ Hz, 3H, iPr CH_3), 1.02 (d, $J = 6.3$ Hz, 3H, iPr CH_3); ^{13}C (125 MHz, CDCl_3) δ 157.5 (Ar C-4), 137.1 (Bn), 130.6 (Ar C-1), 130.2 (Ar C-2), 128.6 (Bn), 128.0 (Bn), 127.5 (Bn), 115.0 (Ar C-3), 70.1 (Bn CH_2), 62.8 (C-1), 57.6 (C-2), 46.3 (iPr CH), 37.4 (C-3), 23.2 (Me), 23.1 (Me); IR (film): 3297, 3269, 2901, 1608, 1581, 1511, 1493; HRMS-ES m/z 300.1961 (M+H calculated for $\text{C}_{19}\text{H}_{25}\text{NO}_2$ requires 300.1958).

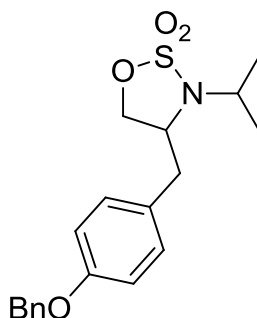
(4*R*,4*S*)-3-(Propan-2-yl)-4-(4-(propyloxy)phenylmethyl)-[1,2,3]oxathiazolidine-2,2-dioxide **84**



Thionyl chloride (120 μ L, 1.6 mmol) was added to a solution of triethylamine (203 μ L, 3.2 mmol) and imidazole (396 mg, 5.8 mmol) in DCM (14 mL) cooled to -60 $^{\circ}$ C. The amino alcohol **82** (365 mg, 1.5 mmol) was added dropwise over 30 min as a solution in DCM (15 mL). The resulting mixture was stirred at -60 $^{\circ}$ C for 3 h before being warmed to and stirred at room temperature overnight. The reaction was quenched by the addition of water (30 mL) and the aqueous phase was washed with DCM (3 \times 30 mL). The organic extracts were combined, washed with water (30 mL), brine (2 \times 30 mL), and dried (MgSO_4). The solvent was removed under reduced pressure to give the crude sulfamidite which was used without further purification. The crude sulfamidite was then dissolved in acetonitrile (7.3 mL) and cooled to 0 $^{\circ}$ C. Sodium periodate (311 mg, 1.0 mmol), ruthenium (III) chloride (4 mg, 1 mol%) and water (7.3 mL) were added sequentially and the resulting mixture was stirred at 0 $^{\circ}$ C for 15 min. The reaction was quenched by the addition of water (10 mL) and the aqueous phase was washed with EtOAc (3 \times 5 mL). The organic extracts were combined, washed with saturated aqueous NaHCO_3 (10 mL), brine (2 \times 10 mL), and dried (MgSO_4). The solvent was removed under reduced pressure to give the crude which was purified by flash chromatography, eluting with 91:9 to 67:33 petrol–EtOAc, to give the *cyclic sulfamidate* **84** (220 mg, 50%) as a light yellow solid, $R_f = 0.3$ (80:20 Petrol–EtOAc); ^1H (500 MHz; CDCl_3) δ 7.10 (d, 2H, $J = 8.4$ Hz, Ar 2-H), 6.86 (d, $J = 8.7$ Hz, 2H, Ar 2-H), 4.28 (dd, $J = 8.7, 6.5$ Hz, 1H, 5- H_A), 4.20 (dd, $J = 8.7, 4.0$ Hz, 1H, 5- H_B), 3.90 (t, $J = 6.6$ Hz, 2H, Pr 1- H_2), 3.88–3.82 (m, 1H, 4-H), 3.70 (hept, $J = 6.7$ Hz, 1H, iPr CH), 3.11 (dd, $J = 13.8, 6.1$ Hz, 1H, 4- CH_A), 2.82 (dd, $J = 13.8, 9.2$ Hz, 1H, 4- CH_B), 1.85–1.75 (m, 2H, Pr 2- H_2), 1.34 (d, $J = 6.7$ Hz, 3H, iPr CH_3), 1.34 (d, $J = 6.7$ Hz, 3H, iPr CH_3), 1.03 (t, $J = 7.43$ Hz, 3H, Pr 3- H_3); ^{13}C (125 MHz, CDCl_3) δ 158.5 (Ar), 130.3 (Ar), 127.5 (Ar), 115.0 (Ar), 70.3 (C-5), 69.6 (Pr C-1), 57.5 (C-4), 49.9 (iPr CH), 39.0 (Bn CH_2), 22.6 (Pr C-2), 20.9 (iPr CH_3), 19.4 (iPr CH_3), 10.5 (Pr C-3); IR (film): 3727,

3037, 2873, 1610, 1581, 1513, 1464; HRMS-ES m/z 336.1236 (M+Na calculated for $C_{15}H_{23}NO_4S$ requires 336.124).

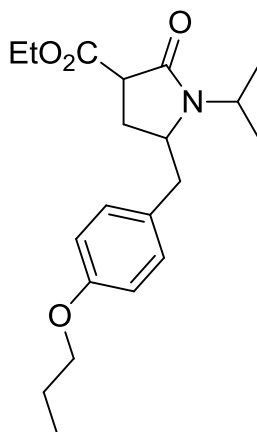
(4*R*,4*S*)-3-(Propan-2-yl)-4-(4-(benzyloxy)phenyl)methyl)-[1,2,3]oxathiazolidine-2,2-dioxide **85**



Thionyl chloride (53 μ L, 0.7 mmol) was added to a solution of triethylamine (196 μ L, 1.4 mmol) and imidazole (174 mg, 2.6 mmol) in DCM (8 mL) cooled to -60 $^{\circ}$ C. The amino alcohol **83** (191 mg, 0.6 mmol) was added dropwise over 30 min as a solution in DCM (5 mL). The resulting mixture was stirred at -60 $^{\circ}$ C for 2 h before being warmed to and stirred at room temperature overnight. The reaction was quenched by the addition of water (7 mL) and the aqueous phase was washed with DCM (3×5 mL). The organic extracts were combined, washed with water (5 mL), brine (2×5 mL), and dried ($MgSO_4$). The solvent was removed under reduced pressure to give the crude sulfamidite which was used without further purification. The crude sulfamidite was then dissolved in acetonitrile (3.2 mL) and cooled to 0 $^{\circ}$ C. Sodium periodate (205 mg, 1.0 mmol), ruthenium (III) chloride (2 mg, 1 mol%) and water (3.2 mL) were added sequentially and the resulting mixture was stirred at 0 $^{\circ}$ C for 15 min. The reaction was quenched by the addition of water (3 mL) and the aqueous phase was washed with EtOAc (3×5 mL). The organic extracts were combined, washed with saturated aqueous $NaHCO_3$ (5 mL), brine (2×5 mL), and dried ($MgSO_4$). The solvent was removed under reduced pressure to give the crude which was purified by flash chromatography, eluting with 75:25 petrol–EtOAc, to give the *cyclic sulfamidate* **85** (128 mg, 53%) as a colourless solid, $R_f = 0.27$ (75:25 Petrol–EtOAc); 1H (500 MHz; $CDCl_3$) δ 7.44–7.30 (m, 5H, OBn), 7.11 (d, $J = 8.5$ Hz, 2H, Ar 2-H), 6.94 (d, $J = 8.7$ Hz, 2H, Ar 3-H), 5.05 (s, 2H, OBn CH_2), 4.29 (dd, $J = 8.7, 6.6$ Hz, 1H, 5- H_A), 4.19 (dd, $J = 8.7, 3.9$ Hz, 1H, 5- H_B), 3.85 (m, 1H, 4-H), 3.70 (hept, $J = 6.8$ Hz, 1H, iPr CH),

3.11 (dd, $J = 13.8, 6.2$ Hz, 1H, 4-CH_A), 2.83 (dd, $J = 13.8, 9.0$ Hz, 1H, 4-CH_B), 1.33 (d, $J = 6.7$ Hz, 3H, iPr CH₃), 1.18 (d, $J = 6.7$ Hz, 3H, iPr CH₃); ¹³C (75 MHz, CDCl₃) δ 158.1 (Ar C-4), 136.8 (OBn), 130.4 (Ar C-2), 128.6 (OBn), 128.1 (Ar C-1), 128.0 (OBn), 127.5 (OBn), 115.3 (Ar C-3), 70.3 (C-5), 70.1 (OBn CH₂), 57.4 (C-4), 50.0 (iPr CH), 39.0 (4-CH₂), 20.9 (Me), 19.4 (Me); IR (film): 3063, 2979, 1611, 1583, 1512, 1465, 1340; HRMS-ES m/z 384.1257 (M+Na calculated for C₁₉H₂₃NO₄S requires 384.124).

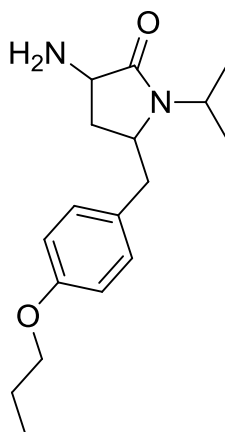
(2*RS*,5*RS*)- and (2*RS*,5*SR*)-Ethyl 2-oxo-1-(propan-2-yl)-5-[(4-propoxyphenyl)methyl]pyrrolidine-3-carboxylate **86**



By method A, diethyl malonate **71** (97 μ L, 0.6 mmol) and the cyclic sulfamidate **84** (100 mg, 0.3 mmol) gave a crude product which was purified by flash chromatography eluting with 80:20 to 50:50 petrol–EtOAc to give the γ -lactam **86** (67 mg, 60%); *trans*–*cis* (67:33), $R_f = 0.38$ (50:50 Petrol–EtOAc); ^1H (500 MHz; CDCl_3) δ 7.13 (d, 2H, $J = 8.6$ Hz, Ar 2- H^{min}), 7.07 (d, $J = 8.6$ Hz, 2H, Ar 2- H^{maj}), 6.85 (d, $J = 8.6$ Hz, 2H, Ar 3- H^{min}), 6.85 (d, $J = 8.6$ Hz, 2H, Ar 3- H^{maj}), 4.26 (q, $J = 7.1$ Hz, 2H, Et 1- H_2^{min}), 4.24–4.14 (m, 3H, Et 1- H_2^{maj} , iPr CH^{min}), 4.14–4.06 (m, 1H, iPr CH^{maj}), 3.94–3.87 (m, 5H, Pr 1- $\text{H}_2^{\text{maj,min}}$, 5- H^{maj}), 3.82–3.75 (app ddd, $J = 15.1, 8.0, 4.0$ Hz, 1H, 5- H^{min}), 3.36–3.29 (m, 2H, 3- $\text{H}^{\text{maj,min}}$), 3.20 (dd, $J = 13.1, 3.8$ Hz, 1H, 5- CH_A^{min}), 3.08 (dd, $J = 13.6, 3.8$ Hz, 1H, 5- CH_A^{maj}), 2.64 (dd, $J = 13.1, 11.1$ Hz, 1H, 5- CH_B^{min}), 2.47 (dd, $J = 13.6, 9.8$ Hz, 1H, 5- CH_B^{maj}), 2.27 (ddd, $J = 13.1, 9.4, 8.2$ Hz, 1H, 4- H_A^{maj}), 2.12 (ddd, $J = 13.5, 5.5, 4.2$ Hz, 1H, 4- H_A^{min}), 2.07–2.01 (m, 1H, 4- H_B^{min}), 1.97 (ddd, $J = 13.1, 8.7, 2.5$ Hz, 1H, 4- H_B^{maj}), 1.84–1.76 (m, 4H, Pr 2- $\text{H}_2^{\text{maj,min}}$), 1.42–1.34 (m, 12H, iPr $\text{CH}_3^{\text{maj,min}}$), 1.33 (t, $J = 7.1$ Hz, 3H, Et 2- H_3^{min}), 1.27 (t, $J = 7.1$ Hz, 3H, Et 2- H_3^{maj}), 1.04 (t, $J = 7.4$ Hz, 6H, Pr 3- $\text{H}_3^{\text{maj,min}}$); ^{13}C (75 MHz, CDCl_3) δ 170.8 (C=O $^{\text{min}}$), 170.4 (C=O $^{\text{maj}}$), 169.9 (C-2 $^{\text{maj}}$), 169.5 (C-2 $^{\text{min}}$), 158.1 (Ar C-4 $^{\text{maj}}$), 158.0 (Ar C-4 $^{\text{min}}$), 130.2 (Ar C-2 $^{\text{maj}}$), 130.1 (Ar C-2 $^{\text{min}}$), 129.2 (Ar C-1 $^{\text{min}}$), 128.8 (Ar C-1 $^{\text{maj}}$), 114.8 (Ar C-3 $^{\text{maj}}$), 114.7 (Ar C-3 $^{\text{min}}$), 68.6 (Pr C-1 $^{\text{maj,min}}$), 61.6 (Et C-1 $^{\text{min}}$), 61.4 (Et C-1 $^{\text{maj}}$), 58.3 (C-5 $^{\text{min}}$), 57.3 (C-5 $^{\text{maj}}$), 48.5 (C-3 $^{\text{min}}$), 47.8 (C-3 $^{\text{maj}}$), 45.7 (iPr CH^{maj}), 45.5 (iPr CH^{min}), 41.0 (5- CH_2^{min}), 40.4 (5- CH_2^{maj}), 28.0 (C-4 $^{\text{maj}}$), 27.0 (C-4 $^{\text{min}}$), 22.6 (Pr C-2 $^{\text{maj,min}}$), 21.4 (iPr CH_3), 19.8 (iPr CH_3), 19.6 (iPr CH_3), 14.2 (Et C-2 $^{\text{maj,min}}$), 10.5 (Pr C-3 $^{\text{maj,min}}$); IR (film): 2971, 2878, 1736, 1692, 1612, 1581, 1512; HRMS-ES m/z 370.1999 (M+Na)

calculated for $C_{20}H_{29}NO_4$ requires 370.1989). Maj and min refer to the major and minor diastereomer, assigned by observation of NOESY correlations between 5-CH₂ and 3-H (major) or 5-H and 3-H (minor).

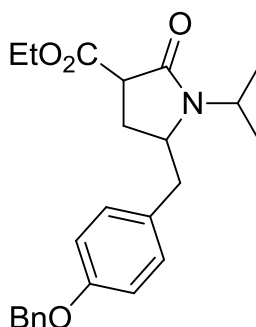
(2*RS*,5*RS*)- and (2*RS*,5*SR*)-3-Amino-1-(propan-2-yl)-5-[(4-propoxyphenyl)methyl]pyrrolidin-2-one **88**



By method A, *N*-(diphenylmethylene)glycine ethyl ester **38** (171 mg, 0.6 mmol) and the cyclic sulfamidate **84** (100 mg, 0.3 mmol) gave a crude product which was purified by flash chromatography eluting with 95:5 DCM–MeOH to give the γ -lactam **88** (31 mg, 33%); *trans*–*cis* (58:42), $R_f = 0.25$ (95:5 DCM–MeOH); ¹H (500 MHz; CDCl₃) δ 7.10–7.06 (m, 4H, Ar 2-H^{maj,min}), 6.87–6.82 (m, 4H, Ar 3-H^{maj,min}), 4.15–4.07 (m, 2H, iPr CH^{maj,min}), 3.90 (t, $J = 6.6$ Hz, 4H, Pr 1-H₂^{maj,min}), 3.78–3.72 (m, 1H, 5-H^{maj}), 3.72–3.65 (m, 1H, 5-H^{min}), 3.43–3.29 (m, 3H, 3-H^{maj,min}, 5-CH_A^{min}), 2.98 (dd, $J = 13.7, 3.7$ Hz, 1H, 5-CH_A^{maj}), 2.52 (dd, $J = 13.7, 9.6$ Hz, 1H, 5-CH_B^{maj}), 2.43 (dd, $J = 13.0, 10.4$ Hz, 1H, 5-CH_B^{min}), 2.25 (app dd, $J = 12.8, 7.9$ Hz, 1H, 4-H_A^{maj}), 2.20 (ddd, $J = 12.9, 8.7, 6.5$ Hz, 1H, 4-H_A^{min}), 1.85–1.76 (m, 4H, Pr 2-H₂^{maj,min}), 1.64 (br s, 4H, NH₂^{maj,min}), 1.55 (ddd, $J = 12.5, 11.0, 8.4$ Hz, 1H, 4-H_B^{maj}), 1.42 (d, $J = 7$ Hz, 3H, iPr CH₃^{min}), 1.38–1.32 (m, 10H, 4-H_B^{min}, iPr CH₃^{maj}, iPr CH₃^{maj,min}), 1.04 (t, $J = 7.4$ Hz, 6H, Pr 3-H₃^{maj,min}); ¹³C (125 MHz, CDCl₃) δ 176.2 (C=O^{min}), 175.9 (C=O^{maj}), 158.1 (Ar C-4^{maj,min}), 130.1 (Ar C-2^{maj}), 130.0 (Ar C-2^{min}), 129.3 (Ar C-1^{maj}), 128.7 (Ar C-1^{min}), 114.7 (Ar C-3^{maj}), 114.7 (Ar C-3^{min}), 69.6 (Pr C-1^{maj,min}), 56.5 (C-5^{min}), 55.4 (C-5^{maj}), 52.7 (C-3^{min}), 51.7 (C-3^{maj}), 45.3 (iPr CH^{maj}), 45.2 (iPr CH^{min}), 41.9 (5-CH₂^{min}), 40.0 (5-CH₂^{maj}), 35.1 (C-4^{min}), 34.2 (C-4^{maj}), 22.6 (Pr C-2^{maj,min}), 21.6 (iPr CH₃), 21.4 (iPr CH₃), 19.7 (iPr CH₃), 19.7 (iPr CH₃), 10.5 (Pr C-3^{maj,min}); IR (film):

3364, 2969, 2935, 2877, 1682, 1613, 1512; HRMS-ES m/z 291.2076 (M+H calculated for $C_{17}H_{26}N_2O_2$ requires 291.2067). Maj and min refer to the major and minor diastereomer, assigned by observation of NOESY correlations between 5-CH₂ and 3-H (major) or 5-H and 3-H (minor).

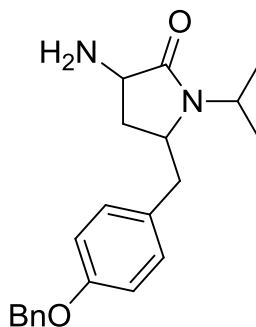
(2RS,5RS)- and (2RS,5SR)-Ethyl 5-[[4-(benzyloxy)phenyl]methyl]-2-oxo-1-(propan-2-yl)pyrrolidine-3-carboxylate **87**



By method A, diethyl malonate **71** (108 μ L, 0.7 mmol) and the cyclic sulfamidate **85** (128 mg, 0.35 mmol) gave a crude product which was purified by flash chromatography eluting with 75:25 petrol–EtOAc to give the γ -lactam **87** (88 mg, 63%); *trans*–*cis* (64:36), $R_f = 0.13$ (75:25 Petrol–EtOAc); ^1H (500 MHz; CDCl_3) δ 7.45–7.30 (m, 10H, $\text{OBn}^{\text{maj,min}}$), 7.15 (d, $J = 8.6$ Hz, 2H, Ar 2- H^{min}), 7.09 (d, $J = 8.6$ Hz, 2H, Ar 2- H^{maj}), 6.93 (d, $J = 8.6$ Hz, 2H, Ar 3- H^{min}), 6.93 (d, $J = 8.7$ Hz, 2H, Ar 3- H^{maj}), 5.05 (s, 4H, $\text{OBn CH}_2^{\text{maj,min}}$), 4.25 (q, $J = 7.1$ Hz, 2H, Et 1- H_2^{min}), 4.24–4.14 (m, 3H, Et 1- H_2^{maj} , iPr CH^{min}), 4.14–4.05 (m, 1H, iPr CH^{maj}), 3.94–3.88 (m, 1H, 5- H^{maj}), 3.79 (ddd, $J = 15.2$, 8.0, 4.0 Hz, 1H, 5- H^{min}), 3.36–3.30 (m, 2H, 3- $\text{H}^{\text{maj,min}}$), 3.20 (dd, $J = 13.1$, 3.8 Hz, 1H, 5- CH_A^{min}), 3.08 (dd, $J = 13.6$, 3.8 Hz, 1H, 5- CH_A^{maj}), 2.65 (dd, $J = 13.1$, 11.1 Hz, 1H, 5- CH_B^{min}), 2.47 (dd, $J = 13.6$, 9.8 Hz, 1H, 5- CH_B^{maj}), 2.28 (ddd, $J = 13.1$, 9.3, 8.2 Hz, 1H, 4- H_A^{maj}), 2.12 (ddd, $J = 13.6$, 5.4, 4.2 Hz, 1H, 4- H_A^{min}), 2.07–2.01 (m, 1H, 4- H_B^{min}), 1.97 (ddd, $J = 13.1$, 8.7, 2.6 Hz, 1H, 4- H_B^{maj}), 1.42–1.32 (m, 12H, iPr $\text{CH}_3^{\text{maj,min}}$), 1.32 (t, $J = 7.1$ Hz, 3H, Et 2- H_3^{min}), 1.27 (t, $J = 7.1$ Hz, 3H, Et 2- H_3^{maj}); ^{13}C (125 MHz, CDCl_3) δ 170.8 ($\text{C}=\text{O}^{\text{min}}$), 170.4 ($\text{C}=\text{O}^{\text{maj}}$), 169.9 ($\text{C}-2^{\text{maj}}$), 169.5 ($\text{C}-2^{\text{min}}$), 157.8 (Ar C-4 $^{\text{maj}}$), 157.7 (Ar C-4 $^{\text{min}}$), 137.0 ($\text{OBn Ar}^{\text{maj,min}}$), 136.9 ($\text{OBn Ar}^{\text{maj,min}}$), 130.2 (Ar C-3 $^{\text{min}}$), 130.1 (Ar C-3 $^{\text{maj}}$), 129.7 (Ar $^{\text{maj,min}}$), 129.3 (Ar $^{\text{maj,min}}$), 128.6 ($\text{OBn Ar}^{\text{maj,min}}$), 128.0 ($\text{OBn Ar}^{\text{maj,min}}$), 127.5 ($\text{OBn Ar}^{\text{maj,min}}$), 115.2 (Ar C-2 $^{\text{maj}}$), 115.1 (Ar C-2 $^{\text{min}}$), 70.1 ($\text{OBn CH}_2^{\text{maj,min}}$), 61.6 (Et C-1 $^{\text{min}}$), 61.4 (Et C-1 $^{\text{maj}}$), 58.2 (C-5 $^{\text{min}}$), 57.2 (C-5 $^{\text{maj}}$), 48.5 (C-3 $^{\text{min}}$), 47.8 (C-3 $^{\text{maj}}$), 45.7 (iPr CH^{maj}), 45.6 (iPr CH^{min}), 41.0 (5- CH_2^{min}), 40.4 (5- CH_2^{maj}), 28.0 (C-4 $^{\text{maj}}$), 27.0 (C-4 $^{\text{min}}$), 21.4 (iPr CH_3), 21.4 (iPr CH_3), 19.8 (iPr CH_3), 19.6 (iPr CH_3), 14.2 (Et 2-C), 14.2 (Et 2-C); IR (film): 3031, 2977, 1735, 1689, 1611, 1583, 1512; HRMS-ES m/z 418.2002 ($\text{M}+\text{Na}$ calculated for $\text{C}_{24}\text{H}_{29}\text{NO}_4$ requires 418.1989). Maj and min refer to the major and minor diastereomer, assigned by

observation of NOESY correlations between 5-CH₂ and 3-H (major) or 5-H and 3-H (minor).

(2RS,5RS)- and (2RS,5SR)-3-Amino-5-[[4-(benzyloxy)phenyl]methyl]-1-(propan-2-yl)pyrrolidin-2-one 89



By method A, *N*-(diphenylmethylene)glycine ethyl ester **38** (144 mg, 0.5 mmol) and the cyclic sulfamidate **85** (97 mg, 0.3 mmol) gave a crude product which was purified by flash chromatography eluting with 90:10 DCM–MeOH to give the γ -lactam **89** (23 mg, 26%); *trans*–*cis* (71:29), $R_f = 0.35$ (90:10 DCM–MeOH); ¹H (500 MHz; CDCl₃) δ 7.45–7.29 (m, 10H, OBn^{maj,min}), 7.13–7.06 (m, 4H, Ar 2-H^{maj,min}), 6.96–6.89 (m, 4H, Ar 3-H^{maj,min}), 5.05 (s, 4H, OBn CH₂^{maj,min}), 4.14–4.07 (m, 2H, iPr CH^{maj,min}), 3.79–3.65 (m, 2H, 5-H^{maj,min}), 3.44–3.36 (m, 1H, 3-H^{maj}), 3.36–3.29 (m, 2H, 3-H^{min}, 5-CH_A^{min}), 2.98 (dd, $J = 13.7, 3.7$ Hz, 1H, 5-CH_A^{maj}), 2.53 (dd, $J = 13.7, 9.6$ Hz, 1H, 5-CH_B^{maj}), 2.44 (dd, $J = 13.0, 10.4$ Hz, 1H, 5-CH_B^{min}), 2.28–2.22 (m, 1H, 4-H_A^{maj}), 2.22–2.16 (m, 1H, 4-H_A^{min}), 1.86 (br s, 4H, NH₂^{maj,min}), 1.62–1.53 (m, 1H, 4-H_B^{maj}), 1.43–1.32 (m, 13H, 4-H_B^{min}, iPr CH₃^{maj,min}); ¹³C (125 MHz, CDCl₃) δ 176.1 (C=O^{min}), 175.8 (C=O^{maj}), 157.7 (Ar C-4^{maj,min}), 137.0 (OBn^{maj,min}), 130.2 (Ar C-2^{maj}), 130.1 (Ar C-2^{min}), 129.8 (Ar C-1^{maj}), 129.2 (Ar C-1^{min}), 128.6 (OBn^{maj,min}), 128.0 (OBn^{maj,min}), 127.5 (OBn^{maj,min}), 115.1 (Ar C-3^{maj}), 115.1 (Ar C-3^{min}), 70.1 (OBn CH₂^{maj,min}), 56.4 (C-5^{min}), 55.4 (C-5^{maj}), 52.6 (C-3^{min}), 51.7 (C-3^{maj}), 45.4 (iPr CH^{maj}), 45.2 (iPr CH^{min}), 41.8 (5-CH₂^{min}), 40.0 (5-CH₂^{maj}), 35.0 (C-4^{min}), 34.1 (C-4^{maj}), 21.6 (iPr CH₃^{maj}), 21.4 (iPr CH₃^{min}), 19.7 (iPr CH₃^{min}), 19.7 (iPr CH₃^{maj}); IR (film): 3363, 2973, 1682, 1611, 1583, 1511, 1454; HRMS-ES m/z 339.2076 (M+H calculated for C₂₁H₂₆N₂O₂ requires 339.2067). Maj and min refer to the major and minor diastereomer, assigned by

observation of NOESY correlations between 5-CH₂ and 3-H (major) or 5-H and 3-H (minor).

8 REFERENCES

- 1 Chanock, R., Roizman, B. & Myers, R. Recovery from infants with respiratory illness of a virus related to chimpanzee coryza agent (CCA). *Am. J. Epidemiol.* **66**, 281-290 (1957).
- 2 Chanock, R. & Finberg, L. Recovery from infants with respiratory illness of a virus related to chimpanzee coryza agent (CCA). *Am. J. Epidemiol.* **66**, 291-300 (1957).
- 3 Collins, P. L. & Crowe, J. E. J. in *Fields virology* Vol. 2 (eds D.M. Knipe *et al.*) 1601-1646 (Lippincott Williams & Wilkins, 2007).
- 4 Diseases, C. o. I. Modified recommendations for use of palivizumab for prevention of respiratory syncytial virus infections. *Pediatrics* **124**, 1694-1701 (2009).
- 5 Zlateva, K. T., Vijgen, L., Dekeersmaeker, N., Naranjo, C. & Van Ranst, M. Subgroup prevalence and genotype circulation patterns of human respiratory syncytial virus in Belgium during ten successive epidemic seasons. *J. Clin. Microbiol.* **45**, 3022-3030 (2007).
- 6 Anderson, L. J. *et al.* Antigenic characterization of respiratory syncytial virus strains with monoclonal antibodies. *J. Infect. Dis.* **151**, 626-633 (1985).
- 7 Mufson, M. A., Örvell, C., Rafnar, B. & Norrby, E. Two distinct subtypes of human respiratory syncytial virus. *J. Gen. Virol.* **66**, 2111-2124 (1985).
- 8 Duprex, W. P., Collins, F. M. & Rima, B. K. Modulating the function of the measles virus RNA-dependent RNA polymerase by insertion of green fluorescent protein into the open reading frame. *J. Virol.* **76**, 7322-7328 (2002).
- 9 Ghildyal, R., Ho, A. & Jans, D. A. Central role of the respiratory syncytial virus matrix protein in infection. *FEMS Microbiol. Rev.* **30**, 692-705 (2006).
- 10 Hall, C. B. Respiratory syncytial virus and parainfluenza virus. *N. Engl. J. Med.* **344**, 1917-1928 (2001).
- 11 Collins, P. L. & Graham, B. S. Viral and host factors in human respiratory syncytial virus pathogenesis. *J. Virol.* **82**, 2040-2055 (2008).
- 12 Hall, C. B. *et al.* The burden of respiratory syncytial virus infection in young children. *N. Engl. J. Med.* **360**, 588-598 (2009).
- 13 Falsey, A. R., Hennessey, P. A., Formica, M. A., Cox, C. & Walsh, E. E. Respiratory syncytial virus infection in elderly and high-risk adults. *N. Engl. J. Med.* **352**, 1749-1759 (2005).
- 14 van Drunen Littel-van den Hurk, S. & Watkiss, E. R. Pathogenesis of respiratory syncytial virus. *Curr. Opin. Virol.* **2**, 300-305 (2012).

- 15 MacLellan, K., Loney, C., Yeo, R. & Bhella, D. The 24-angstrom structure of respiratory syncytial virus nucleocapsid protein-RNA decameric rings. *J. Virol.* **81**, 9519-9524 (2007).
- 16 Hall, C. B. The nosocomial spread of respiratory syncytial viral infections. *Annu. Rev. Med.* **34**, 311-319 (1983).
- 17 Lindsley, W. G. *et al.* Distribution of airborne influenza virus and respiratory syncytial virus in an urgent care medical clinic. *Clin. Infect. Dis.* **50**, 693-698 (2010).
- 18 Bamberger, E. *et al.* What is the clinical relevance of respiratory syncytial virus bronchiolitis?: findings from a multi-center, prospective study. *Eur. J. Clin. Microbiol.*, 1-8 (2012).
- 19 Collins, P. L. & Melerio, J. A. Progress in understanding and controlling respiratory syncytial virus: still crazy after all these years. *Virus Res.* **162**, 80-99 (2011).
- 20 Krishnamoorthy, N. *et al.* Early infection with respiratory syncytial virus impairs regulatory T cell function and increases susceptibility to allergic asthma. *Nat. Med.* **18**, 1525-1530 (2012).
- 21 Sigurs, N. *et al.* Severe respiratory syncytial virus bronchiolitis in infancy and asthma and allergy at age 13. *Am. J. Respir. Crit. Care Med.* **171**, 137-141 (2005).
- 22 Brock, S. C., Goldenring, J. R. & Crowe, J. E. Apical recycling systems regulate directional budding of respiratory syncytial virus from polarized epithelial cells. *Proc. Natl. Acad. Sci. U.S.A.* **100**, 15143-15148 (2003).
- 23 Zhang, L., Peeples, M. E., Boucher, R. C., Collins, P. L. & Pickles, R. J. Respiratory syncytial virus infection of human airway epithelial cells is polarized, specific to ciliated cells, and without obvious cytopathology. *J. Virol.* **76**, 5654-5666 (2002).
- 24 Johnson, J. E., Gonzales, R. A., Olson, S. J., Wright, P. F. & Graham, B. S. The histopathology of fatal untreated human respiratory syncytial virus infection. *Mod. Pathol.* **20**, 108-119 (2006).
- 25 Toolan, H. W. Transplantable human neoplasms maintained in cortisonetreated laboratory animals: H.S. #1; H.Ep. #1; H.Ep. #2; H.Ep. #3; and H.Emb.Rh. #1. *Cancer Res.* **14**, 660-666 (1954).
- 26 Guerrero-Plata, A. *et al.* Differential response of dendritic cells to human metapneumovirus and respiratory syncytial virus. *Am. J. Resp. Cell Mol.* **34**, 320-329 (2006).
- 27 Hornung, V. *et al.* Replication-dependent potent IFN- α induction in human plasmacytoid dendritic cells by a single-stranded RNA virus. *J. Immunol.* **173**, 5935-5943 (2004).
- 28 Stumbles, P. A., Upham, J. W. & Holt, P. G. Airway dendritic cells: co-ordinators of immunological homeostasis and immunity in the respiratory tract. *APMIS* **111**, 741-755 (2003).

- 29 Cowton, V. M., McGivern, D. R. & Fearn, R. Unravelling the complexities of respiratory syncytial virus RNA synthesis. *J. Gen. Virol.* **87**, 1805-1821 (2006).
- 30 Xu, Z., Kuang, M., Okicki, J. R., Cramer, H. & Chaudhary, N. Potent inhibition of respiratory syncytial virus by combination treatment with 2-5A antisense and ribavirin. *Antivir. Res.* **61**, 195-206 (2004).
- 31 Money, V. A., McPhee, H. K., Mosely, J. A., Sanderson, J. M. & Yeo, R. P. Surface features of a Mononegavirales matrix protein indicate sites of membrane interaction. *Proc. Natl. Acad. Sci. U.S.A.* **106**, 4441-4446 (2009).
- 32 Grosfeld, H., Hill, M. & Collins, P. RNA replication by respiratory syncytial virus (RSV) is directed by the N, P, and L proteins; transcription also occurs under these conditions but requires RSV superinfection for efficient synthesis of full-length mRNA. *J. Virol.* **69**, 5677-5686 (1995).
- 33 Dupuy, L. C., Dobson, S., Bitko, V. & Barik, S. Casein kinase 2-mediated phosphorylation of respiratory syncytial virus phosphoprotein P is essential for the transcription elongation activity of the viral polymerase; phosphorylation by casein kinase 1 occurs mainly at Ser215 and is without effect. *J. Virol.* **73**, 8384-8392 (1999).
- 34 Collins, P. L. *et al.* Production of infectious human respiratory syncytial virus from cloned cDNA confirms an essential role for the transcription elongation factor from the 5' proximal open reading frame of the M2 mRNA in gene expression and provides a capability for vaccine development. *Proc. Natl. Acad. Sci. U.S.A.* **92**, 11563-11567 (1995).
- 35 Peeples, M. E. & Collins, P. L. Mutations in the 5' trailer region of a respiratory syncytial virus minigenome which limit RNA replication to one step. *J. Virol.* **74**, 146-155 (2000).
- 36 Bermingham, A. & Collins, P. L. The M2-2 protein of human respiratory syncytial virus is a regulatory factor involved in the balance between RNA replication and transcription. *Proc. Natl. Acad. Sci. U.S.A.* **96**, 11259-11264 (1999).
- 37 Caly, L., Wagstaff, K. M. & Jans, D. A. Nuclear trafficking of proteins from RNA viruses: Potential target for antivirals? *Antivir. Res.* **95**, 202-206 (2012).
- 38 Ghildyal, R., Baulch-Brown, C., Mills, J. & Meanger, J. The matrix protein of human respiratory syncytial virus localises to the nucleus of infected cells and inhibits transcription. *Arch. Virol.* **148**, 1419-1429 (2003).
- 39 Johnson, P. R. & Collins, P. L. The fusion glycoproteins of human respiratory syncytial virus of subgroups A and B: sequence

- conservation provides a structural basis for antigenic relatedness. *J. Gen. Virol.* **69**, 2623-2628 (1988).
- 40 Johnson, P. R., Spriggs, M. K., Olmsted, R. A. & Collins, P. L. The G glycoprotein of human respiratory syncytial viruses of subgroups A and B: extensive sequence divergence between antigenically related proteins. *Proc. Natl. Acad. Sci. U.S.A.* **84**, 5625-5629 (1987).
- 41 Levine, S., Klaiber-Franco, R. & Paradiso, P. R. Demonstration that glycoprotein G is the attachment protein of respiratory syncytial virus. *J. Gen. Virol.* **68**, 2521-2524 (1987).
- 42 Techaarpornkul, S., Collins, P. L. & Peeples, M. E. Respiratory syncytial virus with the fusion protein as its only viral glycoprotein is less dependent on cellular glycosaminoglycans for attachment than complete virus. *Virology* **294**, 296-304 (2002).
- 43 Teng, M. N. & Collins, P. L. Identification of the respiratory syncytial virus proteins required for formation and passage of helper-dependent infectious particles. *J. Virol.* **72**, 5707-5716 (1998).
- 44 Karron, R. A. *et al.* Respiratory syncytial virus (RSV) SH and G proteins are not essential for viral replication in vitro: Clinical evaluation and molecular characterization of a cold-passaged, attenuated RSV subgroup B mutant. *Proc. Natl. Acad. Sci. U.S.A.* **94**, 13961-13966 (1997).
- 45 Hallak, L. K., Kwilas, S. A. & Peeples, M. E. Interaction between respiratory syncytial virus and glycosaminoglycans, including heparan sulfate. *Methods Mol. Biol.* **379**, 15-34 (2007).
- 46 Mastrangelo, P. & Hegele, R. G. The RSV fusion receptor: not what everyone expected it to be. *Microbes Infect.* (2012).
- 47 Tayyari, F. *et al.* Identification of nucleolin as a cellular receptor for human respiratory syncytial virus. *Nat. Med.* **17**, 1132-1135 (2011).
- 48 Leyssen, P., De Clercq, E. & Neyts, J. Molecular strategies to inhibit the replication of RNA viruses. *Antivir. Res.* **78**, 9-25 (2008).
- 49 Carter, S. *et al.* Direct visualization of the small hydrophobic protein of human respiratory syncytial virus reveals the structural basis for membrane permeability. *FEBS Lett.* **584**, 2786-2790 (2010).
- 50 Gan, S.-W. *et al.* The small hydrophobic protein of the human respiratory syncytial virus forms pentameric ion channels. *J. Biol. Chem.* **287**, 24671-24689 (2012).
- 51 Maria Eugenia, G. & Luis, C. Viroporins. *FEBS Lett.* **552**, 28-34 (2003).
- 52 Galloux, M. *et al.* Characterization of a viral phosphoprotein binding site on the surface of the respiratory syncytial nucleoprotein. *J. Virol.*, 8375-8387 (2012).
- 53 Anderson, A. C. The process of structure-based drug design. *Chem. Biol.* **10**, 787-797 (2003).

- 54 Tawar, R. G. *et al.* Crystal structure of a nucleocapsid-like nucleoprotein-RNA complex of respiratory syncytial virus. *Science* **326**, 1279-1283 (2009).
- 55 Battisti, A. J. *et al.* Structure and assembly of a paramyxovirus matrix protein. *Proc. Natl. Acad. Sci. U.S.A.* **109**, 13996-14000 (2012).
- 56 Jo, S., Vargyas, M., Vasko-Szedlar, J., Roux, B. & Im, W. PBEQ-Solver for online visualization of electrostatic potential of biomolecules. *Nucleic Acids Res.* **36**, W270-W275 (2008).
- 57 Brooks, B. R. *et al.* CHARMM: The biomolecular simulation program. *J. Comput. Chem.* **30**, 1545-1614 (2009).
- 58 Colman, P. M. & Lawrence, M. C. The structural biology of type I viral membrane fusion. *Nat. Rev. Mol. Cell Biol.* **4**, 309-319 (2003).
- 59 Chan, D. C. & Kim, P. S. HIV entry and its inhibition. *Cell* **93**, 681-684 (1998).
- 60 Zhao, X., Singh, M., Malashkevich, V. N. & Kim, P. S. Structural characterization of the human respiratory syncytial virus fusion protein core. *Proc. Natl. Acad. Sci. U.S.A.* **97**, 14172-14177 (2000).
- 61 Kim, Y. H. *et al.* Capture and imaging of a prehairpin fusion intermediate of the paramyxovirus PIV5. *Proc. Natl. Acad. Sci. U.S.A.* **108**, 20992-20997 (2011).
- 62 Yin, H.-S., Wen, X., Paterson, R. G., Lamb, R. A. & Jardetzky, T. S. Structure of the parainfluenza virus 5 F protein in its metastable, prefusion conformation. *Nature* **439**, 38-44 (2006).
- 63 McLellan, J. S., Yang, Y., Graham, B. S. & Kwong, P. D. Structure of respiratory syncytial virus fusion glycoprotein in the postfusion conformation reveals preservation of neutralizing epitopes. *J. Virol.* **85**, 7788-7796 (2011).
- 64 Douglas, J. L. *et al.* Small molecules VP-14637 and JNJ-2408068 inhibit respiratory syncytial virus fusion by similar mechanisms. *Antimicrob. Agents Chemother.* **49**, 2460-2466 (2005).
- 65 McLellan, J. S. *et al.* Structural basis of respiratory syncytial virus neutralization by motavizumab. *Nat. Struct. Mol. Biol.* **17**, 248-250 (2010).
- 66 Hughson, F. M. Enveloped viruses: a common mode of membrane fusion? *Curr. Biol.* **7**, R565-R569 (1997).
- 67 Chan, D. C., Fass, D., Berger, J. M. & Kim, P. S. Core structure of gp41 from the HIV envelope glycoprotein. *Cell* **89**, 263-273 (1997).
- 68 Murray, C. W. & Rees, D. C. The rise of fragment-based drug discovery. *Nat. Chem.* **1**, 187-192 (2009).
- 69 Congreve, M., Murray, C. W. & Blundell, T. L. Keynote review: structural biology and drug discovery. *Drug Discov. Today* **10**, 895-907 (2005).

- 70 Gillet, V., Johnson, A. P., Mata, P., Sike, S. & Williams, P. SPROUT: a program for structure generation. *J. Comput. Aided Mol. Des.* **7**, 127-153 (1993).
- 71 Kitchen, D. B., Decornez, H., Furr, J. R. & Bajorath, J. Docking and scoring in virtual screening for drug discovery: methods and applications. *Nat. Rev. Drug Discov.* **3**, 935-949 (2004).
- 72 Kroemer, R. T. Structure-based drug design: docking and scoring. *Curr. Protein Pept. Sci.* **8**, 312-328 (2007).
- 73 Marrone, T. J., Briggs, a., James M. & McCammon, J. A. Structure-based drug design: computational advances. *Annu. Rev. Pharmacol.* **37**, 71-90 (1997).
- 74 S. Ekins, J. M., B. Testa. In silico pharmacology for drug discovery: methods for virtual ligand screening and profiling. *Br. J. Pharmacol.* **152**, 9-20 (2007).
- 75 Murray, C. W., Verdonk, M. L. & Rees, D. C. Experiences in fragment-based drug discovery. *Trends Pharmacol. Sci.* **33**, 224-232 (2012).
- 76 Scott, D. E., Coyne, A. G., Hudson, S. A. & Abell, C. Fragment-Based Approaches in Drug Discovery and Chemical Biology. *Biochemistry* **51**, 4990-5003 (2012).
- 77 Lipinski, C. A., Lombardo, F., Dominy, B. W. & Feeney, P. J. Experimental and computational approaches to estimate solubility and permeability in drug discovery and development settings. *Adv. Drug Deliv. Rev.* **46**, 3-26 (2001).
- 78 Nadin, A., Hattotuwigama, C. & Churcher, I. Lead-oriented synthesis: a new opportunity for synthetic chemistry. *Angew. Chem. Int. Ed. Engl.* **51**, 1114-1122 (2012).
- 79 Teague, S. J., Davis, A. M., Leeson, P. D. & Oprea, T. The design of leadlike combinatorial libraries. *Angew. Chem. Int. Ed. Engl.* **38**, 3743-3748 (1999).
- 80 Boehm, M. *Virtual Screening*. Vol. 48 3-33 (Wiley-VCH, 2011).
- 81 Malo, N., Hanley, J. A., Cerquozzi, S., Pelletier, J. & Nadon, R. Statistical practice in high-throughput screening data analysis. *Nat. Biotech.* **24**, 167-175 (2006).
- 82 Inglese, J. *et al.* High-throughput screening assays for the identification of chemical probes. *Nat. Chem. Biol.* **3**, 466-479 (2007).
- 83 Inglese, J., Shamu, C. E. & Guy, R. K. Reporting data from high-throughput screening of small-molecule libraries. *Nat. Chem. Biol.* **3**, 438-441 (2007).

84

Eli_Lilly_and_company_and_the_Nationale_Institutes_of_Health_Chemical_Genomics_Center. *Assay Guidance Manual Version 5.0*, <http://www.ncgc.nih.gov/guidance/manual_toc.html> (2008).

- 85 Inglese, J. *et al.* Quantitative high-throughput screening: A titration-based approach that efficiently identifies biological activities in large chemical libraries. *Proc. Natl. Acad. Sci. U.S.A.* **103**, 11473-11478 (2006).
- 86 Doman, T. N. *et al.* Molecular docking and high-throughput screening for novel inhibitors of protein tyrosine phosphatase-1B. *J. Med. Chem.* **45**, 2213-2221 (2002).
- 87 Paiva, A. M. *et al.* Inhibitors of dihydrodipicolinate reductase, a key enzyme of the diaminopimelate pathway of *Mycobacterium tuberculosis*. *Biochim. Biophys. Acta* **1545**, 67-77 (2001).
- 88 Shoichet, B. K., McGovern, S. L., Wei, B. & Irwin, J. J. Lead discovery using molecular docking. *Curr. Opin. Chem. Biol.* **6**, 439-446 (2002).
- 89 Kolb, P., Ferreira, R. S., Irwin, J. J. & Shoichet, B. K. Docking and chemoinformatic screens for new ligands and targets. *Curr. Opin. Biotechnol.* **20**, 429-436 (2009).
- 90 Mejías, A. & Ramilo, O. New approaches to reduce the burden of RSV infection. *Drug Discov. Today Ther. Strateg.* **3**, 173-181 (2006).
- 91 Maggon, K. & Barik, S. New drugs and treatment for respiratory syncytial virus. *Rev. Med. Virol.* **14**, 149-168 (2004).
- 92 Georgescu, G. & Chemaly, R. F. Palivizumab: where to from here? *Expert Opin. Biol. Ther.* **9**, 139-147 (2009).
- 93 Bitko, V., Musiyenko, A., Shulyayeva, O. & Barik, S. Inhibition of respiratory viruses by nasally administered siRNA. *Nat. Med.* **11**, 50-55 (2005).
- 94 Boukhvalova, M., Prince, G. & Blanco, J. Inactivation of respiratory syncytial virus by zinc finger reactive compounds. *Virol. J.* **7**, 20 (2010).
- 95 Roymans, D. & Koul, A. Respiratory syncytial virus: a prioritized or neglected target? *Future Med. Chem.* **2**, 1523-1527 (2010).
- 96 Spring, D. R. Chemical genetics to chemical genomics: small molecules offer big insights. *Chem. Soc. Rev.* **34**, 472-482 (2005).
- 97 Olszewska, W. & Openshaw, P. Emerging drugs for respiratory syncytial virus infection. *Expert Opin. Emerg. Drugs* **14**, 207-217 (2009).
- 98 Bonavia, A. *et al.* Identification of broad-spectrum antiviral compounds and assessment of the druggability of their target for efficacy against respiratory syncytial virus (RSV). *Proc. Natl. Acad. Sci. U.S.A.* **108**, 6739-6744 (2011).
- 99 Chapman, J. *et al.* RSV604, a novel inhibitor of respiratory syncytial virus replication. *Antimicrob. Agents Chemother.* **51**, 3346-3353 (2007).

- 100 Alvarez, R. *et al.* RNA interference-mediated silencing of the respiratory syncytial virus nucleocapsid defines a potent antiviral strategy. *Antimicrob. Agents Chemother.* **53**, 3952-3962 (2009).
- 101 StGelais, C. *et al.* Inhibition of hepatitis C virus p7 membrane channels in a liposome-based assay system. *Antivir. Res.* **76**, 48-58 (2007).
- 102 Sudo, K. *et al.* YM-53403, a unique anti-respiratory syncytial virus agent with a novel mechanism of action. *Antivir. Res.* **65**, 125-131 (2005).
- 103 Lambert, D. M. *et al.* Peptides from conserved regions of paramyxovirus fusion (F) proteins are potent inhibitors of viral fusion. *Proc. Natl. Acad. Sci. U.S.A.* **93**, 2186-2191 (1996).
- 104 Shepherd, N. E. *et al.* Modular α -helical mimetics with antiviral activity against respiratory syncytial virus. *J. Am. Chem. Soc.* **128**, 13284-13289 (2006).
- 105 Wu, H. *et al.* Development of motavizumab, an ultra-potent antibody for the prevention of respiratory syncytial virus infection in the upper and lower respiratory tract. *J. Mol. Biol.* **368**, 652-665 (2007).
- 106 Williams, H. in *The Independent* (London, 22/10/2010).
- 107 Andries, K. *et al.* Substituted benzimidazoles with nanomolar activity against respiratory syncytial virus. *Antivir. Res.* **60**, 209-219 (2003).
- 108 Bonfanti, J.-F. *et al.* Selection of a respiratory syncytial virus fusion inhibitor clinical candidate. 2. Discovery of a morpholinopropylaminobenzimidazole derivative (TMC353121). *J. Med. Chem.* **51**, 875-896 (2008).
- 109 Lundin, A. *et al.* Two novel fusion inhibitors of human respiratory syncytial virus. *Antivir. Res.* **88**, 317-324 (2010).
- 110 Douglas, J. L. *et al.* Inhibition of respiratory syncytial virus fusion by the small molecule VP-14637 via specific interactions with F protein. *J. Virol.* **77**, 5054-5064 (2003).
- 111 Cianci, C. *et al.* Orally active fusion inhibitor of respiratory syncytial virus. *Antimicrob. Agents Chemother.* **48**, 413-422 (2004).
- 112 Shah, N. R., Sunderland, A. & Grdzlishvili, V. Z. Cell type mediated resistance of vesicular stomatitis virus and Sendai virus to ribavirin. *PLoS ONE* **5**, e11265 (2010).
- 113 Diseases, C. o. I. Reassessment of the Indications for Ribavirin Therapy in Respiratory Syncytial Virus Infections. *Pediatrics* **97**, 137-140 (1996).
- 114 Gooding, J., Millage, A., Rye, A.-K. & Lacroix, R. The cost and safety of multidose use of palivizumab vials. *Clin. Pediatr. (Phila)* **47**, 160-163 (2008).
- 115 Fairbanks, L. D., Bofill, M., Ruckemann, K. & Simmonds, H. A. Importance of ribonucleotide availability to proliferating T-

- lymphocytes from healthy humans. Disproportionate expansion of pyrimidine pools and contrasting effects of de novo synthesis inhibitors. *J. Biol. Chem.* **270**, 29682-29689 (1995).
- 116 Roymans, D. *et al.* Binding of a potent small-molecule inhibitor of six-helix bundle formation requires interactions with both heptad-repeats of the RSV fusion protein. *Proc. Natl. Acad. Sci. U.S.A.* **107**, 308-313 (2010).
- 117 Olszewska, W. *et al.* Antiviral and lung protective activity of a novel respiratory syncytial virus fusion inhibitor in a mouse model. *Eur. Respir. J.* **38**, 401-408 (2011).
- 118 Hegele, R. G. Respiratory syncytial virus therapy and prophylaxis: have we finally turned the corner? *Eur. Respir. J.* **38**, 246-247 (2011).
- 119 Bonfanti, J.-F. *et al.* Selection of a respiratory syncytial virus fusion inhibitor clinical candidate, part 1: improving the pharmacokinetic profile using the structure-property relationship. *J. Med. Chem.* **50**, 4572-4584 (2007).
- 120 Shelat, A. A. & Guy, R. K. Scaffold composition and biological relevance of screening libraries. *Nat. Chem. Biol.* **3**, 442-446 (2007).
- 121 Kilby, J. M. *et al.* Potent suppression of HIV-1 replication in humans by T-20, a peptide inhibitor of gp41-mediated virus entry. *Nat. Med.* **4**, 1302-1307 (1998).
- 122 Wild, C., Greenwell, T. & Matthews, T. A synthetic peptide from HIV-1 gp41 is a potent inhibitor of virus-mediated cell-cell fusion. *AIDS Res. Hum. Retroviruses* **9**, 1051-1053 (1993).
- 123 DeVincenzo, J. *et al.* A randomized, double-blind, placebo-controlled study of an RNAi-based therapy directed against respiratory syncytial virus. *Proc. Natl. Acad. Sci. U.S.A.* **107**, 8800-8805 (2010).
- 124 Rasmussen, L., Maddox, C., Moore, B. P., Severson, W. & Lucile White, E. A high-throughput screening strategy to overcome virus instability. *Assay Drug. Dev. Technol.* **9**, 184-190 (2011).
- 125 Cannon, M. J. Microplaque immunoperoxidase detection of infectious respiratory syncytial virus in the lungs of infected mice. *J. Virol. Methods* **16**, 293-301 (1987).
- 126 McKimm-Breschkin, J. L. A simplified plaque assay for respiratory syncytial virus-direct visualization of plaques without immunostaining. *J. Virol. Methods* **120**, 113-117 (2004).
- 127 Murphy, B. R., Prince, G. A., Lawrence, L. A., Croen, K. D. & Collins, P. L. Detection of respiratory syncytial virus (RSV) infected cells by in situ hybridization in the lungs of cotton rats immunized with formalin-inactivated virus or purified RSV F and G glycoprotein subunit vaccine and challenged with RSV. *Virus Res.* **16**, 153-162 (1990).

- 128 Mosmann, T. Rapid colorimetric assay for cellular growth and survival: Application to proliferation and cytotoxicity assays. *J. Immunol. Methods* **65**, 55-63 (1983).
- 129 Scudiero, D. A. *et al.* Evaluation of a soluble tetrazolium/formazan assay for cell growth and drug sensitivity in culture using human and other tumor cell lines. *Cancer Res.* **48**, 4827-4833 (1988).
- 130 Severson, W. E. *et al.* Development and validation of a high-throughput screen for inhibitors of SARS CoV and its application in screening of a 100,000-compound library. *J. Biomol. Screen.* **12**, 33-40 (2007).
- 131 Andrei, G., Fiten, P., De Clercq, E., Snoeck, R. & Opdenakker, G. in *Antiviral Methods and Protocols Vol. 24 Methods in Molecular Medicine* (eds D. Kinchington & R. F. Schinazi) 151-170 (Humana Press, 2000).
- 132 Kim, S. S. *et al.* A cell-based, high-throughput screen for small molecule regulators of hepatitis C virus replication. *Gastroenterology* **132**, 311-320 (2007).
- 133 Fan, F. & Wood, K. V. Bioluminescent assays for high-throughput screening. *Assay Drug. Dev. Technol.* **5**, 127-136 (2007).
- 134 Zhang, R. *et al.* A continuous spectrophotometric assay for the hepatitis C virus serine protease. *Anal. Biochem.* **270**, 268-275 (1999).
- 135 Hawker, J. R. Chemiluminescence-based BrdU ELISA to measure DNA synthesis. *J. Immunol. Methods* **274**, 77-82 (2003).
- 136 Zhang, J.-H., Chung, T. D. Y. & Oldenburg, K. R. A simple statistical parameter for use in evaluation and validation of high throughput screening assays. *J. Biomol. Screen.* **4**, 67-73 (1999).
- 137 Iversen, P. W., Eastwood, B. J., Sittampalam, G. S. & Cox, K. L. A comparison of assay performance measures in screening assays: signal window, Z' Factor, and assay variability ratio. *J. Biomol. Screen.* **11**, 247-252 (2006).
- 138 Di, L. & Kerns, E. H. Biological assay challenges from compound solubility: strategies for bioassay optimization. *Drug Discov. Today* **11**, 446-451 (2006).
- 139 Eastwood, B. J. *et al.* The minimum significant ratio: a statistical parameter to characterize the reproducibility of potency estimates from concentration-response assays and estimation by replicate-experiment studies. *J. Biomol. Screen.* **11**, 253-261 (2006).
- 140 Wyde, P. R. *et al.* Use of cotton rats to evaluate the efficacy of antivirals in treatment of measles virus infections. *Antimicrob. Agents Chemother.* **44**, 1146-1152 (2000).
- 141 Markland, W., McQuaid, T. J., Jain, J. & Kwong, A. D. Broad-spectrum antiviral activity of the IMP dehydrogenase inhibitor VX-497: a comparison with ribavirin and demonstration of antiviral

- additivity with alpha interferon. *Antimicrob. Agents Chemother.* **44**, 859-866 (2000).
- 142 Wyde, P. R. *et al.* Antiviral efficacy of VP14637 against respiratory syncytial virus in vitro and in cotton rats following delivery by small droplet aerosol. *Antivir. Res.* **68**, 18-26 (2005).
- 143 Andries, K. *et al.* Piperidine-amino-benzimidazole derivatives as inhibitors of respiratory syncytial virus replication. (2004).
- 144 Gong, Y. & Kato, K. Facile synthesis of o- and p-(1-trifluoromethyl)-alkylated phenols via generation and reaction of quinone methides. *Synlett.* **2002**, 431-434 (2002).
- 145 Hu, Q. *et al.* Pfizer global virtual library (PGVL): a chemistry design tool powered by experimentally validated parallel synthesis information. *ACS Comb. Sci.* **14**, 579-589 (2012).
- 146 Zsoldos, Z., Reid, D., Simon, A., Sadjad, S. B. & Johnson, A. P. eHiTS: a new fast, exhaustive flexible ligand docking system. *J. Mol. Graph. Model.* **26**, 198-212 (2007).
- 147 Zsoldos, Z. in *Library design, search methods, and applications of fragment-based drug design* Vol. 1076 ACS Symposium Series Ch. 6, 91-130 (American Chemical Society, 2011).
- 148 Hopkins, A. L., Groom, C. R. & Alex, A. Ligand efficiency: a useful metric for lead selection. *Drug Discov. Today* **9**, 430-431 (2004).
- 149 MacroModel v. version 9.9 (Schrodinger, LLC, New York, NY, 2011).
- 150 Morton, D., Leach, S., Cordier, C., Warriner, S. & Nelson, A. Synthesis of natural-product-like molecules with over eighty distinct scaffolds. *Angew. Chem. Int. Ed. Engl.* **48**, 104-109 (2009).
- 151 Waldmann, H. Killing 84 birds with one stone. *Nat. Chem. Biol.* **5**, 76-77 (2009).
- 152 Schreiber, S. L. Organic chemistry: molecular diversity by design. *Nature* **457**, 153-154 (2009).
- 153 Galloway, W. R. J. D., Díaz-Gavilán, M., Isidro-Llobet, A. & Spring, D. R. Synthesis of unprecedented scaffold diversity. *Angew. Chem. Int. Ed. Engl.* **48**, 1194-1196 (2009).
- 154 Wolfe, J. P. & Schultz, D. M. Recent developments in palladium-catalyzed alkene aminoarylation reactions for the synthesis of nitrogen heterocycles. *Synthesis* **2012**, 351-361 (2012).
- 155 Tosatti, P., Nelson, A. & Marsden, S. P. Recent advances and applications of iridium-catalysed asymmetric allylic substitution. *Org. Biomol. Chem.* **10**, 3147-3163 (2012).
- 156 Fukuyama, T., Jow, C.-K. & Cheung, M. 2- and 4-Nitrobenzenesulfonamides: exceptionally versatile means for preparation of secondary amines and protection of amines. *Tetrahedron Lett.* **36**, 6373-6374 (1995).

- 157 Baeckvall, J. E., Bystroem, S. E. & Nordberg, R. E. Stereo- and regioselective palladium-catalyzed 1,4-diacetoxylation of 1,3-dienes. *J. Org. Chem.* **49**, 4619-4631 (1984).
- 158 Watson, I. D. G. & Yudin, A. K. New insights into the mechanism of palladium-catalyzed allylic amination. *J. Am. Chem. Soc.* **127**, 17516-17529 (2005).
- 159 Barsanti, P. A. *et al.* Substituted imidazole compounds as KSP inhibitors. United States patent US 7,626,040 B2 (2006).
- 160 Veitía, M. S.-I., Brun, P. L., Jorda, P., Falguières, A. & Ferroud, C. Synthesis of novel N-protected β -amino nitriles: study of their hydrolysis involving a nitrilase-catalyzed step. *Tetrahedron: Asymmetr.* **20**, 2077-2089 (2009).
- 161 Staudinger, H. & Meyer, J. Über neue organische Phosphorverbindungen III. Phosphinmethylenderivate und Phosphinimine. *Helv. Chim. Acta* **2**, 635-646 (1919).
- 162 Chen, Y.-C. *et al.* Multiple dendritic catalysts for asymmetric transfer hydrogenation. *J. Org. Chem.* **67**, 5301-5306 (2002).
- 163 Myers, A. G., Gleason, J. L., Yoon, T. & Kung, D. W. Highly practical methodology for the synthesis of d- and l- α -amino acids, N-protected α -amino acids, and N-methyl- α -amino acids. *J. Am. Chem. Soc.* **119**, 656-673 (1997).
- 164 Nagula, G., Huber, V. J., Lum, C. & Goodman, B. A. Synthesis of α -substituted β -amino acids using pseudoephedrine as a chiral auxiliary. *Org. Lett.* **2**, 3527-3529 (2000).
- 165 Sinha, R. & Imperiali, B. Stereoselective synthesis of a pyridoxamine coenzyme-amino acid chimera: assembly of a polypeptide incorporating the pyridoxamine moiety. *Tetrahedron Lett.* **37**, 2129-2132 (1996).
- 166 Lohse-Fraefel, N. & Carreira, E. M. Polyketide building blocks via diastereoselective nitrile oxide cycloadditions with homoallylic alcohols and monoprotected homoallylic diols. *Chem.-Eur. J.* **15**, 12065-12081 (2009).
- 167 Appel, R. Tertiary phosphane/tetrachloromethane, a versatile reagent for chlorination, dehydration, and P-N linkage. *Angew. Chem. Int. Ed. Engl.* **14**, 801-811 (1975).
- 168 Kozikowski, A. P. & Scripko, J. G. NOC approach to spiroketals. A total synthesis of (+/-)-talaromycin B. *J. Am. Chem. Soc.* **106**, 353-355 (1984).
- 169 Wittig, G. Fortschritte auf dem Gebiet der organischen Aniono-Chemie. *Angew. Chem.* **66**, 10-17 (1954).
- 170 Izquierdo, I., Plaza, M. T., Rodríguez, M. & Tamayo, J. Chiral building-blocks by chemoenzymatic desymmetrization of 2-ethyl-1,3-propanediol for the preparation of biologically active natural products. *Tetrahedron: Asymmetr.* **10**, 449-455 (1999).

- 171 Mori, K. & Takahashi, Y. Synthetic microbial chemistry, XXIV. Synthesis of antibiotic 1233A, an inhibitor of cholesterol biosynthesis. *Liebigs Ann. Chem.* **1991**, 1057-1065 (1991).
- 172 Beckwith, A. L. J. & Meijs, G. F. Iododediazotiation of arenediazonium salts accompanied by aryl radical ring closure. *J. Org. Chem.* **52**, 1922-1930 (1987).
- 173 Tietze, L. F., Stadler, C., Böhnke, N., Brasche, G. & Grube, A. Synthesis of enantiomerically pure cyclopentene building blocks. *Synlett.* **2007**, 485-487 (2007).
- 174 Dore, D. D., Burgeson, J. R., Davis, R. A. & Hitchcock, S. R. Synthesis, reactivity and conformational stability of an L-phenylalanine derived oxadiazinanone. *Tetrahedron: Asymmetr.* **17**, 2386-2392 (2006).
- 175 Deyrup, J. A. & Moyer, C. L. 1,2,3-oxathiazolidines. Heterocyclic system. *J. Org. Chem.* **34**, 175-179 (1969).
- 176 Bower, J. F., Rujirawanich, J. & Gallagher, T. N-Heterocycle construction via cyclic sulfamidates. Applications in synthesis. *Org. Biomol. Chem.* **8**, 1505-1519 (2010).
- 177 Richter, J. M. *et al.* Scope and mechanism of direct indole and pyrrole couplings adjacent to carbonyl compounds: total synthesis of acremoauxin A and oxazinin 3. *J. Am. Chem. Soc.* **129**, 12857-12869 (2007).
- 178 Wolf, C., Francis, C. J., Hawes, P. A. & Shah, M. Enantioselective alkylation of aldehydes promoted by (S)-tyrosine-derived β -amino alcohols. *Tetrahedron: Asymmetr.* **13**, 1733-1741 (2002).
- 179 Oila, M. J., Tois, J. E. & Koskinen, A. M. P. Ligand creation via linking a rapid and convenient method for construction of novel supported PyOX-ligands. *Tetrahedron* **61**, 10748-10756 (2005).
- 180 Lipkus, A. H. *et al.* Structural diversity of organic chemistry. A scaffold analysis of the CAS registry. *J. Org. Chem.* **73**, 4443-4451 (2008).
- 181 Burke, M. D., Berger, E. M. & Schreiber, S. L. Generating diverse skeletons of small molecules combinatorially. *Science* **302**, 613-618 (2003).
- 182 Lachance, H., Wetzel, S., Kumar, K. & Waldmann, H. Charting, navigating, and populating natural product chemical space for drug discovery. *J. Med. Chem.* **55**, 5989-6001 (2012).
- 183 Karageorgis, G. *Targetting the hRSV F protein using a DOS approach* M.Sc. Chemical Biology thesis, University of Leeds, (2011).
- 184 Muller, P. Y. & Milton, M. N. The determination and interpretation of the therapeutic index in drug development. *Nat. Rev. Drug Discov.* **11**, 751-761 (2012).

- 185 Moore, B. P. *et al.* (S)-N-(2,5-Dimethylphenyl)-1-(quinoline-8-ylsulfonyl)pyrrolidine-2-carboxamide as a small molecule inhibitor probe for the study of respiratory syncytial virus Infection. *J. Med. Chem.* **55**, 8582-8587 (2012).
- 186 Wyde, P. R., Meyerson, L. R. & Gilbert, B. E. In vitro evaluation of the antiviral activity of SP-303, an euphorbiaceae shrub extract, against a panel of respiratory viruses. *Drug Dev. Res.* **28**, 467-472 (1993).
- 187 Jorgensen, W. L. Challenges for academic drug discovery. *Angew. Chem. Int. Ed. Engl.* **51**, 11680-11684 (2012).
- 188 Clemons, P. A. *et al.* Small molecules of different origins have distinct distributions of structural complexity that correlate with protein-binding profiles. *Proc. Natl. Acad. Sci. U.S.A.* **107**, 18787-18792 (2010).
- 189 Hert, J., Irwin, J. J., Laggner, C., Keiser, M. J. & Shoichet, B. K. Quantifying biogenic bias in screening libraries. *Nat. Chem. Biol.* **5**, 479-483 (2009).
- 190 Huggins, D. J., Venkitaraman, A. R. & Spring, D. R. Rational methods for the selection of diverse screening compounds. *ACS Chem. Biol.* **6**, 208-217 (2011).
- 191 Wang, R., Fang, X., Lu, Y. & Wang, S. The PDBbind database: collection of binding affinities for protein-ligand complexes with known three-dimensional structures. *J. Med. Chem.* **47**, 2977-2980 (2004).
- 192 Hartshorn, M. J. *et al.* Diverse, high-quality test set for the validation of protein-ligand docking performance. *J. Med. Chem.* **50**, 726-741 (2007).
- 193 Plewczynski, D., Łażniewski, M., Augustyniak, R. & Ginalski, K. Can we trust docking results? Evaluation of seven commonly used programs on PDBbind database. *J. Comput. Chem.* **32**, 742-755 (2011).
- 194 Erickson, J. A., Jalaie, M., Robertson, D. H., Lewis, R. A. & Vieth, M. Lessons in molecular recognition: the effects of ligand and protein flexibility on molecular docking accuracy. *J. Med. Chem.* **47**, 45-55 (2003).
- 195 Abel, R., Young, T., Farid, R., Berne, B. J. & Friesner, R. A. Role of the active-site solvent in the thermodynamics of factor Xa ligand binding. *J. Am. Chem. Soc.* **130**, 2817-2831 (2008).
- 196 Lieber, M., Todaro, G., Smith, B., Szakal, A. & Nelson-Rees, W. A continuous tumor-cell line from a human lung carcinoma with properties of type II alveolar epithelial cells. *Int. J. Cancer* **17**, 62-70 (1976).
- 197 Barretto, N., Hallak, L. K. & Peeples, M. E. Neuraminidase treatment of respiratory syncytial virus-infected cells or virions, but

- not target cells, enhances cell-cell fusion and infection. *Virology* **313**, 33-43 (2003).
- 198 Ho, W. *et al.* Centrifugal enhancement of human immunodeficiency virus type 1 infection and human cytomegalovirus gene expression in human primary monocyte/macrophages in vitro. *J. Leukoc. Biol.* **53**, 208-212 (1993).
- 199 Yoo, S.-M. *et al.* Centrifugal enhancement of Kaposi's sarcoma-associated virus infection of human endothelial cells in vitro. *J. Virol. Methods* **154**, 160-166 (2008).
- 200 Srinivasakumar, N., Ogra, P. L. & Flanagan, T. D. Characteristics of fusion of respiratory syncytial virus with HEp-2 cells as measured by R18 fluorescence dequenching assay. *J. Virol.* **65**, 4063-4069 (1991).
- 201 Grubbs, F. E. Procedures for detecting outlying observations in samples. *Technometrics* **11**, 1-21 (1969).
- 202 Stefansky, W. Rejecting outliers in factorial designs. *Technometrics* **14**, 469-479 (1972).
- 203 Chung, N. *et al.* Median absolute deviation to improve hit selection for genome-scale RNAi screens. *J. Biomol. Screen.* **13**, 149-158 (2008).
- 204 Still, W. C., Kahn, M. & Mitra, A. Rapid chromatographic technique for preparative separations with moderate resolution. *J. Org. Chem.* **43**, 2923-2925 (1978).
- 205 Birmingham, A. *et al.* Statistical methods for analysis of high-throughput RNA interference screens. *Nat. Meth.* **6**, 569-575 (2009).

9 APPENDIX

Appendix 1 Statistics behind a high-throughput screening assay (Sections 2.1.3.2, 2.3)

Appendix 2 – 6 Individual plates (1 to 5) used to determine the overall antiviral effect of Ribavirin (Section 2.3.5.1).

The dose-response to Ribavirin in HEp-2 cells describes a sigmoidal curve. The results are expressed as the ratio to untreated A2-infected cells at an M.O.I. of 0.85, labelled Antiviral. The error bars refer to the standard deviation of three replicates.

Appendix 7 – 8 Establishment of the robustness of the assay (Section 2.3.6).

The dose-response to Ribavirin in HEp-2 cells describes a sigmoidal curve. The results are expressed as the ratio to untreated A2-infected cells at an M.O.I. of 0.55. The error bars refer to the standard deviation of three replicates. Appendix 7: Ribavirin was prepared and added by hand; appendix 8: Ribavirin was prepared and added by the robot.

Appendix 9 Table summarising the statistical parameters analysed in high-throughput screening (Sections 2.3.5.1, 2.3.6).

The following parameters are summarised: mean (μ), standard deviation (σ), coefficient of variation (CV), Z'-factor (for Ribavirin and the maximum and minimum signals), signal window (SW), signal-to-noise (S:N) and signal-to-background (S:B) ratios, the calculated EC_{50} in micromolar as calculated by Origin 7.5. Mock and A2 refers to mock- and A2-infected HEp-2 cells, respectively.

Appendix 10 – 12 Normal distribution of Ribavirin concentrations, (10, Section 2.3.5.3; 11-12, Section 2.3.6).

Representation of the frequencies of normalised Gaussians (normal distribution) for each of the Ribavirin concentrations along with the A2-infected HEp-2 cells (A2) control. M.O.I. was 0.85 for appendix 10 and 0.5 for appendix 11, 12.

Appendix 13 – 18 Input files used for Chapter 3

Appendix 13: building blocks and electrophiles chosen for enumeration of the virtual library described in Section 3.2.1.

Appendix 14: fourteen common substructures identified by vHTS of 53,640 molecules against 3KPE with the bound water using eHiTS (Section 3.2.2)

Appendix 15: twenty-one common scaffolds identified by vHTS of 15,728 molecules against 3KPE with the bound water using eHiTS (Section 3.2.2)

Appendix 16: enumeration of a more focused library (Section 3.2.3)

Appendix 17: enumeration of lead-like library of 85,115 molecules (Section 3.3.1)

Appendix 18 – Biological testing of the vHTS compounds identified as hits after single concentration screening (Section 5.1.3)

Appendix 19 – 23 Dose-response analyses on non-hit controls (Section 5.1.5)

Dose-response analyses (25 μ M to 1.3 nM) carried out on the following compounds groups: four cytotoxic compounds not identified as hits during the screening campaign (Appendices 19-22); and one compound not identified as a hit and not classified as cytotoxic (negative compound, shown in Appendix 23). The results are expressed as the ratio to untreated A2-infected cells at an M.O.I. of 0.5, labelled Antiviral. An additional y-axis has been added to show the cytotoxic dose-response of HEp-2 cells to the hit. The results are expressed as the ratio of the hit-exposed cells to the unexposed cells against logarithm to base 10 of the hit concentrations (in molar). Absorbance was read at 570 nm. The error bars refer to the standard deviation of four replicates.

1 – Statistics behind a high-throughput screening assay (Sections 2.1.3.2, 2.3)

Coefficient of variation: the coefficient of variation is likely to fail when the samples analysed are corresponding to a complete reduction of the signal, hence having a low mean value. In such instances, it is recommended to look at the standard deviation of the data series and to compare it to that of the maximum signal⁸⁴.

Minimum significant ratio: when an assay is carried out with a concentration gradient, it is important to introduce another statistical parameter: the minimum significant ratio (MSR), a measurement of assay performance¹³⁹. This parameter can also be used to assess assay reproducibility, but it needs a minimum of two compounds with reportable potencies¹³⁹. The MSR criterion allows room for variation (standard deviation of the log difference between two runs lower than 0.24). It also means that as long as the difference in log potencies between two runs is consistent (*i.e.* low standard deviation), this criterion will always be satisfied. That is why the limits of agreements MR/MSR and MR×MSR have been introduced¹³⁹. MR is the mean-ratio and is defined as 10^{μ_d} , μ_d is the mean of the d_i (d_i is the difference, between two runs, in log potency for compound i). These two limits should always fall between 0.33 and 3⁸⁴. Therefore, if the difference in log potencies between two runs is consistent but high, the performance of the assay might be rejected.

Hit threshold: the threshold for hit selection, in an unbiased library, is set at three standard deviations, *i.e.* outside the data variability band, from the normalised mean^{81,83,136,203} (Figure A.4). An alternative, more resistant to outliers (*i.e.* false-positive, “hits”), is to use the median and the median absolute deviation^{81,203,205} (M.A.D.):

$$\text{MAD} = 1.4826 \times \text{median}[|x(i,j) - \text{median}(x)|]$$

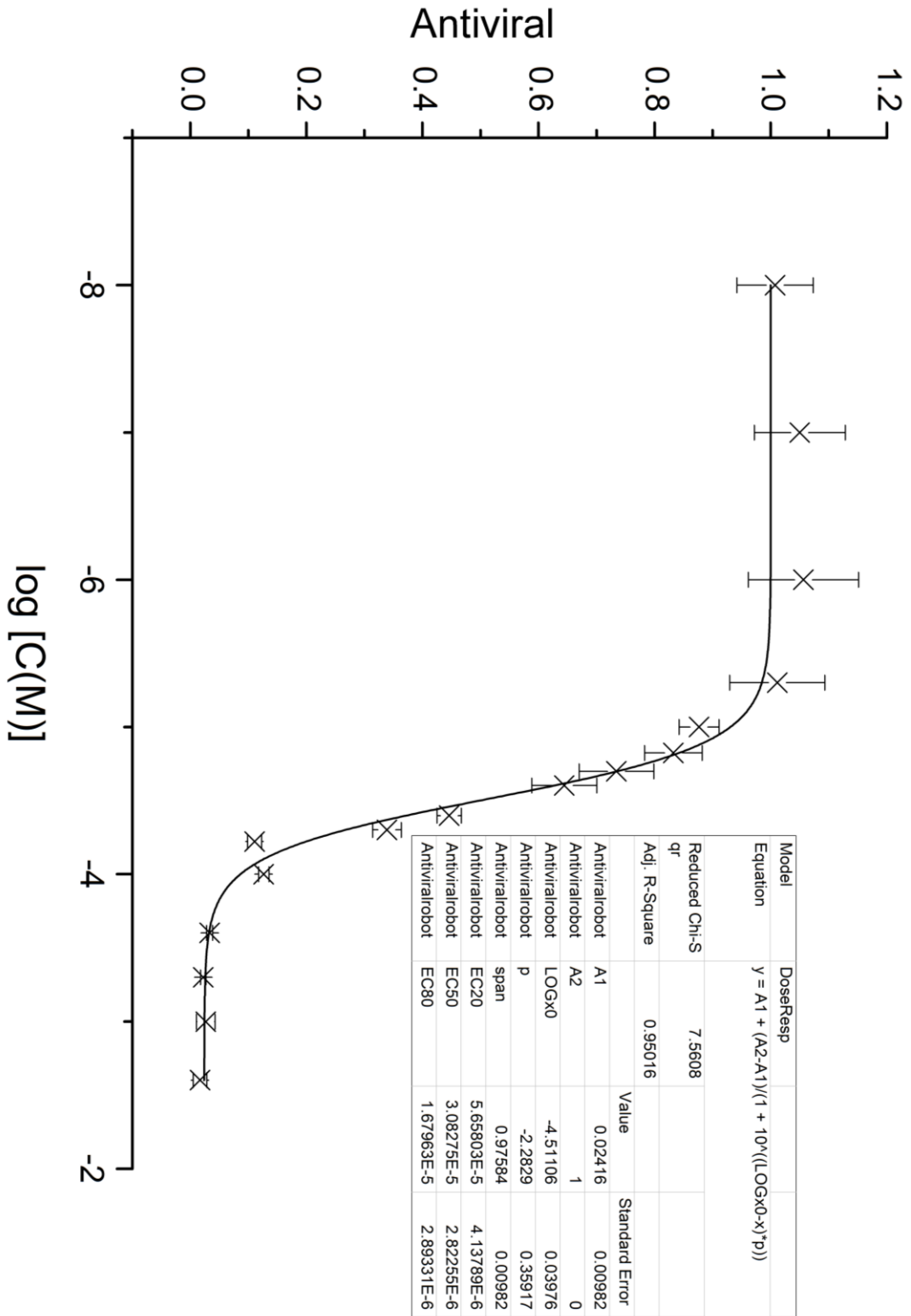
$x(i,j)$ is the sample loaded on the plate in row i , column j , and x is the sample. The 1.4826 coefficient is to allow comparison to the standard deviation when the data fits a normal distribution.

In this instance, the threshold for hit selection is set at three MAD from the median. The downside to this selection method is that it will return several weak “hits”, which will increase the workload for the follow-up screen.

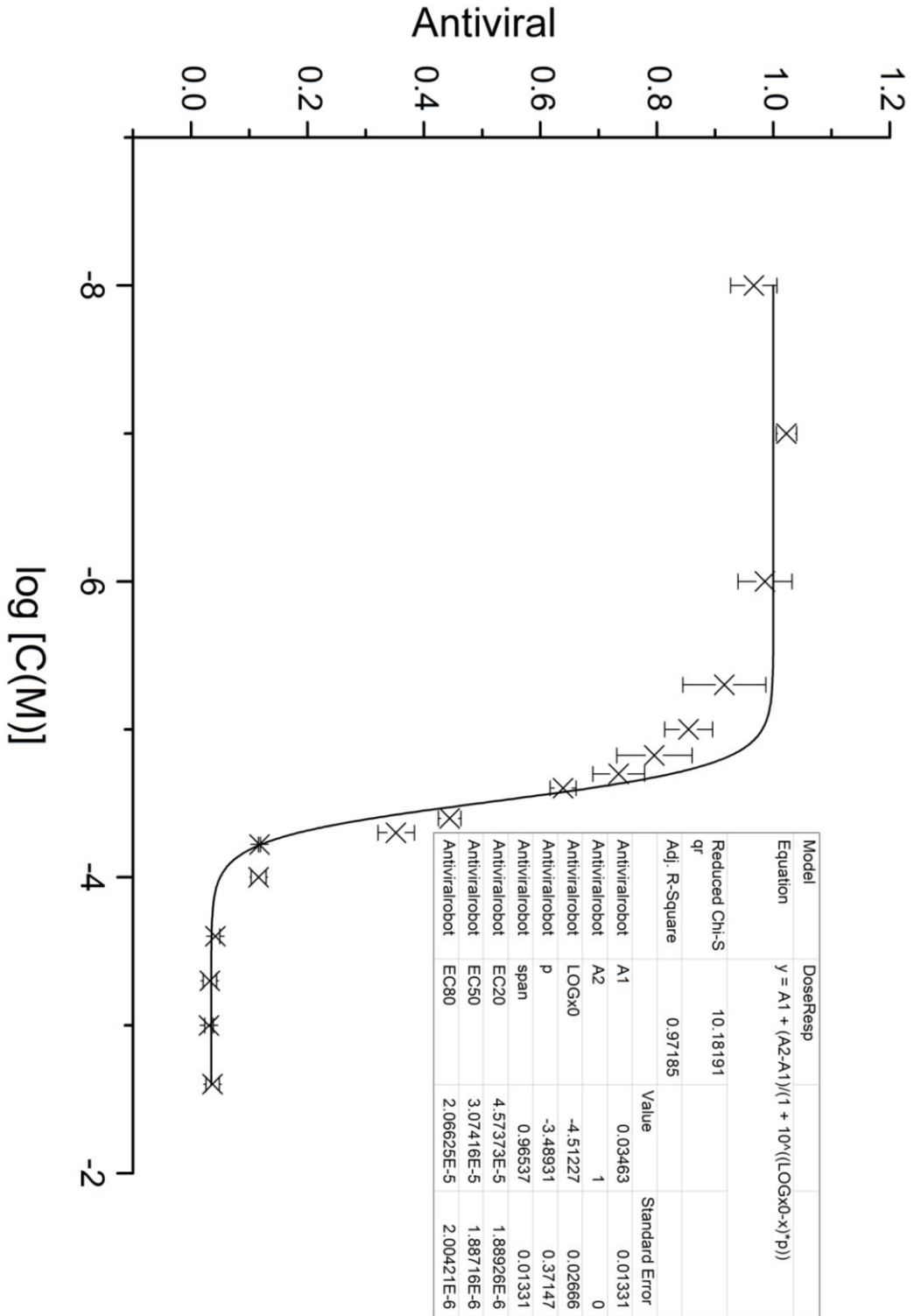
Table 9.1: Statistical parameters required for an assay to be suitable for HTS

Statistical parameters	Equation	Assay validated if
Signal-to-noise ratio	$= \frac{\mu(+ve) - \mu(-ve)}{\sigma(-ve)}$	Strong signal
Signal-to-background ratio	$= \frac{\mu(+ve)}{\mu(-ve)}$	> 2 (good dynamic range)
Coefficient of variation (%)	$= \frac{\sigma(+ve \text{ or } -ve)}{\mu(+ve \text{ or } -ve)}$	< 20% (low well-to-well variability)
Signal window	$= \frac{\mu(+ve) - \mu(-ve) - 3(\sigma(+ve) + \sigma(-ve))}{\sigma(+ve)}$	> 2 (good separation between the controls)
Z'-factor	$= 1 - \frac{3(\sigma(+ve) + \sigma(-ve))}{ \mu(+ve) - \mu(-ve) }$	> 0 ^a (feasible assay)
Z-factor	$Z = 1 - \frac{3(\sigma(sample) + \sigma(control))}{ \mu(sample) - \mu(control) }$	> 0 ^a (feasible assay)
MSR	$MSR = 10^{2\sigma_d^b}$	< 3
Separation band	$= \mu_{+ve} - \mu_{-ve} - 3 \times (\sigma_{+ve} + \sigma_{-ve})$	-

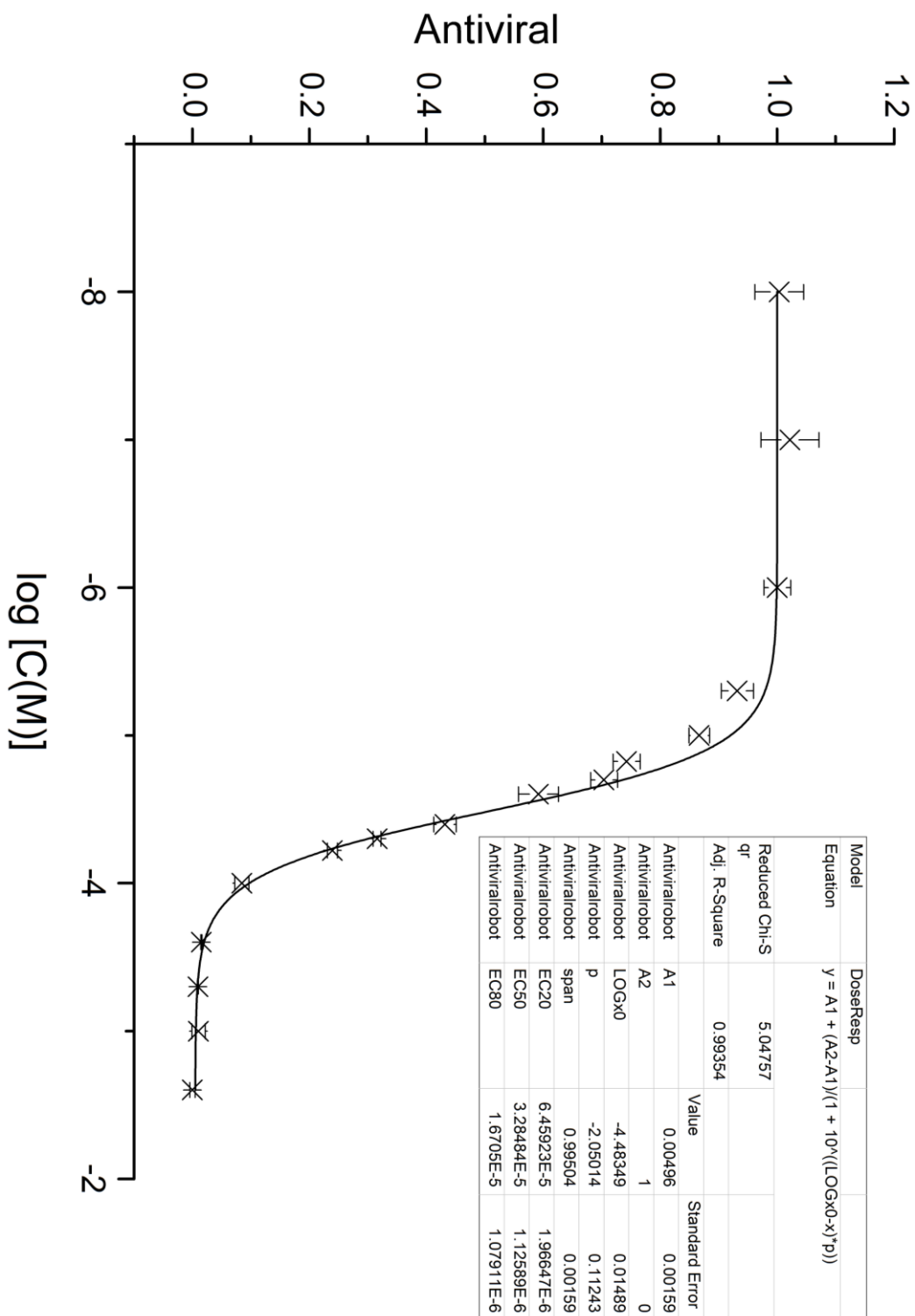
μ and σ refer to the average and standard deviation respectively. The formulae's have been reproduced to match those used in the present assay. +ve refers to the positive control (maximum signal) and -ve refers to the negative control (minimum signal). ^a: a 'good' assay should have $Z' > 0.5$. ^b σ_d is the standard deviation of the d_i for all the compounds, and d_i is the difference, between two runs, in potency (log) for compound i .

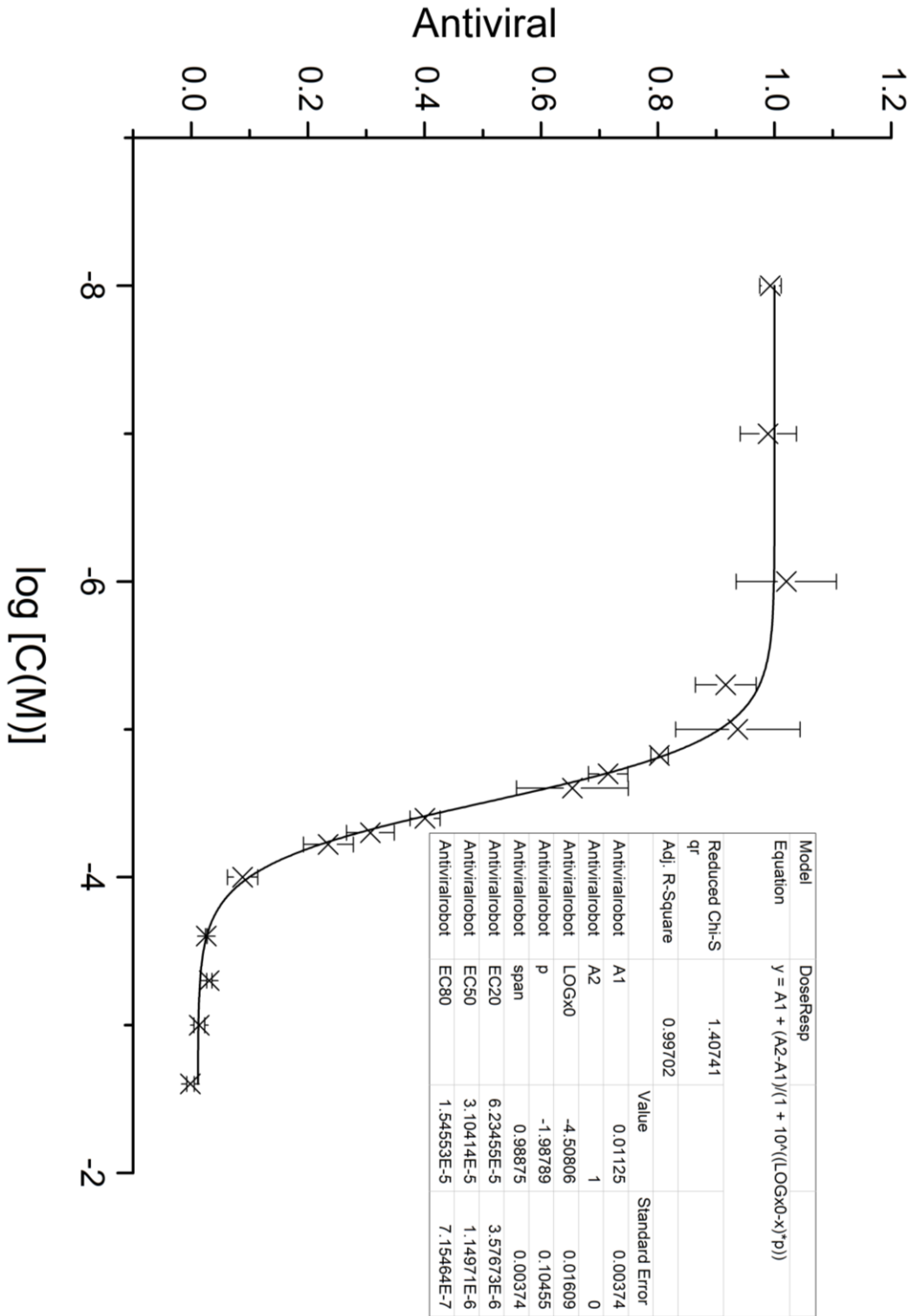


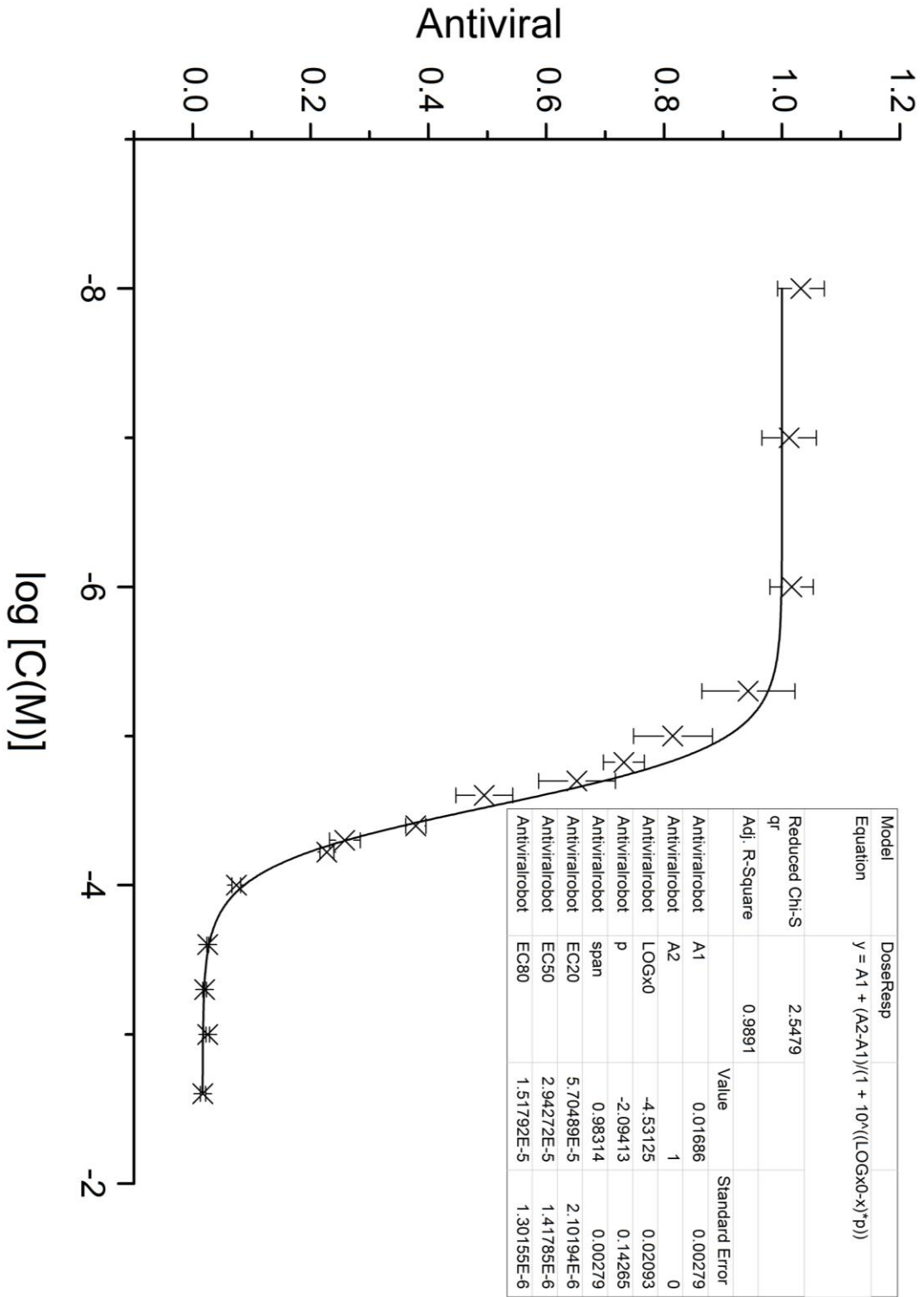
3 – Plate 2 (Section 2.3.5.1)



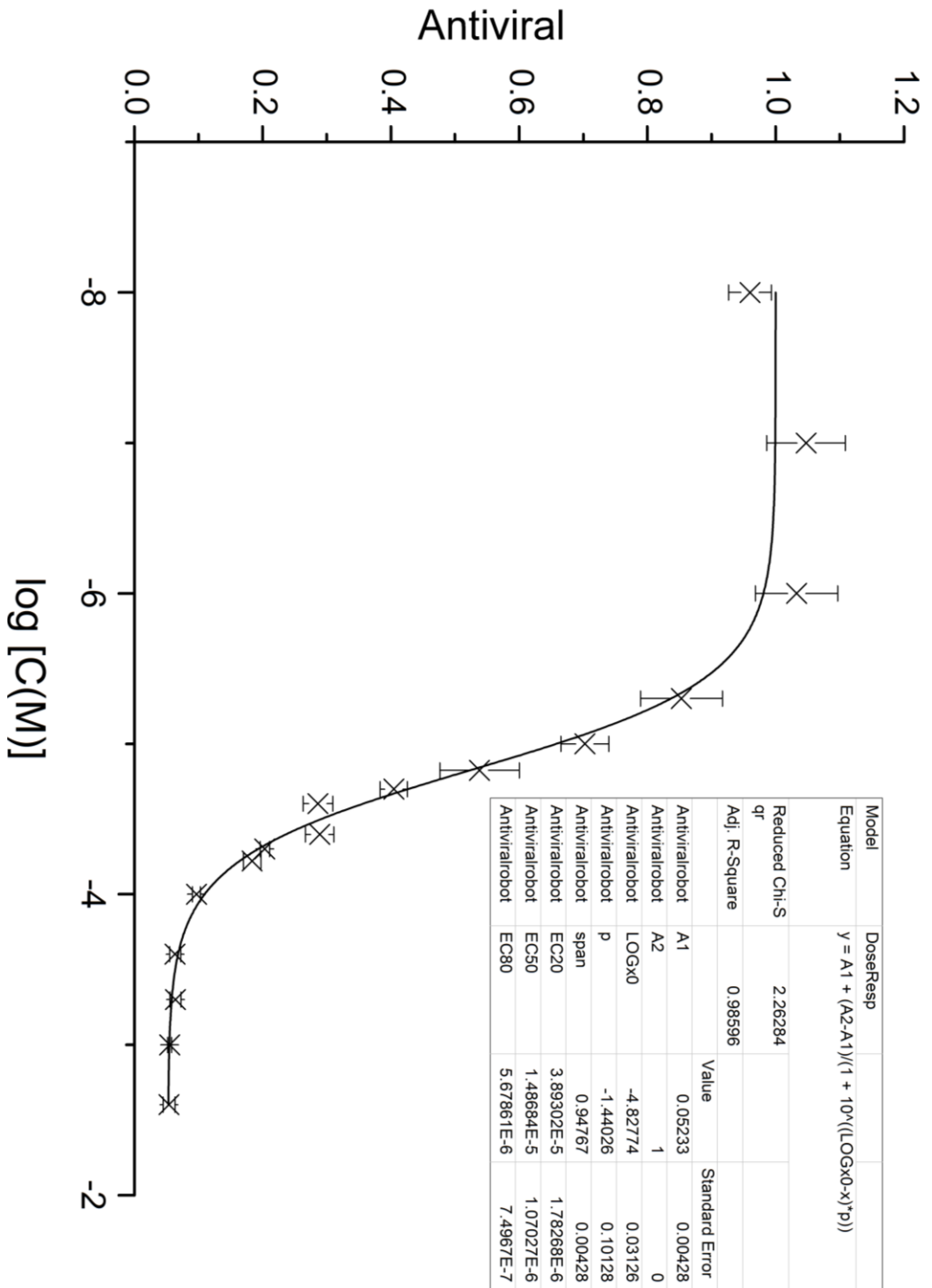
4 – Plate 3 (Section 2.3.5.1)



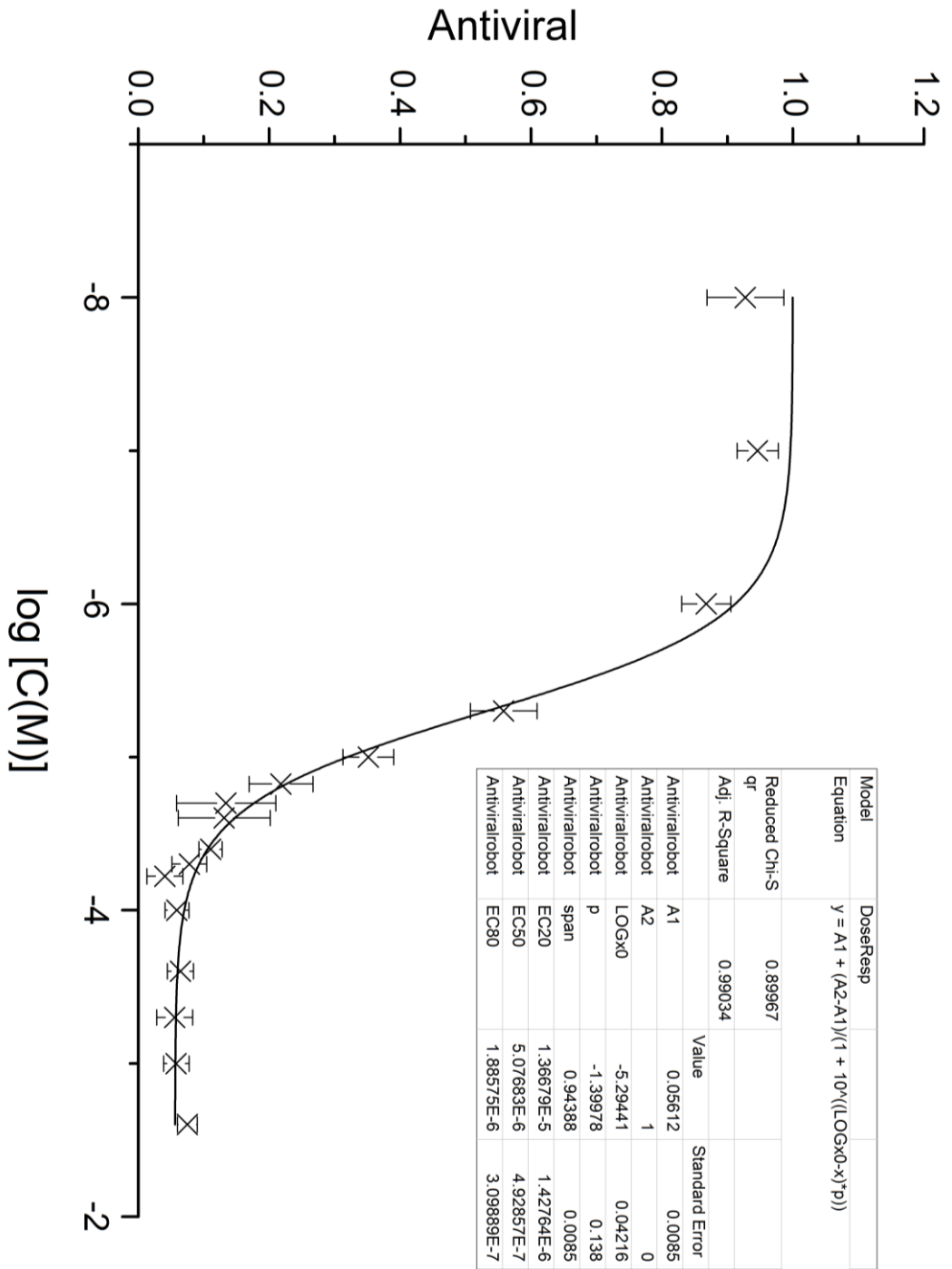




7 – Ribavirin (hand) (Section 2.3.6)



8 – Ribavirin (robot) (Section 2.3.6)



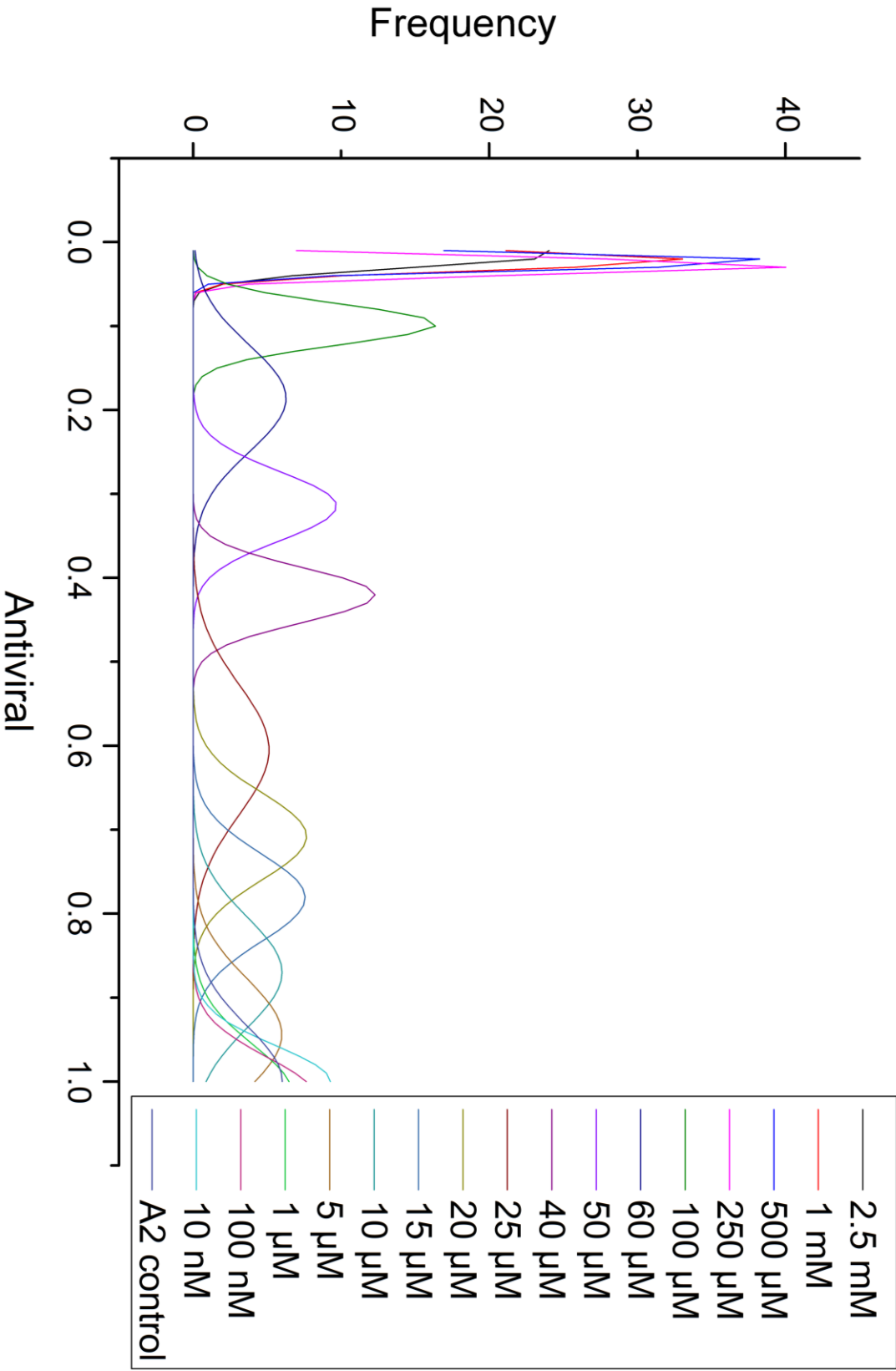
9 – Summary of the statistical parameters (Sections 2.3.5.1, 2.3.6)

	Ribavirin concentration (M)																			
	Mock	A2	2.50E-03	1.00E-03	5.00E-04	2.50E-04	1.00E-04	6.00E-05	5.00E-05	4.00E-05	2.50E-05	2.00E-05	1.50E-05	1.00E-05	5.00E-06	1.00E-06	1.00E-07	1.00E-08		
Plate 1																				
μ	-6.04E-17	1.00E+00	1.67E-02	2.67E-02	2.24E-02	3.33E-02	1.27E-01	1.11E-01	3.39E-01	4.46E-01	6.44E-01	7.34E-01	8.32E-01	8.77E-01	1.01E+00	1.06E+00	1.05E+00	1.01E+00		
σ	9.65E-03	7.41E-02	1.17E-02	1.62E-02	4.60E-03	5.13E-03	9.05E-03	1.22E-02	2.47E-02	2.10E-02	5.60E-02	6.42E-02	4.95E-02	3.44E-02	8.20E-02	9.50E-02	7.81E-02	6.56E-02	6.51	
CV(%)	-1.59E+14	7.41	70.12	60.57	20.56	15.34	7.14	10.96	7.31	4.71	8.69	8.74	5.95	3.92	8.10	9.00	7.44	6.51	6.51	
Z (Ribavirin)	x	x	0.74	0.72	0.76	0.75	0.71	0.71	0.55	0.48	-0.10	-0.56	-1.21	-1.64	-39.63	-8.00	-8.09	-52.97	-52.97	
Z (max/min signal)	0.75	SW	10.1	SN	103.9	SB	3													
EC_{50} (µM)	30.86																			
Plate 2																				
μ	1.04E-17	1.00E+00	3.69E-02	3.09E-02	3.23E-02	4.20E-02	1.16E-01	1.18E-01	3.52E-01	4.44E-01	6.39E-01	7.33E-01	7.96E-01	8.55E-01	9.16E-01	9.86E-01	1.02E+00	9.67E-01	9.67E-01	
σ	7.05E-03	7.50E-02	1.13E-02	7.19E-03	1.14E-02	7.24E-03	1.28E-02	1.64E-03	3.15E-02	1.93E-02	2.24E-02	4.46E-02	6.47E-02	4.13E-02	8.12	4.83	7.78	4.71	1.72	4.13
CV(%)	6.73E+16	7.50	30.62	23.29	35.29	17.23	11.01	1.40	8.94	4.34	3.50	6.07	8.12	8.12	0.04	0.13	0.13	-1.63	-11.02	3.07
Z (Ribavirin)	x	x	0.96	0.98	0.96	0.98	0.96	0.99	0.85	0.90	0.81	0.49	0.04	0.13	0.13	-1.63	-11.02	-11.02	-11.02	-2.91
Z (max/min signal)	0.75	SW	9.8	SN	142.3	SB	3.2													
EC_{50} (µM)	30.74																			
Plate 3																				
μ	-1.01E-17	1.00E+00	3.98E-05	1.04E-02	9.52E-03	1.53E-02	8.45E-02	2.40E-01	3.16E-01	4.32E-01	5.92E-01	7.04E-01	7.43E-01	8.67E-01	9.32E-01	1.00E+00	1.02E+00	1.00E+00	1.00E+00	
σ	6.13E-03	4.20E-02	4.56E-03	1.13E-02	4.59E-04	1.10E-03	1.23E-02	8.76E-03	6.78E-03	1.93E-02	3.43E-02	2.30E-02	2.33E-02	1.75E-02	2.76E-02	2.30E-02	2.30E-02	4.95E-02	4.16E-02	4.16E-02
CV(%)	-6.06E+16	4.20	11440.55	108.82	4.82	7.17	14.57	3.66	2.15	4.46	5.80	3.26	3.13	2.02	2.96	2.30	2.30	4.84	4.14	4.14
Z (Ribavirin)	x	x	0.86	0.83	0.87	0.87	0.82	0.80	0.78	0.67	0.43	0.33	0.23	-0.36	-2.08	-403.82	-12.23	-89.96	-89.96	
Z (max/min signal)	0.85	SW	19.7	SN	163.1	SB	3.1													
EC_{50} (µM)	32.85																			
Plate 4																				
μ	-2.22E-17	1.00E+00	-1.43E-03	1.37E-02	3.09E-02	2.58E-02	8.80E-02	2.35E-01	3.07E-01	4.01E-01	6.53E-01	7.15E-01	8.03E-01	9.37E-01	9.16E-01	1.02E+00	9.89E-01	9.93E-01	9.93E-01	
σ	6.80E-03	5.00E-02	6.59E-03	9.16E-03	4.75E-03	1.35E-03	2.59E-02	4.28E-02	4.09E-02	2.59E-02	9.57E-02	3.37E-02	1.48E-02	1.07E-01	5.22E-02	8.58E-02	4.81E-02	1.83E-02	1.83E-02	
CV(%)	-3.07E+16	5.00	-462.09	66.62	15.35	5.21	29.49	18.20	13.31	6.46	14.65	4.72	1.85	11.40	5.70	8.41	4.86	1.84	1.84	
Z (Ribavirin)	x	x	0.85	0.84	0.85	0.86	0.77	0.65	0.63	0.64	-0.24	0.16	0.07	-6.98	-2.74	-13.95	-57.02	-146.56	-146.56	
Z (max/min signal)	0.83	SW	18.8	SN	147.5	SB	3.1													
EC_{50} (µM)	31.76																			
Plate 5																				
μ	-1.16E-17	1.00E+00	1.73E-02	2.55E-02	2.02E-02	2.56E-02	7.42E-02	2.28E-01	2.88E-01	3.79E-01	4.95E-01	6.52E-01	7.32E-01	8.15E-01	9.43E-01	1.02E+00	1.01E+00	1.03E+00	1.03E+00	
σ	4.53E-02	8.69E-02	4.41E-03	3.03E-03	3.04E-03	1.54E-03	7.29E-03	1.17E-02	2.60E-02	1.73E-02	4.82E-02	6.53E-02	3.49E-02	6.67E-02	7.90E-02	3.66E-02	4.62E-02	3.95E-02	3.95E-02	
CV(%)	-3.92E+17	8.69	25.47	11.88	15.06	5.99	9.84	5.12	10.08	4.57	9.74	10.01	4.77	8.18	8.38	3.61	4.56	3.83	3.83	
Z (Ribavirin)	x	x	0.72	0.72	0.72	0.73	0.69	0.62	0.54	0.50	0.20	-0.31	-0.36	-1.49	-7.71	-21.57	-31.70	-10.75	-10.75	
Z (max/min signal)	0.6	SW	6.9	SN	22.1	SB	3													
EC_{50} (µM)	29.43																			

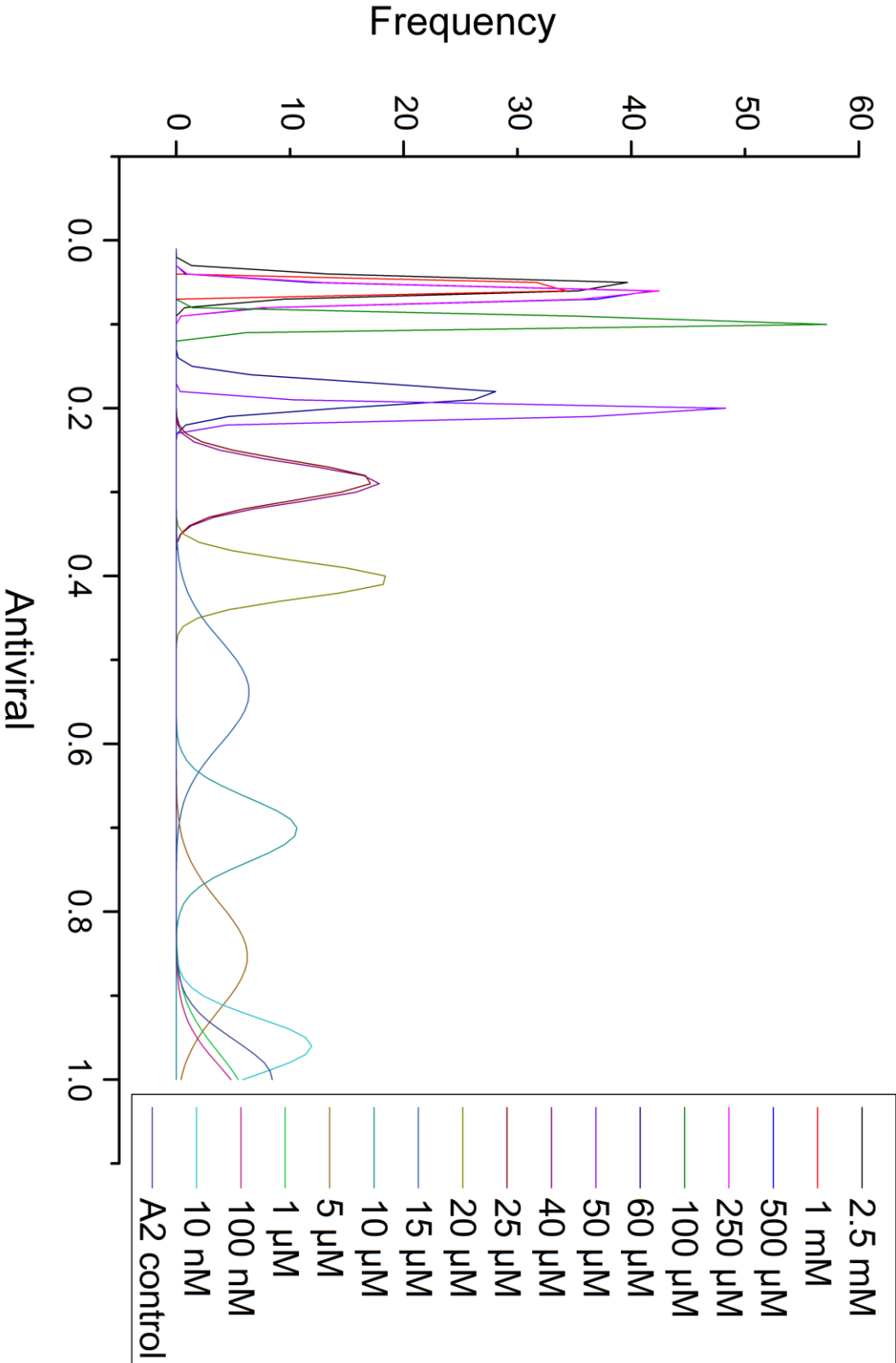
9 – Summary of the statistical parameters (continued) (Sections 2.3.5.1, 2.3.6)

		Rhavirin concentration (AU)																	
	Mock	A2	2.50E-03	1.00E-03	5.00E-04	2.50E-04	1.00E-04	6.00E-05	5.00E-05	4.00E-05	2.50E-05	2.00E-05	1.50E-05	1.00E-05	5.00E-06	1.00E-06	1.00E-07	1.00E-08	
Plates 1, 2, 3, 4, 5																			
O	μ	-1.85E-17	1.00E+00	1.39E-02	2.14E-02	2.31E-02	2.85E-02	9.79E-02	1.86E-01	3.14E-01	4.20E-01	6.05E-01	7.08E-01	7.81E-01	8.70E-01	9.44E-01	1.02E+00	1.00E+00	
V	σ	1.98E-02	6.61E-02	1.61E-02	1.20E-02	9.94E-03	9.85E-03	2.43E-02	6.34E-02	4.11E-02	3.24E-02	7.77E-02	5.20E-02	5.27E-02	6.63E-02	6.65E-02	5.93E-02	4.81E-02	4.30E-02
E	CV(%)	-1.071E+17	6.61	115.72	55.89	43.12	34.58	24.78	34.09	13.09	7.72	12.86	7.34	6.74	7.62	7.04	5.84	4.72	4.30
R	Z (Robust)	x	x	0.75	0.76	0.77	0.77	0.70	0.52	0.53	0.49	-0.09	-0.21	-0.63	-2.06	-6.07	-22.81	-16.80	-552.34
A	Z (max/min signal)	0.7	x	11.2															
L	Separation band	x	SW	7.39E-01	7.44E-01	7.49E-01	7.44E-01	6.31E-01	4.25E-01	3.64E-01	2.84E-01	-3.63E-02	-6.22E-02	-1.37E-01	-2.67E-01	-3.41E-01	-3.92E-01	-3.62E-01	-3.28E-01
L	EC ₅₀ (μM)		31.41																
Hand																			
H	μ	-5.70E-17	1.00E+00	5.40E-02	5.51E-02	6.41E-02	6.37E-02	9.68E-02	1.84E-01	2.03E-01	2.89E-01	2.86E-01	4.05E-01	5.38E-01	7.02E-01	8.53E-01	1.03E+00	1.05E+00	9.60E-01
H	σ	1.09E-02	4.54E-02	9.11E-03	2.99E-03	8.47E-03	8.55E-03	6.07E-03	1.37E-02	7.40E-03	2.23E-02	2.31E-02	2.12E-02	6.21E-02	3.75E-02	6.36E-02	6.42E-02	6.12E-02	3.35E-02
A	CV(%)	-1.92E+16	4.54	16.86	5.43	13.22	13.42	6.27	7.46	3.64	7.72	8.06	5.24	11.53	5.34	7.46	6.22	5.84	3.49
N	Z (Robust)	x	x	0.83	0.85	0.83	0.83	0.83	0.78	0.80	0.71	0.71	0.66	0.30	0.16	-1.23	-9.07	-5.75	-4.93
D	Z (max/min signal)			18.3 SN															
D	EC ₅₀ (μM)		5.1					91.5 SB	2.2										
Robot																			
R	μ	-1.19E-16	1.00E+00	6.45E-02	7.51E-02	5.81E-02	5.57E-02	5.91E-02	4.07E-02	7.82E-02	1.10E-01	1.31E-01	1.34E-01	2.18E-01	3.51E-01	5.58E-01	8.68E-01	9.46E-01	9.27E-01
O	σ	2.50E-02	6.11E-02	1.98E-02	1.53E-02	1.65E-02	2.75E-02	1.81E-02	2.74E-02	2.66E-02	1.76E-02	7.03E-02	7.58E-02	4.87E-02	3.87E-02	5.10E-02	3.77E-02	3.15E-02	5.88E-02
B	CV(%)	-2.11E+16	6.11	30.64	20.42	33.46	49.30	30.68	67.27	34.09	15.92	53.55	56.40	22.33	11.02	9.13	4.34	3.33	6.34
O	Z (Robust)	x	x	0.74	0.75	0.74	0.72	0.75	0.72	0.71	0.73	0.55	0.53	0.58	0.54	0.24	-1.24	-4.16	-3.96
O	Z (max/min signal)			12.1 SN															
T	EC ₅₀ (μM)		5.1					40.0 SB	2.1										

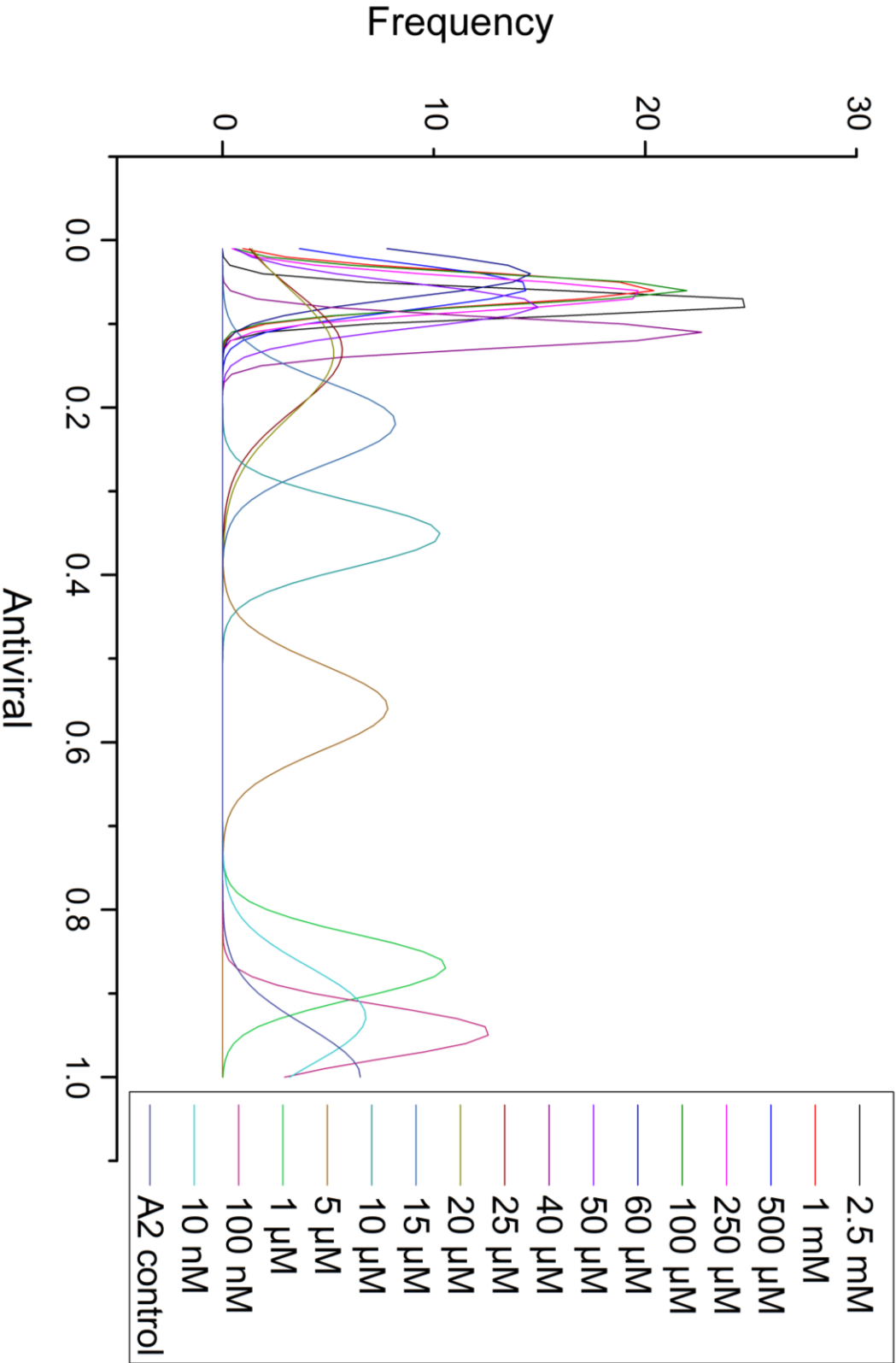
10 – Normal distribution of Ribavirin concentrations (overall) (Section 2.3.5.3)



11 – Normal distribution of Ribavirin concentrations (hand) (Section 2.3.6)

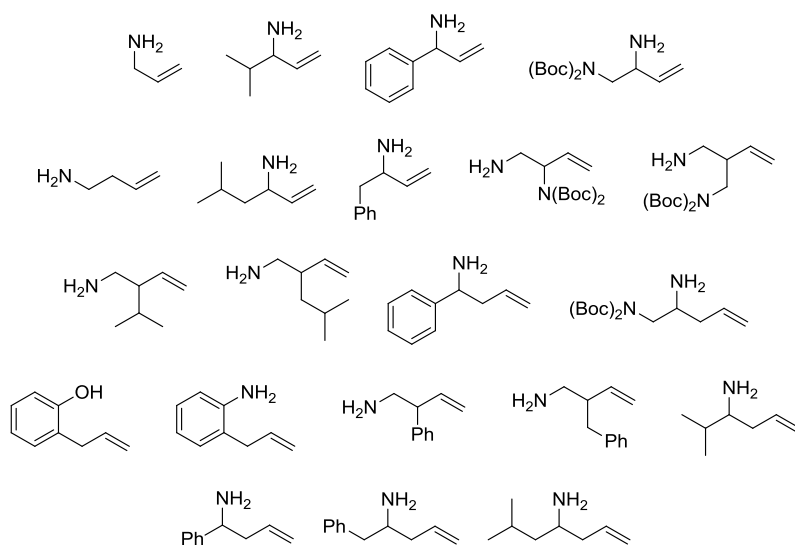


12 – Normal distribution of Ribavirin concentrations (robot) (Section 2.3.6)

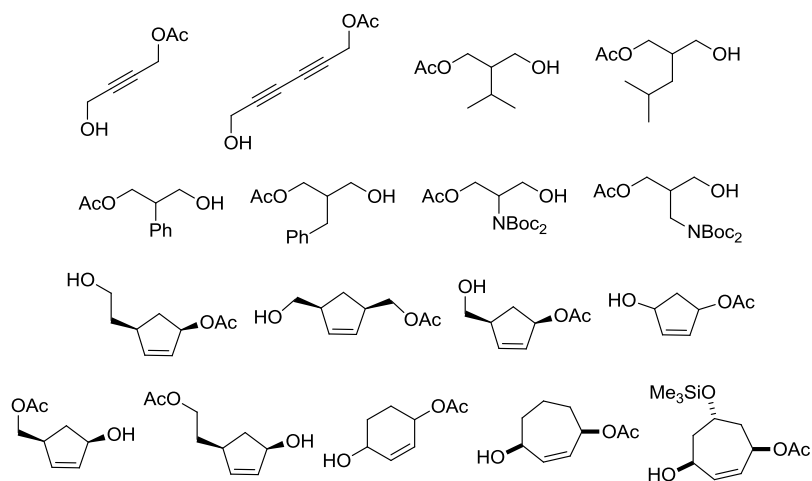


13 – Building blocks and electrophiles chosen for the enumeration of the virtual library described in Section 3.2.1

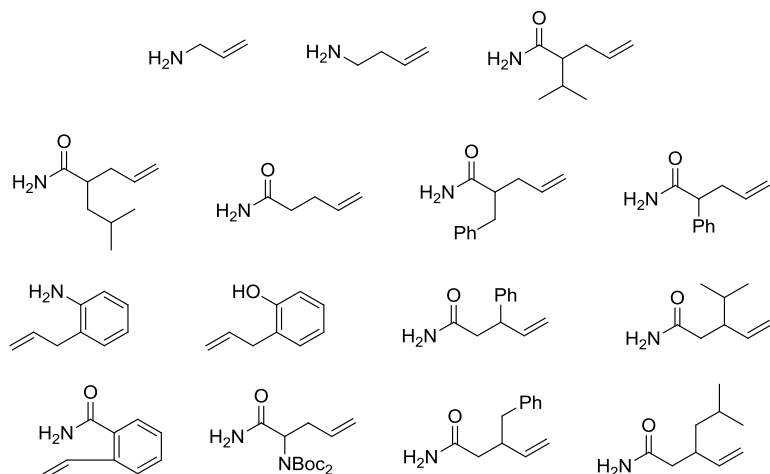
Building blocks (set A):



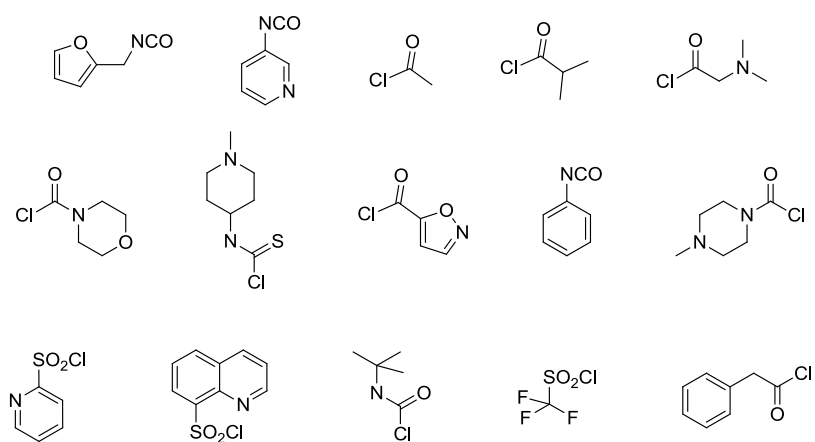
Building blocks (set B):



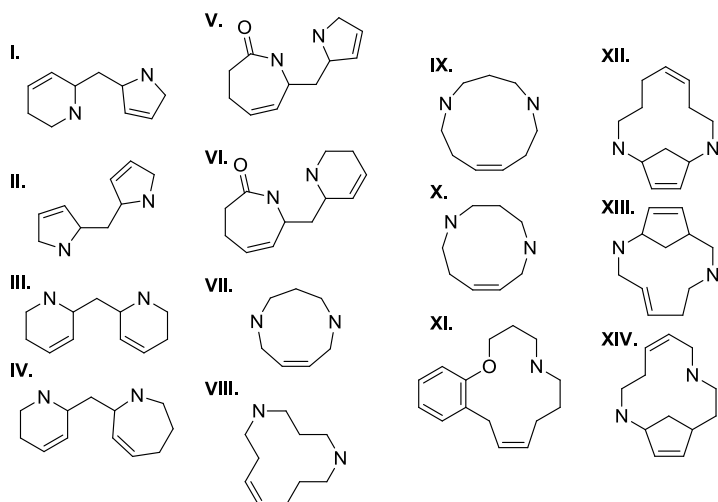
Building blocks (set C):



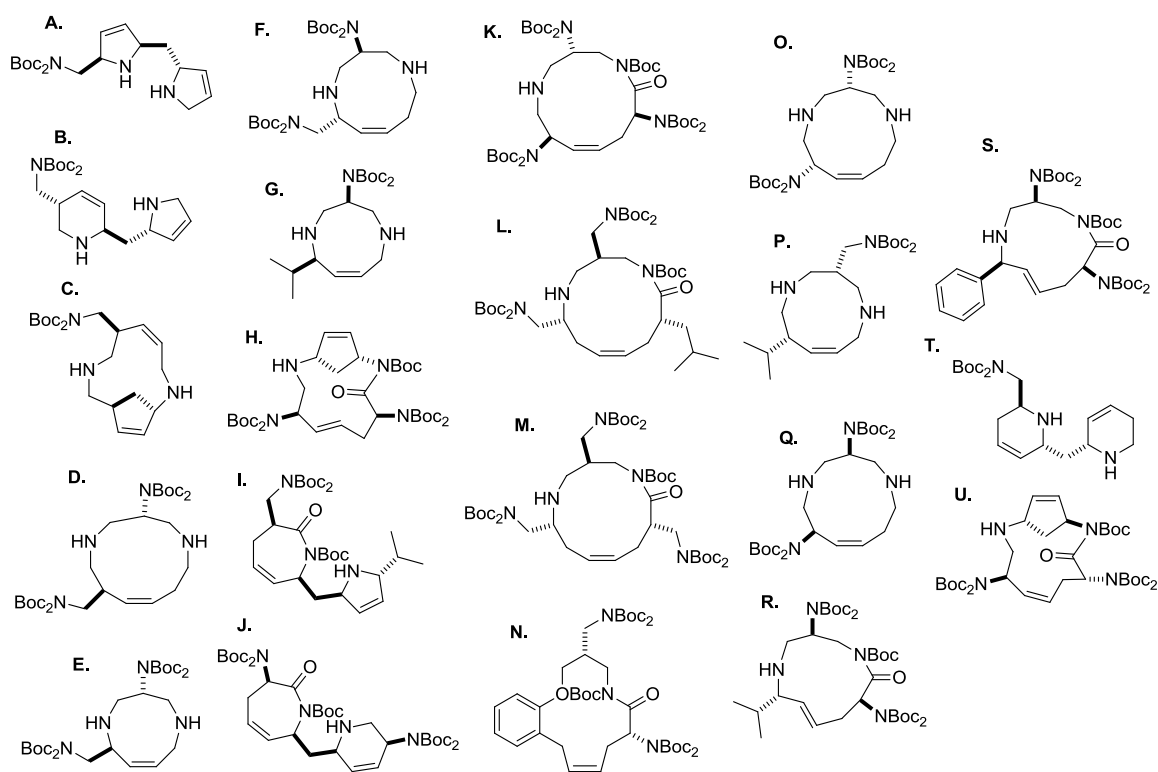
Electrophiles (set D):



Appendix 14 – Fourteen common substructures identified by vHTS of 53,640 molecules against 3KPE with the bound water using eHiTS (Section 3.2.2)

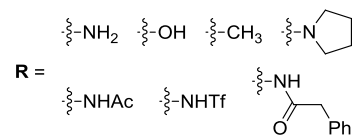


Appendix 15 – Twenty-one common scaffolds identified by vHTS of 15,728 molecules against 3KPE with the bound water using eHiTS (Section 3.2.2)

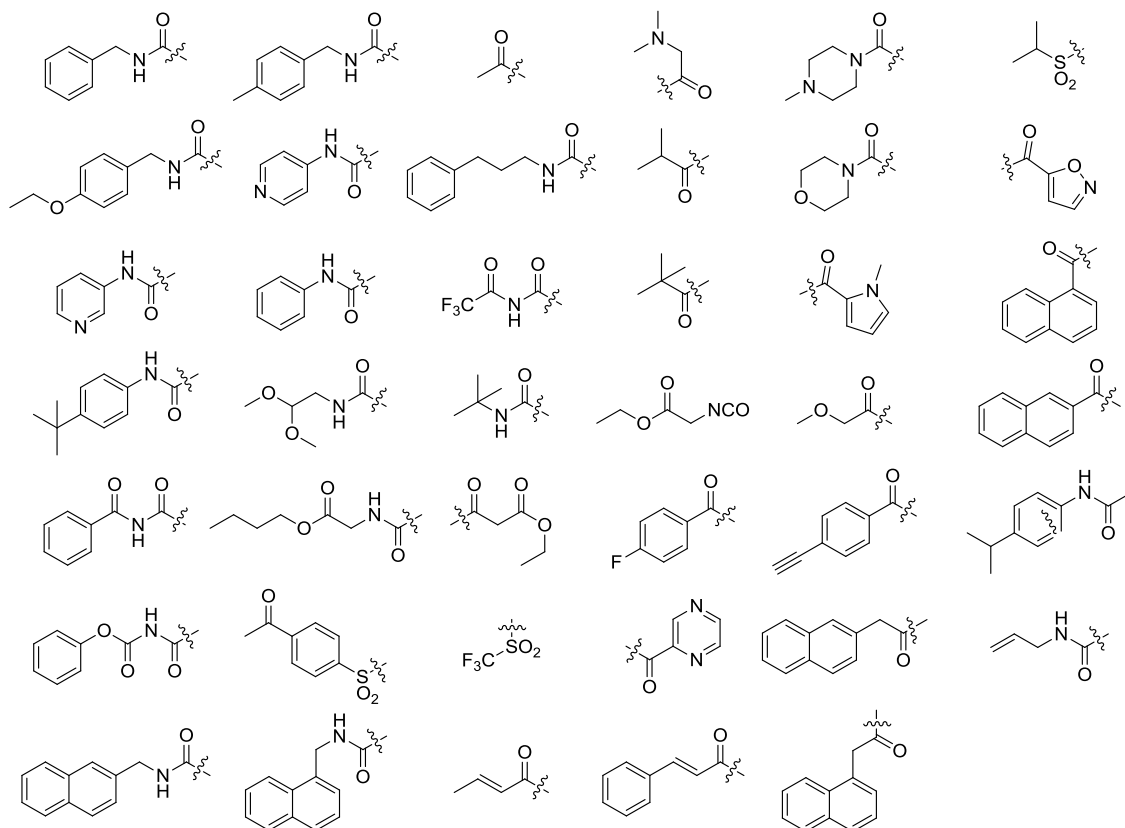


Appendix 16 – Enumeration of a more focused library (Section 3.2.3)

R groups:

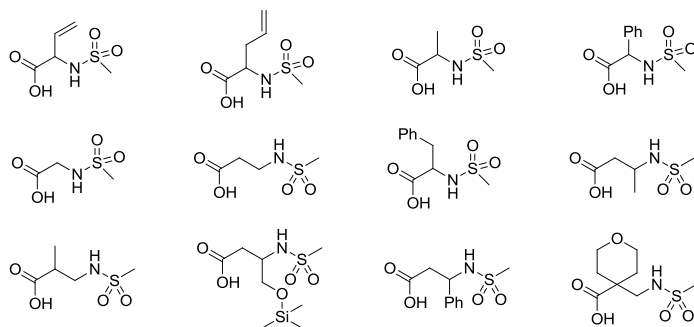


R¹ groups:

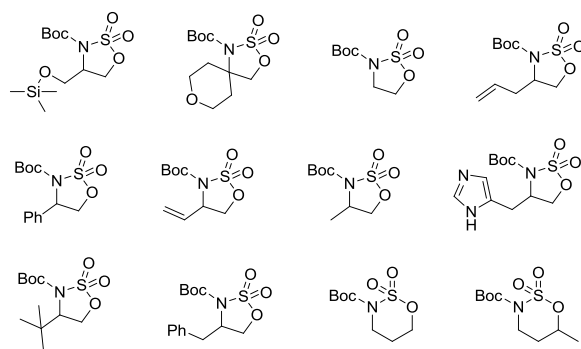


Appendix 17 – Enumeration of a lead-like library of 85,115 molecules (Section 3.3.1)

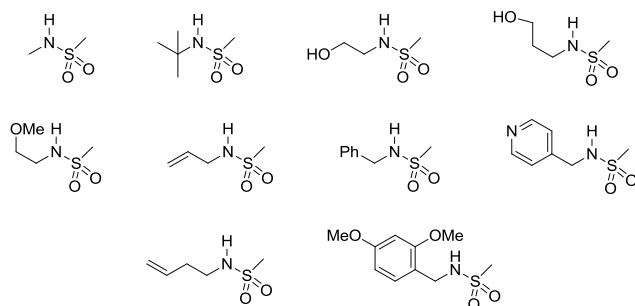
Amino acid derivatives



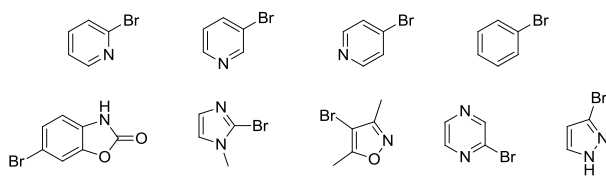
Cyclic sulfamidates



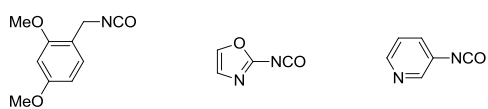
Sulfonamides



Aryl bromides



Isocyanates



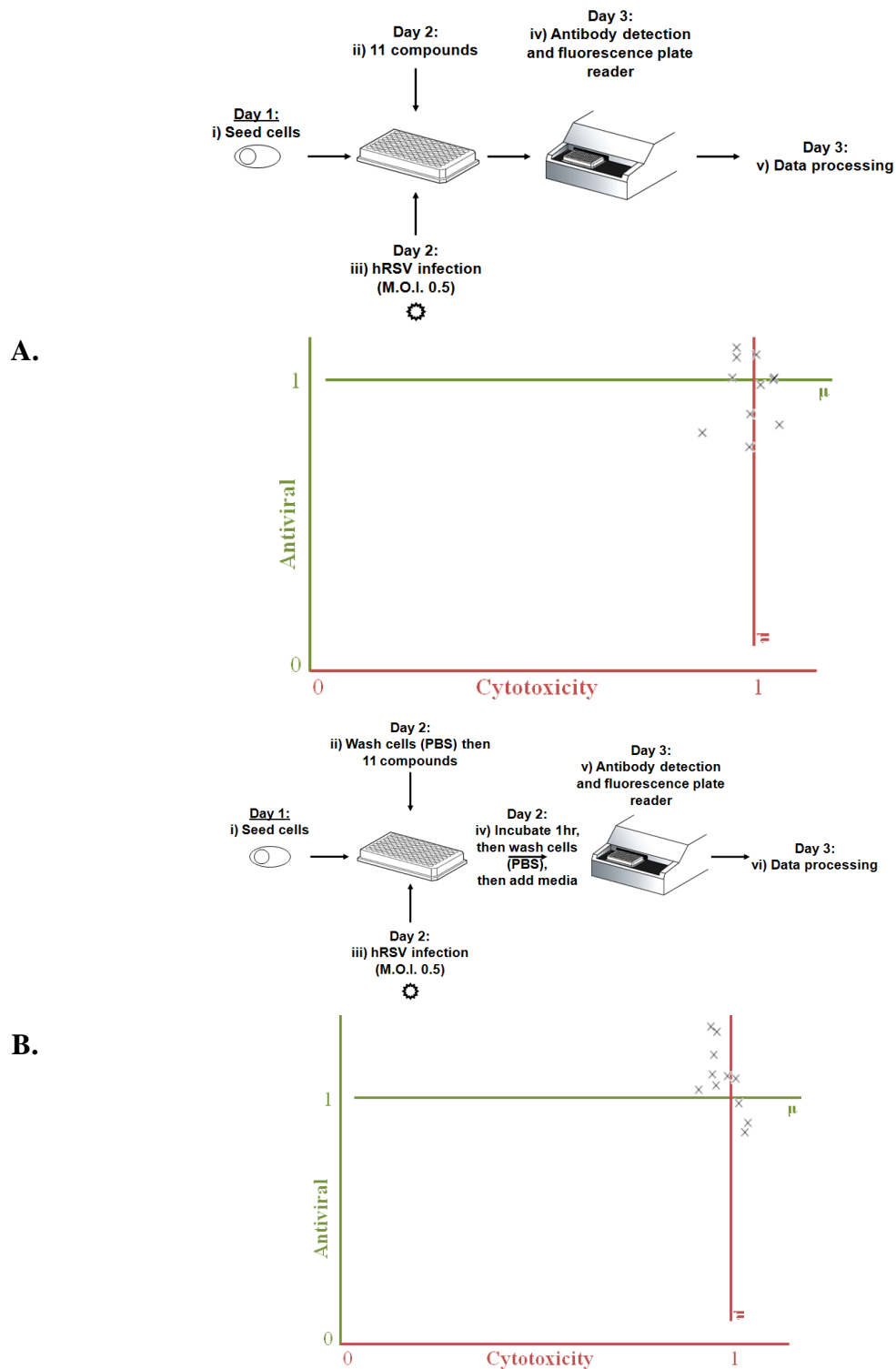
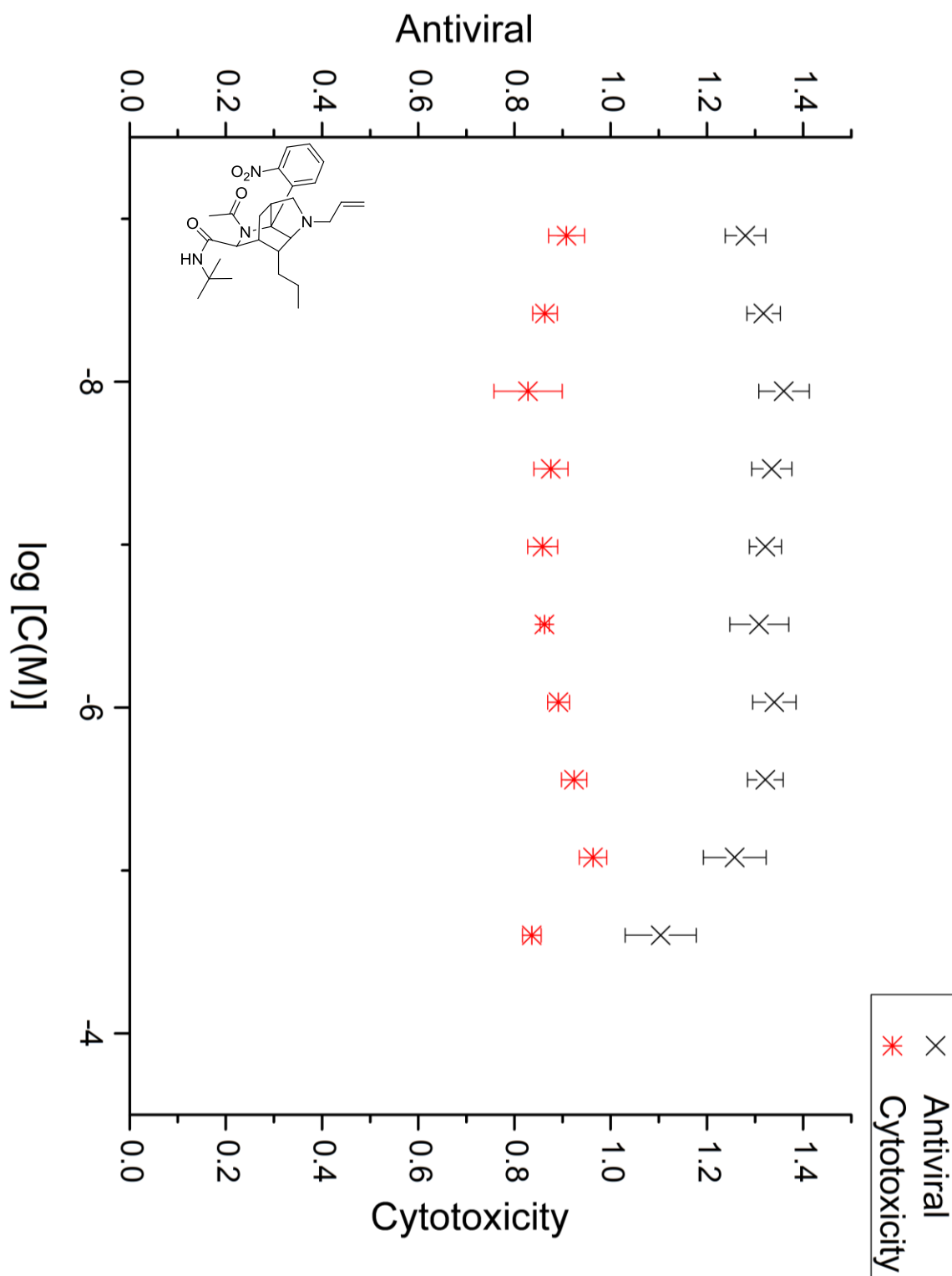
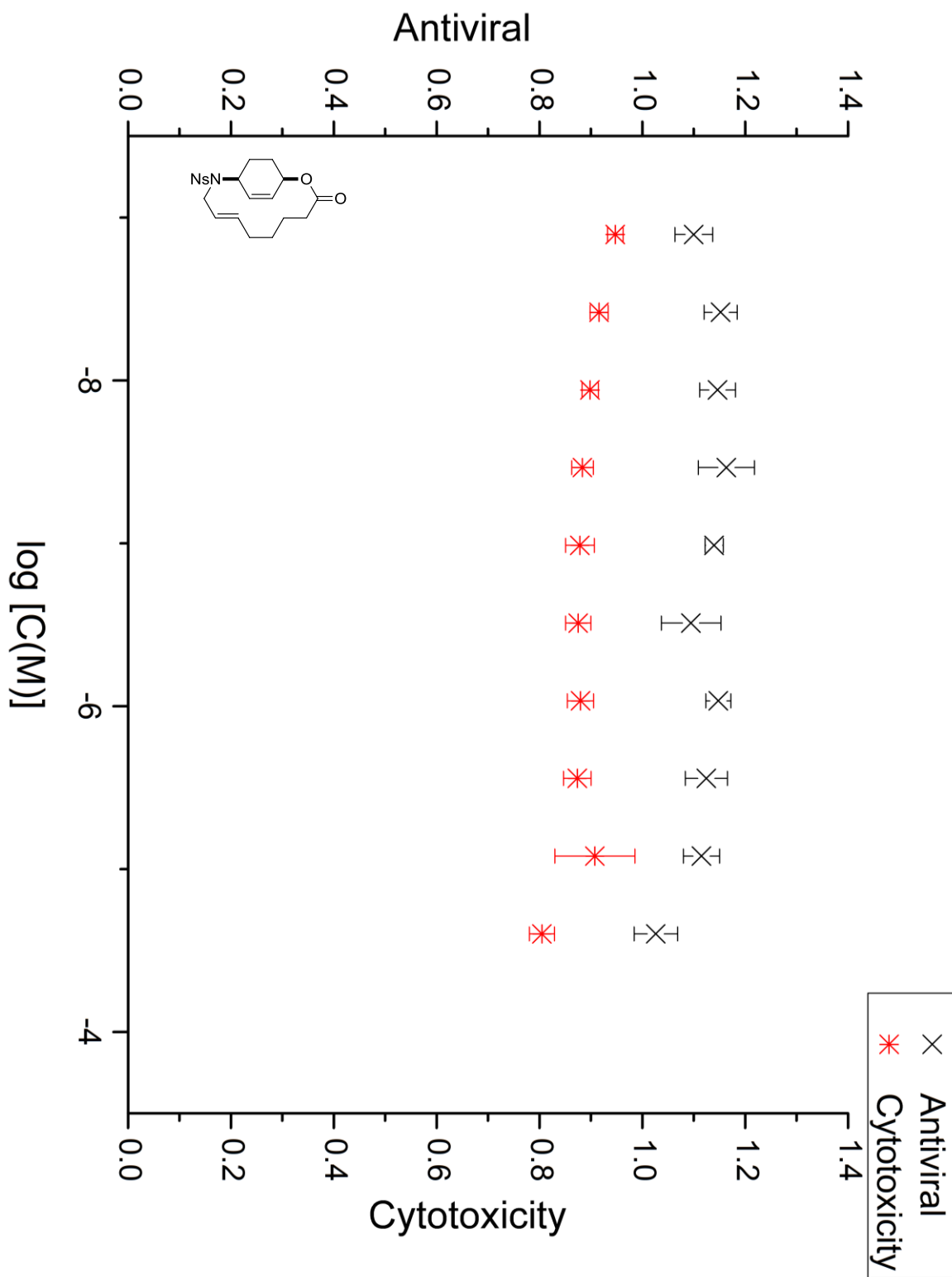


Figure Z.2. Alternative assay conditions used to assay hRSV fusion. A. Day 1: cells, day 2: compounds (25 μ M) then virus and incubate for 24 hr. **B.** Day 1: cells, day 2: compounds (25 μ M) then virus and incubate for 24 hr then wash with PBS and add media, incubate for 24 hr.

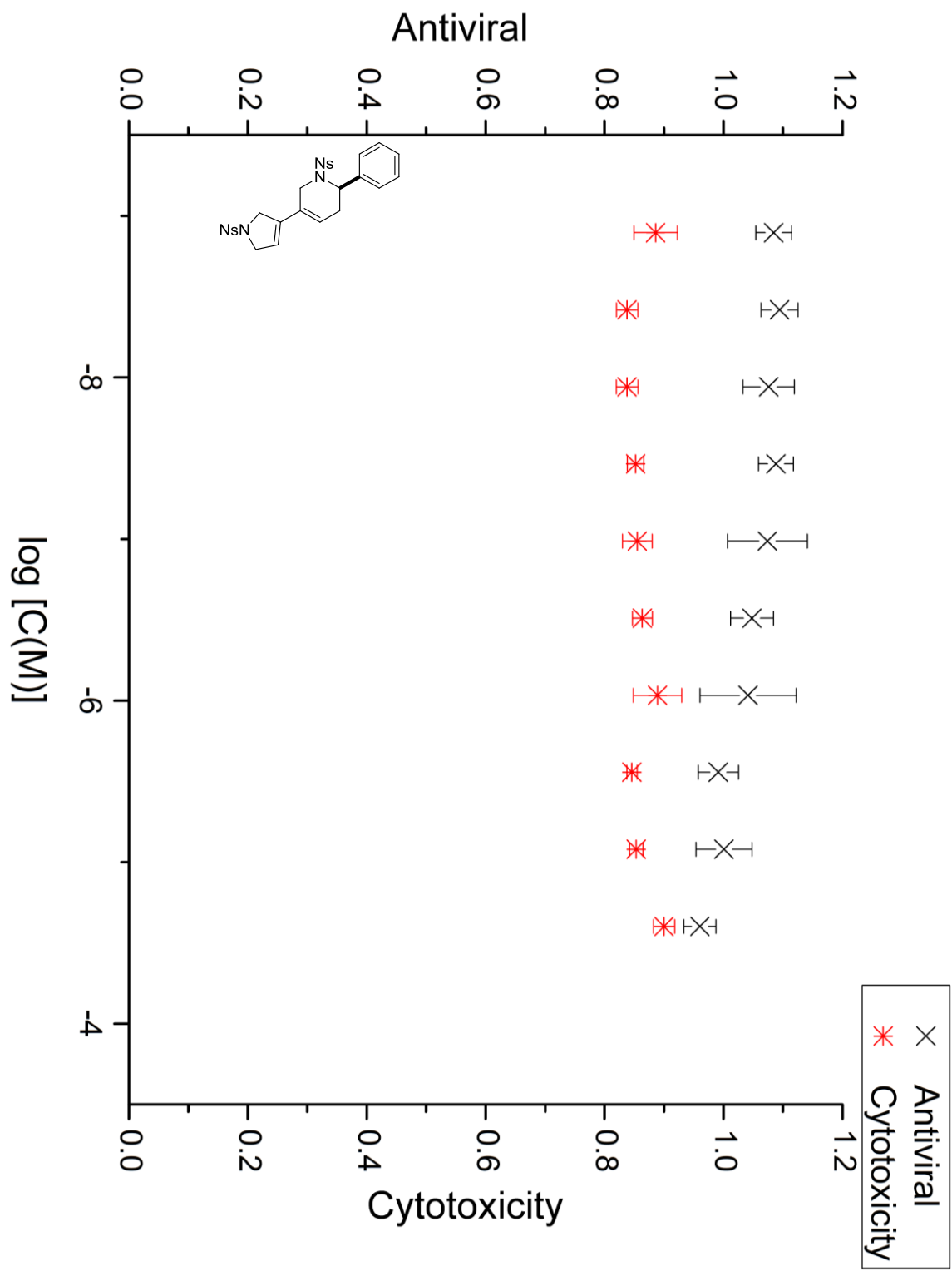
19 – HTS control compound, no antiviral activity but cytotoxicity observed
(Section 5.1.5)



21 – HTS control compound, no antiviral activity but cytotoxicity observed
(Section 5.1.5)



22 – HTS control compound, no antiviral activity but cytotoxicity observed
(Section 5.1.5)



23 – HTS control compound, no antiviral activity, no cytotoxicity observed
(Section 5.1.5)

